

Energy-Based Modeling and Tracking Control of Rigid Body Systems with Practical Multicopter Applications

DISSERTATION
zur Erlangung des Grades
des Doktors der Ingenieurwissenschaften
(Dr.-Ing.)
der Naturwissenschaftlich-Technischen Fakultät II
– Physik und Mechatronik –
der Universität des Saarlandes

von

MATTHIAS KONZ

Saarbrücken

October 20, 2025

Abstract

Many machines, vehicles and robots may be modeled as rigid body systems, i.e. a number of interconnected, undeformable bodies subject to inertia, gravity, and other forces. Energy-based methods for derivation of their equations of motion, like the Lagrange formalism, are standard in engineering education and well established in the dedicated literature. These algorithms commonly rely on the use of a minimal set of generalized coordinates. This is appropriate for many applications, e.g. machines containing only one-dimensional joints. For systems whose configuration space is nonlinear, e.g. mobile robots whose configuration space contains the rigid body attitude, the use of minimal coordinates necessarily leads to singularities. From the point of view of differential geometry, this is a well known fact.

This work resolves this problem by the use of (possibly) redundant configuration coordinates and (possibly) nonholonomic velocity coordinates. The second chapter reviews several established formalisms of analytical mechanics and states them in terms of these more general coordinates. The third chapter applies these results to rigid body systems. Though inertia is the crucial part of the dynamics, this work also investigates dissipation and stiffness. Finally, it presents an algorithm for the derivation of global equations of motion of general rigid body systems.

The literature states computed-torque is a standard approach for tracking control of fully actuated mechanical systems. However, this recipe relies on minimal coordinates and consequently suffers from the problems mentioned above. There is no established “standard” approach for the control of underactuated systems.

This work presents three slightly different algorithms for tracking control of general rigid body systems by means of static state feedback. These essentially minimize the distance between the actual realizable acceleration of the model and a desired acceleration computed from a stable prototype system. The prototype system shares the geometry and kinematics of the actual model, but may have different constitutive properties (inertia, damping, stiffness). The resulting control law can be computed globally and explicitly for any rigid body system. The resulting closed loop system (which may differ from the prototype in the underactuated case), is invariant to the chosen coordinates, i.e. its formulation is covariant. However, so far, there is no general proof of stability. The performance of the proposed approaches are discussed on several examples and simulation results.

The last chapter of this work discusses the experimental realization of the control approach to two small UAVs. The performance is demonstrated on tracking control for several aerobatic maneuvers.

Contents

1	Introduction	1
1.1	Context and state of the art	1
1.2	Motivation example	4
1.3	Goal and outline of this work	6
2	Some math	7
2.1	Coordinates	7
2.1.1	Redundant configuration coordinates	7
2.1.2	Minimal velocity coordinates	8
2.2	Calculus	11
2.2.1	Directional derivative and Hessian	11
2.2.2	Commutation coefficients	12
2.2.3	Linearization about a trajectory	14
2.2.4	Calculus of variations	15
2.2.5	Hamilton's equations	16
2.3	Linear algebra	18
2.3.1	Matrix sets	18
2.3.2	Inner product, norm and metric	18
2.3.3	Vee and wedge	19
2.3.4	Singular value decomposition	20
2.4	An important function on the special orthogonal group	20
3	Analytical mechanics of particle systems	24
3.1	A single free particle	24
3.2	Systems of constrained particles	26

3.2.1	First principles	26
3.2.2	Coordinates	27
3.2.3	Inertia	30
3.2.4	Gravitation	32
3.2.5	Stiffness	33
3.2.6	Dissipation	33
3.2.7	Energy	34
3.3	A single free rigid body	35
3.3.1	Coordinates	35
3.3.2	Inertia	37
3.3.3	Gravitation	39
3.3.4	Stiffness	40
3.3.5	Dissipation	42
3.3.6	Summary and the special Euclidean group	43
3.4	Rigid body systems	47
3.4.1	Parameterization	47
3.4.2	Inertia	53
3.4.3	Gravitation	54
3.4.4	Stiffness	55
3.4.5	Dissipation	56
3.4.6	Summary	56
3.5	Additional general constraints	57
4	Tracking control of rigid body systems	60
4.1	Approach 1: Inspired by particle distribution	61
4.1.1	Particle system	61
4.1.2	Free rigid body	63
4.1.3	Rigid body systems	65
4.2	Approach 2: Body based approach	67
4.2.1	Free rigid body	67
4.2.2	Rigid body systems	68

4.3	Approach 3: Inspired by total energy	69
4.3.1	Overall structure	69
4.3.2	Special cases	70
4.3.3	Free rigid body	71
4.3.4	Rigid body systems	72
4.4	Constant reference and linearization	73
4.5	Underactuated systems	73
4.5.1	Control law through static optimization	74
4.5.2	Matching condition	75
4.5.3	Approximations	76
4.5.4	Systems with input constraints	77
4.6	Summary and recipe	77
4.7	Examples of fully actuated systems	79
4.7.1	Prismatic joint	79
4.7.2	Revolute joint	81
4.7.3	Rigid body orientation	83
4.7.4	Planar rigid body	85
4.7.5	Free rigid body: decoupling of translational and rotational motion .	88
4.7.6	SCARA robot	91
4.7.7	Robot arm	96
4.8	Examples of underactuated systems	99
4.8.1	Two masses connected by a spring	99
4.8.2	PVTOL	101
4.8.3	Quadcopter	104
4.8.4	Bicopter	107
5	Multicopter control realization	112
5.1	Hardware & software realization	113
5.2	Multicopter Models	116
5.2.1	Actuator models	116
5.2.2	Rigid body model	117

5.2.3	Parameter identification	120
5.2.4	Model validation and simplification	125
5.3	Control of the generalized force	129
5.3.1	Servo simulation	129
5.3.2	Propeller tracking control	129
5.3.3	Tricopter force control	131
5.3.4	Quadcopter force vector control	134
5.4	State estimation	137
5.4.1	IMU misalignment correction	139
5.4.2	Angular velocity and torque bias	140
5.4.3	Configuration measurement latency	141
5.4.4	Attitude integration	143
5.4.5	Position, velocity and accelerometer bias	144
5.4.6	Force bias	145
5.5	Reference generation	146
5.6	Experimental results	149
6	Summary and Conclusions	157
A	TBD	159
A.1	On error coordinates	159
A.2	Constraint stabilization	160
A.3	A possible generalization of the rigid body energies	161

Chapter 1

Introduction

1.1 Context and state of the art

Modeling. As the title suggests this work deals with modeling and control of rigid body systems. The procedure of physical modeling is illustrated in Figure 1.1. It starts by approximating the system under consideration by a mechanical model. The mathematical part requires the choice of coordinates \mathbf{z} to capture the state (positions and velocities) of the model. Combining this with principles of mechanics, we may derive a set of ordinary differential equations that capture its motion. This work mainly deals with this second part, i.e. the derivation of *equations of motion*.

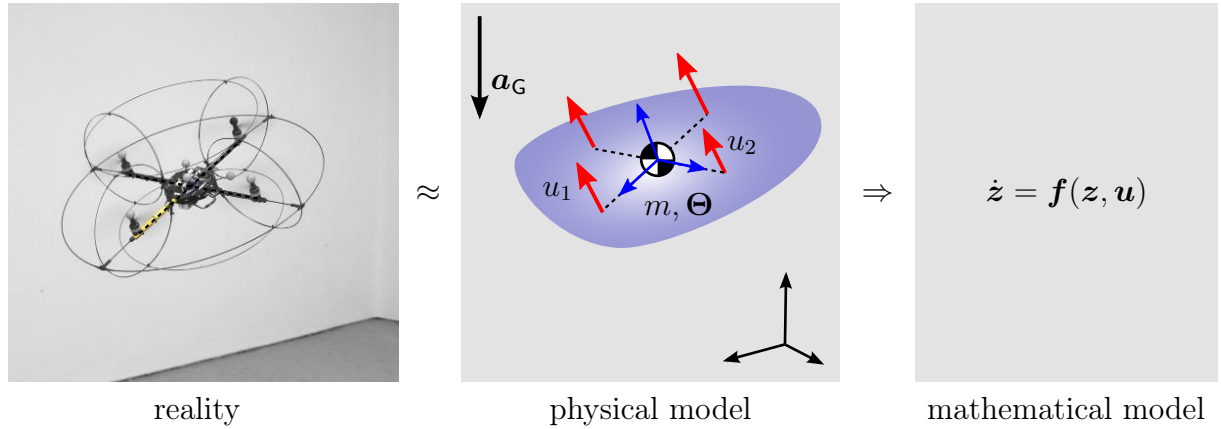


Figure 1.1: Modeling illustration

A very common approach for deriving equations of motion of finite-dimensional, holonomic mechanical systems is the so called *Lagrange formalism*: First, the system is parameterized by so called *generalized coordinates* \mathbf{q} . Then the kinetic energy \mathcal{T} , the potential energy \mathcal{V} and virtual work $\delta\mathcal{W}$ of external forces are formulated in terms of these coordinates and their derivatives $\dot{\mathbf{q}} = d\mathbf{q}/dt$:

$$\mathcal{L}(\mathbf{q}, \dot{\mathbf{q}}) = \mathcal{T}(\mathbf{q}, \dot{\mathbf{q}}) - \mathcal{V}(\mathbf{q}), \quad \delta\mathcal{W}^E = (\delta\mathbf{q})^\top \mathbf{f}^E. \quad (1.1)$$

The equations of motion are derived from the Lagrangian \mathcal{L} as

$$\frac{d}{dt} \frac{\partial \mathcal{L}}{\partial \dot{\mathbf{q}}} - \frac{\partial \mathcal{L}}{\partial \mathbf{q}} = \mathbf{f}^E. \quad (1.2)$$

The kinetic energy for a time-invariant, mechanical system is always strictly quadratic $\mathcal{T} = \frac{1}{2} \dot{\mathbf{q}}^\top \mathbf{M}(\mathbf{q}) \dot{\mathbf{q}}$. Furthermore, we assume that the external forces \mathbf{f}^E is an affine function of the control inputs \mathbf{u} . Then the equations of motion take the structure

$$\mathbf{M}(\mathbf{q})\ddot{\mathbf{q}} + \mathbf{b}(\mathbf{q}, \dot{\mathbf{q}}) = \mathbf{B}(\mathbf{q})\mathbf{u} \quad \Leftrightarrow \quad \underbrace{\frac{d}{dt} \begin{bmatrix} \mathbf{q} \\ \dot{\mathbf{q}} \end{bmatrix}}_z = \underbrace{\begin{bmatrix} \dot{\mathbf{q}} \\ \mathbf{M}^{-1}(\mathbf{q})(\mathbf{B}(\mathbf{q})\mathbf{u} - \mathbf{b}(\mathbf{q}, \dot{\mathbf{q}})) \end{bmatrix}}_{\mathbf{f}(z, \mathbf{u})} \quad (1.3)$$

The right hand side of (1.3) is a standard form for simulation, i.e. numerical solution, or general control design. However, the structure of the left hand side of (1.3) can be exploited for a particular control design.

Feedback Control. From a mathematical point of view, a feedback controller is some map $\mathbf{u} = \mathbf{g}(\mathbf{z}, \mathbf{r})$ that computes the control input \mathbf{u} based on the measured system state \mathbf{z} and some reference input \mathbf{r} . The goal is that the resulting controlled system $\dot{\mathbf{z}} = \mathbf{f}(\mathbf{z}, \mathbf{g}(\mathbf{z}, \mathbf{r})) = \bar{\mathbf{f}}(\mathbf{z}, \mathbf{r})$ has desirable properties.

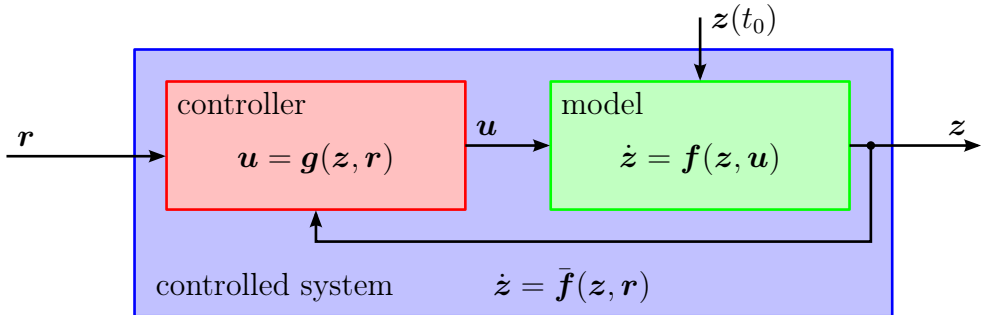


Figure 1.2: Model, controller and controlled system

For a system of the structure (1.3), a typical control objective is, that a given reference trajectory $t \mapsto \mathbf{q}_R(t)$ is a stable trajectory of the controlled system. If there are as many control inputs as degrees of freedom $\dim \mathbf{u} = \dim \mathbf{q} = n$ and the input matrix \mathbf{B} is invertible, there is a popular control approach, commonly called *computed torque*: Defining the error dynamics as

$$\ddot{\mathbf{e}} + \Lambda_1 \dot{\mathbf{e}} + \Lambda_0 \mathbf{e} = \mathbf{0}, \quad \mathbf{e} = \mathbf{q} - \mathbf{q}_R \quad (1.4)$$

with the symmetric, positive definite matrices Λ_0, Λ_1 as tuning parameters. Combining this with the model (1.3) yields the control law

$$\mathbf{u} = \mathbf{B}^{-1}(\mathbf{M}(\mathbf{q})(\ddot{\mathbf{q}}_R - \Lambda_1 \dot{\mathbf{e}} - \Lambda_0 \mathbf{e}) + \mathbf{b}(\mathbf{q}, \dot{\mathbf{q}})) = \mathbf{g}(\underbrace{\mathbf{q}, \dot{\mathbf{q}}}_z, \underbrace{\mathbf{q}_R, \dot{\mathbf{q}}_R, \ddot{\mathbf{q}}_R}_r) \quad (1.5)$$

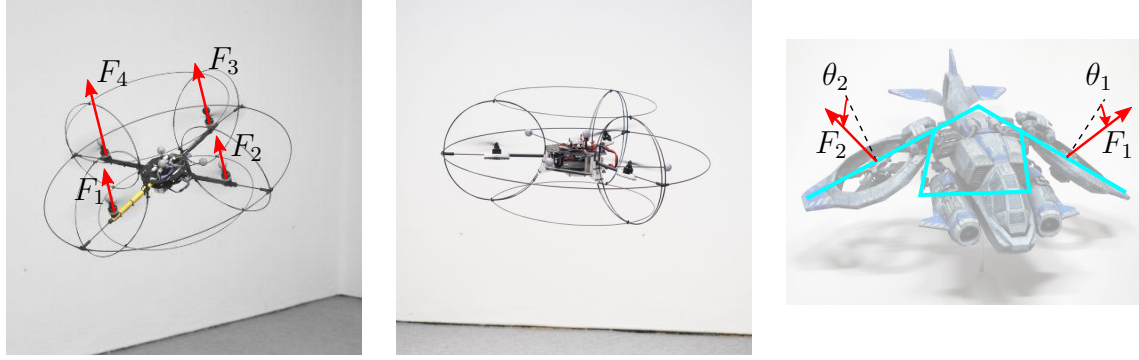


Figure 1.3: lsr-quadcopter (left), lsr-tricopter (middle) and a concept of a bicopter

Multicopters. In contrast to conventional helicopters, multicopters are aerial vehicles that use several rigid (fixed pitch) propellers to generate lift and maneuver. They are usually small and unmanned and are used to carry cameras or other sensors. In particular, the four propeller quadcopter configuration has became quite popular over the last two decades.

The *Chair of Systems Theory and Control Engineering* at Saarland University has developed realizations of a quadcopter and a tricopter with three tilttable propellers (see Figure 1.3). A bicopter with two tilttable and inclined propellers has been studied through simulations. In particular the lsr-quadcopter has an excellent thrust to weight ratio and is consequently well suited for aggressive, aerobatic maneuvers, e.g. a looping as shown in Figure 1.4.

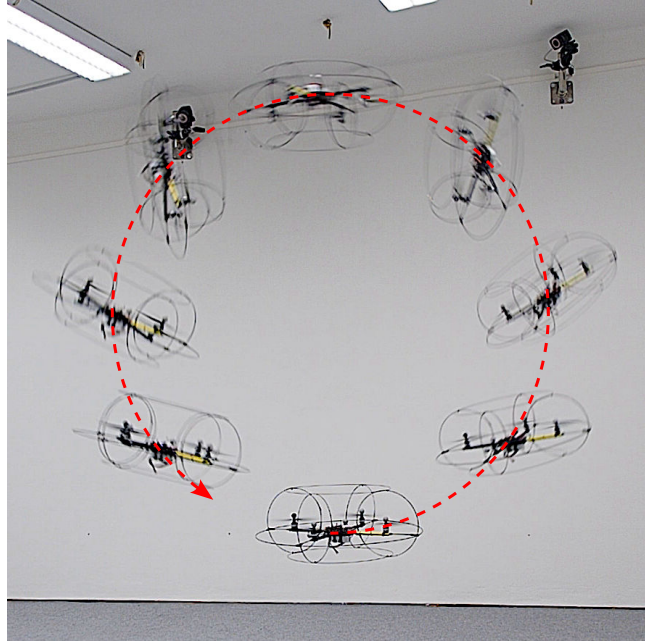


Figure 1.4: Snapshots of the lsr-quadcopter tracking a looping trajectory

From a mechanical point of view, these multicopters may be modelled as a free rigid body moving within Earth's gravity. The difference between them is only the placement of the actuators: the tricopter is fully-actuated, so it poses the easiest control task. The

quadcopter only has four actuators for its six degrees of freedom, i.e. it is underactuated. However, its model is well known to be a configuration flat system and corresponding standard control design approaches may be applied. The bicopter is (probably) not a flat system and consequently, poses the toughest control task.

1.2 Motivation example

Consider a free rigid body as illustrated in the middle of Figure 1.1, but fixed at its center of mass, i.e. it may only rotate about this point. For simplicity, we also assume that the chosen frame coincides with its principle axis and there are three independent control torques about these axis. Then the coefficients of inertia are $\Theta = \text{diag}(\Theta_x, \Theta_y, \Theta_z)$.

Lagrange's equation. For application of the Lagrange formalism we need to parameterize the system by minimal generalized coordinates. A popular choice for the rigid body orientation are Euler angles in the *roll-pitch-yaw* convention:

$$\mathbf{R}(\mathbf{q}) = \begin{bmatrix} c_\varphi c_\beta & -s_\varphi c_\alpha + c_\varphi s_\beta s_\alpha & s_\varphi s_\alpha + c_\varphi s_\beta c_\alpha \\ s_\varphi c_\beta & c_\varphi c_\alpha + s_\varphi s_\beta s_\alpha & -c_\varphi s_\alpha + s_\varphi s_\beta c_\alpha \\ -s_\beta & c_\beta s_\alpha & c_\beta c_\alpha \end{bmatrix}, \quad (1.6a)$$

$$\boldsymbol{\omega}(\mathbf{q}, \dot{\mathbf{q}}) = \underbrace{\begin{bmatrix} 1 & 0 & -s_\beta \\ 0 & c_\alpha & c_\beta s_\alpha \\ 0 & -s_\alpha & c_\beta c_\alpha \end{bmatrix}}_{\mathbf{Y}(\mathbf{q})} \underbrace{\begin{bmatrix} \dot{\alpha} \\ \dot{\beta} \\ \dot{\varphi} \end{bmatrix}}_{\dot{\mathbf{q}}} . \quad (1.6b)$$

The shortcut notation $s_\varphi := \sin(\varphi)$ and $c_\varphi := \cos(\varphi)$ used here, will be used throughout this text. With this, we may formulate the kinetic energy $\mathcal{T}(\mathbf{q}, \dot{\mathbf{q}}) = \frac{1}{2}(\boldsymbol{\omega}(\mathbf{q}, \dot{\mathbf{q}}))^\top \Theta \boldsymbol{\omega}(\mathbf{q}, \dot{\mathbf{q}})$ which coincides with the Lagrangian since there is no potential energy. Evaluation of Lagrange's equation (1.2) yields the equations of motion

$$\underbrace{\begin{bmatrix} \Theta_x & 0 & -\Theta_x s_\beta \\ 0 & \Theta_y c_\alpha^2 + \Theta_z s_\alpha^2 & (\Theta_y - \Theta_z) c_\alpha s_\alpha c_\beta \\ -\Theta_x s_\beta & (\Theta_y - \Theta_z) c_\alpha s_\alpha c_\beta & \Theta_x s_\beta^2 + (\Theta_y s_\alpha^2 + \Theta_z c_\alpha^2) c_\beta^2 \end{bmatrix}}_{\mathbf{M}(\mathbf{q})} \underbrace{\begin{bmatrix} \ddot{\alpha} \\ \ddot{\beta} \\ \ddot{\varphi} \end{bmatrix}}_{\ddot{\mathbf{q}}} + \underbrace{\begin{bmatrix} (\Theta_y - \Theta_z) c_\alpha s_\alpha \dot{\beta}^2 + \dots \\ 2(\Theta_z - \Theta_y) s_\alpha c_\alpha \dot{\beta} \dot{\alpha} + \dots \\ (2(\Theta_y - \Theta_z) c_\alpha^2 - \Theta_x - \Theta_y + \Theta_z) c_\beta \dot{\beta} \dot{\alpha} + \dots \end{bmatrix}}_{\mathbf{b}(\mathbf{q}, \dot{\mathbf{q}})} = \underbrace{\begin{bmatrix} 1 & 0 & 0 \\ 0 & c_\alpha & -s_\alpha \\ -s_\beta & c_\beta s_\alpha & c_\beta c_\alpha \end{bmatrix}}_{\mathbf{Y}^\top(\mathbf{q})} \underbrace{\begin{bmatrix} \tau_x \\ \tau_y \\ \tau_z \end{bmatrix}}_{\mathbf{u}} . \quad (1.7)$$

The entries in \mathbf{b} are not displayed here since they would fill several lines and are actually not of relevance here. What is crucial here is that the model has singularities at $\beta = \pm \frac{\pi}{2}$: $\det \mathbf{M} = \Theta_x \Theta_y \Theta_z c_\beta^2$ and $\det \mathbf{Y} = c_\beta$. For the previous example of aerobatic motions it is should be evident that singularities of this form would be unacceptable for simulation and control design.

Euler's rotation equations. For the particular example of the rigid body orientation one finds another formulation of the equations of motion directly in most textbooks on mechanics, e.g. [Arnold, 1989, p. 143] or [Roberson and Schwertassek, 1988, p. 145]:

$$\underbrace{\frac{d}{dt} \begin{bmatrix} R_x^x & R_y^x & R_z^x \\ R_x^y & R_y^y & R_z^y \\ R_x^z & R_y^z & R_z^z \end{bmatrix}}_R = \underbrace{\begin{bmatrix} R_x^x & R_y^x & R_z^x \\ R_x^y & R_y^y & R_z^y \\ R_x^z & R_y^z & R_z^z \end{bmatrix}}_R \underbrace{\begin{bmatrix} 0 & -\omega_z & \omega_y \\ \omega_z & 0 & -\omega_x \\ -\omega_y & \omega_x & 0 \end{bmatrix}}_{\text{wed } \boldsymbol{\omega}}, \quad (1.8a)$$

$$\underbrace{\begin{bmatrix} \Theta_x & 0 & 0 \\ 0 & \Theta_y & 0 \\ 0 & 0 & \Theta_z \end{bmatrix}}_\Theta \underbrace{\begin{bmatrix} \dot{\omega}_x \\ \dot{\omega}_y \\ \dot{\omega}_z \end{bmatrix}}_\omega + \underbrace{\begin{bmatrix} 0 & -\omega_z & \omega_y \\ \omega_z & 0 & -\omega_x \\ -\omega_y & \omega_x & 0 \end{bmatrix}}_{\text{wed } \boldsymbol{\omega}} \underbrace{\begin{bmatrix} \Theta_x & 0 & 0 \\ 0 & \Theta_y & 0 \\ 0 & 0 & \Theta_z \end{bmatrix}}_\Theta \underbrace{\begin{bmatrix} \omega_x \\ \omega_y \\ \omega_z \end{bmatrix}}_\omega = \underbrace{\begin{bmatrix} \tau_x \\ \tau_y \\ \tau_z \end{bmatrix}}_u. \quad (1.8b)$$

The 9 coefficients of the matrix \mathbf{R} have to obey the constraint $\mathbf{R}^\top \mathbf{R} = \mathbf{I}_3$. However, it can be shown that if this is fulfilled for the initial condition $\mathbf{R}(t_0)$, then the kinematic equation (1.8a) ensures that the condition remains fulfilled. This formulation has no singularities and is well suited for global simulation. Moreover, loosely speaking, its mathematical structure reflects the physical symmetries of the model. The obvious draw-back is that due to the lack of generalized coordinates, its unclear how a method like computed torque could be applied.

Discussion. Euler's equations (1.8) and (1.7) describe the same system. In fact one may plug (1.6b) into (1.8b) and multiply it by \mathbf{Y}^\top to obtain (1.7).

Each of these formulations has its advantages and draw-backs: Euler's equations are more compact and have a symmetric structure in contrast to (1.7). The downside is that they require 9 coordinates, the coefficients of the rotation matrix \mathbf{R} , to parameterize the attitude, whereas the Euler-angles \mathbf{q} only require 3. The crucial advantage of Lagrange's equation (1.2) is, that it holds for *any* finite dimensional and holonomic mechanical system, whereas Euler's equations only hold for this particular example. However, for this example, the equations (1.7) are quite cumbersome and lack an obvious structure. Probably the worst fact is that the inertia matrix $\mathbf{M}(\mathbf{q})$ is singular at the point $\beta = \pm \frac{\pi}{2}$ and consequently $\ddot{\mathbf{q}}$ is undefined at these points.

It should be stressed that there is no physical reason for the singularity in the Lagrangian version (1.7), it is rather a consequence of an unsuitable parameterization of the system. This is pointed out in [Roberson and Schwertassek, 1988, sec. 1.1.1] as: *[The scientists of the Eighteenth Century] recognized that there was something about rotation [...] which somehow made the analysis of rotation a problem of higher order difficulty. We now know that the problem is in the mathematics, not the physics, but the problem is still with us.*

The set of 3-dimensional rotation matrices $\mathbf{R} \in \mathbb{SO}(3)$ captures the actual configuration space of the rigid body orientation well, but it is difficult to work with since the coefficients of the rotation matrix are not independent. Since $\mathbf{R} \in \mathbb{SO}(3)$ is compact while \mathbb{R}^3 is not, there is no bijection between them, see also [Frankel, 1997, sec. 1.1d]. The chosen set of Euler angles may be regarded as a surjective but not injective function from \mathbb{R}^3 to $\mathbf{R} \in \mathbb{SO}(3)$ in a similar manner as latitude and longitude serve as coordinates for Earth's surface. The Euler angles are unsuited at the so called gimbal lock ($\beta = \pm 90^\circ$) just as longitude fails at Earth's poles.

1.3 Goal and outline of this work

The first chapter reviews established methods of analytical mechanics with the addition of allowing redundant coordinates (like the coefficients of a rotation matrix \mathbf{R}) and non-holonomic velocity coordinates (like the coefficients of the angular velocity $\boldsymbol{\omega}$). It will present a formulation that can derive both of the presented equations of motion for the motivation example, but holds for general finite-dimensional mechanical systems.

The second chapter specializes to rigid body systems, i.e. systems that consist of several interconnected rigid bodies. It presents an algorithm that derives the equations of motion based on chosen coordinates and given constitutive parameters. Furthermore, natural formulations of stiffness, dissipation and inertia for a rigid body are established.

The third chapter proposes tracking control algorithms for rigid body systems. Based on the findings of the second chapter it will present three control algorithms motivated by defining desired stiffness, damping and inertia of the resulting controlled system. Furthermore, these algorithms are extended to tackle underactuated systems. These algorithms are discussed through several examples.

The fourth chapter presents the developed quadcopter and tricopter and their performance for real control of aerobatic maneuvers.

Chapter 2

Some math

This chapter reviews some established mathematical concepts in particular for the context of redundant coordinates.

2.1 Coordinates

The example of the rigid body orientation showed that, though its degree of freedom is $n = 3$, it cannot be *globally* parameterized by 3 coordinates without having singularities. In other words, the configuration space of the rigid body orientation is not isomorphic to \mathbb{R}^3 and is called a nonlinear manifold.

If interested in a global parameterization of a n dimensional nonlinear manifold, there are two common approaches:

1. Choose a finite number of overlapping local charts with *minimal* coordinates $\mathbf{q} \in \mathbb{R}^n$, e.g. four distinct sets of Euler angles for the rigid body attitude [Grafarend and Kühnel, 2011]. As this is the common way of defining a smooth manifold, this is always possible.
2. Choose one parameterization with *redundant* coordinates $\mathbf{x} \in \mathbb{R}^\nu$, i.e. coordinates that are constrained by smooth equations of the form $\phi(\mathbf{x}) = \mathbf{0}$. E.g. the coefficients of the rotation matrix as done in (1.8). *Whitney embedding theorem* states that this is always possible with at least $\nu = 2n$ coordinates.

Both approaches have benefits and drawbacks depending on the application, but the first approach and the use of minimal coordinates is far more dominant in the literature. This work utilizes the second approach.

2.1.1 Redundant configuration coordinates

In the notation of this work, we use $\nu > 0$ coordinates $\mathbf{x}(t) = [x^1(t), \dots, x^\nu(t)]^\top \in \mathbb{R}^\nu$ that might be constrained by $c \geq 0$ smooth functions of the form $\phi(\mathbf{x}) = [\phi^1(\mathbf{x}), \dots, \phi^c(\mathbf{x})]^\top =$

0. For $c > 0$ these coordinates are not independent and are commonly called *redundant*. The set of mutually admissible coordinates is called the configuration space \mathbb{X} :

$$\mathbb{X} = \{\boldsymbol{x} \in \mathbb{R}^\nu \mid \boldsymbol{\phi}(\boldsymbol{x}) = \mathbf{0}\}. \quad (2.1)$$

Assuming that the rank of $\frac{\partial \boldsymbol{\phi}}{\partial \boldsymbol{x}}$ is constant, the dimension of the configuration space is

$$n = \dim \mathbb{X} = \nu - \text{rank } \frac{\partial \boldsymbol{\phi}}{\partial \boldsymbol{x}}. \quad (2.2)$$

For holonomic systems, n is also called its degree of freedom.

Whitney embedding theorem (see e.g. [Lee, 2003, Theo. 6.14]) states that: *Every smooth manifold of dimension n can be smoothly embedded in the Euclidean space \mathbb{R}^{2n} .* The number $2n$ is a worst case bound, i.e. for a particular example a lower dimension for the embedding space \mathbb{R}^ν might work and a higher dimension is permitted anyway. For this work, it essentially guarantees the existence of a global parameterization by the set \mathbb{X} for any smooth manifold.

2.1.2 Minimal velocity coordinates

For the following it is crucial to note that a geometric constraint is equivalent to its derivative supplemented with a suitable initial condition

$$\phi^\kappa(\boldsymbol{x}) = 0 \quad (2.3a)$$

$$\Leftrightarrow \quad \frac{\partial \phi^\kappa}{\partial x^\alpha}(\boldsymbol{x}) \dot{x}^\alpha = 0, \quad \phi^\kappa(\boldsymbol{x}_0) = 0 \quad (2.3b)$$

$$\Leftrightarrow \quad \frac{\partial \phi^\kappa}{\partial x^\alpha}(\boldsymbol{x}) \ddot{x}^\alpha + \frac{\partial^2 \phi^\kappa}{\partial x^\alpha \partial x^\beta}(\boldsymbol{x}) \dot{x}^\beta \dot{x}^\alpha = 0, \quad \phi^\kappa(\boldsymbol{x}_0) = 0, \quad \frac{\partial \phi^\kappa}{\partial x^\alpha}(\boldsymbol{x}_0) \dot{x}_0^\alpha = 0 \quad (2.3c)$$

...

where $\boldsymbol{x}_0 = \boldsymbol{x}(t_0)$. Even though (2.3a) might be nonlinear, its derivative (2.3b) is always *linear* in the velocities $\dot{\boldsymbol{x}}$. So here it is reasonable to choose *minimal velocity coordinates*: Let $\mathbf{A}(\boldsymbol{x}) \in \mathbb{R}^{\nu \times n}$ be a matrix with the properties $\frac{\partial \boldsymbol{\phi}}{\partial \boldsymbol{x}} \mathbf{A} = \mathbf{0}$ and $\text{rank } \mathbf{A} = n$. The first property of $\mathbf{A}(\boldsymbol{x})$ is that these columns of $\mathbf{A}(\boldsymbol{x})$ are orthogonal to the rows of $\frac{\partial \boldsymbol{\phi}}{\partial \boldsymbol{x}}(\boldsymbol{x})$. The second property implies that the columns of $\mathbf{A}(\boldsymbol{x})$ are linearly independent. So the columns of $\mathbf{A}(\boldsymbol{x})$ can be interpreted as a *basis vectors* for the tangent space $T_{\boldsymbol{x}} \mathbb{X}$. We can capture all allowed velocities $\dot{\boldsymbol{x}}(t)$ by the minimal velocity coordinates $\boldsymbol{\xi}(t) \in \mathbb{R}^n$ through

$$\dot{\boldsymbol{x}} = \mathbf{A}(\boldsymbol{x}) \boldsymbol{\xi} \quad (2.4)$$

This kinematic relation (2.4) ensures that the time derivative (2.3b) of the geometric constraint is fulfilled, and consequently the geometric constraint only has to be imposed on the initial condition $\boldsymbol{\phi}(\boldsymbol{x}(t_0)) = \mathbf{0}$.

Example 1. Consider a single particle constrained to a circle of radius ρ as illustrated in Figure 2.1.

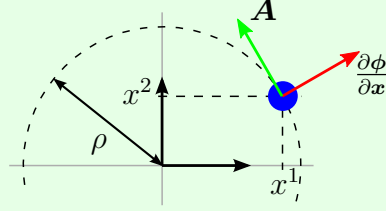


Figure 2.1: Particle on a circle

We use its Cartesian position $[x^1, x^2]^\top \in \mathbb{R}^2$ constrained by $\phi = (x^1)^2 + (x^2)^2 - \rho^2 = 0$ as configuration coordinates. A reasonable choice for the kinematics matrix \mathbf{A} is

$$\underbrace{\begin{bmatrix} 2x^1 & 2x^2 \end{bmatrix}}_{\frac{\partial \phi}{\partial \mathbf{x}}} \underbrace{\begin{bmatrix} -x^2 \\ x^1 \end{bmatrix}}_{\mathbf{A}} = 0 \quad (2.5)$$

Example 2. Consider the motivation example of the rigid body orientation from section 1.2. Instead of parameterizing the rotation matrix \mathbf{R} by minimal coordinates, we take its 9 coefficients $\mathbf{x} = [R_x^x, R_x^y, R_x^z, R_y^x, R_y^y, R_y^z, R_z^x, R_z^y, R_z^z]^\top \in \mathbb{R}^9$ as configuration coordinates. The constraints $\mathbf{R}^\top \mathbf{R} = \mathbf{I}_3$ and $\det \mathbf{R} = 1$ read

$$\phi(\mathbf{x}) = \begin{bmatrix} (R_x^x)^2 + (R_x^y)^2 + (R_x^z)^2 - 1 \\ (R_y^x)^2 + (R_y^y)^2 + (R_y^z)^2 - 1 \\ (R_z^x)^2 + (R_z^y)^2 + (R_z^z)^2 - 1 \\ R_y^x R_z^x + R_y^y R_z^y + R_y^z R_z^z \\ R_x^x R_z^x + R_x^y R_z^y + R_x^z R_z^z \\ R_x^y R_z^x + R_x^y R_z^y + R_x^z R_z^y \\ R_x^x R_y^x + R_x^y R_y^y + R_x^z R_y^z \\ R_x^x R_y^y R_z^z + R_y^x R_z^y R_x^z + R_z^x R_x^y R_y^z - R_x^x R_z^y R_y^z - R_y^x R_z^y R_x^z - R_z^x R_y^y R_x^z - 1 \end{bmatrix} = \mathbf{0}. \quad (2.6)$$

The 9 conditions $\mathbf{R}^\top \mathbf{R} = \mathbf{I}_3$ yields due to symmetry only 6 constraints and already imply $\det \mathbf{R} = \pm 1$. Since the determinant is a smooth function, the corresponding manifold must consist of two disjoint components, one with $\det \mathbf{R} = +1$ (proper rotations) and one with $\det \mathbf{R} = -1$ (rotations with reflection). So the additional constraint $\det \mathbf{R} = +1$ does not change the dimension of the configuration space. Formally this means $\text{rank } \frac{\partial \phi}{\partial \mathbf{x}} = 6$ and consequently $\dim \mathbb{X} = 9 - 6 = 3$. A kinematics matrix with $\frac{\partial \phi}{\partial \mathbf{x}} \mathbf{A} = \mathbf{0}$ and $\text{rank } \mathbf{A} = 3$

is given by

$$\mathbf{A}(\mathbf{x}) = \begin{bmatrix} 0 & -R_z^x & R_y^x \\ 0 & -R_z^y & R_y^y \\ 0 & -R_z^z & R_y^z \\ R_z^x & 0 & -R_x^x \\ R_z^y & 0 & -R_x^y \\ R_z^z & 0 & -R_x^z \\ -R_y^x & R_x^x & 0 \\ -R_y^y & R_x^y & 0 \\ -R_y^z & R_x^z & 0 \end{bmatrix}. \quad (2.7)$$

The resulting kinematic equation $\dot{\mathbf{x}} = \mathbf{A}(\mathbf{x})\xi$ can be reordered to the matrix equation $\dot{\mathbf{R}} = \mathbf{R} \text{wed}(\xi)$ by introducing the *wedge operator* defined as

$$\text{wed} \begin{bmatrix} \xi^1 \\ \xi^2 \\ \xi^3 \end{bmatrix} = \begin{bmatrix} 0 & -\xi^3 & \xi^2 \\ \xi^3 & 0 & -\xi^1 \\ -\xi^2 & \xi^1 & 0 \end{bmatrix}. \quad (2.8)$$

Pseudoinverse For any matrix $\mathbf{S} \in \mathbb{R}^{m \times n}$ there exists a unique (*Moore-Penrose*) pseudoinverse $\mathbf{S}^+ \in \mathbb{R}^{n \times m}$ determined by the following conditions [Penrose, 1955, Theo. 1]:

$$\mathbf{S}\mathbf{S}^+\mathbf{S} = \mathbf{S}, \quad (2.9a)$$

$$\mathbf{S}^+\mathbf{S}\mathbf{S}^+ = \mathbf{S}^+, \quad (2.9b)$$

$$(\mathbf{S}\mathbf{S}^+)^\top = \mathbf{S}\mathbf{S}^+, \quad (2.9c)$$

$$(\mathbf{S}^+\mathbf{S})^\top = \mathbf{S}^+\mathbf{S}. \quad (2.9d)$$

If the matrix \mathbf{S} has linearly independent columns, its pseudoinverse is $\mathbf{S}^+ = (\mathbf{S}^\top \mathbf{S})^{-1} \mathbf{S}^\top$. Similarly, if \mathbf{S} has linearly independent rows, its pseudoinverse is $\mathbf{S}^+ = \mathbf{S}^\top (\mathbf{S} \mathbf{S}^\top)^{-1}$. Consequently, if \mathbf{S} is invertible (independent rows and columns) the pseudoinverse coincides with the inverse $\mathbf{S}^+ = \mathbf{S}^{-1}$.

Some identities involving the pseudo-inverse. Define $\mathbf{Y}(\mathbf{x}) \in \mathbb{R}^{n \times \nu}$ as $\mathbf{Y} = \mathbf{A}^+ = (\mathbf{A}^\top \mathbf{A})^{-1} \mathbf{A}^\top$, i.e. the pseudoinverse of the kinematics matrix \mathbf{A} . Note that this implies $\mathbf{Y}\mathbf{A} = \mathbf{I}_n$, but $\mathbf{A}\mathbf{Y} \neq \mathbf{I}_\nu$. We also introduce the matrices $\boldsymbol{\Phi} = \frac{\partial \phi}{\partial \mathbf{x}}$ and $\boldsymbol{\Psi} = \boldsymbol{\Phi}^+$. With $\boldsymbol{\Phi}\mathbf{A} = \mathbf{0}$ and the Penrose conditions (2.9), we can show¹ that $\boldsymbol{\Psi}^\top \mathbf{A} = \mathbf{0}$ and $\mathbf{Y}^\top \boldsymbol{\Phi} = \mathbf{0}$. Furthermore, since $\text{rank } \boldsymbol{\Psi} = \text{rank } \boldsymbol{\Phi} = \nu - n$ the columns of $\boldsymbol{\Psi}(\mathbf{x})$ span the complementary space $(T_{\mathbf{x}} \mathbb{X})^\perp$ though they might not be a basis since the columns might not be linearly independent.

The matrix $\mathbf{P} = \mathbf{A}\mathbf{Y}$ is an *orthogonal projector*, i.e. $\mathbf{P}^2 = \mathbf{P}$ and $\mathbf{P}^\top = \mathbf{P}$ which result directly from the Penrose conditions (2.9). Since $\boldsymbol{\Psi}$ spans the complementary

¹ $\boldsymbol{\Psi}^\top \mathbf{A} = (\boldsymbol{\Psi}\boldsymbol{\Phi}\boldsymbol{\Psi})^\top \mathbf{A} = \boldsymbol{\Psi}^\top (\boldsymbol{\Psi}\boldsymbol{\Phi})^\top \mathbf{A} = \boldsymbol{\Psi}^\top \boldsymbol{\Psi}\boldsymbol{\Phi}\mathbf{A} = \mathbf{0}$

space $(T_{\bar{\mathbf{x}}}\mathbb{X})^\perp$, the unique orthogonal projector from \mathbb{R}^ν to $(T_{\bar{\mathbf{x}}}\mathbb{X})^\perp$ can be expressed as $\mathbf{P}^\perp = \Psi\Phi$. The identity $\mathbf{P} + \mathbf{P}^\perp = \mathbf{I}_\nu$ implies

$$\mathbf{A}\mathbf{Y} + \Psi\Phi = \mathbf{I}_\nu. \quad (2.10)$$

2.2 Calculus

This section reviews some of the established tools of calculus for the context of redundant coordinates and nonholonomic velocity coordinates as introduced in the previous section.

2.2.1 Directional derivative and Hessian

Consider a function $\mathcal{V} : \mathbb{R}^\nu \rightarrow \mathbb{R}$ and a curve $\mathbf{x} : \mathbb{R} \rightarrow \mathbb{X}$. Since $\mathbb{X} \subset \mathbb{R}^\nu$, their composition $\mathcal{V} \circ \mathbf{x} = f : \mathbb{R} \rightarrow \mathbb{R}$ is a scalar function and has the Taylor expansion

$$\begin{aligned} \underbrace{\mathcal{V}(\mathbf{x}(t))}_{f(t)} &= \underbrace{\mathcal{V}(\mathbf{x}(0))}_{f(0)} + t \underbrace{\frac{\partial \mathcal{V}}{\partial x^\alpha}(\mathbf{x}(0)) \dot{x}^\alpha(0)}_{\dot{f}(0)} \\ &\quad + \underbrace{\frac{1}{2}t^2 \left(\frac{\partial^2 \mathcal{V}}{\partial x^\beta \partial x^\alpha}(\mathbf{x}(0)) \dot{x}^\alpha(0) \dot{x}^\beta(0) + \frac{\partial \mathcal{V}}{\partial x^\alpha}(\mathbf{x}(0)) \ddot{x}^\alpha(0) \right)}_{\ddot{f}(0)} + \mathcal{O}(t^3). \end{aligned} \quad (2.11)$$

Now let the curve be parameterized by $\dot{\mathbf{x}}(t) = \mathbf{A}(\mathbf{x}(t))\xi(t)$ and we use the shorthand notations $\bar{\mathbf{x}} = \mathbf{x}(0)$, $\bar{\xi} = \xi(0)$ and $\bar{\mathbf{A}} = \mathbf{A}(\mathbf{x}(0))$ to write

$$\begin{aligned} \mathcal{V}(\mathbf{x}(t)) &= \mathcal{V}(\bar{\mathbf{x}}) + t \frac{\partial \mathcal{V}}{\partial x^\alpha}(\bar{\mathbf{x}}) \bar{A}_i^\alpha \bar{\xi}^i \\ &\quad + \frac{1}{2}t^2 \left(\frac{\partial^2 \mathcal{V}}{\partial x^\beta \partial x^\alpha}(\bar{\mathbf{x}}) \bar{A}_i^\alpha \bar{A}_j^\beta \bar{\xi}^i \bar{\xi}^j + \frac{\partial \mathcal{V}}{\partial x^\alpha}(\bar{\mathbf{x}}) \left(\frac{\partial A_i^\alpha}{\partial x^\beta}(\bar{\mathbf{x}}) \bar{A}_j^\beta \bar{\xi}^i \bar{\xi}^j + \bar{A}_i^\alpha \dot{\bar{\xi}}^i \right) \right) + \mathcal{O}(t^3) \end{aligned} \quad (2.12)$$

Introducing the notation

$$\partial_i = A_i^\alpha \frac{\partial}{\partial x^\alpha}, \quad i = 1, \dots, n \quad (2.13)$$

for the derivative in the direction of the i -th basis vector, we can state the Taylor expansion as

$$\mathcal{V}(\mathbf{x}(t)) = \mathcal{V}(\bar{\mathbf{x}}) + t \partial_i \mathcal{V}(\bar{\mathbf{x}}) \bar{\xi}^i + \frac{1}{2}t^2 (\partial_i \partial_j \mathcal{V}(\bar{\mathbf{x}}) \bar{\xi}^i \bar{\xi}^j + \partial_i \mathcal{V}(\bar{\mathbf{x}}) \dot{\bar{\xi}}^i) + \mathcal{O}(t^3). \quad (2.14)$$

There are two more things we can derive from this equation:

- If $\partial_i \mathcal{V}(\bar{\mathbf{x}}) = 0, i = 1, \dots, n$ then $\bar{\mathbf{x}}$ is called a *critical point* of \mathcal{V} . At a critical point the expansion (2.14) reduces to

$$\mathcal{V}(\mathbf{x}(t)) = \mathcal{V}(\bar{\mathbf{x}}) + \frac{1}{2}t^2 \underbrace{(\partial_i \partial_j \mathcal{V})(\bar{\mathbf{x}})}_{\bar{H}_{ij}} \bar{\xi}^i \bar{\xi}^j + \mathcal{O}(t^3). \quad (2.15)$$

This relation holds for any sufficiently smooth curve $t \mapsto \mathbf{x}(t)$ through $\bar{\mathbf{x}}$ and consequently for any velocity vector $\bar{\xi}$ at the critical point. So if the matrix \bar{H} is positive (negative) definite, then $\bar{\mathbf{x}}$ is a local minimum (maximum) of \mathcal{V} .

- Assume the curve $t \mapsto \mathbf{x}(t)$ is a *geodesic*, i.e. $\dot{\xi}^i = -\Gamma_{jk}^i \xi^j \xi^k$ with the connection coefficients Γ_{jk}^i that will be discussed later. Plugging this into (2.14) we find a coordinate form of the *Hessian tensor* $\nabla^2 \mathcal{V}$ of the potential:

$$\mathcal{V}(\mathbf{x}(t)) = \mathcal{V}(\bar{\mathbf{x}}) + t(\partial_i \mathcal{V})(\bar{\mathbf{x}}) \bar{\xi}^i + \frac{1}{2} t^2 \underbrace{(\partial_i \partial_j \mathcal{V} - \Gamma_{ij}^k \partial_k \mathcal{V})(\bar{\mathbf{x}})}_{(\nabla^2 \mathcal{V})_{ij}} \bar{\xi}^i \bar{\xi}^j + \mathcal{O}(t^3). \quad (2.16)$$

At a critical point $\bar{\mathbf{x}}$, the Hessian of the potential is independent of the connection coefficients Γ_{jk}^i and consequently of the underlying metric. There it coincides with the matrix $\bar{\mathbf{H}}$ defined in (2.15).

2.2.2 Commutation coefficients

For a function $\mathcal{V} : \mathbb{R}^\nu \rightarrow \mathbb{R}$ we are used to the fact that partial derivatives commute, i.e. $\partial^2 \mathcal{V} / \partial x^\alpha \partial x^\beta = \partial^2 \mathcal{V} / \partial x^\beta \partial x^\alpha$. Unfortunately this is (in general) not the case for a directional derivatives like ∂_i defined in (2.13). Consequently we investigate the following commutation relation

$$\begin{aligned} \partial_i \partial_j \mathcal{V} - \partial_j \partial_i \mathcal{V} &= A_i^\alpha \frac{\partial}{\partial x^\alpha} \left(A_j^\beta \frac{\partial \mathcal{V}}{\partial x^\beta} \right) - A_j^\beta \frac{\partial}{\partial x^\beta} \left(A_i^\alpha \frac{\partial \mathcal{V}}{\partial x^\alpha} \right) \\ &= A_i^\alpha \frac{\partial A_j^\beta}{\partial x^\alpha} \frac{\partial \mathcal{V}}{\partial x^\beta} - A_j^\beta \frac{\partial A_i^\alpha}{\partial x^\beta} \frac{\partial \mathcal{V}}{\partial x^\alpha} + A_i^\alpha A_j^\beta \underbrace{\left(\frac{\partial^2 \mathcal{V}}{\partial x^\alpha \partial x^\beta} - \frac{\partial^2 \mathcal{V}}{\partial x^\beta \partial x^\alpha} \right)}_{=0} \\ &= \left(A_i^\beta \frac{\partial A_j^\alpha}{\partial x^\beta} - A_j^\beta \frac{\partial A_i^\alpha}{\partial x^\beta} \right) \frac{\partial \mathcal{V}}{\partial x^\alpha}. \end{aligned} \quad (2.17)$$

Now using the identity (2.10) with $\Phi_\alpha^\kappa = \frac{\partial \phi^\kappa}{\partial x^\alpha}$ and $\Phi_\alpha^\kappa A_i^\alpha = 0 \Rightarrow \Phi_\alpha^\kappa \frac{\partial A_i^\alpha}{\partial x^\beta} = -\frac{\partial \Phi_\alpha^\kappa}{\partial x^\beta} A_i^\alpha$ to shape this expression a bit further

$$\begin{aligned} \partial_i \partial_j \mathcal{V} - \partial_j \partial_i \mathcal{V} &= \left(A_i^\beta \frac{\partial A_j^\alpha}{\partial x^\beta} - A_j^\beta \frac{\partial A_i^\alpha}{\partial x^\beta} \right) \overbrace{(A_k^\sigma Y_\alpha^k + \Psi_\kappa^\sigma \Phi_\alpha^\kappa)}^{\delta_\alpha^\sigma} \frac{\partial \mathcal{V}}{\partial x^\sigma} \\ &= \left(A_i^\beta \frac{\partial A_j^\alpha}{\partial x^\beta} - A_j^\beta \frac{\partial A_i^\alpha}{\partial x^\beta} \right) Y_\alpha^k A_k^\sigma \frac{\partial \mathcal{V}}{\partial x^\sigma} - \left(A_i^\beta A_j^\alpha \frac{\partial \Phi_\alpha^\kappa}{\partial x^\beta} - A_j^\beta A_i^\alpha \frac{\partial \Phi_\alpha^\kappa}{\partial x^\beta} \right) \Psi_\kappa^\sigma \frac{\partial \mathcal{V}}{\partial x^\sigma} \\ &= \underbrace{\left(A_i^\beta \frac{\partial A_j^\alpha}{\partial x^\beta} - A_j^\beta \frac{\partial A_i^\alpha}{\partial x^\beta} \right)}_{\gamma_{ij}^k} \underbrace{Y_\alpha^k A_k^\sigma \frac{\partial \mathcal{V}}{\partial x^\sigma}}_{\partial_k \mathcal{V}} - A_j^\beta A_i^\alpha \underbrace{\left(\frac{\partial^2 \phi^\kappa}{\partial x^\alpha \partial x^\beta} - \frac{\partial^2 \phi^\kappa}{\partial x^\beta \partial x^\alpha} \right)}_{=0} \Psi_\kappa^\sigma \frac{\partial \mathcal{V}}{\partial x^\sigma}. \end{aligned} \quad (2.18)$$

Since this relation holds for any function \mathcal{V} we can state it in operator form and introduce the *commutation coefficients* γ_{ij}^k as

$$\partial_i \partial_j - \partial_j \partial_i = \gamma_{ij}^k \partial_k, \quad \gamma_{ij}^k = (\partial_i A_j^\alpha - \partial_j A_i^\alpha)(A^+)_\alpha^k. \quad (2.19)$$

Note the skew symmetry $\gamma_{ij}^k = -\gamma_{ji}^k$.

Example 3. The commutation coefficients γ_{ij}^k associated with the kinematics matrix \mathbf{A} from (2.7) are

$$\begin{aligned}\gamma_{23}^1 &= \gamma_{31}^2 = \gamma_{12}^3 = +1, \\ \gamma_{32}^1 &= \gamma_{13}^2 = \gamma_{21}^3 = -1, \\ \gamma_{11}^1 &= \gamma_{12}^1 = \gamma_{13}^1 = \gamma_{21}^1 = \gamma_{22}^1 = \gamma_{31}^1 = \gamma_{33}^1 = 0, \\ \gamma_{11}^2 &= \gamma_{12}^2 = \gamma_{21}^2 = \gamma_{22}^2 = \gamma_{23}^2 = \gamma_{32}^2 = \gamma_{33}^2 = 0, \\ \gamma_{11}^3 &= \gamma_{13}^3 = \gamma_{22}^3 = \gamma_{23}^3 = \gamma_{31}^3 = \gamma_{32}^3 = \gamma_{33}^3 = 0.\end{aligned}$$

This coincides with the three dimensional Levi-Civita symbol commonly defined as

$$\gamma_{ij}^k = \begin{cases} +1, & (i, j, k) \text{ even permutation of } (1, 2, 3) \\ -1, & (i, j, k) \text{ odd permutation of } (1, 2, 3) \\ 0, & \text{else} \end{cases}. \quad (2.20)$$

It is related to the 3 dimensional *cross product* by $\mathbf{a}, \mathbf{b} \in \mathbb{R}^3 : [\gamma_{ij}^k a^i b^j]_{k=1..3} = \mathbf{a} \times \mathbf{b}$ and to the previously defined wed operator by $\mathbf{a} \in \mathbb{R}^3 : [\gamma_{ij}^k a^i]_{j,k=1..3} = \text{wed}(\mathbf{a})$.

The right hand side of (2.19) appears in the context of Lagrange's equation in [Boltzmann, 1902, p. 687] and [Hamel, 1904a, p. 10] for the case of minimal configuration coordinates and consequently with a square matrix \mathbf{A} . In the contemporary literature on this context, the quantities γ_{ij}^k are sometimes called the *Boltzmann three-index symbols* [Lurie, 2002, sec. 1.8] or *Hamel coefficients* [Bremer, 2008, p. 75]. The left hand side of (2.19) appears in the context of tensor algebra in [Misner et al., 1973, Box 8.4] where γ_{ij}^k are called the *commutation coefficients*. From the way γ_{ij}^k is defined here, this naming seems most fitting and will be used throughout this work.

The case of redundant configuration coordinates and consequently a non-square matrix \mathbf{A} as derived above, is not established in the literature to the best of the authors knowledge.

It is worth noting that the commutation coefficients are *invariant* to the choice of configuration coordinates \mathbf{x} , even though the coordinates appear explicitly in the definition: For a change of configuration coordinates $\mathbf{x} = f(\hat{\mathbf{x}})$ the commutation symbols transform like $\hat{\gamma}_{ij}^k(\hat{\mathbf{x}}) = \gamma_{ij}^k(f(\hat{\mathbf{x}}))$. This might be obvious from a geometric point of view, but the explicit calculation of the coordinate transformation is shown in see [sec:TrafoRules]. It will even turn out that for most of our examples the coefficients will be constants.

The commutation coefficients γ_{jk}^i vanish if the corresponding velocity coordinates ξ^i are *integrable*, i.e.

$$\begin{aligned}\exists \pi^i : \dot{\pi}^i = \xi^i = Y_\alpha^i \dot{x}^\alpha &\Rightarrow Y_\alpha^i = \frac{\partial \pi^i}{\partial x^\beta} \\ &\Rightarrow \frac{\partial Y_\alpha^i}{\partial x^\alpha} = \frac{\partial^2 \pi^i}{\partial x^\beta \partial x^\alpha} = \frac{\partial Y_\beta^i}{\partial x^\alpha}, \quad \Rightarrow \quad \gamma_{jk}^i = 0.\end{aligned} \quad (2.21)$$

This is not the case in general. Nevertheless the quantities π are introduced as *nonholonomic coordinates* in [Boltzmann, 1902] or as *quasi coordinates* in [Lurie, 2002, sec. 1.5].

Then we could write $\partial_i(\partial_j f) - \partial_j(\partial_i f) = \partial^2 f / \partial \pi^i \partial \pi^j - \partial^2 f / \partial \pi^j \partial \pi^i \neq 0$ what might lead to the conception that partial derivatives do not commute. The commutativity clearly holds, the issue is rather π are no proper coordinates. To avoid confusion of this kind we do not pick up this notation here. See also [Hamel, 1904b] for an extensive discussion on this topic.

2.2.3 Linearization about a trajectory

Let $\bar{\mathbf{x}} : [t_1, t_2] \rightarrow \mathbb{X}$ be a smooth curve with the velocity coordinates $\bar{\boldsymbol{\xi}} : [t_1, t_2] \rightarrow \mathbb{R}^n : t \mapsto \mathbf{A}^+(\bar{\mathbf{x}}(t))\dot{\bar{\mathbf{x}}}(t)$. For a small deviation $\mathbf{x} \approx \bar{\mathbf{x}}$ with $\mathbf{x} \in \mathbb{X}$ we may approximate the geometric constraint as

$$\phi(\mathbf{x}) \approx \underbrace{\phi(\bar{\mathbf{x}})}_{=0} + \frac{\partial \phi}{\partial \mathbf{x}}(\bar{\mathbf{x}})(\mathbf{x} - \bar{\mathbf{x}}) = 0. \quad (2.22)$$

Since this constraint is affine w.r.t. \mathbf{x} it is reasonable to use a the basis $\boldsymbol{\varepsilon}(t) \in \mathbb{R}^n$ for the deviated configuration coordinates:

$$\mathbf{x} = \bar{\mathbf{x}} + \mathbf{A}(\bar{\mathbf{x}})\boldsymbol{\varepsilon}, \quad \boldsymbol{\varepsilon} = \mathbf{A}^+(\bar{\mathbf{x}})(\mathbf{x} - \bar{\mathbf{x}}), \quad (2.23)$$

For the velocity coordinates $\boldsymbol{\xi}$ of the deviated curve \mathbf{x} we use again the first order approximation and $\mathbf{Y} = \mathbf{A}^+$:

$$\begin{aligned} \xi^i &= Y_\alpha^i(\mathbf{x})\dot{x}^\alpha \\ &\approx Y_\alpha^i(\bar{\mathbf{x}} + \mathbf{A}(\bar{\mathbf{x}})\boldsymbol{\varepsilon}) \frac{d}{dt} (\bar{x}^\alpha + A_j^\alpha(\bar{\mathbf{x}})\varepsilon^j) \\ &\approx Y_\alpha^i(\bar{\mathbf{x}}) (\dot{x}_R^\alpha + \frac{\partial A_j^\alpha}{\partial x^\beta}(\bar{\mathbf{x}}) \dot{x}_R^\beta \varepsilon^j + A_j^\alpha(\bar{\mathbf{x}}) \dot{\varepsilon}^j) + \frac{\partial Y_\alpha^i}{\partial x^\beta}(\bar{\mathbf{x}}) A_j^\beta(\bar{\mathbf{x}}) \varepsilon^j \dot{x}_R^\alpha \\ &= \bar{\xi}^i + \dot{\varepsilon}^i + \gamma_{kj}^i(\bar{\mathbf{x}}) \bar{\xi}^k \varepsilon^j \end{aligned} \quad (2.24)$$

Using these results we may formulate an approximation of a general smooth function f along the trajectory $t \mapsto \bar{\mathbf{x}}(t)$ as

$$\begin{aligned} f(\mathbf{x}, \boldsymbol{\xi}, \dot{\boldsymbol{\xi}}) &\approx f(\bar{\mathbf{x}}, \bar{\boldsymbol{\xi}}, \dot{\bar{\boldsymbol{\xi}}}) + \frac{\partial f}{\partial x^\alpha}(\bar{\mathbf{x}}, \bar{\boldsymbol{\xi}}, \dot{\bar{\boldsymbol{\xi}}})(x^\alpha - \bar{x}^\alpha) + \frac{\partial f}{\partial \xi^i}(\bar{\mathbf{x}}, \bar{\boldsymbol{\xi}}, \dot{\bar{\boldsymbol{\xi}}})(\xi^i - \bar{\xi}^i) \\ &\quad + \frac{\partial f}{\partial \dot{\xi}^i}(\bar{\mathbf{x}}, \bar{\boldsymbol{\xi}}, \dot{\bar{\boldsymbol{\xi}}})(\dot{\xi}^i - \dot{\bar{\xi}}^i) \\ &\approx f(\bar{\mathbf{x}}, \bar{\boldsymbol{\xi}}, \dot{\bar{\boldsymbol{\xi}}}) + (\partial_i f)(\bar{\mathbf{x}}, \bar{\boldsymbol{\xi}}, \dot{\bar{\boldsymbol{\xi}}})\varepsilon^i + \frac{\partial f}{\partial \xi^i}(\bar{\mathbf{x}}, \bar{\boldsymbol{\xi}}, \dot{\bar{\boldsymbol{\xi}}})(\dot{\varepsilon}^i + \gamma_{kj}^i(\bar{\mathbf{x}}) \bar{\xi}^k \varepsilon^j) \\ &\quad + \frac{\partial f}{\partial \dot{\xi}^i}(\bar{\mathbf{x}}, \bar{\boldsymbol{\xi}}, \dot{\bar{\boldsymbol{\xi}}})(\ddot{\varepsilon}^i + \gamma_{kj}^i(\bar{\mathbf{x}}) \bar{\xi}^k \dot{\varepsilon}^j + \gamma_{kj}^i(\bar{\mathbf{x}}) \dot{\bar{\xi}}^k \varepsilon^j + \partial_l \gamma_{kj}^i(\bar{\mathbf{x}}) \bar{\xi}^l \bar{\xi}^k \varepsilon^j) \\ &= \bar{f} + \bar{F}_i^0 \varepsilon^i + \bar{F}_i^1 \dot{\varepsilon}^i + \bar{F}_i^2 \ddot{\varepsilon}^i \end{aligned} \quad (2.25)$$

where

$$\begin{aligned}\bar{f} &= f(\bar{\boldsymbol{x}}, \bar{\boldsymbol{\xi}}, \dot{\bar{\boldsymbol{\xi}}}), \\ \bar{F}_i^0 &= (\partial_i f)(\bar{\boldsymbol{x}}, \bar{\boldsymbol{\xi}}, \dot{\bar{\boldsymbol{\xi}}}) + \frac{\partial f}{\partial \xi^j}(\bar{\boldsymbol{x}}, \bar{\boldsymbol{\xi}}, \dot{\bar{\boldsymbol{\xi}}}) \gamma_{ki}^j(\bar{\boldsymbol{x}}) \bar{\xi}^k + \frac{\partial f}{\partial \dot{\xi}^j}(\bar{\boldsymbol{x}}, \bar{\boldsymbol{\xi}}, \dot{\bar{\boldsymbol{\xi}}}) (\gamma_{ki}^j(\bar{\boldsymbol{x}}) \dot{\bar{\xi}}^k + \partial_l \gamma_{ki}^j(\bar{\boldsymbol{x}}) \bar{\xi}^l \bar{\xi}^k), \\ \bar{F}_i^1 &= \frac{\partial f}{\partial \xi^i}(\bar{\boldsymbol{x}}, \bar{\boldsymbol{\xi}}, \dot{\bar{\boldsymbol{\xi}}}) + \frac{\partial f}{\partial \dot{\xi}^j}(\bar{\boldsymbol{x}}, \bar{\boldsymbol{\xi}}, \dot{\bar{\boldsymbol{\xi}}}) \gamma_{ki}^j(\bar{\boldsymbol{x}}) \bar{\xi}^k, \\ \bar{F}_i^2 &= \frac{\partial f}{\partial \dot{\xi}^i}(\bar{\boldsymbol{x}}, \bar{\boldsymbol{\xi}}, \dot{\bar{\boldsymbol{\xi}}}).\end{aligned}$$

Evidently, the expressions simplify significantly if the velocity coordinates are holonomic, i.e. $\gamma = 0$, or if the approximation is about a static point $\bar{\boldsymbol{x}} = \text{const.} \Rightarrow \boldsymbol{\xi} = \mathbf{0}$.

2.2.4 Calculus of variations

The calculus of variations is concerned with the extrema of functionals, i.e. functions of functions. For the particular context of classical mechanics we are interested in the curves $t \mapsto \boldsymbol{x}(t)$ for which the functional

$$\mathcal{J}[\boldsymbol{x}] = \int_{t_1}^{t_2} \mathcal{L}(\boldsymbol{x}(t), \boldsymbol{\xi}(t), t) dt \quad (2.26)$$

for given boundary conditions $\boldsymbol{x}(t_1)$ and $\boldsymbol{x}(t_2)$ is *stationary*. The *Lagrangian* \mathcal{L} is here a function of the configuration coordinates \boldsymbol{x} , its derivatives $\dot{\boldsymbol{x}} = \mathbf{A}\boldsymbol{\xi}$ parameterized in the velocity coordinates $\boldsymbol{\xi}$ and may depend explicitly on the time t as well.

For the standard case, $\boldsymbol{x} = \boldsymbol{q}$ and $\boldsymbol{\xi} = \dot{\boldsymbol{q}}$, a derivation may be found in e.g. [Courant and Hilbert, 1924, chap. 4, §3], [Lanczos, 1986, ch. II] or [Arnold, 1989, sec. 12]. For the present case we modify the well known derivation slightly: Suppose that $\boldsymbol{x} : [t_1, t_2] \mapsto \mathbb{X}$ is the solution to the variational problem. With the function $\boldsymbol{\chi}(t) \in \mathbb{R}^\nu$ and the parameter $\varepsilon \in \mathbb{R}$ we define a perturbation to it by

$$\bar{\boldsymbol{x}} = \boldsymbol{x} + \varepsilon \boldsymbol{\chi}. \quad (2.27)$$

We need $\bar{\boldsymbol{x}}(t) \in \mathbb{X}$ and consequently $\phi(\bar{\boldsymbol{x}}) = \mathbf{0}$. Assuming ε to be sufficiently small, we may use the first order approximation analog to subsection 2.2.3: With the *variation coordinates* $\boldsymbol{h} : [t_1, t_2] \rightarrow \mathbb{R}^n$ we parameterize $\boldsymbol{\chi} = \mathbf{A}(\boldsymbol{x})\boldsymbol{h}$. Using the inverse kinematic relation $\boldsymbol{\xi} = \mathbf{Y}(\boldsymbol{x})\dot{\boldsymbol{x}}$ we can write the functional for the varied path as

$$\mathcal{J}[\bar{\boldsymbol{x}}] = \int_{t_1}^{t_2} \mathcal{L}(\boldsymbol{x} + \varepsilon \mathbf{A}(\boldsymbol{x})\boldsymbol{h}, \mathbf{Y}(\boldsymbol{x} + \varepsilon \mathbf{A}(\boldsymbol{x})\boldsymbol{h}) \frac{d}{dt}(\boldsymbol{x} + \varepsilon \mathbf{A}(\boldsymbol{x})\boldsymbol{h}), t) dt =: \mathcal{P}(\varepsilon) \quad (2.28)$$

Now if $\boldsymbol{x}(t)$ is indeed the solution to the variational problem, then $\mathcal{P}(\varepsilon)$ must have a minimum at $\mathcal{P}(0)$ and consequently $\partial \mathcal{P} / \partial \varepsilon(0) = 0$. Evaluation of this “ordinary” differentiation yields

$$\begin{aligned}0 &= \frac{\partial \mathcal{P}}{\partial \varepsilon} \Big|_{\varepsilon=0} = \int_{t_1}^{t_2} \left(\frac{\partial \mathcal{L}}{\partial x^\alpha} A_i^\alpha h^i + \frac{\partial \mathcal{L}}{\partial \xi^i} \left(\frac{\partial Y_\alpha^i}{\partial x^\beta} A_j^\beta h^j \dot{x}^\alpha + Y_\alpha^i \frac{\partial A_j^\alpha}{\partial x^\beta} h^j \dot{x}^\beta + \dot{h}^i \right) \right) dt \\ &= \int_{t_1}^{t_2} \left(\partial_i \mathcal{L} h^i + \frac{\partial \mathcal{L}}{\partial \xi^i} (\gamma_{kj}^i h^j \xi^k + \dot{h}^i) \right) dt\end{aligned} \quad (2.29)$$

where we have found again the commutation coefficients γ_{kj}^i previously derived in (2.19). Integrating by parts with the boundary conditions $\mathbf{h}(t_1) = \mathbf{h}(t_2) = \mathbf{0}$ gives

$$\int_{t_1}^{t_2} h^i \left(A_i^\alpha \frac{\partial \mathcal{L}}{\partial x^\alpha} - \frac{d}{dt} \frac{\partial \mathcal{L}}{\partial \xi^i} - \gamma_{ij}^k \xi^j \frac{\partial \mathcal{L}}{\partial \xi^k} \right) dt = 0. \quad (2.30)$$

Since the variation coordinates $h^i, i = 1, \dots, n$ are independent by definition, the *fundamental lemma of the calculus of variations* (see e.g. [Courant and Hilbert, 1924, p. 166] or [Arnold, 1989, p. 57]) states that, for the integral to vanish, the terms in the brackets have to vanish. Together with the kinematic equation, we have the following necessary conditions for the functional (2.26) to be stationary:

$$\dot{x}^\alpha = A_i^\alpha \xi^i, \quad \alpha = 1 \dots \nu, \quad (2.31a)$$

$$\frac{d}{dt} \frac{\partial \mathcal{L}}{\partial \xi^i} + \gamma_{ij}^k \xi^j \frac{\partial \mathcal{L}}{\partial \xi^k} - \partial_i \mathcal{L} = 0, \quad i = 1, \dots, n. \quad (2.31b)$$

For the special case $\mathbf{x}(t) = \mathbf{q}(t) \in \mathbb{R}^n$ and $\boldsymbol{\xi}(t) = \dot{\mathbf{q}}(t)$ we have $\mathbf{A} = \mathbf{I}_n$ and $\gamma = 0$. Then (2.31) coincides with the *Euler-Lagrange equation* (1.2).

Example 4. Consider again the configuration coordinates $\mathbf{x} = [\mathbf{R}_x^\top, \mathbf{R}_y^\top, \mathbf{R}_z^\top]^\top$ and the velocity coordinates $\boldsymbol{\xi} = \boldsymbol{\omega}$ related by $\dot{\mathbf{R}} = \mathbf{R}_{\text{wed}}(\boldsymbol{\omega})$ as discussed in the previous example (2.7). The commutation coefficients were derived in (2.20).

For the Lagrangian

$$\mathcal{L} = \frac{1}{2} \boldsymbol{\omega}^\top \boldsymbol{\Theta} \boldsymbol{\omega} \quad (2.32)$$

we obtain

$$\left[\frac{d}{dt} \frac{\partial \mathcal{L}}{\partial \xi^i} + \gamma_{ij}^k \xi^j \frac{\partial \mathcal{L}}{\partial \xi^k} - A_i^\alpha \frac{\partial \mathcal{L}}{\partial x^\alpha} \right]_{i=1,2,3} = \boldsymbol{\Theta} \dot{\boldsymbol{\omega}} + \boldsymbol{\omega} \times \boldsymbol{\Theta} \boldsymbol{\omega}. \quad (2.33)$$

2.2.5 Hamilton's equations

Legendre transformation. Define the *generalized momentum* \mathbf{p} as

$$p_i = \frac{\partial \mathcal{L}}{\partial \dot{x}^i}, \quad i = 1, \dots, n. \quad (2.34)$$

and assume that these relations can be inverted to express the velocity $\boldsymbol{\xi} = \boldsymbol{\zeta}(\mathbf{x}, \mathbf{p}, t)$ in terms of the momentum. Then define the *Hamiltonian* \mathcal{H} as

$$\mathcal{H}(\mathbf{x}, \mathbf{p}, t) = \left[p_i \xi^i - \mathcal{L}(\mathbf{x}, \boldsymbol{\xi}, t) \right]_{\boldsymbol{\xi}=\boldsymbol{\zeta}(\mathbf{x}, \mathbf{p}, t)} = p_i \zeta^i(\mathbf{x}, \mathbf{p}, t) - \mathcal{L}(\mathbf{x}, \boldsymbol{\zeta}(\mathbf{x}, \mathbf{p}, t), t). \quad (2.35)$$

The definitions (2.34) and (2.35) describe the *Legendre transformation* $(\mathcal{L}, \boldsymbol{\xi}) \rightarrow (\mathcal{H}, \mathbf{p})$, see [Lanczos, 1986, ch. VI.1] or [Arnold, 1989, sec. 14] for some geometric background. Note that the configuration coordinates \mathbf{x} and the time t do not participate in the transformation.

Hamilton's canonical equations. Evaluation of the differentials of (2.35), we get the relations

$$\partial_j \mathcal{H} = p_i \partial_j \zeta^i - \partial_j \mathcal{L} - \frac{\partial \mathcal{L}}{\partial \xi^i} \partial_j \zeta^i = -\partial_j \mathcal{L} \quad (2.36a)$$

$$\frac{\partial \mathcal{H}}{\partial p_j} = \zeta^j + p_i \frac{\partial \zeta^i}{\partial p_j} - \frac{\partial \mathcal{L}}{\partial \xi^i} \frac{\partial \zeta^i}{\partial p_j} = \xi^j \quad (2.36b)$$

$$\frac{\partial \mathcal{H}}{\partial t} = p_i \frac{\partial \zeta^i}{\partial t} - \frac{\partial \mathcal{L}}{\partial \xi^i} \frac{\partial \zeta^i}{\partial t} - \frac{\partial \mathcal{L}}{\partial t} = -\frac{\partial \mathcal{L}}{\partial t}, \quad (2.36c)$$

With this we can express the Euler-Lagrange equation (2.31) in terms of the generalized momentum \mathbf{p} and the Hamiltonian \mathcal{H} as

$$\dot{x}^\alpha = A_i^\alpha \frac{\partial \mathcal{H}}{\partial p_i}, \quad \alpha = 1, \dots, \nu, \quad (2.37a)$$

$$\dot{p}_i + \gamma_{ij}^k \frac{\partial \mathcal{H}}{\partial p_j} p_k + \partial_i \mathcal{H} = 0, \quad i = 1, \dots, n. \quad (2.37b)$$

For the special case of minimal configuration coordinates \mathbf{q} and velocity coordinates $\boldsymbol{\xi} = \dot{\mathbf{q}}$ we have $\mathbf{A} = \mathbf{I}_n$ and (2.37) is called *Hamilton's canonical equations*.

Conservation law. The time derivative of the Hamiltonian along the the solutions of (2.37) is

$$\frac{d\mathcal{H}}{dt} = \frac{\partial \mathcal{H}}{\partial x^\alpha} \dot{x}^\alpha + \frac{\partial \mathcal{H}}{\partial p_i} \dot{p}_i + \frac{\partial \mathcal{H}}{\partial t} = \underbrace{\frac{\partial \mathcal{H}}{\partial x^\alpha} A_i^\alpha \frac{\partial \mathcal{H}}{\partial p_i}}_0 - \underbrace{\frac{\partial \mathcal{H}}{\partial p_i} A_i^\alpha \frac{\partial \mathcal{H}}{\partial x^\alpha}}_0 - p_k \underbrace{\gamma_{ij}^k \frac{\partial \mathcal{H}}{\partial p_i} \frac{\partial \mathcal{H}}{\partial p_j}}_0 + \frac{\partial \mathcal{H}}{\partial t} \quad (2.38)$$

and consequently

$$\frac{d\mathcal{H}}{dt} = \frac{\partial \mathcal{H}}{\partial t} = -\frac{\partial \mathcal{L}}{\partial t}. \quad (2.39)$$

This is the well known conservation law for the Hamiltonian, see e.g. [Lanczos, 1986, ch. VI.6]. The remarkable aspect of the conservation law (and for the Legendre transformation) is that there is no particular assumption on the structure of the Lagrangian \mathcal{L} .

Example 5. Consider a Lagrangian as

$$\mathcal{L}(\mathbf{x}, \boldsymbol{\xi}, t) = \frac{1}{2} M_{ij}(\mathbf{x}, t) \xi^j \xi^i + b_i(\mathbf{x}, t) \xi^i + c(\mathbf{x}, t). \quad (2.40)$$

The corresponding generalized momentum and Hamiltonian are

$$p_i = \frac{\partial \mathcal{L}}{\partial \xi^i} = M_{ij} \xi^j + b_i \quad \Leftrightarrow \quad \xi^i = M^{ij} (p_j - b_j) \quad (2.41)$$

$$\mathcal{H} = \frac{1}{2} M^{ij} (p_i - b_i) (p_j - b_j) - c. \quad (2.42)$$

Evaluation of (2.37) yields

$$\dot{x}^\alpha = A_i^\alpha M^{ij}(p_j - b_j), \quad (2.43a)$$

$$\dot{p}_i + (\gamma_{il}^k M^{lj} p_k + \frac{1}{2} \partial_i M^{kj} (p_k - b_k) - M^{kj} \partial_i b_k)(p_j - b_j) + \partial_i c = 0, \quad (2.43b)$$

The Euler-Lagrange equation evaluates to

$$\dot{x}^\alpha = A_i^\alpha \xi^i, \quad (2.44a)$$

$$M_{ij} \dot{\xi}^j + (\partial_k M_{ij} + \gamma_{ij}^l M_{lk} - \frac{1}{2} \partial_i M_{kj}) \xi^j \xi^k + \left(\frac{\partial M_{ij}}{\partial t} + \gamma_{ij}^k b_k \right) \xi^j + \frac{\partial b_i}{\partial t} - \partial_i c \quad (2.44b)$$

Note that the Hamiltonian in terms of Lagrangian coordinates reads

$$\mathcal{H} = \frac{1}{2} M_{ij} \xi^i \xi^j - c. \quad (2.45)$$

2.3 Linear algebra

2.3.1 Matrix sets

The following sets of real matrices that are frequently used in the work:

$$(\text{symmetric}) \quad \mathbb{S}\mathbb{Y}\mathbb{M}(n) = \{ \mathbf{A} \in \mathbb{R}^{n \times n} \mid \mathbf{A} = \mathbf{A}^\top \}, \quad (2.46a)$$

$$(\text{symmetric, pos. def.}) \quad \mathbb{S}\mathbb{Y}\mathbb{M}^+(n) = \{ \mathbf{A} \in \mathbb{S}\mathbb{Y}\mathbb{M}(n) \mid \mathbf{x}^\top \mathbf{A} \mathbf{x} > 0 \forall \mathbf{x} \in \mathbb{R}^n \setminus \{\mathbf{0}\} \}, \quad (2.46b)$$

$$(\text{sym., pos. semi-def.}) \quad \mathbb{S}\mathbb{Y}\mathbb{M}_0^+(n) = \{ \mathbf{A} \in \mathbb{S}\mathbb{Y}\mathbb{M}(n) \mid \mathbf{x}^\top \mathbf{A} \mathbf{x} \geq 0 \forall \mathbf{x} \in \mathbb{R}^n \setminus \{\mathbf{0}\} \}, \quad (2.46c)$$

$$(\text{unit sphere}) \quad \mathbb{S}^n = \{ \mathbf{a} \in \mathbb{R}^n \mid \mathbf{a}^\top \mathbf{a} = 1 \}, \quad (2.46d)$$

$$(\text{orthogonal}) \quad \mathbb{O}(n) = \{ \mathbf{A} \in \mathbb{R}^{n \times n} \mid \mathbf{A}^\top \mathbf{A} = \mathbf{I}_n \}, \quad (2.46e)$$

$$(\text{special orthogonal}) \quad \mathbb{SO}(n) = \{ \mathbf{R} \in \mathbb{O}(n) \mid \det \mathbf{R} = +1 \}, \quad (2.46f)$$

2.3.2 Inner product, norm and metric

Inner product. For matrices $\mathbf{A}, \mathbf{B} \in \mathbb{R}^{n \times m}$ and a symmetric, positive definite matrix $\mathbf{K} \in \mathbb{S}\mathbb{Y}\mathbb{M}^+(n)$, define an *inner product* as

$$\langle \mathbf{A}, \mathbf{B} \rangle_{\mathbf{K}} = \text{tr}(\mathbf{A}^\top \mathbf{K} \mathbf{B}). \quad (2.47)$$

Setting $\mathbf{K} = \mathbf{I}_n$ in the definition (2.47) is called the *Frobenius inner product* in [Horn and Johnson, 1985, sec. 5.2] or *Hilbert-Schmidt inner product* in [Hall, 2015, sec. A.6]. Furthermore, for $\mathbf{A}, \mathbf{B} \in \mathbb{R}^{n \times 1}$ it coincides with the common *dot product*.

Norm. The inner product (2.47) induces the norm

$$\|\mathbf{A}\|_{\mathbf{K}} = \sqrt{\langle \mathbf{A}, \mathbf{A} \rangle_{\mathbf{K}}}. \quad (2.48)$$

Again for $\mathbf{K} = \mathbf{I}_n$ this coincides with the established *Frobenius norm*, e.g. [Golub and Loan, 1996, p 55]. Furthermore, for $\mathbf{A}, \mathbf{B} \in \mathbb{R}^{n \times 1}$ it coincides with the common *Euclidean norm* or 2-norm.

Metric. The norm (2.48) induces the metric

$$d_{\mathbf{K}}(\mathbf{A}, \mathbf{B}) = \|\mathbf{A} - \mathbf{B}\|_{\mathbf{K}}. \quad (2.49)$$

Again for $\mathbf{K} = \mathbf{I}_n$ this coincides with the established *Euclidean metric*.

The introduced inner product, norm and metric may be regarded as weighted versions of their established forms. For $\mathbf{K} = \mathbf{I}_n$, this work uses the shorthand notation

$$\langle \cdot, \cdot \rangle \equiv \langle \cdot, \cdot \rangle_{\mathbf{I}_n}, \quad \|\cdot\| \equiv \|\cdot\|_{\mathbf{I}_n}, \quad d(\cdot, \cdot) \equiv d_{\mathbf{I}_n}(\cdot, \cdot). \quad (2.50)$$

2.3.3 Vee and wedge

Established definitions. Define the wedge operator as

$$\text{wed} : \mathbb{R}^3 \rightarrow \mathbb{R}^{3 \times 3} : \begin{bmatrix} \omega_1 \\ \omega_2 \\ \omega_3 \end{bmatrix} \mapsto \begin{bmatrix} 0 & -\omega_3 & \omega_2 \\ \omega_3 & 0 & -\omega_1 \\ -\omega_2 & \omega_1 & 0 \end{bmatrix} \quad (2.51a)$$

Its inverse is denoted vee(\cdot), i.e. $\text{vee}(\text{wed}(\boldsymbol{\omega})) = \boldsymbol{\omega}$. The wed and vee operators are well established in the literature, see e.g. [Murray et al., 1994, sec. 2.3.2], and have already been used in previous sections.

New definitions. The following operators are not established in the literature, but will prove quite useful for this work. Define the vee2 operator through: $\mathbf{M} \in \mathbb{R}^{3 \times 3}$:

$$\text{tr}(\mathbf{M}(\text{wed } \boldsymbol{\omega})^\top) = \boldsymbol{\omega}^\top \text{vee2}(\mathbf{M}), \quad (2.52)$$

this is

$$\text{vee2} : \mathbb{R}^{3 \times 3} \rightarrow \mathbb{R}^3 : \mathbf{M} \mapsto \text{vee}(\mathbf{M} - \mathbf{M}^\top) \quad (2.53)$$

Note that we have $\text{vee2}(\text{wed } \boldsymbol{\omega}) = 2 \text{vee}(\text{wed } \boldsymbol{\omega}) = 2\boldsymbol{\omega}$, thus giving the motivation for the name.

Define the Vee operator through

$$\text{tr}(\text{wed } \boldsymbol{\omega} \mathbf{M}(\text{wed } \boldsymbol{\eta})^\top) = \boldsymbol{\eta}^\top (\text{Vee } \mathbf{M}) \boldsymbol{\omega}, \quad (2.54)$$

this is

$$\text{Vee} : \mathbb{R}^{3 \times 3} \rightarrow \mathbb{R}^{3 \times 3} : \mathbf{M} \mapsto \text{tr}(\mathbf{M}) \mathbf{I}_3 - \mathbf{M} \quad (2.55)$$

Noting that $\text{tr}(\text{Vee}(\mathbf{M})) = 2 \text{tr}(\mathbf{M})$, we may write the inverse $\text{Wed}(\text{Vee}(\mathbf{M})) = \mathbf{M}$ as

$$\text{Wed} : \mathbb{R}^{3 \times 3} \rightarrow \mathbb{R}^{3 \times 3} : \mathbf{M} \mapsto \frac{1}{2} \text{tr}(\mathbf{M}) \mathbf{I}_3 - \mathbf{M}. \quad (2.56)$$

Identities. For $\mathbf{a}, \mathbf{b}, \mathbf{c} \in \mathbb{R}^3$ and $\mathbf{M} \in \mathbb{R}^{3 \times 3}$, the following identities may be checked by direct computation:

$$\text{wed}(\mathbf{a})^\top = -\text{wed}(\mathbf{a}), \quad (2.57a)$$

$$\text{wed}(\mathbf{a})\mathbf{b} = \text{vee2}(\mathbf{b}\mathbf{a}^\top), \quad (2.57b)$$

$$\text{wed}(\mathbf{a})\text{wed}(\mathbf{b}) = \mathbf{b}\mathbf{a}^\top - (\mathbf{b}^\top \mathbf{a})\mathbf{I}_3 = -\text{Vee}(\mathbf{b}\mathbf{a}^\top), \quad (2.57c)$$

$$\text{wed}(\mathbf{a})\text{wed}(\mathbf{b})\mathbf{c} + \text{wed}(\mathbf{b})\text{wed}(\mathbf{c})\mathbf{a} + \text{wed}(\mathbf{c})\text{wed}(\mathbf{a})\mathbf{b} = \mathbf{0}, \quad (2.57d)$$

$$\text{vee2}(\text{wed}(\mathbf{b})\mathbf{M}) = \text{Vee}(\mathbf{M})\mathbf{b}. \quad (2.57e)$$

2.3.4 Singular value decomposition

Definition [Golub and Loan, 1996, Theo. 2.5.2]: For any matrix $\mathbf{M} \in \mathbb{R}^{n \times m}$ there exist orthonormal matrices $\mathbf{X} \in \mathbb{O}(n)$, $\mathbf{Y} \in \mathbb{O}(m)$ and a matrix $\boldsymbol{\Sigma} \in \mathbb{R}^{n \times m}$ with $i \neq j : \Sigma_{ij} = 0$, $\Sigma_{ii} = \sigma_i$ with $\sigma_1 \geq \dots \geq \sigma_p \geq 0$, $p = \max(n, m)$ such that $\mathbf{M} = \mathbf{X}\boldsymbol{\Sigma}\mathbf{Y}^\top$.

- The columns of \mathbf{X} are eigenvectors of $\mathbf{M}\mathbf{M}^\top = \mathbf{X}(\boldsymbol{\Sigma}\boldsymbol{\Sigma}^\top)\mathbf{X}^\top$
- The columns of \mathbf{Y} are eigenvectors of $\mathbf{M}^\top\mathbf{M} = \mathbf{Y}(\boldsymbol{\Sigma}^\top\boldsymbol{\Sigma})\mathbf{Y}^\top$
- The square of the non-zero singular values σ_i^2 coincide with the non-zero eigenvalues of $\mathbf{M}\mathbf{M}^\top$ and $\mathbf{M}^\top\mathbf{M}$

Due to the descending order of the singular values, the matrix $\boldsymbol{\Sigma}$ is unique. The matrices \mathbf{X} and \mathbf{Y} are unique up to orthogonal transformations of the subspaces of each singular value and the kernel and co-kernel of \mathbf{M} .

2.4 An important function on the special orthogonal group

Motivation. In the context of satellite navigation, the following problem [Wahba, 1965] arose, now commonly called *Wahba's problem*: given $\mathbf{u}_k, \mathbf{v}_k \in \mathbb{R}^3$, find $\mathbf{R} \in \mathbb{SO}(3)$ that minimizes

$$\begin{aligned} \mathcal{V}_1(\mathbf{R}) &= \sum_k \|\mathbf{u}_k - \mathbf{R}\mathbf{v}_k\|^2 = \sum_k (\|\mathbf{u}_k\|^2 + \|\mathbf{v}_k\|^2 - \langle \mathbf{u}_k, \mathbf{R}\mathbf{v}_k \rangle) \\ &= \underbrace{\sum_k (\|\mathbf{u}_k\|^2 + \|\mathbf{v}_k\|^2)}_{\text{const.}} - \text{tr} \left(\mathbf{R} \underbrace{\sum_k \mathbf{v}_k \mathbf{u}_k^\top}_{\mathbf{P}_1} \right). \end{aligned} \quad (2.58)$$

In [Koditschek, 1989] the following function with parameters $\mathbf{K} \in \mathbb{SYM}^+(3)$ and $\mathbf{R}_R \in \mathbb{SO}(3)$ is called a *navigation function on $\mathbb{SO}(3)$* :

$$\mathcal{V}_2(\mathbf{R}) = \text{tr} \left(\mathbf{K} (\mathbf{I}_3 - \mathbf{R}_R^\top \mathbf{R}) \right) = \underbrace{\text{tr} \mathbf{K}}_{\text{const.}} - \underbrace{\text{tr} (\mathbf{K} \mathbf{R}_R^\top \mathbf{R})}_{\mathbf{P}_2}. \quad (2.59)$$

Using the metric from (2.49) with a weight $\mathbf{K} \in \mathbb{SYM}^+(3)$ we may ask for the rotation matrix $\mathbf{R} \in \mathbb{SO}(3)$ which is closest to a given matrix $\mathbf{Q} \in \mathbb{R}^{3 \times 3}$, i.e. which minimizes

$$\begin{aligned}\mathcal{V}_3(\mathbf{R}) &= \frac{1}{2}d_{\mathbf{K}}^2(\mathbf{Q}, \mathbf{R}) = \frac{1}{2} \operatorname{tr}((\mathbf{Q} - \mathbf{R})^\top \mathbf{K}(\mathbf{Q} - \mathbf{R})) \\ &= \underbrace{\frac{1}{2} \operatorname{tr}(\mathbf{Q}^\top \mathbf{K} \mathbf{Q} + \mathbf{K})}_{\text{const.}} - \operatorname{tr}(\underbrace{\mathbf{Q}^\top \mathbf{K} \mathbf{R}}_{\mathbf{P}_3})\end{aligned}\quad (2.60)$$

Each of these problems essentially asks for an $\mathbf{R} \in \mathbb{SO}(3)$ which minimizes $\mathcal{V} = -\operatorname{tr}(\mathbf{P}\mathbf{R})$ for some given $\mathbf{P} \in \mathbb{R}^{3 \times 3}$.

Solutions to Wahba's problem are given in [Davenport, 1968] using attitude quaternions and in [Kabsch, 1976] using the singular value decomposition. A proof of a unique minimum in [Bullo and Murray, 1999] relies on \mathbf{P} having distinct singular values.

In the following we extend these results in the sense that, we do not impose assumptions on \mathbf{P} and are also interested other extrema of \mathcal{V} .

Problem definition. Similar problems to the ones above will also appear in this work. So we are interested in the extrema, and their nature, of the function

$$\mathcal{V} : \mathbb{SO}(3) \rightarrow \mathbb{R} : \mathbf{R} \mapsto -\operatorname{tr}(\mathbf{P}\mathbf{R}) \quad (2.61)$$

with the parameter $\mathbf{P} \in \mathbb{R}^{3 \times 3}$.

Coordinate transformation. Consider a singular value decomposition $\mathbf{P} = \mathbf{X}\boldsymbol{\Sigma}\mathbf{Y}^\top$ with $\mathbf{X}, \mathbf{Y} \in \mathbb{O}(3)$ and $\boldsymbol{\Sigma} = \operatorname{diag}(\sigma_1, \sigma_2, \sigma_3)$, $\sigma_1 \geq \sigma_2 \geq \sigma_3 \geq 0$. [Kabsch, 1976]: Define

$$\bar{\mathbf{X}} = \mathbf{X} \operatorname{diag}(1, 1, \det \mathbf{X}) \in \mathbb{SO}(3), \quad (2.62a)$$

$$\bar{\mathbf{Y}} = \mathbf{Y} \operatorname{diag}(1, 1, \det \mathbf{Y}) \in \mathbb{SO}(3), \quad (2.62b)$$

$$\bar{\boldsymbol{\Sigma}} = \operatorname{diag}(\sigma_1, \sigma_2, \bar{\sigma}_3), \quad \bar{\sigma}_3 = \det \mathbf{X} \det \mathbf{Y} \sigma_3 \quad (2.62c)$$

which yields a decomposition $\mathbf{P} = \bar{\mathbf{X}} \bar{\boldsymbol{\Sigma}} \bar{\mathbf{Y}}^\top$ with proper rotations. Using the cyclic permutation property of the trace we get

$$\mathcal{V}(\mathbf{R}) = -\operatorname{tr}(\bar{\mathbf{X}} \bar{\boldsymbol{\Sigma}} \bar{\mathbf{Y}}^\top \mathbf{R}) = -\operatorname{tr}(\bar{\boldsymbol{\Sigma}} \underbrace{\bar{\mathbf{Y}}^\top \mathbf{R} \bar{\mathbf{X}}}_{\bar{\mathbf{R}}}) =: \bar{\mathcal{V}}(\bar{\mathbf{R}}) \quad (2.63)$$

Since the SVD is not unique in general, the transformed function $\bar{\mathcal{V}}$ is neither. However, since the coordinate transformation $\mathbf{R} = \bar{\mathbf{Y}} \bar{\boldsymbol{\Sigma}} \bar{\mathbf{X}}^\top$ is bijective, no information is lost here.

Critical points. Using the operators defined above, we may formulate the differential and Hessian of the transformed function as

$$\nabla \bar{\mathcal{V}}(\bar{\mathbf{R}}) = \operatorname{vee2}(\bar{\boldsymbol{\Sigma}} \bar{\mathbf{R}}), \quad (2.64)$$

$$\nabla^2 \bar{\mathcal{V}}(\bar{\mathbf{R}}) = \operatorname{Vee}(\bar{\boldsymbol{\Sigma}} \bar{\mathbf{R}})^\top. \quad (2.65)$$

For a critical point $\bar{\mathbf{R}}_0 : \nabla \bar{\mathcal{V}}(\bar{\mathbf{R}}_0) = \mathbf{0}$ we need the matrix $\bar{\Sigma} \bar{\mathbf{R}}_0$ to be symmetric. For the following it will be useful to substitute the entries/eigenvalues of $\text{Vee}(\bar{\Sigma}) = \text{diag}(\lambda_1, \lambda_2, \lambda_3) = \Lambda$ as

$$\left. \begin{array}{l} \lambda_1 = \sigma_2 + \bar{\sigma}_3, \\ \lambda_2 = \bar{\sigma}_3 + \sigma_1, \\ \lambda_3 = \sigma_1 + \sigma_2 \end{array} \right\} \Leftrightarrow \left\{ \begin{array}{l} \sigma_1 = \frac{1}{2}(\lambda_2 + \lambda_3 - \lambda_1), \\ \sigma_2 = \frac{1}{2}(\lambda_3 + \lambda_1 - \lambda_2), \\ \bar{\sigma}_3 = \frac{1}{2}(\lambda_1 + \lambda_2 - \lambda_3) \end{array} \right. \quad (2.66)$$

Note that $\sigma_1 \geq \sigma_2 \geq |\bar{\sigma}_3| \geq 0$ implies $\lambda_3 \geq \lambda_2 \geq \lambda_1 \geq 0$. Depending on the constellation of the eigenvalues we have the following critical points:

- Distinct eigenvalues: $\lambda_3 > \lambda_2 > \lambda_1 > 0$: We have the critical points

$$\bar{\mathbf{R}}_0 = \mathbf{I}_3 : \quad \mathcal{V}(\bar{\mathbf{R}}_0) = -\frac{\lambda_1}{2} - \frac{\lambda_2}{2} - \frac{\lambda_3}{2}, \quad \text{eig}(\nabla^2 \bar{\mathcal{V}}(\bar{\mathbf{R}}_0)) = \{\lambda_3, \lambda_2, \lambda_1\} \quad (2.67a)$$

$$\bar{\mathbf{R}}_1 = \text{diag}(1, -1, -1) : \quad \mathcal{V}(\bar{\mathbf{R}}_1) = \frac{3\lambda_1 - \lambda_2 - \lambda_3}{2}, \quad \text{eig}(\nabla^2 \bar{\mathcal{V}}(\bar{\mathbf{R}}_1)) = \{\lambda_3 - \lambda_1, \lambda_2 - \lambda_1, -\lambda_1\} \quad (2.67b)$$

$$\bar{\mathbf{R}}_2 = \text{diag}(-1, 1, -1) : \quad \mathcal{V}(\bar{\mathbf{R}}_2) = \frac{3\lambda_2 - \lambda_1 - \lambda_3}{2}, \quad \text{eig}(\nabla^2 \bar{\mathcal{V}}(\bar{\mathbf{R}}_2)) = \{\lambda_3 - \lambda_2, \lambda_1 - \lambda_2, -\lambda_2\} \quad (2.67c)$$

$$\bar{\mathbf{R}}_3 = \text{diag}(-1, -1, 1) : \quad \mathcal{V}(\bar{\mathbf{R}}_3) = \frac{3\lambda_3 - \lambda_1 - \lambda_2}{2}, \quad \text{eig}(\nabla^2 \bar{\mathcal{V}}(\bar{\mathbf{R}}_3)) = \{\lambda_2 - \lambda_3, \lambda_1 - \lambda_3, -\lambda_3\} \quad (2.67d)$$

so $\bar{\mathbf{R}}_0$ is a minimum, $\bar{\mathbf{R}}_1$ and $\bar{\mathbf{R}}_2$ are saddle points, and $\bar{\mathbf{R}}_3$ is a maximum.

- Double eigenvalue: $\lambda_3 > \lambda_2 = \lambda_1 > 0$: We have a minimum at $\bar{\mathbf{R}}_0$, a maximum at $\bar{\mathbf{R}}_3$ and a saddle on the circular manifold

$$\bar{\mathbf{R}}_4 = \begin{bmatrix} -c & s & 0 \\ s & c & 0 \\ 0 & 0 & -1 \end{bmatrix}, \quad c^2 + s^2 = 1 : \quad \mathcal{V}(\bar{\mathbf{R}}_4) = \lambda_1 - \frac{\lambda_3}{2}, \quad \text{eig}(\nabla^2 \bar{\mathcal{V}}(\bar{\mathbf{R}}_4)) = \{\lambda_3 - \lambda_1, 0, -\lambda_1\} \quad (2.67e)$$

which includes the points $\bar{\mathbf{R}}_1$ and $\bar{\mathbf{R}}_2$.

- Double eigenvalue: $\lambda_3 = \lambda_2 > \lambda_1 > 0$: Analog to above we have a minimum at $\bar{\mathbf{R}}_0$, a saddle at $\bar{\mathbf{R}}_1$ and a maximum on the circular manifold

$$\bar{\mathbf{R}}_5 = \begin{bmatrix} -1 & 0 & 0 \\ 0 & c & s \\ 0 & s & -c \end{bmatrix}, \quad c^2 + s^2 = 1 : \quad \mathcal{V}(\bar{\mathbf{R}}_5) = \lambda_2 - \frac{\lambda_1}{2}, \quad \text{eig}(\nabla^2 \bar{\mathcal{V}}(\bar{\mathbf{R}}_5)) = \{0, \lambda_1 - \lambda_2, -\lambda_2\} \quad (2.67f)$$

which includes the points $\bar{\mathbf{R}}_2$ and $\bar{\mathbf{R}}_3$.

- Triple eigenvalue: $\lambda_3 = \lambda_2 = \lambda_1 > 0$: Minimum at $\bar{\mathbf{R}}_0$ and a maximum on the spherical manifold

$$\bar{\mathbf{R}}_6 = \begin{bmatrix} q_x^2 - q_y^2 - q_z^2 & 2q_x q_y & 2q_x q_z \\ 2q_x q_y & q_y^2 - q_x^2 + q_z^2 & 2q_y q_z \\ 2q_x q_z & 2q_y q_z & q_z^2 - q_x^2 - q_y^2 \end{bmatrix}, \quad q_x^2 + q_y^2 + q_z^2 = 1 : \quad \mathcal{V}(\bar{\mathbf{R}}_6) = \frac{\lambda_1}{2}, \quad \text{eig}(\nabla^2 \bar{\mathcal{V}}(\bar{\mathbf{R}}_6)) = \{0, 0, -\lambda_1\} \quad (2.67g)$$

which includes the points $\bar{\mathbf{R}}_1$, $\bar{\mathbf{R}}_2$ and $\bar{\mathbf{R}}_3$ and the circles $\bar{\mathbf{R}}_4$ and $\bar{\mathbf{R}}_5$. It corresponds to a 180° rotation about an arbitrary axis $[q_x, q_y, q_z]^\top \in \mathbb{S}^2$.

- One zero eigenvalue: $\lambda_3 > \lambda_2 > \lambda_1 = 0$: We have a minimum on the circular manifold

$$\bar{\mathbf{R}}_7 = \begin{bmatrix} 1 & 0 & 0 \\ 0 & c & -s \\ 0 & s & c \end{bmatrix}, \quad c^2 + s^2 = 1 : \\ \mathcal{V}(\bar{\mathbf{R}}_7) = -\frac{\lambda_2 + \lambda_3}{2}, \quad \text{eig}(\nabla^2 \bar{\mathcal{V}}(\bar{\mathbf{R}}_7)) = \{\lambda_3, \lambda_2, 0\} \quad (2.67h)$$

which includes $\bar{\mathbf{R}}_0$ and $\bar{\mathbf{R}}_1$. Furthermore we have a saddle point at $\bar{\mathbf{R}}_2$ and a maximum at $\bar{\mathbf{R}}_3$.

- Double eigenvalue and zero eigenvalue: $\lambda_3 = \lambda_2 > \lambda_1 = 0$: We have a minimum on $\bar{\mathbf{R}}_7$ and a maximum on $\bar{\mathbf{R}}_5$.
- Two zero eigenvalues: $\lambda_3 > \lambda_2 = \lambda_1 = 0$: We have a minimum on the spherical manifold

$$\bar{\mathbf{R}}_8 = \begin{bmatrix} q_w^2 + q_x^2 - q_y^2 & 2q_x q_y & 2q_w q_y \\ 2q_x q_y & q_w^2 - q_x^2 + q_y^2 & -2q_w q_x \\ -2q_w q_x & 2q_w q_x & q_w^2 - q_x^2 - q_y^2 \end{bmatrix}, \quad q_w^2 + q_x^2 + q_y^2 = 1 : \\ \mathcal{V}(\bar{\mathbf{R}}_8) = -\frac{\lambda_3}{2}, \quad \text{eig}(\nabla^2 \bar{\mathcal{V}}(\bar{\mathbf{R}}_8)) = \{\lambda_3, 0, 0\} \quad (2.67i)$$

which includes $\bar{\mathbf{R}}_0$, $\bar{\mathbf{R}}_1$ and $\bar{\mathbf{R}}_2$ and corresponds to an arbitrary rotation about an axis $[q_x, q_y, 0]^\top$. Furthermore we have a maximum at $\bar{\mathbf{R}}_3$.

- All zero Eigenvalues: $\lambda_3 = \lambda_2 = \lambda_1 = 0$: for this we have $\bar{\Sigma} = \mathbf{P} = \mathbf{0}$ and the function is $\mathcal{V} = 0$.

We may conclude that the function $\bar{\mathcal{V}}$ has a minimum at $\bar{\mathbf{R}}_0 = \mathbf{I}_3$ and a maximum at $\bar{\mathbf{R}}_3 = \text{diag}(-1, -1, 1)$, though they may not be strict. The minimum is strict if and only if $\lambda_1 > 0$. The maximum is strict if and only if $\lambda_3 > \lambda_2$.

It should also be noted that the results of this paragraph would be much more “symmetric” if we would not have required the descending order of the singular values σ_i . This did however reduce the number of cases to distinguish.

Original coordinates. The original function \mathcal{V} has a minimum at $\mathbf{R}_0 = \bar{\mathbf{Y}} \bar{\mathbf{X}}^\top$. The minimum \mathbf{R}_0 is strict, if, and only if, $\lambda_i > 0, i = 1, 2, 3$ or equivalently if $\mathbf{K} \in \text{SYM}_0^+(3)$ is positive definite:

$$\mathbf{K} = \nabla^2 \mathcal{V}(\mathbf{R}_0) = \text{Vee}(\mathbf{P} \mathbf{R}_0) = \text{Vee}(\bar{\mathbf{X}} \bar{\Sigma} \bar{\mathbf{Y}}^\top \bar{\mathbf{Y}} \bar{\mathbf{X}}^\top) = \bar{\mathbf{X}} \text{Vee}(\bar{\Sigma}) \bar{\mathbf{X}}^\top = \bar{\mathbf{X}} \Lambda \bar{\mathbf{X}}^\top. \quad (2.68)$$

Special polar decomposition. From the results of this section we may also conclude the following: For any matrix $\mathbf{M} \in \mathbb{R}^{3 \times 3}$ there is a matrix $\mathbf{R} \in \text{SO}(3)$ and a unique matrix $\mathbf{K} \in \text{SYM}_0^+(3)$, such that $\mathbf{M} = \mathbf{R} \text{Wed}(\mathbf{K})$. The matrix \mathbf{R} is unique if, and only if, the matrix \mathbf{K} is positive definite. Within this work, this will be called the *special polar decomposition*.

Chapter 3

Analytical mechanics of particle systems

Goal. Established approaches of analytical mechanics commonly rely on the parameterization of the system in terms of *minimal* generalized coordinates \mathbf{q} and their derivatives $\dot{\mathbf{q}}$. In this section we like to generalize this to handle redundant configuration coordinates $\mathbf{x}(t) \in \mathbb{X}$ and nonholonomic velocity coordinates $\boldsymbol{\xi}(t) \in \mathbb{R}^n$ as introduced in the previous section. The resulting formulations might become more cumbersome, but with some examples we like to show that it is worth it.

3.1 A single free particle

[Landau and Lifshitz, 1960, §1]: *One of the fundamental concepts of mechanics is that of a particle, also called material point.* This abstracts a body whose dimensions may be neglected and all its mass \mathfrak{m} is located at a point with the Cartesian coordinates $\mathbf{r}(t) \in \mathbb{R}^3$ at time t . Its motion obeys Newton's second law [Newton, 1687, p. 13, lex II], english translation [Newton, 1846, p. 83]: *The alteration of motion is ever proportional to the motive force impressed; and is made in the direction of the right line in which that force is impressed.* The contemporary version reads (e.g. [Lurie, 2002, eq. 6.1.1] or [Goldstein, 1951, eq. 1.3])

$$\mathfrak{m}\ddot{\mathbf{r}} = \mathfrak{F}^A. \quad (3.1)$$

where $\ddot{\mathbf{r}} \equiv d^2\mathbf{r}/dt^2$ is Newton's notation of differentiation and the applied force \mathfrak{F}^A collects all other (non inertial) influences on the particle. In this work we will investigate three sources of applied forces: gravity, linear springs and viscous friction.

Gravity. For far most engineering applications we are dealing with systems that move close to the surface of the Earth and where Galilei's gravitation principle [Galilei, 1638, Day 3] holds. In a contemporary formulation it states that a particle with mass \mathfrak{m}_p is subject to the gravitational force

$$\mathfrak{F}^G = \mathfrak{m}a_G \quad (3.2)$$

where \mathbf{a}_G are the coefficients of the gravitational acceleration of the earth w.r.t. the chosen reference frame. Commonly the reference frame is chosen such that the e_z axis is opposing gravity and we have $\mathbf{a}_G = [0, 0, -g]^\top$ with the *gravity of earth* $g = 9.8 \frac{\text{m}}{\text{s}^2}$.

Linear spring. Let the particle be connected with a spring to a point \mathbf{r}_0 . The simplest model of a spring is that of Hooke's law [Hooke, 1678]: The force \mathfrak{F}^K on the particle is opposite and proportional by a factor $k \in \mathbb{R}^+$ to the spring displacement $\mathbf{r} - \mathbf{r}_0$, i.e.

$$\mathfrak{F}^K = -k(\mathbf{r} - \mathbf{r}_0). \quad (3.3)$$

Viscous friction. [Rayleigh, 1877, §81]: *There is another group of forces whose existence is often advantageous to recognize specially, namely those arising from friction or viscosity. [...] we suppose that each particle is retarded by forces proportional to its component velocities.* We may think of the particle to be immersed in a viscous fluid which, at the particle position, has the velocity \mathbf{v}_0 . The force on the particle is

$$\mathfrak{F}^D = -d(\dot{\mathbf{r}} - \mathbf{v}_0) \quad (3.4)$$

with the damping parameter $d \in \mathbb{R}^+$.

Equation of motion. A single free particle that is subject to all the aforementioned forces and a general, not further specified external force \mathfrak{F}^E , i.e. $\mathfrak{F}^A = \mathfrak{F}^G + \mathfrak{F}^K + \mathfrak{F}^D + \mathfrak{F}^E$, has the equation of motion

$$m(\ddot{\mathbf{r}} - \mathbf{a}_G) + d(\dot{\mathbf{r}} - \mathbf{v}_0) + k(\mathbf{r} - \mathbf{r}_0) = \mathfrak{F}^E. \quad (3.5)$$

Control engineering. From a control engineering perspective the structure of this system is already nice enough to consider it as a desired closed loop dynamics: If we want the particle to track a sufficiently smooth reference trajectory $t \mapsto \mathbf{r}_R(t)$ a reasonable desired closed loop dynamics is

$$\mathbf{r}_E = \mathbf{r} - \mathbf{r}_0, \quad m\ddot{\mathbf{r}}_E + \bar{d}\dot{\mathbf{r}}_E + \bar{k}\mathbf{r}_E = \mathbf{0}. \quad (3.6)$$

This is essentially the same as above (3.5), but we replaced the spring origin \mathbf{r}_0 with the reference position \mathbf{r}_R , the fluid velocity \mathbf{v}_0 with the reference velocity $\dot{\mathbf{r}}_R$ and the free-fall acceleration \mathbf{a}_G with the reference acceleration $\ddot{\mathbf{r}}_R$. Furthermore, we replaced the spring stiffness k and viscosity d by analog tuning parameters $\bar{k}, \bar{d} \in \mathbb{R}^+$. Plugging the desired dynamics (3.6) into the plant dynamics (3.5) yields the required control law

$$\mathfrak{F}^E = m(\ddot{\mathbf{r}}_R - \mathbf{a}_G) + \bar{d}(\dot{\mathbf{r}} - \mathbf{v}_0) + k(\mathbf{r} - \mathbf{r}_0) - \bar{d}(\dot{\mathbf{r}} - \dot{\mathbf{r}}_R) - \bar{k}(\mathbf{r} - \mathbf{r}_R) - ma_G. \quad (3.7)$$

As this control approach is so closely related to basic mechanics, it could be more intuitive for an engineer than other generic mathematical approaches.

3.2 Systems of constrained particles

System under consideration. For this section we consider a system of \mathfrak{N} particles under geometric constraints: The *position* of a particle with respect to a given inertial frame at a given time t is $\mathbf{r}_p(t) \in \mathbb{R}^3, p = 1, \dots, \mathfrak{N}$ and the collection of all particle positions is $\mathbf{x} = [\mathbf{r}_1^\top, \dots, \mathbf{r}_{\mathfrak{N}}^\top]^\top \in \mathbb{R}^{3\mathfrak{N}}$. *Geometric constraints* on the particles are captured in $\mathfrak{H} \geq 0$ smooth functions of the form $\mathbf{c}(\mathbf{x}) = [\mathbf{c}^1(\mathbf{x}), \dots, \mathbf{c}^{\mathfrak{H}}(\mathbf{x})]^\top = \mathbf{0}$. The set of all mutually admissible particle positions

$$\mathfrak{X} = \{\mathbf{x} \in \mathbb{R}^{3\mathfrak{N}} \mid \mathbf{c}(\mathbf{x}) = \mathbf{0}\} \quad (3.8)$$

is called the *configuration space*. We require $\frac{\partial \mathbf{c}}{\partial \mathbf{x}}(\mathbf{x})$ to have a constant, though not necessarily full rank.

3.2.1 First principles

Principle of constraint release. The principle of constraint release (see e.g. [Hamel, 1949, sec. 32] or [Lurie, 2002, sec. 6.1]) states that the motion of system of geometrically constrained particles is governed by

$$\mathbf{c}(\mathbf{x}) = \mathbf{0}, \quad \mathfrak{m}_p \ddot{\mathbf{r}}_p = \mathfrak{F}_p^A + \lambda_\kappa \frac{\partial \mathbf{c}^\kappa}{\partial \mathbf{r}_p}, \quad p = 1, \dots, \mathfrak{N}. \quad (3.9)$$

Lagrange-d'Alembert principle. For a system of geometrically constrained particles states (e.g. [Goldstein, 1951, sec. 1.4] or [Lurie, 2002, sec. 6.3]):

$$\sum_{p=1}^{\mathfrak{N}} \langle \delta \mathbf{r}_p, \mathfrak{F}_p^A - \mathfrak{m}_p \ddot{\mathbf{r}}_p \rangle = 0 \quad \forall \quad \frac{\partial \mathbf{c}}{\partial \mathbf{x}} \delta \mathbf{x} = \mathbf{0}. \quad (3.10)$$

The *virtual displacements* $\delta \mathbf{r}_p$ are tangents to possible motions: For particle positions constrained by $\mathbf{c}(\mathbf{x}) = \mathbf{0}$ the displacements have to fulfill $\frac{\partial \mathbf{c}}{\partial \mathbf{x}} \delta \mathbf{x} = \mathbf{0}$.

Gauß principle. Gauss's principle of least constraint was originally described in [Gauß, 1829] in words rather than equations. Maybe because of this, one finds somewhat different mathematical formulations in more contemporary sources, e.g. [Päsler, 1968, sec. 7], [Lanczos, 1986, sec. IV.8], [Bremer, 2008, sec. 2.2].

For the system given above, Gauss' principle states that the particle accelerations $\ddot{\mathbf{r}}_p, p = 1, \dots, \mathfrak{N}$ minimize the so-called Gaussian constrain \mathcal{G} :

$$\begin{aligned} \min_{\ddot{\mathbf{r}} \in \mathbb{R}^{3\mathfrak{N}}} \quad & \mathcal{G} = \frac{1}{2} \sum_{p=1}^{\mathfrak{N}} \mathfrak{m}_p \|\ddot{\mathbf{r}}_p - \ddot{\mathbf{r}}_p^f\|^2 \\ \text{s. t.} \quad & \ddot{\mathbf{c}}(\mathbf{x}, \dot{\mathbf{x}}, \ddot{\mathbf{x}}) = \mathbf{0} \end{aligned} \quad (3.11)$$

where $\ddot{\mathbf{r}}_p^f$ are the *unconstrained* particle accelerations, i.e. Newtons's second law $\ddot{\mathbf{r}}_p^f = \frac{\mathfrak{F}_p^A}{\mathfrak{m}_p}$. Its crucial to note that the constraint equations $\ddot{\mathbf{c}}(\mathbf{x}, \dot{\mathbf{x}}, \ddot{\mathbf{x}}) = \mathbf{0}$ are *linear* in the accelerations $\ddot{\mathbf{x}}$. Consequently, as stressed in [Gauß, 1829], the principle (3.11) is a (static) quadratic optimization problem with linear constraints.

Hamilton's principle. [Lanczos, 1986, p. 113]: *Hamilton's principle states that the motion of a mechanical system occurs in such a way that the action $\mathcal{A} = \int_{t_0}^{t_1} \mathcal{L} dt$ becomes stationary for arbitrary possible variations of the configuration of the system, provided the initial and final conditions are prescribed. The Lagrangian $\mathcal{L} = \mathcal{T} - \mathcal{V}$ is the excess of kinetic energy \mathcal{T} over potential energy \mathcal{V} .* For the system considered here, the kinetic energy is $\mathcal{T} = \frac{1}{2} \sum_{p=1}^{\mathfrak{N}} \mathfrak{m}_p \|\dot{\mathbf{r}}_p\|^2$. The potential energy may have various origins, some of them will be discussed later.

The remarkable quality of the principle of stationary action is that it is used interdisciplinary: With appropriate formulation of the Lagrangian \mathcal{L} it has applications in all branches of physics e.g. general relativity [Einstein, 1916], electromagnetic field theory [Landau and Lifshitz, 1971, ch. 4] or optics, the original context of Hamilton [Klein, 1926, p. 192]. Apart from physics, there is optimal control that builds up on essentially the same idea e.g. [Bryson, 1975].

For the context of this work, the statement above is actually not that useful since it does not allow for generic impressed forces \mathfrak{F}_p^A . To mend this one finds a similar statement in e.g. [Lurie, 2002, eq. 12.2.14] or [Szabó, 1956, sec. I.3]:

$$\delta' \mathcal{A} = \int_{t_1}^{t_2} (\delta \mathcal{T} - \delta' \mathcal{W}) dt = 0, \quad \mathcal{T} = \frac{1}{2} \sum_p \mathfrak{m}_p \|\dot{\mathbf{r}}_p\|^2, \quad \delta' \mathcal{W} = \langle \delta \mathbf{r}_p, \mathfrak{F}_p^A \rangle. \quad (3.12)$$

Here $\delta' \mathcal{W}$ is an variational quantity, but in general, there is no \mathcal{W} that it is the variation of, unless the impressed forces \mathfrak{F}_p^A may be derived from a potential. Consequently, there is generally no quantity \mathcal{A} which becomes stationary, thus the naming is not suitable here.

3.2.2 Coordinates

Generalized coordinates. In most cases we are not really interested in the motion of the individual particles but rather in the system as a whole. Using the constraint equations it is possible to capture the configuration of the system by $\dim \mathfrak{X} = 3\mathfrak{N} - \text{rank } \frac{\partial \mathbf{c}}{\partial \mathbf{x}} = n$ coordinates, commonly called *generalized coordinates* and commonly denoted by \mathbf{q} . Its components, in contrast to the Cartesian particle coordinates, may be lengths, angles or some completely generic quantity stressed by the term “generalized”. What is more crucial but usually implicit, is that they have to be independent from another to parameterize the n dimensional configuration space with its n components. Whenever used in this work, these coordinates are referred to as *minimal generalized coordinates* $\mathbf{q} \in \mathbb{R}^n$.

Redundant configuration coordinates and velocity coordinates. As motivated in section 2.1, in some cases it can be beneficial to use a slightly larger number of *redundant* generalized coordinates $\mathbf{x}(t) \in \mathbb{X} = \{\mathbf{x} \in \mathbb{R}^\nu \mid \phi(\mathbf{x}) = \mathbf{0}\}$ and *minimal* velocity coordinates $\boldsymbol{\xi}(t) \in \mathbb{R}^n$ related by $\dot{\mathbf{x}} = \mathbf{A}\boldsymbol{\xi}$. Of course this includes common minimal parameterization $\mathbf{x} = \mathbf{q} \in \mathbb{R}^n$ and $\boldsymbol{\xi} = \dot{\mathbf{q}} \in \mathbb{R}^n$ as the special case $\mathbb{X} = \mathbb{R}^n$ and $\mathbf{A} = \mathbf{I}_n$.

Particle parameterization. Let the admissible particle positions $\mathfrak{x} \in \mathfrak{X}$ be parameterized $\mathfrak{r}_p = \mathfrak{r}_p(\mathbf{x}, t)$ by possibly redundant coordinates $\mathbf{x} \in \mathbb{X}$. This means $\phi(\mathbf{x}) =$

$\mathbf{0} \Rightarrow \mathbf{c}(\mathbf{x}(x, t)) = \mathbf{0}$ and consequently $\mathbf{x} \in \mathbb{X} \Rightarrow \mathbf{x}(x) \in \mathfrak{X}$. The particle velocities and accelerations in terms of the coordinates we have

$$\dot{\mathbf{r}}_p = \partial_i \mathbf{r}_p \xi^i + \frac{\partial \mathbf{r}_p}{\partial t} \quad (3.13a)$$

$$\ddot{\mathbf{r}}_p = \partial_i \mathbf{r}_p \dot{\xi}^i + \partial_j \partial_i \mathbf{r}_p \xi^i \xi^j + \underbrace{\left(\partial_i \frac{\partial \mathbf{r}_p}{\partial t} + \frac{\partial}{\partial t} \partial_i \mathbf{r}_p \right)}_{\mathbf{a}_p^E} \xi^i + \frac{\partial^2 \mathbf{r}_p}{\partial t^2}. \quad (3.13b)$$

The following relations will be useful for the next steps of this section:

- From (3.13) it is evident that

$$\partial_i \mathbf{r}_p = \frac{\partial \dot{\mathbf{r}}_p}{\partial \xi^i} = \frac{\partial \ddot{\mathbf{r}}_p}{\partial \dot{\xi}^i}. \quad i = 1, \dots, n. \quad (3.14)$$

- From $\frac{d}{dt} \partial_i \mathbf{r}_p = \partial_j \partial_i \mathbf{r}_p \xi^j + \frac{\partial}{\partial t} \partial_i \mathbf{r}_p = (\partial_i \partial_j - \gamma_{ij}^k \partial_k) \mathbf{r}_p \xi^j + \partial_i \frac{\partial \mathbf{r}_p}{\partial t} = \partial_i \dot{\mathbf{r}}_p - \gamma_{ij}^k \partial_k \mathbf{r}_p \xi^j$ with the commutation coefficients γ_{ij}^k established in subsection 2.2.2, we obtain the commutation relation

$$\partial_i \dot{\mathbf{r}}_p - \frac{d}{dt} \partial_i \mathbf{r}_p = \gamma_{ij}^k \partial_k \mathbf{r}_p \xi^j, \quad i = 1, \dots, n. \quad (3.15)$$

- As $\frac{d}{dt} \mathbf{c}^\kappa = \sum_p \frac{\partial \mathbf{c}^\kappa}{\partial \mathbf{r}_p} \dot{\mathbf{r}}_p = \sum_p \frac{\partial \mathbf{c}^\kappa}{\partial \mathbf{r}_p} (\partial_i \mathbf{r}_p \xi^i + \frac{\partial \mathbf{r}_p}{\partial t}) = 0$ has to hold for any ξ we have

$$\sum_p \frac{\partial \mathbf{c}^\kappa}{\partial \mathbf{r}_p} \partial_i \mathbf{r}_p = 0, \quad \kappa = 1, \dots, \mathfrak{H}, \quad i = 1, \dots, n \quad (3.16a)$$

$$\sum_p \frac{\partial \mathbf{c}^\kappa}{\partial \mathbf{r}_p} \frac{\partial \mathbf{r}_p}{\partial t} = 0, \quad \kappa = 1, \dots, \mathfrak{H}. \quad (3.16b)$$

Application to the principle of constraint release. Summing up the projections of (3.9) on $\partial_i \mathbf{r}_p$ eliminates the constraint forces $\boldsymbol{\lambda}$ due to (3.16a):

$$\underbrace{\sum_p \langle \partial_i \mathbf{r}_p, \mathbf{m}_p \ddot{\mathbf{r}}_p \rangle}_{f_i^M} = \underbrace{\sum_p \langle \partial_i \mathbf{r}_p, \mathfrak{F}_p^A \rangle}_{f_i^A} + \lambda_\kappa \underbrace{\sum_p \langle \partial_i \mathbf{r}_p, \frac{\partial \mathbf{c}^\kappa}{\partial \mathbf{r}_p} \rangle}_0, \quad i = 1, \dots, n. \quad (3.17)$$

We call \mathbf{f}^M the generalized inertia force and \mathbf{f}^A the generalized applied force.

Parameterizing the particle accelerations $\ddot{\mathbf{r}}_p$ in terms of the chosen coordinates (3.13b) yields

$$\begin{aligned} & \sum_p \mathbf{m}_p \langle \partial_i \mathbf{r}_p, \overbrace{\partial_j \mathbf{r}_p \dot{\xi}^j + \partial_k \partial_j \mathbf{r}_p \xi^k \xi^j + \mathbf{a}_p^E}^{\ddot{\mathbf{r}}_p} \rangle = \sum_p \langle \partial_i \mathbf{r}_p, \mathfrak{F}_p^A \rangle, \quad i = 1, \dots, n \\ \Leftrightarrow & \underbrace{\sum_p \mathbf{m}_p \langle \partial_i \mathbf{r}_p, \partial_j \mathbf{r}_p \rangle}_{M_{ij}} \dot{\xi}^j = \underbrace{\sum_p \langle \partial_i \mathbf{r}_p, \mathfrak{F}_p^A - \mathbf{m}_p (\partial_k \partial_j \mathbf{r}_p \xi^k \xi^j + \mathbf{a}_p^E) \rangle}_{b_i}, \quad i = 1, \dots, n. \end{aligned} \quad (3.18)$$

Mathematically, the matrix \mathbf{M} is symmetric and (assuming $\mathfrak{m}_p \geq 0$) is positive semidefinite. Physically, we may assume that \mathbf{M} is actually positive definite, otherwise there is a degree of freedom with no inertia attached which would rather be an error in modeling. For this work we will assume that \mathbf{M} is symmetric positive definite and consequently invertible. Then the acceleration coordinates can be expressed as

$$\dot{\boldsymbol{\xi}} = \mathbf{M}^{-1} \mathbf{b}. \quad (3.19)$$

Application to the Lagrange-d'Alembert principle. Analog to the velocity, we may parameterize virtual displacements as $\delta \mathbf{r}_p = \partial_i \mathbf{r}_p h^i, p = 1, \dots, \mathfrak{N}$ in terms of *minimal* displacements coordinates $\mathbf{h} \in \mathbb{R}^n$. Plugging this into (3.10) we get

$$h^i \sum_p \langle \partial_i \mathbf{r}_p, \tilde{\mathbf{f}}_p^A - \mathfrak{m}_p \ddot{\mathbf{r}}_p \rangle = 0 \quad \forall \mathbf{h} \in \mathbb{R}^n. \quad (3.20)$$

Since this has to hold for any \mathbf{h} , we have the identical result as above (3.17).

Application to the Gauß principle. Parameterizing the particle accelerations $\ddot{\mathbf{r}}_p = \ddot{\mathbf{r}}_p(\mathbf{x}, \boldsymbol{\xi}, \dot{\boldsymbol{\xi}})$ in terms of the chosen coordinates (3.13b) in Gauss' principle (3.11) eliminates the constraints. So it essentially transforms it to an *unconstrained* minimization problem. The Gaussian constraint now reads

$$\begin{aligned} \mathcal{G} &= \frac{1}{2} \sum_p \mathfrak{m}_p \left\| \overbrace{\partial_j \mathbf{r}_p \dot{\xi}^j + \partial_k \partial_j \mathbf{r}_p \xi^k \xi^j + \mathbf{a}_p^E}^{\ddot{\mathbf{r}}_p} - \frac{\tilde{\mathbf{f}}_p^A}{\mathfrak{m}_p} \right\|^2 \\ &= \underbrace{\frac{1}{2} \sum_p \mathfrak{m}_p \langle \partial_i \mathbf{r}_p, \partial_j \mathbf{r}_p \rangle}_{M_{ij}} \dot{\xi}^i \dot{\xi}^j - \underbrace{\sum_p \langle \partial_i \mathbf{r}_p, \tilde{\mathbf{f}}_p^A - \mathfrak{m}_p (\partial_k \partial_j \mathbf{r}_p \xi^k \xi^j + \mathbf{a}_p^E) \rangle}_{b_i} \dot{\xi}^i \\ &\quad + \underbrace{\frac{1}{2} \sum_p \frac{1}{\mathfrak{m}_p} \|\tilde{\mathbf{f}}_p^A - \mathfrak{m}_p (\partial_k \partial_j \mathbf{r}_p \xi^k \xi^j + \mathbf{a}_p^E)\|^2}_{\mathcal{G}_0} \\ &= \frac{1}{2} \boldsymbol{\xi}^\top \mathbf{M} \boldsymbol{\xi} - \boldsymbol{\xi}^\top \mathbf{b} + \mathcal{G}_0. \end{aligned} \quad (3.21)$$

The necessary condition for a critical point is

$$\frac{\partial \mathcal{G}}{\partial \dot{\boldsymbol{\xi}}} = \mathbf{0} \quad \Leftrightarrow \quad \mathbf{M} \dot{\boldsymbol{\xi}} = \mathbf{b}. \quad (3.22)$$

Which is, again, the same result as above. Since $\partial^2 \mathcal{G} / \partial \dot{\boldsymbol{\xi}} \partial \dot{\boldsymbol{\xi}} = \mathbf{M}$ is positive definite, the solution $\dot{\boldsymbol{\xi}} = \mathbf{M}^{-1} \mathbf{b}$ is a minimum of the Gaussian constraint \mathcal{G} .

Application to Hamilton's principle. As discussed above, Hamilton's principle of stationary action is not applicable for generic forces as assumed here. However, it might still be instructive to apply it to our system when setting $\mathbf{f}^A = \mathbf{0}$ and $\mathcal{L} = \mathcal{T}$.

The kinetic energy \mathcal{T} in terms of the chosen coordinates is

$$\mathcal{T}(\mathbf{x}, \boldsymbol{\xi}, t) = \frac{1}{2} \sum_p \mathfrak{m}_p \|\dot{\mathbf{r}}_p(\mathbf{x}, \boldsymbol{\xi}, t)\|^2, \quad \dot{\mathbf{r}}_p(\mathbf{x}, \boldsymbol{\xi}, t) = \partial_i \mathbf{r}_p(\mathbf{x}) \xi^i + \frac{\partial \mathbf{r}_p}{\partial t}(\mathbf{x}, t) \quad (3.23)$$

As this is the structure assumed in (2.26) we may use the result (2.31) from the calculus of variations to obtain

$$f_i^M = \frac{d}{dt} \frac{\partial \mathcal{T}}{\partial \xi^i} + \gamma_{ij}^k \xi^j \frac{\partial \mathcal{T}}{\partial \xi^k} - \partial_i \mathcal{T} = 0 \quad i = 1, \dots, n. \quad (3.24)$$

Evaluation and some rearrangement using the identities (3.14) and (3.15) yields

$$\begin{aligned} f_i^M &= \sum_p m_p \left(\frac{d}{dt} \langle \frac{\partial \ddot{\mathbf{r}}_p}{\partial \xi^i}, \dot{\mathbf{r}}_p \rangle + \gamma_{ij}^k \xi^j \langle \frac{\partial \ddot{\mathbf{r}}_p}{\partial \xi^k}, \dot{\mathbf{r}}_p \rangle - \langle \partial_i \dot{\mathbf{r}}_p, \dot{\mathbf{r}}_p \rangle \right) \\ &= \sum_p m_p \left(\langle \partial_i \dot{\mathbf{r}}_p, \ddot{\mathbf{r}}_p \rangle + \underbrace{\langle \frac{d}{dt} \partial_i \dot{\mathbf{r}}_p + \gamma_{ij}^k \xi^j \partial_k \dot{\mathbf{r}}_p - \partial_i \dot{\mathbf{r}}_p, \dot{\mathbf{r}}_p \rangle}_0 \right) \end{aligned} \quad (3.25)$$

Which matches the generalized inertial force derived above (3.17).

3.2.3 Inertia

In (3.17) we have introduced the generalized inertia force $\mathbf{f}^M = \sum_p \langle \partial_i \dot{\mathbf{r}}_p, \mathfrak{F}_p^M \rangle$ as the projection of the particle inertia forces $\mathfrak{F}_p^M = m_p \ddot{\mathbf{r}}_p$. With this we will review some established formalisms and extend them for the use of redundant configuration coordinates.

Gibbs-Appell formulation. Using the identity of the differentials (3.14) we may formulate

$$f_i^M = \sum_p \langle \frac{\partial \ddot{\mathbf{r}}_p}{\partial \dot{\xi}^i}, -m_p \ddot{\mathbf{r}}_p \rangle = -\frac{\partial}{\partial \dot{\xi}^i} \underbrace{\left(\frac{1}{2} \sum_p m_p \|\ddot{\mathbf{r}}_p\|^2 \right)}_S, \quad i = 1, \dots, n. \quad (3.26)$$

So the generalized inertia force \mathbf{f}^M may be derived from the function $S = S(\mathbf{x}, \boldsymbol{\xi}, \dot{\boldsymbol{\xi}}, t)$ which is commonly called the *acceleration energy* though its dimension is *not* that of energy.

This formulation was first proposed by [Gibbs, 1879] for Cartesian, minimal coordinates and by [Appell, 1900] also using nonholonomic velocity coordinates. Some historic overview is given in [Lewis, 1996, sec. 1].

Euler-Lagrange formulation. Using the identity of the differentials (3.14), the commutation relation (3.15) and the product rule of differentiation we may formulate

$$\begin{aligned} f_i^M &= \sum_p \langle \frac{\partial \ddot{\mathbf{r}}_p}{\partial \dot{\xi}^i}, \frac{d}{dt} (m_p \dot{\mathbf{r}}_p) \rangle \\ &= \sum_p m_p \left(\frac{d}{dt} \langle \frac{\partial \ddot{\mathbf{r}}_p}{\partial \dot{\xi}^i}, \dot{\mathbf{r}}_p \rangle - \langle \frac{d}{dt} \frac{\partial \ddot{\mathbf{r}}_p}{\partial \dot{\xi}^i}, \dot{\mathbf{r}}_p \rangle \right) \\ &= \sum_p m_p \left(\frac{d}{dt} \langle \frac{\partial \ddot{\mathbf{r}}_p}{\partial \dot{\xi}^i}, \dot{\mathbf{r}}_p \rangle - \langle \partial_i \dot{\mathbf{r}}_p - \gamma_{ij}^k \frac{\partial \ddot{\mathbf{r}}_p}{\partial \dot{\xi}^k} \xi^j, \dot{\mathbf{r}}_p \rangle \right) \\ &= \left(\frac{d}{dt} \frac{\partial}{\partial \dot{\xi}^i} + \gamma_{ij}^k \xi^j \frac{\partial}{\partial \dot{\xi}^k} - \partial_i \right) \underbrace{\left(\frac{1}{2} \sum_p m_p \|\dot{\mathbf{r}}_p\|^2 \right)}_{\mathcal{T}}, \quad i = 1, \dots, n. \end{aligned} \quad (3.27)$$

So the generalized inertia force \mathbf{f}^M may be derived from the *kinetic energy* $\mathcal{T} = \mathcal{T}(\mathbf{x}, \boldsymbol{\xi}, t)$ formulated in terms of the chosen coordinates. This has already been shown in (3.24) and the computation is essentially (3.25) backwards.

For the special case of minimal configuration coordinates $\mathbf{x} = \mathbf{q}$ and the holonomic velocity coordinates $\boldsymbol{\xi} = \dot{\mathbf{q}}$, which implies $\gamma = 0$, this formulation and its derivation may be found in any graduate textbook on mechanics and is commonly called the *Euler-Lagrange equation*. A nearly identical form as (3.27) can be found in [Hamel, 1904a, p. 17]. The difference is that, in contrast to this work, the directional derivative ∂_i and the commutation coefficients γ_{ij}^k are therein restricted to minimal configuration coordinates.

It is worth noting that the quantity $2\mathcal{T}$ which appeared in this context, was called *vis viva* in older publications and translated to *living force* or *lebendige Kraft* [Hamel, 1904a]. The contemporary term *kinetic energy* seems to have established in the early 20th century.

Levi-Civita formulation. Formulation of the particle accelerations $\ddot{\mathbf{r}}_p$ explicitly in terms of the chosen coordinates (3.13b) yields

$$\begin{aligned} f_i^M &= \sum_p \langle \partial_i \mathbf{r}_p, \mathbf{m}_p \overbrace{(\partial_j \mathbf{r}_p \dot{\xi}^j + \partial_k \partial_j \mathbf{r}_p \xi^k \xi^j + \mathbf{a}_p^E)}^{\ddot{\mathbf{r}}_p} \rangle \\ &= \underbrace{\sum_p \mathbf{m}_p \langle \partial_i \mathbf{r}_p, \partial_j \mathbf{r}_p \rangle}_{M_{ij}} \dot{\xi}^j + \underbrace{\sum_p \mathbf{m}_p \langle \partial_i \mathbf{r}_p, \partial_k \partial_j \mathbf{r}_p \rangle}_{\Gamma_{ijk}} \xi^k \xi^j + \sum_p \mathbf{m}_p \langle \partial_i \mathbf{r}_p, \mathbf{a}_p^E \rangle, \quad i = 1, \dots, n. \end{aligned} \quad (3.28)$$

The inertia matrix \mathbf{M} was already discussed above. Here we are interested in the terms denoted by Γ_{ijk} . Based on their definition in (3.28) one may validate the following identities

$$\partial_k M_{ij} = \Gamma_{ijk} + \Gamma_{jik}, \quad (3.29a)$$

$$\gamma_{ij}^s M_{sk} = \Gamma_{kji} - \Gamma_{kij}. \quad (3.29b)$$

Plugging these together while permuting the indices, we find

$$\begin{aligned} \Gamma_{ijk} &= \partial_k M_{ij} - \Gamma_{jik} \\ &= \partial_k M_{ij} + \gamma_{ik}^s M_{sj} - \Gamma_{jki} \\ &= \partial_k M_{ij} + \gamma_{ik}^s M_{sj} - \partial_i M_{kj} + \Gamma_{kji} \\ &= \partial_k M_{ij} + \gamma_{ik}^s M_{sj} - \partial_i M_{kj} + \gamma_{ij}^s M_{sk} + \Gamma_{kij} \\ &= \partial_k M_{ij} + \gamma_{ik}^s M_{sj} - \partial_i M_{kj} + \gamma_{ij}^s M_{sk} + \partial_j M_{ik} - \Gamma_{ikj} \\ &= \partial_k M_{ij} + \gamma_{ik}^s M_{sj} - \partial_i M_{kj} + \gamma_{ij}^s M_{sk} + \partial_j M_{ik} - \gamma_{kj}^s M_{si} - \Gamma_{ijk} \end{aligned} \quad (3.30)$$

$$\Leftrightarrow \Gamma_{ijk} = \frac{1}{2} (\partial_k M_{ij} + \partial_j M_{ik} - \partial_i M_{jk} + \gamma_{ij}^s M_{sk} + \gamma_{ik}^s M_{sj} - \gamma_{kj}^s M_{si}). \quad (3.31)$$

This means the coefficients Γ_{ijk} are completely determined by the inertia matrix \mathbf{M} and the geometric matrix \mathbf{A} which determines the directional derivative ∂_i and the commutation coefficients γ .

A similar, coordinate free derivation can be found in [Abraham and Marsden, 1978, proof of Theorem 2.7.6] for the proof of the fundamental theorem of Riemannian geometry,

i.e. the existence and uniqueness of the *Levi-Civita connection*. However, all coordinate versions therein are restricted to minimal holonomic coordinates. For this *special case*, i.e. $\mathbf{x} = \mathbf{q}$, $\dot{\mathbf{q}} = \dot{\mathbf{q}}$, $\mathbf{A} = \mathbf{I}_n$ and consequently $\gamma = 0$, (3.31) simplifies to the familiar definition of the *Christoffel symbols* $\Gamma_{ijk} = \frac{1}{2} \left(\frac{\partial M_{ij}}{\partial q^k} + \frac{\partial M_{ik}}{\partial q^j} - \frac{\partial M_{jk}}{\partial q^i} \right)$, see e.g. [Abraham and Marsden, 1978, p. 145] or [Spivak, 1999, Vol. 2, p. 221]. In [Frankel, 1997, sec. 9.2] it is pointed out that the name Christoffel symbols is exclusive for the holonomic case, whereas in general Γ_{ijk} are referred to as the *(Levi-Civita) connection coefficients*. To the best of the authors knowledge, the only popular source that states the coordinate version (3.31) explicitly is [Misner et al., 1973, eq. 8.24], though restricted to minimal coordinates and in a rather different context of relativistic point masses. Since the directional derivative ∂_i and the commutation coefficients γ_{ij}^s are defined in a setting supporting redundant coordinates, so does (3.31) as definition of the connection coefficients.

3.2.4 Gravitation

Earth's gravity acts on a system of particles just as on a single particle (3.2), i.e. with a force $\mathfrak{F}_p^G = \mathfrak{m}_p \mathbf{a}_G$ on each particle. The resulting generalized force on the system is

$$f_i^G = \sum_p \langle \partial_i \mathbf{r}_p, \mathfrak{F}_p^G \rangle = \sum_p \mathfrak{m}_p \langle \partial_i \mathbf{r}_p, \mathbf{a}_G \rangle = \partial_i \underbrace{\sum_p \mathfrak{m}_p \langle \mathbf{r}_p, -\mathbf{a}_G \rangle}_{\mathcal{V}^G}. \quad (3.32)$$

The force may also be derived from the *gravitational potential* \mathcal{V}^G of the system which is simply the sum of the potentials of the individual particles.

The *gravitational mass* \mathfrak{m}_p in (3.32) takes the same value as the *inertial mass* from the previous section. This is sometimes referred to as the *(Galilean) equivalence principle* and is crucial topic for general relativity, see e.g., [Misner et al., 1973, chap. 16]. In this context, there is no *absolute* acceleration $\ddot{\mathbf{r}}_p$, instead, we are interested in the deviation from the free fall acceleration \mathbf{a}_G . This motivates the following formulation for the sum of generalized inertial and gravitational force

$$\begin{aligned} f_i^M + f_i^G &= \sum_p \mathfrak{m}_p \langle \partial_i \mathbf{r}_p, \ddot{\mathbf{r}}_p - \mathbf{a}_G \rangle = \sum_p \mathfrak{m}_p \langle \frac{\partial \ddot{\mathbf{r}}_p}{\partial \xi^i}, \ddot{\mathbf{r}}_p - \mathbf{a}_G \rangle \\ &= \underbrace{\frac{\partial}{\partial \xi^i} \left(\frac{1}{2} \sum_p \mathfrak{m}_p \|\ddot{\mathbf{r}}_p - \mathbf{a}_G\|^2 \right)}_{\mathcal{S}^G}, \quad i = 1, \dots, n. \end{aligned} \quad (3.33)$$

The quantity \mathcal{S}^G may be regarded as a metric for the deviation of the system to its natural acceleration, the free fall.

Taking this one step further, we may consider the free fall velocities $\mathfrak{v}_{pG}(t) = \mathbf{a}_G t + \mathfrak{v}_{p0}$

with arbitrary initial velocities $\mathbf{v}_{p0} \in \mathbb{R}^3, p = 1, \dots, \mathfrak{N}$ and compute analog to (3.27):

$$\begin{aligned} f_i^M + f_i^G &= \sum_p \mathfrak{m}_p \left\langle \frac{\partial \dot{\mathbf{r}}_p}{\partial \xi^i}, \frac{d}{dt} (\dot{\mathbf{r}}_p - \mathbf{v}_{pG}) \right\rangle \\ &= \sum_p \mathfrak{m}_p \left(\frac{d}{dt} \left\langle \frac{\partial \dot{\mathbf{r}}_p}{\partial \xi^i}, \dot{\mathbf{r}}_p - \mathbf{v}_{pG} \right\rangle - \left\langle \frac{d}{dt} \frac{\partial \dot{\mathbf{r}}_p}{\partial \xi^i}, \dot{\mathbf{r}}_p - \mathbf{v}_{pG} \right\rangle \right) \\ &= \sum_p \mathfrak{m}_p \left(\frac{d}{dt} \left\langle \frac{\partial \dot{\mathbf{r}}_p}{\partial \xi^i}, \dot{\mathbf{r}}_p - \mathbf{v}_{pG} \right\rangle - \left\langle \partial_i \dot{\mathbf{r}}_p - \gamma_{ij}^k \frac{\partial \dot{\mathbf{r}}_p}{\partial \xi^k} \xi^j, \dot{\mathbf{r}}_p - \mathbf{v}_{pG} \right\rangle \right) \\ &= \left(\frac{d}{dt} \frac{\partial}{\partial \xi^i} + \gamma_{ij}^k \xi^j \frac{\partial}{\partial \xi^k} - \partial_i \right) \underbrace{\left(\frac{1}{2} \sum_p \mathfrak{m}_p \|\dot{\mathbf{r}}_p - \mathbf{v}_{pG}\|^2 \right)}_{\mathcal{T}^G}, \quad i = 1, \dots, n. \end{aligned} \quad (3.34)$$

3.2.5 Stiffness

Consider that *one* particle \mathbf{r}_p of the system is connected by a linear spring with stiffness \mathfrak{k}_p to a position \mathbf{p}_p . The force on this one particle, as proposed in (3.3), is $\mathfrak{F}_p^K = \mathfrak{k}_p(\mathbf{p}_p - \mathbf{r}_p)$. The generalized force on the system is

$$f_i^K = \langle \partial_i \mathbf{r}_p, \mathfrak{F}_p^K \rangle = \mathfrak{k}_p \langle \partial_i \mathbf{r}_p, \mathbf{p}_p - \mathbf{r}_p \rangle = -\partial_i \underbrace{\left(\frac{1}{2} \mathfrak{k}_p \|\mathbf{r}_p - \mathbf{p}_p\|^2 \right)}_{\mathcal{V}_p^K}. \quad (3.35)$$

We may also consider a spring with stiffness \mathfrak{k}_{pq} between two particles of the system: Then we have the force $\mathfrak{F}_p^K = \mathfrak{k}_{pq}(\mathbf{r}_q - \mathbf{r}_p)$ on particle \mathbf{r}_p and the opposite force $\mathfrak{F}_q^K = \mathfrak{k}_{pq}(\mathbf{r}_p - \mathbf{r}_q)$ on particle \mathbf{r}_q . The generalized force on the system is

$$f_i^K = \langle \partial_i \mathbf{r}_p, \mathfrak{F}_p^K \rangle + \langle \partial_i \mathbf{r}_q, \mathfrak{F}_q^K \rangle = -\mathfrak{k}_{pq} \langle \partial_i (\mathbf{r}_p - \mathbf{r}_q), \mathbf{r}_p - \mathbf{r}_q \rangle = -\partial_i \underbrace{\left(\frac{1}{2} \mathfrak{k}_{pq} \|\mathbf{r}_p - \mathbf{r}_q\|^2 \right)}_{\mathcal{V}_{pq}^K}. \quad (3.36)$$

In both cases the generalized force can be derived from a potential \mathcal{V}^K .

For a system with an arbitrary number of linear springs, one may simply sum up the individual potentials to obtain the stiffness potential \mathcal{V}^K and derive the corresponding generalized force $\mathbf{f}^K = \nabla \mathcal{V}^K$. Note that non-negativity of the spring constants $\mathfrak{k} \geq 0$ implies non-negativity of the potential $\mathcal{V}^K \geq 0$.

3.2.6 Dissipation

Let the system of particles move within a viscous fluid with velocities \mathbf{v}_p^D at the positions \mathbf{r}_p of the particles. Then, as proposed in (3.4), each particle is subject to a friction force $\mathfrak{F}_p^D = -\mathfrak{d}_p(\dot{\mathbf{r}}_p - \mathbf{v}_p^D)$. The generalized force on the system is

$$f_i^D = \sum_p \langle \partial_i \mathbf{r}_p, \mathfrak{F}_p^D \rangle = -\sum_p \mathfrak{d}_p \left\langle \frac{\partial \dot{\mathbf{r}}_p}{\partial \xi^i}, \dot{\mathbf{r}}_p - \mathbf{v}_p^D \right\rangle = -\frac{\partial}{\partial \xi^i} \underbrace{\left(\frac{1}{2} \sum_p \mathfrak{d}_p \|\dot{\mathbf{r}}_p - \mathbf{v}_p^D\|^2 \right)}_{\mathcal{R}}. \quad (3.37)$$

This dissipative force may be derived from \mathcal{R} , which is commonly called *Rayleigh dissipation function*, e.g. [Goldstein, 1951, p. 24]. Its dimension is that of power, i.e. watts. Note that non-negativity of the damping parameters $\mathfrak{d} \geq 0$ implies non-negativity of the dissipation function $\mathcal{V}^K \geq 0$.

3.2.7 Energy

Total energy. The time derivative of the kinetic energy may be formulated as

$$\dot{\mathcal{T}} = \sum_p \mathfrak{m}_p \langle \dot{\mathbf{r}}_p, \ddot{\mathbf{r}}_p \rangle = \xi^i \underbrace{\sum_p \mathfrak{m}_p \langle \partial_i \mathbf{r}_p, \ddot{\mathbf{r}}_p \rangle}_{f_i^M} + \sum_p \mathfrak{m}_p \langle \frac{\partial \mathbf{r}_p}{\partial t}, \ddot{\mathbf{r}}_p \rangle. \quad (3.38)$$

In subsection 3.2.4 and subsection 3.2.4 we have seen potentials of the form $\mathcal{V}(\mathbf{x}, t)$ and their associated generalized force $f_i^V = \partial_i \mathcal{V}$. The time derivative of this potential is

$$\dot{\mathcal{V}} = \xi^i \underbrace{\partial_i \mathcal{V}}_{f_i^V} + \frac{\partial \mathcal{V}}{\partial t}. \quad (3.39)$$

The sum $\mathcal{W} = \mathcal{T} + \mathcal{V}$ is commonly called the *total energy*. Its time derivative is

$$\dot{\mathcal{W}} = \boldsymbol{\xi}^\top (\mathbf{f}^M + \mathbf{f}^V) + \sum_p \mathfrak{m}_p \langle \frac{\partial \mathbf{r}_p}{\partial t}, \ddot{\mathbf{r}}_p \rangle + \frac{\partial \mathcal{V}}{\partial t}. \quad (3.40)$$

Note that the equation of motion implies $\mathbf{f}^M + \mathbf{f}^V = \mathbf{f}^E - \mathbf{f}^D$.

A mechanical system is called scleronic (otherwise rheonomic) if it does not contain explicit time dependency. For this important case the change of total energy may be expressed by the external and dissipative forces alone

$$\dot{\mathcal{W}} = \boldsymbol{\xi}^\top (\mathbf{f}^E - \mathbf{f}^D). \quad (3.41)$$

Lagrangian and Hamiltonian. Define the *Lagrangian* as $\mathcal{L} = \mathcal{T} - \mathcal{V}$ which according to subsection 2.2.5 implies the generalized momentum and *Hamiltonian* as

$$p_i = \frac{\partial \mathcal{L}}{\partial \xi^i} = \sum_p \mathfrak{m}_p \langle \partial_i \mathbf{r}_p, \dot{\mathbf{r}}_p \rangle, \quad i = 1, \dots, n, \quad (3.42)$$

$$\mathcal{H} = p_i \xi^i - \mathcal{L} = \underbrace{\frac{1}{2} \sum_p \mathfrak{m}_p \|\dot{\mathbf{r}}_p\|^2}_{\mathcal{W}} + \mathcal{V} - \sum_p \mathfrak{m}_p \langle \frac{\partial \mathbf{r}_p}{\partial t}, \dot{\mathbf{r}}_p \rangle. \quad (3.43)$$

Extending the derivation from subsection 2.2.5 with the non-conservative forces \mathbf{f}^D and \mathbf{f}^E we find the change of the Hamiltonian along the solutions of the equations of motion as

$$\dot{\mathcal{H}} = \boldsymbol{\xi}^\top (\mathbf{f}^E - \mathbf{f}^D) - \frac{\partial \mathcal{L}}{\partial t} = \boldsymbol{\xi}^\top (\mathbf{f}^E - \mathbf{f}^D) - \sum_p \mathfrak{m}_p \langle \frac{\partial \dot{\mathbf{r}}_p}{\partial t}, \dot{\mathbf{r}}_p \rangle + \frac{\partial \mathcal{V}}{\partial t} \quad (3.44)$$

Note that for a scleronic system, the Hamiltonian \mathcal{H} coincides with the total energy \mathcal{W} .

3.3 A single free rigid body

Established textbooks on physics (e.g. [Goldstein, 1951, chap. 4], [Landau and Lifshitz, 1960, §31] or [Boltzmann, 1897, §44]) define a *rigid body* as a system of a *finite* number \mathfrak{N} particles such that the distances $d_{pq} = \|\mathbf{r}_p - \mathbf{r}_q\|$ between their positions \mathbf{r}_p are constant. Textbooks that are more focused on engineering like [Hamel, 1949, sec. 8, § 1], [Bremer, 2008, sec. 4.1] or [Roberson and Schwertassek, 1988, sec. 6.1.1] rather define a rigid body as a rigid volume over which mass is continuously distributed. Both modeling assumptions eventually lead to the same equations of motion when using the same generalized coordinates. They differ in the computation of the inertial parameters of total mass, center of mass and moment of inertia: The physics perspective uses a finite sum over the particles, whereas the engineering point of view requires an integral over the body volume. This work will consider a finite number of particles.

In contrast to the sources mentioned above, this section will investigate apart from inertia and gravitation, also stiffness and damping for a rigid body. In particular for the latter two parts, the model of concentrated particles is more intuitive in the authors humble opinion.

3.3.1 Coordinates

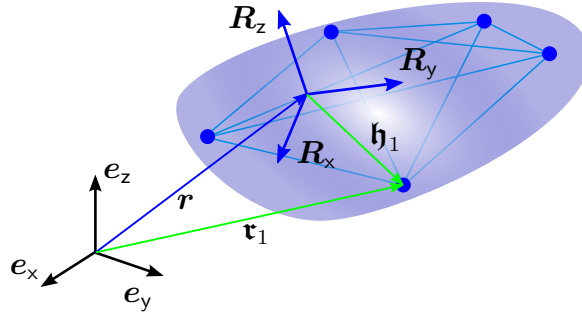


Figure 3.1: body fixed frame and particle positions

Body fixed frame. A common approach for modeling the rigid body (used in all sources above) is the use of a *body fixed frame*. This is the choice of a position $\mathbf{r} \in \mathbb{R}^3$ and a triple of orthonormal, right handed vectors $[\mathbf{R}_x, \mathbf{R}_y, \mathbf{R}_z] = \mathbf{R} \in \mathbb{SO}(3)$ which are rigidly attached to the body, i.e. move with it, see Figure 3.1. With this, the position of any particle of the body may then be written as

$$\mathbf{r}_p = \mathbf{r} + \mathbf{R}\mathbf{h}_p, \quad p = 1, \dots, \mathfrak{N} \quad (3.45)$$

where the relative particle positions $\mathbf{h}_p \in \mathbb{R}^3$ to the body fixed frame are *constant*. Consequently, the motion of the rigid body is completely captured by the position $\mathbf{r}(t) \in \mathbb{R}^3$ and orientation $\mathbf{R}(t) \in \mathbb{SO}(3)$ of the body fixed frame.

Usefulness of these particular coordinates. This is an example par excellence for the use of redundant parameters as discussed in the previous chapter: The system

of particles has \mathfrak{N} has $\nu = 3\mathfrak{N}$ coordinates, the coefficients of the particle positions $\mathbf{r}_p, p = 1, \dots, \mathfrak{N}$, and $c = \frac{1}{2}\mathfrak{N}(\mathfrak{N} - 1)$ fixing their distances to each other. Actually, just fixing the distances between the particles still allows a mirroring of the rigid body, which from a physical perspective is not permitted. To resolve this there should be additional constraints on the “handedness” of the particles. Even without the “handedness” constraints, the number of distance constraints c surpasses the number of coordinates ν for larger number of particles. Consequently, the distance constraints cannot be independent. All these issues discourage us from working with the particle positions as configuration parameters.

On the other hand, since the configuration space of the rigid body $\mathbb{X} \cong \mathbb{R}^3 \times \mathbb{SO}(3)$ contains $\mathbb{SO}(3)$, any set of $n = \dim \mathbb{X} = 6$ minimal generalized coordinates will lead to singularities as discussed in section 1.2.

This particular choice of coordinates (\mathbf{r}, \mathbf{R}) may be regarded as a trade-off between these two extremes: It uses a fixed number of $\nu = 12$ coordinates and constraints and respects the topology of the configuration space. Furthermore, the interpretation of \mathbf{r} and the columns of \mathbf{R} as a body fixed frame are quite intuitive for practical applications.

Velocity. For parameterization of the velocity of the rigid body, we will use the body fixed velocity $\mathbf{v}(t) \in \mathbb{R}^3$ and the angular velocity $\boldsymbol{\omega}(t) \in \mathbb{R}^3$ which are related to the configuration by

$$\dot{\mathbf{r}} = \mathbf{R}\mathbf{v}, \quad \dot{\mathbf{R}} = \mathbf{R} \text{wed}(\boldsymbol{\omega}). \quad (3.46)$$

With this we may express the velocity and accelerations of the body particles as

$$\dot{\mathbf{r}}_p = \mathbf{R}(\mathbf{v} - \text{wed}(\mathbf{h}_p)\boldsymbol{\omega}), \quad (3.47a)$$

$$\ddot{\mathbf{r}}_p = \mathbf{R}(\dot{\mathbf{v}} - \text{wed}(\mathbf{h}_p)\dot{\boldsymbol{\omega}} + \text{wed}(\boldsymbol{\omega})(\mathbf{v} - \text{wed}(\mathbf{h}_p)\boldsymbol{\omega})), \quad p = 1, \dots, \mathfrak{N} \quad (3.47b)$$

Compliance with the framework. In order to comply to the framework from the previous chapter we may group the configuration coordinates as $\mathbf{x} = [\mathbf{r}^\top, \mathbf{R}_x^\top, \mathbf{R}_y^\top, \mathbf{R}_z^\top]^\top \in \mathbb{X} \subset \mathbb{R}^{12}$ and their geometric constraint as $\phi(\mathbf{x}) = \mathbf{0}$ are the constraints of $\mathbb{SO}(3)$ as given in (2.6). The vector form of the kinematic relation (3.46) is

$$\underbrace{\begin{bmatrix} \dot{\mathbf{r}} \\ \dot{\mathbf{R}}_x \\ \dot{\mathbf{R}}_y \\ \dot{\mathbf{R}}_z \end{bmatrix}}_{\dot{\mathbf{x}}} = \underbrace{\begin{bmatrix} \mathbf{R}_x & \mathbf{R}_y & \mathbf{R}_z & \mathbf{0} & \mathbf{0} & \mathbf{0} \\ \mathbf{0} & \mathbf{0} & \mathbf{0} & \mathbf{0} & -\mathbf{R}_z & \mathbf{R}_y \\ \mathbf{0} & \mathbf{0} & \mathbf{0} & \mathbf{R}_z & \mathbf{0} & -\mathbf{R}_x \\ \mathbf{0} & \mathbf{0} & \mathbf{0} & -\mathbf{R}_y & \mathbf{R}_x & \mathbf{0} \end{bmatrix}}_A \underbrace{\begin{bmatrix} v_x \\ v_y \\ v_z \\ \omega_x \\ \omega_y \\ \omega_z \end{bmatrix}}_{\xi}. \quad (3.48)$$

Commutation coefficients. Plugging the kinematic matrix \mathbf{A} from (3.48) into the definition (2.19) of the commutation symbols γ yields

$$\begin{aligned} \gamma_{26}^1 &= \gamma_{53}^1 = \gamma_{34}^2 = \gamma_{61}^2 = \gamma_{15}^3 = \gamma_{42}^3 = \gamma_{56}^4 = \gamma_{64}^5 = \gamma_{45}^6 = 1, \\ \gamma_{62}^1 &= \gamma_{35}^1 = \gamma_{43}^2 = \gamma_{16}^2 = \gamma_{51}^3 = \gamma_{24}^3 = \gamma_{65}^4 = \gamma_{46}^5 = \gamma_{54}^6 = -1 \end{aligned} \quad (3.49)$$

and the remaining coefficients vanish. With this we have

$$[\gamma_{ij}^k \xi^j]_{i=1 \dots 6}^{k=1 \dots 6} = \begin{bmatrix} \text{wed}(\boldsymbol{\omega}) & 0 \\ \text{wed}(\mathbf{v}) & \text{wed}(\boldsymbol{\omega}) \end{bmatrix} = -\text{ad}_{\boldsymbol{\xi}}^{\top} \quad (3.50)$$

whose naming will be discussed later.

3.3.2 Inertia

The previous section derived several formulations for the generalized inertial force \mathbf{f}^M . These will now be applied to the the rigid body and the chosen coordinates.

Kinetic energy. With the particle velocities $\dot{\mathbf{r}}_p$ in terms of the chosen coordinates (3.47a) we obtain the kinetic energy \mathcal{T} of a free rigid body as

$$\begin{aligned} \mathcal{T} &= \frac{1}{2} \sum_p m_p \left\| \overbrace{\mathbf{R}(\mathbf{v} - \text{wed}(\mathbf{h}_p)\boldsymbol{\omega})}^{\dot{\mathbf{r}}_p} \right\|^2 \\ &= \frac{1}{2} \underbrace{\sum_p m_p \|\mathbf{v}\|^2}_{m} - \underbrace{\mathbf{v}^{\top} \sum_p m_p \text{wed}(\mathbf{h}_p) \boldsymbol{\omega}}_{m \text{wed}(\mathbf{s})} + \frac{1}{2} \underbrace{\boldsymbol{\omega}^{\top} \sum_p m_p \text{wed}(\mathbf{h}_p)^{\top} \text{wed}(\mathbf{h}_p) \boldsymbol{\omega}}_{\boldsymbol{\Theta}} \\ &= \frac{1}{2} \underbrace{[\mathbf{v}^{\top} \boldsymbol{\omega}^{\top}]}_{\boldsymbol{\xi}^{\top}} \underbrace{\begin{bmatrix} m\mathbf{I}_3 & m \text{wed}(\mathbf{s})^{\top} \\ m \text{wed}(\mathbf{s}) & \boldsymbol{\Theta} \end{bmatrix}}_{\mathbf{M}} \underbrace{[\mathbf{v} \ \boldsymbol{\omega}]}_{\boldsymbol{\xi}}. \end{aligned} \quad (3.51)$$

Here we have substituted some well established inertia parameters: the total mass m , the center of mass $\mathbf{s} = m^{-1} \sum_p m_p \mathbf{h}_p$ and the moment of inertia $\boldsymbol{\Theta} = \boldsymbol{\Theta}^{\top}$. Assuming that the particle masses are positive $m_p > 0, p = 1, \dots, \mathfrak{N}$ implies that the total mass is positive $m > 0$. Furthermore, if the rigid body has at least three particles that do not lie on a line, the inertia matrix is positive definite $\boldsymbol{\Theta} > 0$. It is important to notice that the inertia matrix \mathbf{M} for the chosen coordinates is *constant*¹.

Plugging the the kinetic energy (3.51) into the corresponding formulation (3.27) of the generalized inertia force and using the commutation symbols from (3.50) yields

$$\mathbf{f}^M = \underbrace{\begin{bmatrix} m\mathbf{I}_3 & m \text{wed}(\mathbf{s})^{\top} \\ m \text{wed}(\mathbf{s}) & \boldsymbol{\Theta} \end{bmatrix}}_{\mathbf{M}} \underbrace{[\dot{\mathbf{v}} \ \dot{\boldsymbol{\omega}}]}_{\boldsymbol{\xi}} + \underbrace{\begin{bmatrix} \text{wed}(\boldsymbol{\omega}) & 0 \\ \text{wed}(\mathbf{v}) & \text{wed}(\boldsymbol{\omega}) \end{bmatrix}}_{-\text{ad}_{\boldsymbol{\xi}}^{\top}} \underbrace{\begin{bmatrix} m\mathbf{I}_3 & m \text{wed}(\mathbf{s})^{\top} \\ m \text{wed}(\mathbf{s}) & \boldsymbol{\Theta} \end{bmatrix}}_{\mathbf{M}} \underbrace{[\mathbf{v} \ \boldsymbol{\omega}]}_{\boldsymbol{\xi}} \quad (3.52)$$

¹One reason for the choice of \mathbf{v} as velocity coordinates it the fact that the inertia matrix \mathbf{M} is *constant*. If we choose instead $\dot{\mathbf{r}}$ as velocity coordinates we have

$$\mathcal{T} = \frac{1}{2} [\dot{\mathbf{r}}^{\top}, \boldsymbol{\omega}^{\top}] \begin{bmatrix} m\mathbf{I}_3 & m\mathbf{R} \text{wed}(\mathbf{s})^{\top} \\ m \text{wed}(\mathbf{s})\mathbf{R}^{\top} & \boldsymbol{\Theta} \end{bmatrix} [\dot{\mathbf{r}} \ \boldsymbol{\omega}].$$

Obviously the body inertia matrix depends on the orientation \mathbf{R} of the body and is not constant unless the reference position \mathbf{r} coincides with the *center of mass*, i.e. $\mathbf{s} = 0$. Actually many textbooks, e.g. [Murray et al., 1994, p. 167] or [Shabana, 2005, p. 153], restrict to this case for their expressions of the kinetic energy. In the next section on rigid body systems we will see that it can be quite useful to use *geometrically* meaningful body fixed frames rather than restricting to the center of mass.

Acceleration energy. With the particle accelerations $\ddot{\mathbf{r}}_p$ in terms of the coordinates (3.47b) and using the Jacobi identity (2.57d) we find the acceleration energy \mathcal{S} for the free rigid body as

$$\begin{aligned}
\mathcal{S} &= \frac{1}{2} \sum_p m_p \left\| \overbrace{\mathbf{R}(\dot{\mathbf{v}} - \text{wed}(\mathbf{h}_p)\dot{\boldsymbol{\omega}} + \text{wed}(\boldsymbol{\omega})(\mathbf{v} - \text{wed}(\mathbf{h}_p)\boldsymbol{\omega}))}^{\ddot{\mathbf{r}}_p} \right\|^2 \\
&= \underbrace{\frac{1}{2} \sum_p m_p \|\dot{\mathbf{v}}\|^2}_{m} - \dot{\mathbf{v}}^\top \underbrace{\sum_p m_p \text{wed}(\mathbf{h}_p) \dot{\boldsymbol{\omega}}}_{m \text{ wed}(\mathbf{s})} + \underbrace{\frac{1}{2} \dot{\boldsymbol{\omega}}^\top \sum_p m_p \text{wed}(\mathbf{h}_p)^\top \text{wed}(\mathbf{h}_p) \dot{\boldsymbol{\omega}}}_{\boldsymbol{\Theta}} \\
&\quad + \dot{\mathbf{v}}^\top \text{wed}(\boldsymbol{\omega}) \left(\underbrace{\sum_p m_p \mathbf{v}}_{m} - \underbrace{\sum_p m_p \text{wed}(\mathbf{h}_p) \boldsymbol{\omega}}_{m \text{ wed}(\mathbf{s})} \right) \\
&\quad + \dot{\boldsymbol{\omega}}^\top \left(\underbrace{\sum_p m_p \text{wed}(\mathbf{h}_p)}_{m \text{ wed}(\mathbf{s})} \text{wed}(\boldsymbol{\omega}) \mathbf{v} + \text{wed}(\boldsymbol{\omega}) \underbrace{\sum_p m_p \text{wed}(\mathbf{h}_p)^\top \text{wed}(\mathbf{h}_p) \boldsymbol{\omega}}_{\boldsymbol{\Theta}} \right) \\
&\quad + \underbrace{\frac{1}{2} \sum_p m_p \|\text{wed}(\boldsymbol{\omega})\mathbf{v}\|^2}_{m} + \mathbf{v}^\top \text{wed}(\boldsymbol{\omega})^2 \underbrace{\sum_p m_p \text{wed}(\mathbf{h}_p) \boldsymbol{\omega}}_{m \text{ wed}(\mathbf{s})} \\
&\quad + \underbrace{\frac{1}{2} \text{tr} \left(\underbrace{\sum_p m_p \mathbf{h}_p \mathbf{h}_p^\top}_{\boldsymbol{\Theta}' = \frac{1}{2} \text{tr}(\boldsymbol{\Theta}) \mathbf{I}_3 - \boldsymbol{\Theta}'} \text{wed}(\boldsymbol{\omega})^4 \right)}_{(3.53)}
\end{aligned}$$

Not at all surprisingly, we found the same inertia parameters m , \mathbf{s} and $\boldsymbol{\Theta}$ as for the kinetic energy \mathcal{T} in (3.51). Collecting these further in the inertia matrix \mathbf{M} we have

$$\begin{aligned}
\mathcal{S} &= \frac{1}{2} \underbrace{[\dot{\mathbf{v}}^\top \dot{\boldsymbol{\omega}}^\top]}_{\dot{\boldsymbol{\xi}}^\top} \underbrace{\begin{bmatrix} m\mathbf{I}_3 & m \text{wed}(\mathbf{s})^\top \\ m \text{wed}(\mathbf{s}) & \boldsymbol{\Theta} \end{bmatrix}}_{\mathbf{M}} \underbrace{[\dot{\mathbf{v}} \dot{\boldsymbol{\omega}}]}_{\dot{\boldsymbol{\xi}}} \\
&\quad + \underbrace{[\dot{\mathbf{v}}^\top \dot{\boldsymbol{\omega}}^\top]}_{\dot{\boldsymbol{\xi}}^\top} \underbrace{\begin{bmatrix} \text{wed}(\boldsymbol{\omega}) & \mathbf{0} \\ \text{wed}(\mathbf{v}) & \text{wed}(\boldsymbol{\omega}) \end{bmatrix}}_{-\text{ad}_{\boldsymbol{\xi}}^\top} \underbrace{\begin{bmatrix} m\mathbf{I}_3 & m \text{wed}(\mathbf{s})^\top \\ m \text{wed}(\mathbf{s}) & \boldsymbol{\Theta} \end{bmatrix}}_{\mathbf{M}} \underbrace{[\mathbf{v} \boldsymbol{\omega}]}_{\boldsymbol{\xi}} \\
&\quad + \underbrace{\frac{1}{2} m \|\text{wed}(\boldsymbol{\omega})\mathbf{v}\|^2 + \mathbf{v}^\top \text{wed}(\boldsymbol{\omega})^2 m \text{wed}(\mathbf{s}) \boldsymbol{\omega} + \frac{1}{2} \text{tr} (\boldsymbol{\Theta}' \text{wed}(\boldsymbol{\omega})^4)}_{\mathcal{S}_0}. \quad (3.54)
\end{aligned}$$

Plugging this into the corresponding formulation (3.26) of the generalized inertia force, i.e. $\mathbf{f}^M = \partial \mathcal{S} / \partial \dot{\boldsymbol{\xi}}$, we obviously find the same expression as above (3.52). Note that \mathcal{S}_0 is independent of the generalized acceleration $\dot{\boldsymbol{\xi}}$ and consequently does not contribute to the inertia force.

Inertia matrix and connection coefficients. We can compute the Jacobian of the particle positions from

$$\boldsymbol{\nabla} \mathbf{r}_p = \left[\partial_i \mathbf{r}_p \right]_{i=1,\dots,6} = \left[\frac{\partial \mathbf{r}_p}{\partial \xi^i} \right]_{i=1,\dots,6} = \left[\frac{\partial}{\partial \xi^i} \right]^\top \overbrace{\mathbf{R}(\mathbf{v} - \text{wed}(\mathbf{h}_p)\boldsymbol{\omega})}^{\dot{\mathbf{r}}_p} = \mathbf{R} [\mathbf{I}_3 \text{ wed}(\mathbf{h}_p)^\top]. \quad (3.55)$$

With this, the rigid body inertia matrix may be written as

$$\begin{aligned} \mathbf{M} &= \left[\sum_p \mathfrak{m}_p \langle \partial_i \mathbf{r}_p, \partial_j \mathbf{r}_p \rangle \right]_{i,j=1,\dots,6} = \sum_p \mathfrak{m}_p (\nabla \mathbf{r}_p)^\top \nabla \mathbf{r}_p \\ &= \sum_p \mathfrak{m}_p \begin{bmatrix} \mathbf{I}_3 & \text{wed}(\mathbf{h}_p)^\top \\ \text{wed}(\mathbf{h}_p) & \text{wed}(\mathbf{h}_p) \text{wed}(\mathbf{h}_p)^\top \end{bmatrix} = \begin{bmatrix} m \mathbf{I}_3 & m \text{wed}(\mathbf{s})^\top \\ m \text{wed}(\mathbf{s}) & \boldsymbol{\Theta} \end{bmatrix} \end{aligned} \quad (3.56)$$

which obviously coincides with what we found from the kinetic energy (3.51) and from the acceleration energy (3.54).

As already pointed out above, for the chosen velocity coordinates $\xi = (\mathbf{v}, \boldsymbol{\omega})$, the coefficients of the rigid body inertia matrix M_{ij} are constant. Consequently, since $\partial_k M_{ij} \equiv 0$, the corresponding connection coefficients Γ_{ijk} only consist of the terms with the commutation coefficients γ :

$$\Gamma_{ijk} = \frac{1}{2} (\gamma_{ij}^s M_{sk} + \gamma_{ik}^s M_{sj} - \gamma_{jk}^s M_{si}) = -\Gamma_{jik}. \quad (3.57)$$

Using the commutation coefficients γ given in (3.49) and taking into account the skew symmetry above, the non-zero connection coefficients are

$$\Gamma_{324} = \Gamma_{135} = \Gamma_{216} = m, \quad (3.58a)$$

$$\Gamma_{254} = \Gamma_{364} = \Gamma_{515} = \Gamma_{616} = ms_x, \quad (3.58b)$$

$$\Gamma_{424} = \Gamma_{145} = \Gamma_{365} = \Gamma_{626} = ms_y, \quad (3.58c)$$

$$\Gamma_{434} = \Gamma_{535} = \Gamma_{146} = \Gamma_{256} = ms_z, \quad (3.58d)$$

$$\Gamma_{654} = \Theta'_{xx} = \frac{1}{2} (\Theta_{yy} + \Theta_{zz} - \Theta_{xx}), \quad (3.58e)$$

$$\Gamma_{465} = \Theta'_{yy} = \frac{1}{2} (\Theta_{xx} + \Theta_{zz} - \Theta_{yy}), \quad (3.58f)$$

$$\Gamma_{546} = \Theta'_{zz} = \frac{1}{2} (\Theta_{xx} + \Theta_{yy} - \Theta_{zz}), \quad (3.58g)$$

$$\Gamma_{464} = \Gamma_{655} = \Theta'_{xy} = -\Theta_{xy}, \quad (3.58h)$$

$$\Gamma_{544} = \Gamma_{656} = \Theta'_{xz} = -\Theta_{xz}, \quad (3.58i)$$

$$\Gamma_{545} = \Gamma_{466} = \Theta'_{yz} = -\Theta_{yz}. \quad (3.58j)$$

Note that the quantity $\boldsymbol{\Theta}' = \frac{1}{2} \text{tr}(\boldsymbol{\Theta}) \mathbf{I}_3 - \boldsymbol{\Theta}$ also appeared above in the formulation of the acceleration energy (3.53).

Finally, assembling the terms $f_i^M = M_{ij} \dot{\xi}^j + \Gamma_{ijk} \xi^j \xi^k$ we may check that this is indeed identical to (3.52).

3.3.3 Gravitation

The potential energy \mathcal{V}^G of a rigid body due to a gravitational acceleration \mathbf{a}_G according to (3.32) in terms of the chosen coordinates is

$$\mathcal{V}^G = \sum_p \overbrace{\langle \mathbf{r} + \mathbf{R} \mathbf{h}_p, -\mathfrak{m}_p \mathbf{a}_G \rangle}^{\mathfrak{r}_p} = - \underbrace{\langle \sum_p \mathfrak{m}_p \mathbf{r} + \mathbf{R} \sum_p \mathfrak{m}_p \mathbf{h}_p, \mathbf{a}_G \rangle}_{m \mathbf{s}} = -m \langle \mathbf{r} + \mathbf{R} \mathbf{s}, \mathbf{a}_G \rangle. \quad (3.59)$$

Note that the parameters of total mass m and center of mass \mathbf{s} are the same as found above for the inertia matrix. The resulting generalized force is

$$\mathbf{f}^G = \nabla \mathcal{V}^G = -m \begin{bmatrix} \mathbf{R}^\top \mathbf{a}_G \\ \text{wed}(\mathbf{s}) \mathbf{R}^\top \mathbf{a}_G \end{bmatrix}. \quad (3.60)$$

3.3.4 Stiffness

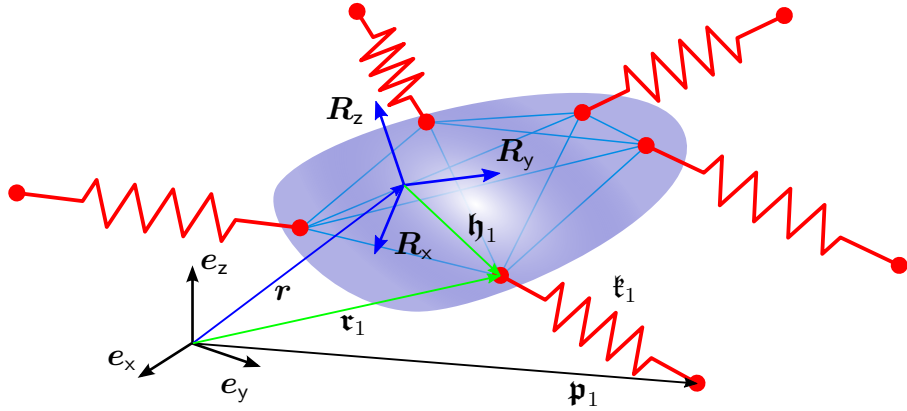


Figure 3.2: springs attached to a rigid body

Assume that every particle of the rigid body with position \mathbf{r}_p is connected to a position $\mathbf{p}_p \in \mathbb{R}^3$ by a linear spring with stiffness $\mathbf{k}_p \in \mathbb{R}^{(+)}$, see Figure 3.2. The resulting potential energy in terms of the rigid body coordinates $\mathbf{x} \cong (\mathbf{r}, \mathbf{R})$ is

$$\mathcal{V}^K(\mathbf{x}) = \frac{1}{2} \sum_p \mathbf{k}_p \|\mathbf{r} + \mathbf{R}\mathbf{h}_p - \mathbf{p}_p\|^2. \quad (3.61)$$

Stiffness parameters. Using the identities above we may rearrange (3.61) to

$$\begin{aligned} \mathcal{V}^K(\mathbf{x}) &= \frac{1}{2} \sum_p \mathbf{k}_p \|\mathbf{r} + \mathbf{R}\mathbf{h}_p - \mathbf{p}_p\|^2 \\ &= \frac{1}{2} \sum_p \mathbf{k}_p \left(\|\mathbf{r}\|^2 + \underbrace{\|\mathbf{R}\mathbf{h}_p\|^2}_{\text{const.}} + \underbrace{\|\mathbf{p}_p\|^2}_{\text{const.}} + 2\langle \mathbf{r}, \mathbf{R}\mathbf{h}_p \rangle - 2\langle \mathbf{r}, \mathbf{p}_p \rangle - 2\langle \mathbf{R}\mathbf{h}_p, \mathbf{p}_p \rangle \right) \\ &= \frac{1}{2} k \|\mathbf{r}\|^2 + k \langle \mathbf{r}, \mathbf{R}\mathbf{h} \rangle - k \langle \mathbf{r}, \mathbf{p} \rangle - \text{tr}(\mathbf{P}\mathbf{R}) + \underbrace{\frac{1}{2} \sum_p \mathbf{k}_p (\|\mathbf{h}_p\|^2 + \|\mathbf{p}_p\|^2)}_{\mathcal{V}_c^K = \text{const.}} \end{aligned} \quad (3.62)$$

with substitution of the constant parameters

$$k = \sum_p \mathbf{k}_p, \quad \mathbf{h} = k^{-1} \sum_p \mathbf{k}_p \mathbf{h}_p, \quad \mathbf{p} = k^{-1} \sum_p \mathbf{k}_p \mathbf{p}_p, \quad \mathbf{P} = \sum_p \mathbf{k}_p \mathbf{h}_p \mathbf{p}_p^\top. \quad (3.63)$$

Note that there was no specific assumption for the particle and spring distribution, i.e. on the values of \mathbf{h}_p , \mathbf{p}_p and \mathbf{k}_p . Consequently, any constellation may be captured by the $1 + 3 + 3 + 9 + 1 = 17$ parameters within $(k, \mathbf{h}, \mathbf{p}, \mathbf{P}, \mathcal{V}_c^K)$.

Critical points. The time derivatives of the potential may be written as

$$\begin{aligned} \frac{d}{dt}\mathcal{V}^K &= k\langle \mathbf{r}, \mathbf{Rv} \rangle + k\langle \mathbf{Rv}, \mathbf{Rh} \rangle + k\langle \mathbf{r}, \mathbf{R} \text{wed}(\boldsymbol{\omega})\mathbf{h} \rangle - k\langle \mathbf{Rv}, \mathbf{p} \rangle - \text{tr}(\mathbf{P}\mathbf{R} \text{wed}(\boldsymbol{\omega})) \\ &= \boldsymbol{\xi}^\top \underbrace{\left[\begin{array}{c} k(\mathbf{R}^\top(\mathbf{r} - \mathbf{p}) + \mathbf{h}) \\ k \text{wed}(\mathbf{h})\mathbf{R}^\top\mathbf{r} + \text{vee2}(\mathbf{P}\mathbf{R}) \end{array} \right]}_{\nabla\mathcal{V}^K} \quad (3.64) \end{aligned}$$

$$\frac{d^2}{dt^2}\mathcal{V}^K = \dot{\boldsymbol{\xi}}^\top \nabla\mathcal{V}^K + \boldsymbol{\xi}^\top \underbrace{\left[\begin{array}{cc} k\mathbf{I}_3 & k \text{wed}(\mathbf{R}^\top(\mathbf{r} - \mathbf{p})) \\ k \text{wed}(\mathbf{h}) & k \text{wed}(\mathbf{h}) \text{wed}(\mathbf{R}^\top\mathbf{r}) + \text{tr}(\mathbf{P}\mathbf{R})\mathbf{I}_3 - (\mathbf{P}\mathbf{R})^\top \end{array} \right]}_{\nabla^2\mathcal{V}^K} \boldsymbol{\xi} \quad (3.65)$$

We are interested in configurations $\mathbf{x}_R \cong (\mathbf{r}_R, \mathbf{R}_R)$ at which the potential is stationary $\nabla\mathcal{V}^K(\mathbf{x}_R) = \mathbf{0}$: From the upper part of (3.64) we get the condition

$$\mathbf{r}_R = \mathbf{p} - \mathbf{R}_R\mathbf{h}. \quad (3.66)$$

Plugging this into the lower part of (3.64) we obtain

$$k \text{wed}(\mathbf{h})\mathbf{R}_R^\top(\mathbf{p} - \mathbf{R}_R\mathbf{h}) + \text{vee2}(\mathbf{P}\mathbf{R}_R) = \text{vee2}(\underbrace{(\mathbf{P} - k\mathbf{h}\mathbf{p}^\top)\mathbf{R}_R}_{\mathbf{P}_s}) = \mathbf{0}. \quad (3.67)$$

The solution to this subproblem $\text{vee2}(\mathbf{P}_s\mathbf{R}_R) = \mathbf{0}, \mathbf{R}_R \in \mathbb{SO}(3)$ is discussed in great detail in section 2.4: Let $\mathbf{P}_s^\top = \mathbf{X} \text{Wed}(\boldsymbol{\Pi}_s)$ with $\mathbf{X} \in \mathbb{SO}(3), \boldsymbol{\Pi}_s \in \mathbb{SYM}_0^+(3)$ be a *special polar decomposition*. Then $\mathbf{R}_R = \mathbf{X}$ is clearly a critical point. Plugging $\mathbf{P} = \text{Wed}(\boldsymbol{\Pi}_s)\mathbf{R}_R^\top + k\mathbf{h}\mathbf{p}^\top$ into the Hessian matrix, we have

$$\begin{aligned} \nabla^2\mathcal{V}^K(\mathbf{x}_R) &= \begin{bmatrix} k\mathbf{I}_3 & k \text{wed}(\mathbf{h})^\top \\ k \text{wed}(\mathbf{h}) & \boldsymbol{\Pi}_s - k \text{wed}(\mathbf{h})^2 \end{bmatrix} \\ &= \begin{bmatrix} \mathbf{I}_3 & \mathbf{0} \\ \text{wed}(\mathbf{h}) & \mathbf{I}_3 \end{bmatrix} \begin{bmatrix} k\mathbf{I}_3 & \mathbf{0} \\ \mathbf{0} & \boldsymbol{\Pi}_s \end{bmatrix} \begin{bmatrix} \mathbf{I}_3 & \text{wed}(\mathbf{h})^\top \\ \mathbf{0} & \mathbf{I}_3 \end{bmatrix} \quad (3.68) \end{aligned}$$

By Sylvester's law of inertia, the definiteness of $\nabla^2\mathcal{V}^K(\mathbf{x}_R)$ coincides with the definiteness of $k \geq 0$ and $\boldsymbol{\Pi}_s \geq 0$. Using the results from section 2.4 we may conclude that \mathbf{x}_R is a minimum, and it is strict and global, if, and only if, $k > 0$ and $\boldsymbol{\Pi}_s > 0$.

Stiffness parameters cont'd. We may express the parameters \mathbf{p} and \mathbf{P} in terms of the minimum configuration $(\mathbf{r}_R, \mathbf{R}_R)$ and the matrix $\boldsymbol{\Pi}_s$ as

$$\mathbf{p} = \mathbf{r}_R + \mathbf{R}_R\mathbf{h}, \quad \mathbf{P} = \text{Wed}(\boldsymbol{\Pi}_s)\mathbf{R}_R^\top + k\mathbf{h}(\mathbf{r}_R + \mathbf{R}_R\mathbf{h})^\top \quad (3.69)$$

Plugging this into (3.62) we may reformulate the potential energy as

$$\begin{aligned} \mathcal{V}^K(\mathbf{x}) &= \frac{1}{2}k\|\mathbf{r}\|^2 + k\langle \mathbf{r}, \mathbf{Rv} \rangle - k\langle \mathbf{r}, \mathbf{r}_R + \mathbf{R}_R\mathbf{h} \rangle - k\langle \mathbf{r}_R + \mathbf{R}_R\mathbf{h}, \mathbf{Rh} \rangle \\ &\quad - \text{tr}(\text{Wed}(\boldsymbol{\Pi}_s)\mathbf{R}_R^\top\mathbf{R}) + \frac{1}{2}\sum_p \mathfrak{k}_p(\|\mathbf{h}_p\|^2 + \|\mathbf{p}_p\|^2) \\ &= \frac{1}{2}k\|\mathbf{r} + \mathbf{Rh} - (\mathbf{r}_R + \mathbf{R}_R\mathbf{h})\|^2 + \text{tr}(\text{Wed}(\boldsymbol{\Pi}_s)(\mathbf{I}_3 - \mathbf{R}_R^\top\mathbf{R})) \\ &\quad - \underbrace{\frac{1}{2}k\|\mathbf{r}_R + \mathbf{R}_R\mathbf{h}\|^2 - \frac{1}{2}k\|\mathbf{h}\|^2 - \text{tr}(\text{Wed}(\boldsymbol{\Pi}_s)) + \frac{1}{2}\sum_p \mathfrak{k}_p(\|\mathbf{h}_p\|^2 + \|\mathbf{p}_p\|^2)}_{\mathcal{V}_0^K = \mathcal{V}^K(\mathbf{x}_R)} \\ &= \frac{1}{2}k\|\mathbf{r} - \mathbf{r}_R\|^2 + k\langle \mathbf{r} - \mathbf{r}_R, (\mathbf{R} - \mathbf{R}_R)\mathbf{h} \rangle + \text{tr}(\text{Wed}(\boldsymbol{\Pi})(\mathbf{I}_3 - \mathbf{R}_R^\top\mathbf{R})) + \mathcal{V}_0^K \quad (3.70) \end{aligned}$$

where $\boldsymbol{\Pi} = \boldsymbol{\Pi}_s + k \text{wed}(\mathbf{h}) \text{wed}(\mathbf{h})^\top$ and \mathcal{V}_0^K is the minimal potential, i.e. the potential of the residual displacement of the springs at the minimum \mathbf{x}_R . The differential may be written as

$$\nabla \mathcal{V}^K(\mathbf{x}) = \begin{bmatrix} k \mathbf{R}^\top (\mathbf{r} - \mathbf{r}_R) + (\mathbf{I}_3 - \mathbf{R}^\top \mathbf{R}_R) k \mathbf{h} \\ k \text{wed}(\mathbf{h}) \mathbf{R}^\top (\mathbf{r} - \mathbf{r}_R) + \text{vee2}(\text{Wed}(\boldsymbol{\Pi}) \mathbf{R}_R^\top \mathbf{R}) \end{bmatrix}. \quad (3.71)$$

The Hessian at the minimum is

$$\nabla^2 \mathcal{V}^K(\mathbf{x}_R) = \begin{bmatrix} k \mathbf{I}_3 & k \text{wed}(\mathbf{h})^\top \\ k \text{wed}(\mathbf{h}) & \boldsymbol{\Pi} \end{bmatrix} \geq 0 \quad (3.72)$$

Conclusion. The conclusion of this subsection is that any constellation of linear springs attached to a rigid body may be captured by the potential \mathcal{V}^K from (3.70) and the resulting force $\mathbf{f}^K = \nabla \mathcal{V}^K$ from (3.71). It is parameterized by 6 parameters within $(\mathbf{r}_R, \mathbf{R}_R) \in \mathbb{R}^3 \times \mathbb{SO}(3)$ which describe the configuration at the minimum, the $1+3+6 = 10$ parameters within $k \in \mathbb{R}_0^+$, $\mathbf{h} \in \mathbb{R}^3$ and $\boldsymbol{\Pi} \in \mathbb{SYM}_0^+(3)$, and the minimum \mathcal{V}_0^K : $\mathcal{V}^K(\mathbf{x}) \geq \mathcal{V}_0^K \geq 0$. The minimum is strict and global if, and only if, $k > 0$ and $\boldsymbol{\Pi}_s = \boldsymbol{\Pi} - k \text{wed}(\mathbf{h}) \text{wed}(\mathbf{h})^\top > 0$.

The rigid body stiffness matrix $\mathbf{K} = \nabla^2 \mathcal{V}^K(\mathbf{x}_R)$ has the same structure as the inertia matrix $\mathbf{M} = \partial^2 \mathcal{T} / \partial \xi \partial \xi$ for the chosen coordinates. Due to these analogies to the established inertia parameters, we refer to the rigid body stiffness parameters in the following as: total stiffness k , center of stiffness \mathbf{h} , moment of stiffness $\boldsymbol{\Pi}$, and moment of stiffness at the center of stiffness $\boldsymbol{\Pi}_s$.

3.3.5 Dissipation

As motivated in the previous section we may motivate damping as particles moving within a viscous fluid which produce a drag force proportional to the particles velocity $\dot{\mathbf{r}}_p$. Different volumes of the particles may motivate different drag coefficients \mathfrak{d}_p , see Figure 3.3.

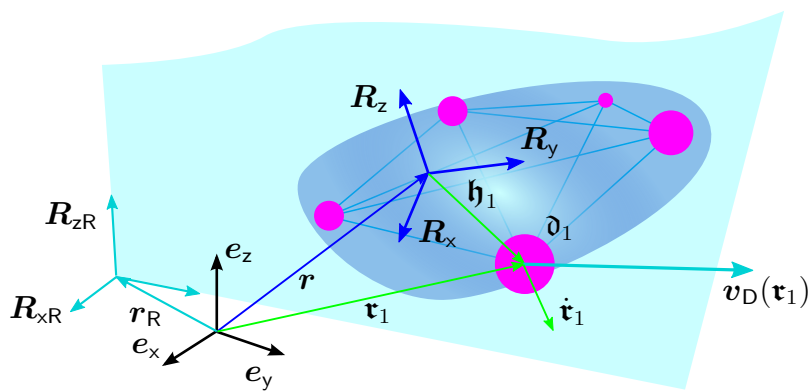


Figure 3.3: rigid body within viscous fluid

General fluid motion. Let the fluid at the position of p -th particle position have the velocity $\mathbf{v}_{Dp}(t) \in \mathbb{R}^3$ and let its drag coefficient be $\mathfrak{d}_p \in \mathbb{R}_0^+$. Overall, the dissipation function is

$$\begin{aligned}\mathcal{R} &= \frac{1}{2} \sum_p \mathfrak{d}_p \left\| \overbrace{\mathbf{R}(\mathbf{v} - \text{wed}(\mathbf{h}_p)\boldsymbol{\omega})}^{\mathbf{r}_p} - \mathbf{v}_{Dp} \right\|^2 \\ &= \frac{1}{2} \underbrace{\sum_p \mathfrak{d}_p \|\mathbf{v}\|^2}_{d} - \mathbf{v}^\top \underbrace{\sum_p \mathfrak{d}_p \text{wed}(\mathbf{h}_p)}_{d \text{ wed}(\mathbf{l})} \boldsymbol{\omega} + \frac{1}{2} \boldsymbol{\omega}^\top \underbrace{\sum_p \mathfrak{d}_p \text{wed}(\mathbf{h}_p)^\top \text{wed}(\mathbf{h}_p)}_{\mathbf{r}} \boldsymbol{\omega} \\ &\quad - \mathbf{v}^\top \sum_p \mathfrak{d}_p \mathbf{R}^\top \mathbf{v}_{Dp} + \boldsymbol{\omega}^\top \sum_p \mathfrak{d}_p \text{wed}(\mathbf{h}_p) \mathbf{R}^\top \mathbf{v}_{Dp} + \frac{1}{2} \sum_p \mathfrak{d}_p \|\mathbf{v}_{Dp}\|^2\end{aligned}\quad (3.73)$$

The resulting generalized force is

$$\mathbf{f}^D = \frac{\partial \mathcal{R}}{\partial \xi} = \underbrace{\begin{bmatrix} d\mathbf{I}_3 & d \text{ wed}(\mathbf{l})^\top \\ d \text{ wed}(\mathbf{l}) & \mathbf{r} \end{bmatrix}}_{\mathbf{D}} \underbrace{\begin{bmatrix} \mathbf{v} \\ \boldsymbol{\omega} \end{bmatrix}}_{\xi} + \sum_p \mathfrak{d}_p \begin{bmatrix} -\mathbf{I}_3 \\ \text{wed}(\mathbf{h}_p) \end{bmatrix} \mathbf{R}^\top \mathbf{v}_{Dp}. \quad (3.74)$$

Again we found parameters similar to the established inertia parameters. In analogy to them we call $d \in \mathbb{R}_0^+$ the total damping, $\mathbf{l} \in \mathbb{R}^3$ the center of damping, and $\mathbf{r} \in \text{SYM}_0^+(3)$ the moment of damping.

Rigid fluid motion. Let us consider a special case in which the fluid velocity also obeys a rigid body motion parameterized by $(\mathbf{r}_R, \mathbf{R}_R)$ and the velocity $(\mathbf{v}_R, \boldsymbol{\omega}_R)$, see Figure 3.3. The absolute fluid velocity at the particle position is then $\mathbf{v}_{Dp} = \mathbf{R}_R(\mathbf{v}_R + \text{wed}(\boldsymbol{\omega}_R)\mathbf{R}_R^\top(\mathbf{r}_p - \mathbf{r}_R))$. The we have the dissipation function

$$\begin{aligned}\mathcal{R} &= \frac{1}{2} \sum_p \mathfrak{d}_p \left\| \overbrace{\mathbf{R}(\mathbf{v} - \text{wed}(\mathbf{h}_p)\boldsymbol{\omega})}^{\mathbf{r}_p} - \overbrace{\mathbf{R}_R(\mathbf{v}_R + \text{wed}(\boldsymbol{\omega}_R)\mathbf{R}_R^\top(\mathbf{r} + \mathbf{R}\mathbf{h}_p - \mathbf{r}_R))}^{\mathbf{v}_{Dp}} \right\|^2 \\ &= \frac{1}{2} \sum_p \mathfrak{d}_p \left\| \underbrace{\mathbf{v} - \mathbf{R}^\top(\mathbf{R}_R \mathbf{v}_R - \text{wed}(\mathbf{r} - \mathbf{r}_R) \mathbf{R}_R \boldsymbol{\omega}_R)}_{\mathbf{v}_E} - \text{wed}(\mathbf{h}_p) \underbrace{(\boldsymbol{\omega} - \mathbf{R}^\top \mathbf{R}_R \boldsymbol{\omega}_R)}_{\boldsymbol{\omega}_E} \right\|^2 \\ &= \frac{1}{2} \underbrace{[\mathbf{v}_E^\top, \boldsymbol{\omega}_E^\top]}_{\xi_E^\top} \underbrace{\begin{bmatrix} d\mathbf{I}_3 & d \text{ wed}(\mathbf{l})^\top \\ d \text{ wed}(\mathbf{l}) & \mathbf{r} \end{bmatrix}}_{\mathbf{D}} \underbrace{\begin{bmatrix} \mathbf{v}_E \\ \boldsymbol{\omega}_E \end{bmatrix}}_{\xi_E}\end{aligned}\quad (3.75)$$

The resulting generalized force is

$$\mathbf{f}^D = \frac{\partial \mathcal{R}}{\partial \xi} = \frac{\partial \mathcal{R}}{\partial \xi_E} = \mathbf{D} \xi_E \quad (3.76)$$

3.3.6 Summary and the special Euclidean group

Special Euclidean group. Instead of collecting the configuration coordinates in a tuple $\mathbf{x} = [\mathbf{r}^\top, \mathbf{R}_x^\top, \mathbf{R}_y^\top, \mathbf{R}_z^\top]^\top \in \mathbb{X}$ as proposed in the previous chapter, it can also be useful to arrange them within a matrix:

$$\mathbf{G} = \begin{bmatrix} \mathbf{R} & \mathbf{r} \\ \mathbf{0} & 1 \end{bmatrix} \in \text{SE}(3) = \left\{ \begin{bmatrix} \mathbf{R} & \mathbf{r} \\ \mathbf{0} & 1 \end{bmatrix} \mid \mathbf{r} \in \mathbb{R}^3, \mathbf{R} \in \text{SO}(3) \right\} \quad (3.77)$$

which is commonly referred to as the *homogeneous representation*, e.g. [Murray et al., 1994, sec. 2.3.1]. The set $\mathbb{SE}(3)$ combined with matrix multiplication forms a Lie group which is called the *special Euclidean group*. Euclidean denotes to the fact that its transformations preserve the Euclidean distance, while special denotes to the fact that it does not permit reflections (analog to the special orthogonal group $\mathbb{SO}(3)$).

Operators. This section already used the wed on \mathbb{R}^3 quite extensively. On \mathbb{R}^6 we define it as

$$\text{wed} : \mathbb{R}^3 \rightarrow \mathfrak{so}(3) : \begin{bmatrix} \omega_1 \\ \omega_2 \\ \omega_3 \end{bmatrix} \mapsto \begin{bmatrix} 0 & -\omega_3 & \omega_2 \\ \omega_3 & 0 & -\omega_1 \\ -\omega_2 & \omega_1 & 0 \end{bmatrix} \quad (3.78a)$$

$$\text{wed} : \mathbb{R}^6 \rightarrow \mathfrak{se}(3) : \begin{bmatrix} \mathbf{v} \\ \boldsymbol{\omega} \end{bmatrix} \mapsto \begin{bmatrix} \text{wed } \boldsymbol{\omega} & \mathbf{v} \\ \mathbf{0} & 0 \end{bmatrix} \quad (3.78b)$$

Its inverse is denoted vee(\cdot), i.e. $\text{vee}(\text{wed}(\boldsymbol{\xi})) = \boldsymbol{\xi}$. The wed and vee operators are well established in the literature, see e.g. [Murray et al., 1994, sec. 2.3.2].

Using the wed operator may rewrite the rigid body kinematics from (3.46) in matrix form as:

$$\underbrace{\begin{bmatrix} \dot{\mathbf{R}} & \dot{\mathbf{r}} \\ \mathbf{0} & 0 \end{bmatrix}}_{\dot{\mathbf{G}}} = \underbrace{\begin{bmatrix} \mathbf{R} & \mathbf{r} \\ \mathbf{0} & 1 \end{bmatrix}}_{\mathbf{G}} \underbrace{\begin{bmatrix} \text{wed}(\boldsymbol{\omega}) & \mathbf{v} \\ \mathbf{0} & 0 \end{bmatrix}}_{\text{wed}(\boldsymbol{\xi})} \quad (3.79)$$

More operators. The following operators are not established in the literature, but will prove quite useful for this work. Define the vee2 operator through

$$\text{tr}(\mathbf{A}(\text{wed } \boldsymbol{\xi})^\top) = \boldsymbol{\xi}^\top \text{vee2}(\mathbf{A}), \quad (3.80)$$

this is

$$\text{vee2} : \mathbb{R}^{3 \times 3} \rightarrow \mathbb{R}^3 : \mathbf{A} \mapsto \text{vee}(\mathbf{A} - \mathbf{A}^\top) \quad (3.81a)$$

$$\text{vee2} : \mathbb{R}^{4 \times 4} \rightarrow \mathbb{R}^6 : \begin{bmatrix} \mathbf{A} & \mathbf{b} \\ * & * \end{bmatrix} \mapsto \begin{bmatrix} \mathbf{b} \\ \text{vee2 } \mathbf{A} \end{bmatrix}. \quad (3.81b)$$

Note that for $\boldsymbol{\Omega} \in \mathfrak{so}(3) \subset \mathbb{R}^{3 \times 3}$ we have $\text{vee2}(\boldsymbol{\Omega}) = 2 \text{vee}(\boldsymbol{\Omega})$, thus giving the motivation for the name. Define the Vee operator through

$$\text{tr}(\text{wed } \boldsymbol{\xi} \mathbf{A}(\text{wed } \boldsymbol{n})^\top) = \boldsymbol{n}^\top (\text{Vee } \mathbf{A}) \boldsymbol{\xi}, \quad (3.82)$$

this is

$$\text{Vee} : \mathbb{R}^{3 \times 3} \rightarrow \mathbb{R}^{3 \times 3} : \mathbf{A} \mapsto \text{tr}(\mathbf{A}) \mathbf{I}_3 - \mathbf{A} \quad (3.83a)$$

$$\text{Vee} : \mathbb{R}^{4 \times 4} \rightarrow \mathbb{R}^{6 \times 6} : \begin{bmatrix} \mathbf{A} & \mathbf{b} \\ \mathbf{c}^\top & d \end{bmatrix} \mapsto \begin{bmatrix} d \mathbf{I}_3 & (\text{wed } \mathbf{b})^\top \\ \text{wed } \mathbf{c} & \text{Vee } \mathbf{A} \end{bmatrix}. \quad (3.83b)$$

Let Wed(\cdot) denote its inverse. Combining the definitions (3.82) and (3.80) also yields

$$\text{vee2}(\text{wed } \boldsymbol{\xi} \mathbf{A}) = \text{Vee}(\mathbf{A}) \boldsymbol{\xi} \quad (3.84)$$

Adjoint representation. Define

$$\mathbf{G} = \begin{bmatrix} \mathbf{R} & \mathbf{r} \\ \mathbf{0} & 1 \end{bmatrix} : \quad \text{Ad}_{\mathbf{G}} = \begin{bmatrix} \mathbf{R} & \text{wed}(\mathbf{r})\mathbf{R} \\ \mathbf{0} & \mathbf{R} \end{bmatrix} \quad (3.85a)$$

$$\boldsymbol{\xi} = \begin{bmatrix} \mathbf{v} \\ \boldsymbol{\omega} \end{bmatrix} : \quad \text{ad}_{\boldsymbol{\xi}} = \begin{bmatrix} \text{wed}(\boldsymbol{\omega}) & \text{wed}(\mathbf{v}) \\ \mathbf{0} & \text{wed}(\boldsymbol{\omega}) \end{bmatrix} \quad (3.85b)$$

The notation is due to the established notation for the *adjoint representation* for Lie groups and their associated Lie algebras, see e.g. [Hall, 2015, Def. 3.32 & 3.7]. Using this background we have the obvious relations:

$$\text{Ad}_{\mathbf{G}_1}\mathbf{G}_2 = \text{Ad}_{\mathbf{G}_1}\text{Ad}_{\mathbf{G}_2}, \quad \text{Ad}_{\mathbf{G}}^{-1} = \text{Ad}_{\mathbf{G}^{-1}}, \quad \text{Ad}_{\mathbf{I}_4} = \mathbf{I}_6, \quad (3.86a)$$

$$\text{ad}_{\boldsymbol{\xi}_1}\boldsymbol{\xi}_2 = -\text{ad}_{\boldsymbol{\xi}_2}\boldsymbol{\xi}_1, \quad \text{ad}_{\boldsymbol{\xi}}\boldsymbol{\xi} = \mathbf{0}. \quad (3.86b)$$

Furthermore, for $\frac{d}{dt}\mathbf{G} = \mathbf{G} \text{ wed}(\boldsymbol{\xi})$ we have

$$\frac{d}{dt}\text{Ad}_{\mathbf{G}} = \text{Ad}_{\mathbf{G}}\text{ad}_{\boldsymbol{\xi}}. \quad (3.87)$$

Though the Lie group theory can be extremely useful for rigid body mechanics, for this work it is sufficient to regard $\text{Ad}_{(.)}$ and $\text{ad}_{(.)}$ as simple algebraic operators with the identities (3.86).

Rigid body energies. Notice that for $\mathbf{x}, \mathbf{h}_p \in \mathbb{R}^n, \mathbf{X} \in \mathbb{R}^{n \times n}$ we have

$$\begin{aligned} \sum_p \mathfrak{m}_p \|\mathbf{x} + \mathbf{X}\mathbf{h}_p\|^2 &= \sum_p \mathfrak{m}_p \text{tr}((\mathbf{x} + \mathbf{X}\mathbf{h}_p)(\mathbf{x} + \mathbf{X}\mathbf{h}_p)^\top) \\ &= \sum_p \mathfrak{m}_p \text{tr}\left(\left(\begin{bmatrix} \mathbf{X} & \mathbf{x} \\ \mathbf{0} & 0 \end{bmatrix} \begin{bmatrix} \mathbf{h}_p \\ 1 \end{bmatrix}\right) \left(\begin{bmatrix} \mathbf{X} & \mathbf{x} \\ \mathbf{0} & 0 \end{bmatrix} \begin{bmatrix} \mathbf{h}_p \\ 1 \end{bmatrix}\right)^\top\right) \\ &= \text{tr}\left(\underbrace{\begin{bmatrix} \mathbf{X} & \mathbf{x} \\ \mathbf{0} & 0 \end{bmatrix}}_{\Xi} \underbrace{\left(\sum_p \mathfrak{m}_p \begin{bmatrix} \mathbf{h}_p \mathbf{h}_p^\top & \mathbf{h}_p^\top \\ \mathbf{h}_p & 1 \end{bmatrix}\right)}_{\mathbf{M}'} \underbrace{\begin{bmatrix} \mathbf{X}^\top & \mathbf{0} \\ \mathbf{x}^\top & 0 \end{bmatrix}}_{\Xi^\top}\right) \\ &= \|\Xi^\top\|_{\mathbf{M}'}^2 \end{aligned} \quad (3.88)$$

with the weighted Frobenius norm motivated in (2.48). Furthermore, for the special case $\Xi = \text{wed } \boldsymbol{\xi}$ we have due to (3.82):

$$\|\text{wed}(\boldsymbol{\xi})^\top\|_{\mathbf{M}'}^2 = \|\boldsymbol{\xi}\|_{\text{Vee } \mathbf{M}'}^2, \quad (3.89)$$

Using this, we may rewrite the kinetic energy \mathcal{T} of a free rigid body (3.51), the acceleration energy \mathcal{S} from (3.53), the dissipation function \mathcal{R} in (3.75), the potential energy \mathcal{V} due to linear springs (3.70) and the potential energy \mathcal{V}^G due to earth's gravitation from (3.59)

as

$$\mathcal{T} = \frac{1}{2} \sum_p \mathfrak{m}_p \left\| \overbrace{\dot{\mathbf{r}} + \dot{\mathbf{R}} \mathfrak{h}_p}^{\mathfrak{t}_p} \right\|^2 = \frac{1}{2} \|\dot{\mathbf{G}}^\top\|_{\mathbf{M}'}^2 = \frac{1}{2} \|\boldsymbol{\xi}\|_{\mathbf{M}}^2 \quad (3.90a)$$

$$\mathcal{T}^G = \frac{1}{2} \sum_p \mathfrak{m}_p \left\| \overbrace{\dot{\mathbf{r}} + \dot{\mathbf{R}} \mathfrak{h}_p}^{\mathfrak{t}_p} - \mathbf{a}_G t \right\|^2 = \frac{1}{2} \|(\dot{\mathbf{G}} - \text{wed}(\boldsymbol{\alpha}_G t))^\top\|_{\mathbf{M}'}^2 \quad \boldsymbol{\alpha}_G = \begin{bmatrix} \mathbf{a}_G \\ \mathbf{0}_{3 \times 1} \end{bmatrix} \quad (3.90b)$$

$$\mathcal{S} = \frac{1}{2} \sum_p \mathfrak{m}_p \left\| \overbrace{\ddot{\mathbf{r}} + \ddot{\mathbf{R}} \mathfrak{h}_p}^{\mathfrak{t}_p} \right\|^2 = \frac{1}{2} \|\ddot{\mathbf{G}}^\top\|_{\mathbf{M}'}^2 \quad (3.90c)$$

$$\mathcal{S}^G = \frac{1}{2} \sum_p \mathfrak{m}_p \left\| \overbrace{\ddot{\mathbf{r}} + \ddot{\mathbf{R}} \mathfrak{h}_p}^{\mathfrak{t}_p} - \mathbf{a}_G \right\|^2 = \frac{1}{2} \|(\ddot{\mathbf{G}} - \text{wed}(\boldsymbol{\alpha}_G))^\top\|_{\mathbf{M}'}^2 \quad (3.90d)$$

$$\mathcal{R} = \frac{1}{2} \sum_p \mathfrak{d}_p \left\| \overbrace{\dot{\mathbf{r}} + \dot{\mathbf{R}} \mathfrak{h}_p}^{\mathfrak{t}_p} \right\|^2 = \frac{1}{2} \|\dot{\mathbf{G}}^\top\|_{\mathbf{D}'}^2 = \frac{1}{2} \|\boldsymbol{\xi}\|_{\mathbf{D}}^2 \quad (3.90e)$$

$$\mathcal{V}^K = \frac{1}{2} \sum_p \mathfrak{k}_p \left\| \overbrace{\mathbf{r} + \mathbf{R} \mathfrak{h}_p}^{\mathfrak{r}_p} - \overbrace{(\mathbf{r}_R + \mathbf{R}_R \mathfrak{h}_p)}^{\mathfrak{r}_{pR}} \right\|^2 = \frac{1}{2} \|(\mathbf{G} - \mathbf{G}_R)^\top\|_{\mathbf{K}'}^2 \quad (3.90f)$$

$$\mathcal{V}^G = \sum_p \langle \overbrace{\mathbf{r} + \mathbf{R} \mathfrak{h}_p}^{\mathfrak{r}_p}, -\mathfrak{m}_p \mathbf{a}_G \rangle = \langle \mathbf{G}^\top, \text{wed}(-\boldsymbol{\alpha}_G)^\top \rangle_{\mathbf{M}'}, \quad (3.90g)$$

where

$$\mathbf{M}' = \sum_p \mathfrak{m}_p \begin{bmatrix} \mathfrak{h}_p \mathfrak{h}_p^\top & \mathfrak{h}_p^\top \\ \mathfrak{h}_p & 1 \end{bmatrix} = \begin{bmatrix} \boldsymbol{\Theta}' & m\mathbf{s} \\ m\mathbf{s}^\top & m \end{bmatrix} = \text{Wed}(\mathbf{M}) \quad (3.91a)$$

$$\mathbf{D}' = \sum_p \mathfrak{d}_p \begin{bmatrix} \mathfrak{h}_p \mathfrak{h}_p^\top & \mathfrak{h}_p^\top \\ \mathfrak{h}_p & 1 \end{bmatrix} = \begin{bmatrix} \boldsymbol{\Upsilon}' & d\mathbf{l} \\ d\mathbf{l}^\top & d \end{bmatrix} = \text{Wed}(\mathbf{D}) \quad (3.91b)$$

$$\mathbf{K}' = \sum_p \mathfrak{k}_p \begin{bmatrix} \mathfrak{h}_p \mathfrak{h}_p^\top & \mathfrak{h}_p^\top \\ \mathfrak{h}_p & 1 \end{bmatrix} = \begin{bmatrix} \boldsymbol{\Pi}' & k\mathbf{h} \\ k\mathbf{h}^\top & k \end{bmatrix} = \text{Wed}(\mathbf{K}) \quad (3.91c)$$

Note that m , $m\mathbf{s}$ and $\boldsymbol{\Theta}'$ correspond to the zeroth, first and second *mathematical moments* of the distribution $\mathfrak{m}_p \mathfrak{h}_p$, $p = 1, \dots, \mathfrak{N}$. Their collection in the matrix $\mathbf{M}' \in \text{SYM}(4)$ is bijective to the previously encountered inertia matrix $\mathbf{M}' = \text{Wed}(\mathbf{M}) \Leftrightarrow \mathbf{M} = \text{Vee}(\mathbf{M}')$. Obviously, the same holds for the damping \mathbf{K}' and stiffness matrix \mathbf{D}' .

Rigid body forces. The corresponding forces forces which were already derived in the previous subsections can be written in a more compact form:

$$\mathbf{f}^M = \frac{\partial \mathcal{S}}{\partial \dot{\boldsymbol{\xi}}} = \text{vee2}((\text{wed}(\dot{\boldsymbol{\xi}}) + \text{wed}(\boldsymbol{\xi})^2)\mathbf{M}') = \mathbf{M}\dot{\boldsymbol{\xi}} - \text{ad}_{\boldsymbol{\xi}}^\top \mathbf{M}\boldsymbol{\xi} \quad (3.92a)$$

$$\mathbf{f}^D = \frac{\partial \mathcal{R}}{\partial \dot{\boldsymbol{\xi}}} = \text{vee2}(\text{wed}(\boldsymbol{\xi})\mathbf{D}') = \mathbf{D}\dot{\boldsymbol{\xi}} \quad (3.92b)$$

$$\mathbf{f}^K = \nabla \mathcal{V}^K = \text{vee2}((\mathbf{I}_4 - \mathbf{G}^{-1}\mathbf{G}_R)\mathbf{K}') \quad (3.92c)$$

$$\mathbf{f}^G = \nabla \mathcal{V}^G = \text{vee2}(\mathbf{G}^\top \text{wed}(-\boldsymbol{\alpha}_G)\mathbf{M}') = -\mathbf{M}\text{Ad}_{\mathbf{G}}^{-1}\boldsymbol{\alpha}_G. \quad (3.92d)$$

Equation of motion. Combining the results above, the equations of motion of a free rigid body subject to inertia, gravity, viscous friction, linear springs and a generalized force \mathbf{f}^E may be written as

$$\dot{\mathbf{G}} = \mathbf{G} \text{ wed}(\boldsymbol{\xi}), \quad (3.93a)$$

$$\dot{\boldsymbol{\xi}} = \text{Ad}_{\mathbf{G}}^{-1} \boldsymbol{\alpha}_G + \mathbf{M}^{-1} (\mathbf{f}^E + (\text{ad}_{\boldsymbol{\xi}}^\top \mathbf{M} - \mathbf{D}) \boldsymbol{\xi} - \text{vee2}((\mathbf{I}_4 - \mathbf{G}^{-1} \mathbf{G}_R) \mathbf{K}')). \quad (3.93b)$$

There are three sets of ingredients:

- The chosen coordinates are collected within $\mathbf{G}(t) \in \mathbb{SE}(3)$ and $\boldsymbol{\xi}(t) \in \mathbb{R}^6$.
- The matrices $\mathbf{M}', \mathbf{D}', \mathbf{K}' \in \mathbb{SYM}(4)$ capture the distribution of mass, damping and stiffness.
- External influences are collected within the gravity wrench $\boldsymbol{\alpha}_G^\top = [\mathbf{a}_G^\top, \mathbf{0}_{1 \times 3}]$, the equilibrium configuration of the springs $\mathbf{G}_R(t) \in \mathbb{SE}(3)$ and the generalized external force $\mathbf{f}^E(t) \in \mathbb{R}^6$.

3.4 Rigid body systems

A rigid body system is a system of $N \geq 1$ rigid bodies which may be constrained to each other and/or to the surrounding space. As before, this section restricts to geometric constraints.

There are many established textbooks on this subject e.g. [Roberson and Schwertassek, 1988], [Murray et al., 1994], [Kane and Levinson, 1985]. However, all these excellent texts restrict to *minimal* generalized coordinates or are even more restrictive by requiring Denavit–Hartenberg parameters [Denavit and Hartenberg, 1955]. While this is just fine when dealing only with one-dimensional joints, it may be too restrictive when dealing with multidimensional joints as e.g. mobile robots. Furthermore, the texts mentioned above mostly focus on inertia but not dissipation and stiffness.

This section deals with the derivation of equations of motion for rigid body systems subject to inertia, gravity, linear springs and viscous friction. It allows for a quite general parameterization as motivated in the previous sections.

3.4.1 Parameterization

Configuration coordinates. As motivated for the single rigid body, let there be a body fixed frame for each body of the system as illustrated in Figure 3.4. The components of the position of the b -th body w.r.t. the inertial frame are ${}_b^0\mathbf{r} \in \mathbb{R}^3$ and the components of its attitude are ${}_b^0\mathbf{R} = [{}^0_b\mathbf{R}_x, {}^0_b\mathbf{R}_y, {}^0_b\mathbf{R}_z] \in \mathbb{SO}(3)$.

The configuration can also be expressed w.r.t. any other body: ${}_b^a\mathbf{r}$ is the position of the b -th frame w.r.t. the frame of the a -th body and analog of the attitude ${}_b^a\mathbf{R}$. The left side indices are used for readability but also to emphasize their different nature compared

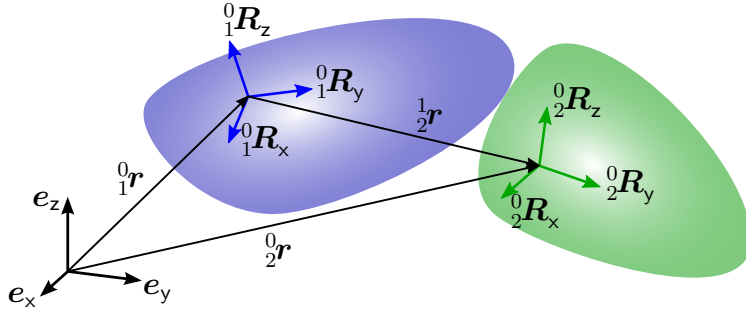


Figure 3.4: reference frame and body fixed frames

to the right side indices. The sum convention does not apply to these indices. For the positions and attitudes we have the following relations

$${}_c^a \mathbf{r} = {}_b^a \mathbf{r} + {}_b^a \mathbf{R} {}_c^b \mathbf{r}, \quad {}_c^a \mathbf{R} = {}_b^a \mathbf{R} {}_c^b \mathbf{R}, \quad (3.94a)$$

$${}^b_a \mathbf{r} = - {}_a^b \mathbf{R}^\top {}_b^a \mathbf{r}, \quad {}_a^b \mathbf{R} = {}_b^a \mathbf{R}^\top, \quad (3.94b)$$

$${}^a_a \mathbf{r} = \mathbf{0}, \quad {}_a^a \mathbf{R} = \mathbf{I}_3, \quad a, b, c = 0, \dots, N. \quad (3.94c)$$

As motivated in the previous section, it will be convenient to merge position ${}_b^a \mathbf{r} \in \mathbb{R}^3$ and rotation matrix ${}_b^a \mathbf{R} \in \mathbb{SO}(3)$ into the (rigid body) configuration matrix

$${}_b^a \mathbf{G} = \begin{bmatrix} {}_b^a \mathbf{R} & {}_b^a \mathbf{r} \\ 0 & 1 \end{bmatrix} \in \mathbb{SE}(3). \quad (3.95)$$

Then (3.94) is equivalent to

$${}_c^a \mathbf{G} = {}_b^a \mathbf{G} {}_c^b \mathbf{G}, \quad (3.96a)$$

$${}^b_a \mathbf{G} = {}_a^b \mathbf{G}^{-1}, \quad (3.96b)$$

$${}^a_a \mathbf{G} = \mathbf{I}_4, \quad a, b, c = 0, \dots, N. \quad (3.96c)$$

For a system of N body fixed frames and a reference frame there are $(N + 1)^2$ transformations, but due to the rules (3.96), only N of them can be independent. So, a RBS can have at most $6N$ degrees of freedom, which is only the case if there are no constraints (like joints) between the bodies. Constraints of a joint between body a and b can be captured inside the corresponding transformation ${}_b^a \mathbf{G}$. We will discuss this in the following example.

Example 6. Tricopter with suspended load: configuration. Consider the Tricopter with a suspended load as shown in Figure 3.5. The top part of the figure shows the body fixed frames which are attached to geometrically meaningful points. The numbering of the bodies is rather arbitrary.

The Tricopter flies freely in space, i.e. there are no constraints between the reference frame and any body of the system. So we chose to describe the configuration of the central body w.r.t. the reference frame as

$${}_1^0 \mathbf{G} = \begin{bmatrix} {}_1^0 R_x^x & {}_1^0 R_y^x & {}_1^0 R_z^x & {}_1^0 r^x \\ {}_1^0 R_x^y & {}_1^0 R_y^y & {}_1^0 R_z^y & {}_1^0 r^y \\ {}_1^0 R_x^z & {}_1^0 R_y^z & {}_1^0 R_z^z & {}_1^0 r^z \\ 0 & 0 & 0 & 1 \end{bmatrix}. \quad (3.97a)$$

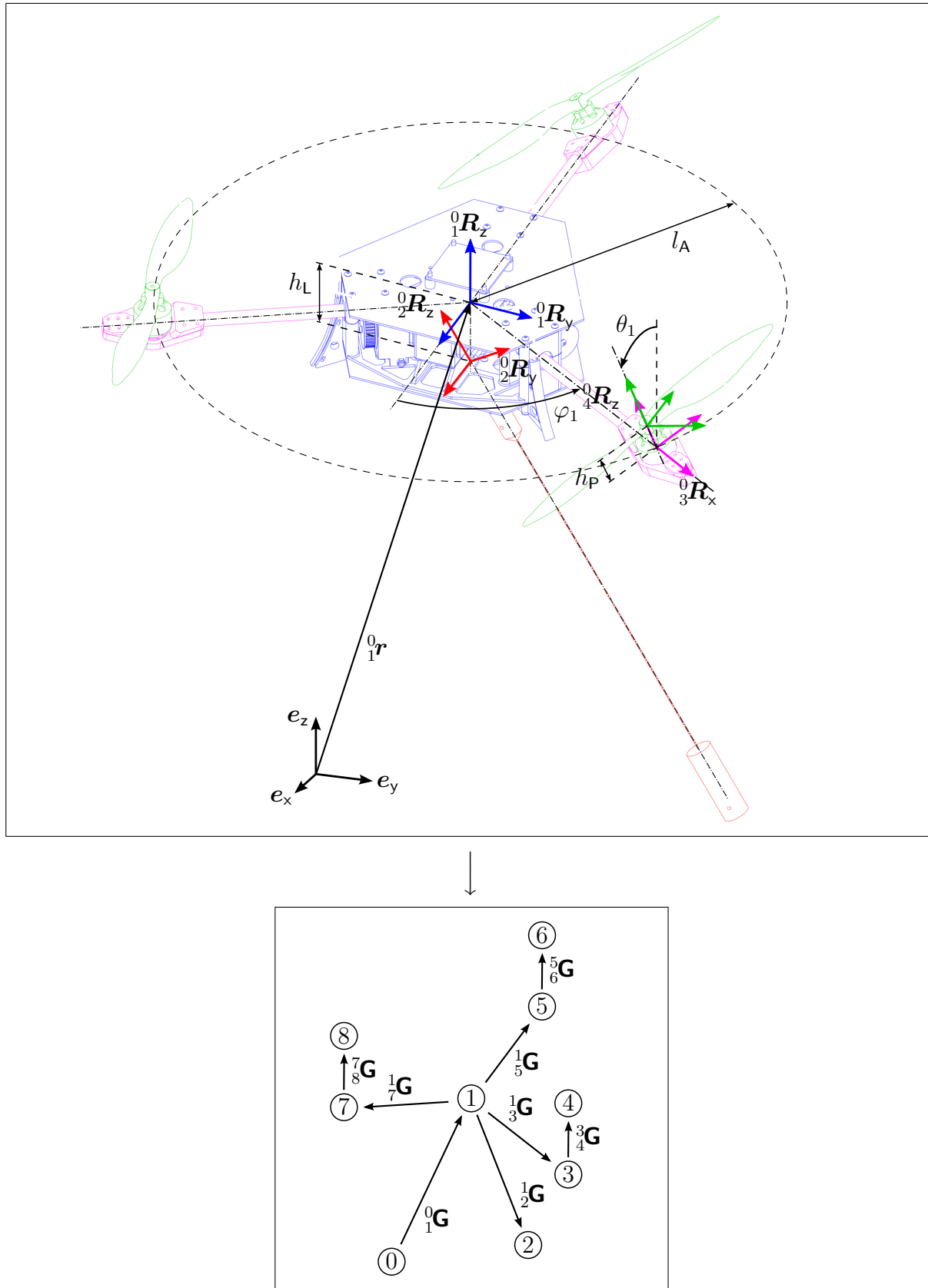


Figure 3.5: Frames attached to the Tricopter bodies (top) and the configuration graph (bottom)

The suspended load is a rigid body that is attached by a spherical joint to the central body. The body fixed frame of the load is placed in the center of this spherical joint. As a consequence, the position of the load (the position of its body fixed frame not the position of its center of mass) w.r.t. the central body is constant. This is reflected by the configuration

$${}^1\mathbf{G} = \begin{bmatrix} {}^1R_x^x & {}^1R_y^x & {}^1R_z^x & 0 \\ {}^1R_x^y & {}^1R_y^y & {}^1R_z^y & 0 \\ {}^1R_x^z & {}^1R_y^z & {}^1R_z^z & h_L \\ 0 & 0 & 0 & 1 \end{bmatrix}. \quad (3.97b)$$

The three arms are connected to the central body each by revolute joints with tilt angles θ_k , $k = 1, 2, 3$. The joint axis lie in the plane spanned by ${}^0\mathbf{R}_x$ and ${}^0\mathbf{R}_y$ and their angles to ${}^0\mathbf{R}_x$ are $\varphi_1 = \frac{\pi}{3}$, $\varphi_2 = \pi$, $\varphi_3 = -\frac{\pi}{3}$. The body fixed axes are placed such that ${}_{2k+1}{}^0\mathbf{R}_x$ coincide with the tilt axis and ${}_{2k+1}{}^0\mathbf{R}_z$, $k = 1, 2, 3$ coincide with the propeller spinning axis. The configuration of the k -th arm w.r.t. the central body is

$${}^{2k+1}\mathbf{G} = \begin{bmatrix} \cos \varphi_k & -\sin \varphi_k \cos \theta_k & \sin \varphi_k \sin \theta_k & l_A \cos \varphi_k \\ \sin \varphi_k & \cos \varphi_k \cos \theta_k & -\cos \varphi_k \sin \theta_k & l_A \sin \varphi_k \\ 0 & \sin \theta_k & \cos \theta_k & 0 \\ 0 & 0 & 0 & 1 \end{bmatrix}, \quad k = 1, \dots, 3. \quad (3.97c)$$

The propellers are connected by revolute joints to the arms. The body fixed frame is attached to the geometric center of the propeller (which will be an important point for its aerodynamic model). The configuration w.r.t. the corresponding arm is

$${}^{2k+2}\mathbf{G} = \begin{bmatrix} c_k & -s_k & 0 & 0 \\ s_k & c_k & 0 & 0 \\ 0 & 0 & 1 & h_P \\ 0 & 0 & 0 & 1 \end{bmatrix}, \quad k = 1, \dots, 3. \quad (3.97d)$$

The set of configurations $\mathcal{G}_0 = \{{}^0\mathbf{G}, {}^1\mathbf{G}, {}^2\mathbf{G}, {}^3\mathbf{G}, {}^4\mathbf{G}, {}^5\mathbf{G}, {}^6\mathbf{G}, {}^7\mathbf{G}, {}^8\mathbf{G}\}$ form a directed graph as shown at the bottom of Figure 3.5. With them and the rules from (3.96) we can compute the configuration ${}^a\mathbf{G}$ of any body w.r.t. any other body or the reference frame.

The configurations can be seen as functions ${}^a\mathbf{G}(\mathbf{x})$ of the system coordinates

$$\mathbf{x} = [{}^0r^x, {}^0r^y, {}^0r^z, {}^0R_x^x, \dots, {}^0R_z^x, {}^1R_x^x, \dots, {}^1R_z^x, \theta_1, \theta_2, \theta_3, c_1, s_1, c_2, s_2, c_3, s_3]^T \in \mathbb{R}^{30} \quad (3.98)$$

and the constant parameters $h_L, l_A, \varphi_1, \varphi_2, \varphi_3, h_P$. From the rules (3.96) emerge the geometric constraints

$$\phi(\mathbf{x}) = \mathbf{0} \quad \cong \quad \begin{cases} {}^0\mathbf{R}^T {}^0\mathbf{R} = \mathbf{I}_3, \det {}^0\mathbf{R} = +1, \\ {}^1\mathbf{R}^T {}^1\mathbf{R} = \mathbf{I}_3, \det {}^1\mathbf{R} = +1, \\ (c_k)^2 + (s_k)^2 = 1, \quad k = 1, 2, 3 \end{cases} \quad (3.99)$$

The configuration space of the rigid body system is

$$\mathbb{X} = \{\mathbf{x} \in \mathbb{R}^{30} \mid \phi(\mathbf{x}) = 0\} \cong \mathbb{SE}(3) \times \mathbb{SO}(3) \times \mathbb{R}^3 \times (\mathbb{S}^1)^3. \quad (3.100)$$

This example was mainly chosen as the Tricopter will be discussed in the following chapters. However, it is also an example of a system that is complex enough that one probably does not want to derive the equations of motion without a formalism. It also covers the most common manifolds encountered in rigid body mechanics. Even though the revolute joints for the propeller tilt and the propeller spinning axes both imply a \mathbb{S}^1 manifold, the local parameterization by the angle $\theta_k, k = 1, 2, 3$ is chosen. This has a practical motivation: The tilt mechanism also twists the cables to the propeller motor and so $\theta_k = 0$ and $\theta_k = 2\pi$ are really different situations in practice. On the other hand it should also show that the following algorithm handles minimal coordinates just as fine.

A generalization of the example states: A rigid body system can be parameterized by a set of ν (possibly redundant) coordinates \boldsymbol{x} which again parameterize a set of configurations ${}^a_b \mathbf{G}(\boldsymbol{x})$ which form a *connected* graph. The property connected is essential: it ensures that, with the rules (3.96), all remaining configurations of the graph can be computed, i.e. the corresponding *complete* graph. Loops in the graph and the property ${}^a_b \mathbf{G} \in \mathbb{SE}(3)$ may imply geometric constraints.

The use of graph theory in the context of algorithms for rigid body systems is quite common, see e.g. [Roberson and Schwertassek, 1988, sec. 8.2] or [Wittenburg, 2008, sec. 5.3]. However, we will not go any deeper into this. All we need for the following is that any configuration ${}^a_b \mathbf{G}(\boldsymbol{x}), a, b = 0 \dots N$ can be expressed in terms of the configuration coordinates \boldsymbol{x} .

Body velocity. The previous section motivated particular velocity coordinates $\boldsymbol{\xi} = [\mathbf{v}^\top, \boldsymbol{\omega}^\top]^\top$ for the free rigid body, which did lead to a convenient mathematical expressions. In the context of rigid body systems we may associate a *body velocity* ${}^a_b \boldsymbol{\xi} = [{}^a_b \mathbf{v}^\top, {}^a_b \boldsymbol{\omega}^\top]^\top$ with any configuration ${}^a_b \mathbf{G}, a, b = 0, \dots, N$ defined by

$${}^a_b \boldsymbol{\xi} = \text{vee}({}^b_a \mathbf{G} {}^a_b \dot{\mathbf{G}}), \quad a, b = 0, \dots, N. \quad (3.101)$$

From the rules (3.96) for the configurations we can conclude similar rules for their velocities: For the composition ${}^c_b \mathbf{G} = {}^a_b \mathbf{G} {}^b_c \mathbf{G}$ we get

$${}^c_b \boldsymbol{\xi} = \text{vee}({}^c_b \mathbf{G} {}^b_a \mathbf{G} ({}^a_b \dot{\mathbf{G}} {}^b_c \mathbf{G} + {}^a_b \mathbf{G} {}^b_c \dot{\mathbf{G}})) = \text{vee}({}^c_b \mathbf{G} \text{wed}({}^a_b \boldsymbol{\xi}) {}^b_c \mathbf{G}) + {}^b_c \boldsymbol{\xi} = \text{Ad}_{{}^c_b \mathbf{G}} {}^a_b \boldsymbol{\xi} + {}^b_c \boldsymbol{\xi} \quad (3.102a)$$

with the adjoint representation introduced in (3.85a). Differentiation of ${}^a_b \mathbf{G} {}^b_a \mathbf{G} = \mathbf{I}$ yields

$$\frac{d}{dt}({}^a_b \mathbf{G} {}^b_a \mathbf{G}) = {}^a_b \dot{\mathbf{G}} {}^b_a \mathbf{G} + {}^a_b \mathbf{G} {}^b_a \dot{\mathbf{G}} = {}^a_b \mathbf{G} \text{wed}({}^a_b \boldsymbol{\xi}) {}^b_a \mathbf{G} + \text{wed}({}^a_b \boldsymbol{\xi}) {}^b_a \mathbf{G} = \mathbf{0} \quad \Leftrightarrow \quad {}^a_b \boldsymbol{\xi} = -\text{Ad}_{{}^a_b \mathbf{G}} {}^a_b \boldsymbol{\xi} \quad (3.102b)$$

and obviously

$${}^a_a \boldsymbol{\xi} = \mathbf{0}. \quad (3.102c)$$

System velocity and body Jacobians. Based on their definition (3.101), the body velocities ${}^a_b \boldsymbol{\xi}$ can be seen as a function of the system coordinates \boldsymbol{x} and their derivatives

$\dot{\mathbf{x}} = \mathbf{A}(\mathbf{x})\boldsymbol{\xi}$. Crucially the velocity is linear in $\dot{\mathbf{x}}$ and consequently linear in the system velocity $\boldsymbol{\xi}$ and we can write

$${}^a_b\boldsymbol{\xi}(\mathbf{x}, \boldsymbol{\xi}) = {}^a_b\mathbf{J}(\mathbf{x})\boldsymbol{\xi}, \quad {}^a_b\mathbf{J}(\mathbf{x}) = \frac{\partial {}^a_b\boldsymbol{\xi}}{\partial \boldsymbol{\xi}}(\mathbf{x}) = \frac{\partial}{\partial \dot{\mathbf{x}}} \text{vee} \left({}^b_a\mathbf{G}(\mathbf{x}) \frac{d}{dt}({}^a_b\mathbf{G}(\mathbf{x})) \right) \mathbf{A}. \quad (3.103)$$

The matrix ${}^a_b\mathbf{J}(\mathbf{x}) \in \mathbb{R}^{6 \times n}$ that maps the system velocity $\boldsymbol{\xi}$ to the body velocity ${}^a_b\boldsymbol{\xi}$ is commonly called the *body Jacobian*. An alternative formula for the body Jacobian, which might give additional geometric insight, is given in [eq:AppendixDefBodyJac]. The following rules emerge directly from (3.102):

$${}^a_c\mathbf{J} = \text{Ad}_{{}^b_a\mathbf{G}} {}^a_b\mathbf{J} + {}^b_c\mathbf{J}, \quad {}^b_a\mathbf{J} = -\text{Ad}_{{}^a_b\mathbf{G}} {}^a_b\mathbf{J}, \quad {}^a_a\mathbf{J} = \mathbf{0}. \quad (3.104)$$

Example 7. Tricopter with suspended load: kinematics. For the tricopter with load from Example 6 we chose the following velocity coordinates: The components of the body velocity ${}^0\boldsymbol{\xi}$ of the central body w.r.t. the inertial frame, the components of the angular velocity ${}^0\boldsymbol{\omega}$ of the load w.r.t. the inertial frame, the angular velocities $\dot{\theta}_k, k = 1, 2, 3$ of the arm tilt mechanism and the angular velocities $\varpi_k, k = 1, 2, 3$ of the propellers w.r.t. the arms. These velocity coordinates $\boldsymbol{\xi} = [{}^0_1\boldsymbol{\xi}^\top, {}^0_2\boldsymbol{\omega}^\top, \dot{\theta}_1, \dot{\theta}_2, \dot{\theta}_3, \varpi_1, \varpi_2, \varpi_3]^\top$ are related to the configuration coordinates $\boldsymbol{\xi}$ by the kinematic equation

$$\dot{\mathbf{x}} = \mathbf{A}\boldsymbol{\xi} \quad \approx \quad \begin{cases} {}^0_1\dot{\mathbf{G}} = {}^0_1\mathbf{G} \text{ wed}({}^0_1\boldsymbol{\xi}), \\ {}^1_2\dot{\mathbf{R}} = {}^1_2\mathbf{R} \text{ wed}({}^0_2\boldsymbol{\omega}) - \text{wed}({}^0_1\boldsymbol{\omega}) {}^1_2\mathbf{R}, \\ \dot{\theta}_k = \dot{\theta}_k, \quad k = 1, 2, 3 \\ \dot{\varpi}_k = -s_k \varpi_k, \quad k = 1, 2, 3 \\ \dot{s}_k = c_k \varpi_k, \quad k = 1, 2, 3 \end{cases}. \quad (3.105)$$

The relative velocity ${}^1_2\boldsymbol{\omega} = \text{vee}({}^1_2\mathbf{R}^\top {}^1_2\dot{\mathbf{R}})$ of the load would be another possible and probably more obvious choice. The absolute velocity ${}^0_2\boldsymbol{\omega}$ is mainly chosen to demonstrate the flexibility of the presented approach but the use of absolute velocities also leads to less cumbersome terms in the system inertia matrix.

The body velocities associated with the configuration matrices from (3.97) are

$${}^0_1\boldsymbol{\xi} = \begin{bmatrix} {}^0_1v^x \\ {}^0_1v^y \\ {}^0_1v^z \\ {}^0_1\omega^x \\ {}^0_1\omega^y \\ {}^0_1\omega^z \end{bmatrix}, \quad {}^1_2\boldsymbol{\xi} = \begin{bmatrix} 0 \\ 0 \\ 0 \\ {}^0_2\omega^x - \frac{1}{2}R_x^x {}^0_2\omega^x - \frac{1}{2}R_y^x {}^0_2\omega^y - \frac{1}{2}R_z^x {}^0_2\omega^z \\ {}^0_2\omega^y - \frac{1}{2}R_x^y {}^0_2\omega^x - \frac{1}{2}R_y^y {}^0_2\omega^y - \frac{1}{2}R_z^y {}^0_2\omega^z \\ {}^0_2\omega^z - \frac{1}{2}R_x^z {}^0_2\omega^x - \frac{1}{2}R_y^z {}^0_2\omega^y - \frac{1}{2}R_z^z {}^0_2\omega^z \end{bmatrix}, \quad (3.106a)$$

$${}^{2k+1}_2\boldsymbol{\xi} = \begin{bmatrix} 0 \\ 0 \\ 0 \\ \dot{\theta}_k \\ 0 \\ 0 \end{bmatrix}, \quad {}^{2k+2}\boldsymbol{\xi} = \begin{bmatrix} 0 \\ 0 \\ 0 \\ 0 \\ 0 \\ \varpi_k \end{bmatrix}, \quad k = 1, 2, 3. \quad (3.106b)$$

From this it should clear how the corresponding body Jacobians look like, e.g. ${}^0_1\mathbf{J} = [\mathbf{I}_6 \ 0]$.

For the formulation of the kinetic energy in the following subsection we will need the body Jacobians ${}^0_b\mathbf{J}$, $b = 1, \dots, N$. From the graph structure and the rules (3.104) we can compute them iteratively as

$${}^0_2\mathbf{J} = \text{Ad}_{{}^1_1\mathbf{G}} {}^0_1\mathbf{J} + {}^1_2\mathbf{J}, \quad (3.107a)$$

$${}^{2k+1}_{2k+1}\mathbf{J} = \text{Ad}_{{}^{2k+1}_1\mathbf{G}} {}^0_1\mathbf{J} + {}^{2k+1}_{2k+1}\mathbf{J}, \quad (3.107b)$$

$${}^{2k+2}_{2k+2}\mathbf{J} = \text{Ad}_{{}^{2k+2}_{2k+1}\mathbf{G}} {}^{2k+1}_{2k+1}\mathbf{J} + {}^{2k+2}_{2k+2}\mathbf{J}. \quad (3.107c)$$

These terms are significantly more cumbersome, so they are not displayed explicitly.

3.4.2 Inertia

Kinetic energy and inertia matrix. The kinetic energy \mathcal{T} of a rigid body system is simply the sum of the kinetic energies of its bodies. Combining this with the kinetic energy (3.51) of a single free rigid body and the formulation of the absolute body velocities ${}^0_b\boldsymbol{\xi}$ in terms of the chosen coordinates using the body Jacobian ${}^0_b\mathbf{J}$ from (3.103), yields

$$\mathcal{T} = \sum_b \frac{1}{2} {}^0_b\boldsymbol{\xi}^\top {}^0_b\mathbf{M} {}^0_b\boldsymbol{\xi} = \frac{1}{2} \boldsymbol{\xi}^\top \underbrace{\sum_b {}^0_b\mathbf{J}^\top {}^0_b\mathbf{M} {}^0_b\mathbf{J}}_{\mathbf{M}} \boldsymbol{\xi}. \quad (3.108)$$

Recall from the previous section, that the constant *body* inertia matrix ${}^0_b\mathbf{M} \in \mathbb{R}^{6 \times 6}$ collects the inertia parameters of the rigid body with index b and w.r.t. its body fixed frame. The matrix $\mathbf{M}(\mathbf{x}) \in \mathbb{R}^{n \times n}$ is called the *system* inertia matrix.

Connection coefficients. With a rather cumbersome computation (see [eq: ??]), it can be shown that the connection coefficients Γ_{ijk} associated to the system inertia matrix \mathbf{M} from (3.108) can be expressed in terms of the body Jacobians ${}^0_b\mathbf{J}$, the body inertia matrices ${}^0_b\mathbf{M}$ and the body connection coefficients ${}^0_b\Gamma_{pqr}$ from (3.58) or the body commutation coefficients γ_{pq}^h from (3.49) as

$$\Gamma_{ijk} = \sum_b {}^0_b J_i^p \left({}^0_b M_{pq} \partial_k {}^0_b J_j^q + \underbrace{\frac{1}{2} (\gamma_{pq}^h {}^0_b M_{hr} + \gamma_{pr}^h {}^0_b M_{hq} - \gamma_{qr}^h {}^0_b M_{hp}) {}^0_b J_j^q {}^0_b J_k^r}_{{}^0_b \Gamma_{pqr}} \right) \quad (3.109)$$

Acceleration energy. As with the kinetic energy, the acceleration energy of a rigid body system is simply the sum of the acceleration energies of its bodies. Summing up the body acceleration energies from (3.90c) and plugging in the body velocities ${}^0_b\boldsymbol{\xi} = {}^0_b\mathbf{J}\boldsymbol{\xi}$

yields

$$\begin{aligned}
\mathcal{S} &= \sum_b \frac{1}{2} \|({}^0_b\ddot{\mathbf{G}})^\top\|_{{}^0_b\mathbf{M}'}^2 \\
&= \sum_b \frac{1}{2} \|(\text{wed}({}^0_b\mathbf{J}\dot{\boldsymbol{\xi}} + {}^0_b\dot{\mathbf{J}}\boldsymbol{\xi}) + \text{wed}({}^0_b\mathbf{J}\boldsymbol{\xi})^2)^\top\|_{{}^0_b\mathbf{M}'}^2 \\
&= \sum_b \frac{1}{2} \|(\text{wed}({}^0_b\mathbf{J}\dot{\boldsymbol{\xi}}))^\top\|_{{}^0_b\mathbf{M}'}^2 + \sum_b \text{tr} (\text{wed}({}^0_b\mathbf{J}\dot{\boldsymbol{\xi}}){}^0_b\mathbf{M}'(\text{wed}({}^0_b\mathbf{J}\boldsymbol{\xi}) + \text{wed}({}^0_b\mathbf{J}\boldsymbol{\xi})^2)^\top) \\
&\quad + \underbrace{\sum_b \frac{1}{2} \|(\text{wed}({}^0_b\dot{\mathbf{J}}\boldsymbol{\xi}) + \text{wed}({}^0_b\mathbf{J}\boldsymbol{\xi})^2)^\top\|_{{}^0_b\mathbf{M}'}^2}_{\mathcal{S}_0} \\
&= \frac{1}{2} \dot{\boldsymbol{\xi}}^\top \underbrace{\sum_b {}^0_b\mathbf{J}^\top {}^0_b\mathbf{M} {}^0_b\mathbf{J}}_{\mathbf{M}} \dot{\boldsymbol{\xi}} + \dot{\boldsymbol{\xi}}^\top \underbrace{\sum_b {}^0_b\mathbf{J}^\top ({}^0_b\mathbf{M} {}^0_b\mathbf{J} - \text{ad}^\top_{{}^0_b\mathbf{J}\boldsymbol{\xi}} {}^0_b\mathbf{M} {}^0_b\mathbf{J}) \boldsymbol{\xi}}_{\mathbf{c}} + \mathcal{S}_0. \tag{3.110}
\end{aligned}$$

Obviously, we found again the system inertia matrix \mathbf{M} and one may check that indeed $c_i = \Gamma_{ijk}\dot{\xi}^j\xi^k$ with the connection coefficients Γ_{ijk} from (3.109). Note that \mathcal{S}_0 is independent of $\boldsymbol{\xi}$, so it does not contribute to the generalized inertia force.

Inertia force. As before, there are several equivalent ways for computing the inertia force \mathbf{f}^M of a rigid body system: We may use the Lagrange operator on the kinetic energy from (3.108), use the inertia matrix and connection coefficients from (3.109), or taking the differential of the acceleration energy from (3.110). Each of these approaches will yield

$$\mathbf{f}^M = \underbrace{\sum_b {}^0_b\mathbf{J}^\top {}^0_b\mathbf{M} {}^0_b\mathbf{J}}_{\mathbf{M}} \dot{\boldsymbol{\xi}} + \underbrace{\sum_b {}^0_b\mathbf{J}^\top ({}^0_b\mathbf{M} {}^0_b\mathbf{J} - \text{ad}^\top_{{}^0_b\mathbf{J}\boldsymbol{\xi}} {}^0_b\mathbf{M} {}^0_b\mathbf{J}) \boldsymbol{\xi}}_{\mathbf{c}}. \tag{3.111}$$

Similar results are called *the projection equation* in [Bremer, 2008, sec. 4.2.5] and *the Kane equations* [Kane and Levinson, 1985, chap. 6]. There is some controversy (starting in [Desloge, 1987]) about the naming, since the equations result rather directly (as shown above) from the Gibbs-Appell formulation. See [Lesser, 1992] or [Papastavridis, 2002, p. 714] for an overview.

In contrast to the sources above, the derivation here does allow for redundant configuration coordinates \mathbf{x} and general velocity coordinates $\boldsymbol{\xi}$. This is mostly due to the more general formulation (3.103) of the body jacobian ${}^0_b\mathbf{J}$, whereas the formulation of the inertia matrix \mathbf{M} and gyroscopic terms \mathbf{c} should look familiar.

3.4.3 Gravitation

The potential energy of gravitation of a rigid body system is the sum of the potentials of the individual bodies (3.90g). This is

$$\mathcal{V}^G = \sum_b \langle ({}^0_b\mathbf{G})^\top, \text{wed}(\boldsymbol{\alpha}_G)^\top \rangle_{{}^0_b\mathbf{M}'}, \quad \boldsymbol{\alpha}_G^\top = [\mathbf{a}_G^\top, \mathbf{0}_{1 \times 3}], \tag{3.112}$$

where ${}^0_b\mathbf{M}' = \text{Vee}({}^0_b\mathbf{M})$ is the body inertia matrix and $\boldsymbol{\alpha}_G$ is Earth's gravity wrench.

Finally, the generalized force of gravity on a rigid body system may be formulated as

$$\begin{aligned} \mathbf{f}^G = \nabla \mathcal{V}^G &= \frac{\partial \dot{\mathcal{V}}^G}{\partial \boldsymbol{\xi}} = \frac{\partial}{\partial \boldsymbol{\xi}} \sum_b \text{tr} \left({}_0^b \mathbf{G} \text{wed}({}_b^0 \boldsymbol{\xi}) {}_b^0 \mathbf{M}' \text{wed}(\boldsymbol{\alpha}_G)^\top \right) \\ &= \sum_b \left(\frac{\partial {}_b^0 \boldsymbol{\xi}}{\partial \boldsymbol{\xi}} \right)^\top \text{vee2} \left({}_b^0 \mathbf{G}^\top \text{wed}(\boldsymbol{\alpha}_G) {}_b^0 \mathbf{M}' \right) = \sum_b {}_b^0 \mathbf{J}^\top {}_b^0 \mathbf{M} \text{Ad}_{{}_b^0 \mathbf{G}}^{-1} \boldsymbol{\alpha}_G. \quad (3.113) \end{aligned}$$

3.4.4 Stiffness

In subsection 3.3.4 we considered linear springs between arbitrary points of the body and the inertial frame. For a system of rigid bodies we may consider the same for each body, but additionally we may also consider springs connecting the bodies to each other, see Figure 3.6.

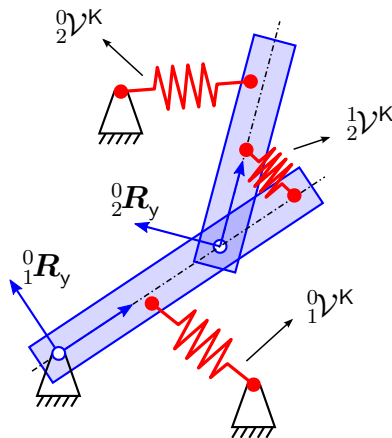


Figure 3.6: MultibodyStiffnessIllustration

The total potential energy \mathcal{V}^K is the sum of the potentials of the individual springs. Here it will make sense to group them differently: Let ${}^a_b \mathcal{V}^K$ with $0 \leq a < b \leq N$ denote the combined potential of all springs connecting body a and b . The total energy is

$$\mathcal{V}^K = \sum_{a=0}^{N-1} \sum_{b=a+1}^N {}^a_b \mathcal{V}^K \quad (3.114)$$

Using the results from subsection 3.3.4 it may be shown that each potential can be formulated as

$${}^a_b \mathcal{V}^K = \frac{1}{2} \|({}^a_b \mathbf{G} - {}^a_b \mathbf{G}_R)^\top\|_{b \mathbf{K}'}^2 = \frac{1}{2} \|({}^a_b \mathbf{G}_R^{-1} {}^a_b \mathbf{G} - \mathbf{I}_4)^\top\|_{b \mathbf{K}'}^2 \quad (3.115)$$

with the constant parameters ${}^a_b \mathbf{K}' \in \text{SYM}(4)$ and ${}^a_b \mathbf{G}_R \in \mathbb{SE}(3)$ resulting from the particular spring distribution between body a and b .

Finally, the generalized force due to an arbitrary constellation of linear springs on a rigid

body system may be formulated as

$$\begin{aligned} \mathbf{f}^K &= \nabla \mathcal{V}^K = \frac{\partial \dot{\mathcal{V}}^K}{\partial \boldsymbol{\xi}} = \frac{\partial}{\partial \boldsymbol{\xi}} \sum_{a,b} \text{tr} \left(\left({}_b^a \mathbf{G} - {}_b^a \mathbf{G}_R \right) {}_b^a \mathbf{K}' ({}_b^a \mathbf{G} \text{ wed}({}_b^a \boldsymbol{\xi}))^\top \right) \\ &= \sum_{a,b} \left(\frac{\partial {}_b^a \boldsymbol{\xi}}{\partial \boldsymbol{\xi}} \right)^\top \text{vee2} \left({}_b^a \mathbf{G}^\top ({}_b^a \mathbf{G} - {}_b^a \mathbf{G}_R) {}_b^a \mathbf{K}' \right) \\ &= \sum_{a,b} {}_b^a \mathbf{J}^\top \text{vee2} \left((\mathbf{I}_4 - {}_b^a \mathbf{G}^{-1} {}_b^a \mathbf{G}_R) {}_b^a \mathbf{K}' \right) \end{aligned} \quad (3.116)$$

3.4.5 Dissipation

Similar to the previous subsection we may consider viscous friction of the bodies to each other and to the inertial frame. Let the body with index b move through a viscous fluid that is attached to the body with index a . The corresponding dissipation function ${}_b^a \mathcal{R}$ was derived in (3.75):

$${}_b^a \mathcal{R} = \frac{1}{2} {}_b^a \boldsymbol{\xi}^\top {}_b^a \mathbf{D} {}_b^a \boldsymbol{\xi} \quad (3.117)$$

with the body dissipation matrix ${}_b^a \mathbf{D}$. Notice that in contrast to stiffness, the dissipation is, in general, not symmetric in the sense ${}_b^a \mathcal{R} \neq {}_a^b \mathcal{R}$. But due to ${}_a^a \boldsymbol{\xi} = \mathbf{0}$ we have ${}_a^a \mathcal{R} = 0$. For system of rigid bodies we have the dissipation function

$$\mathcal{R} = \sum_{a=0}^N \sum_{b=0, b \neq a}^N {}_b^a \mathcal{R} = \frac{1}{2} \boldsymbol{\xi}^\top \underbrace{\sum_{a=0}^N \sum_{b=0, b \neq a}^N {}_b^a \mathbf{J}^\top {}_b^a \mathbf{D} {}_b^a \mathbf{J} \boldsymbol{\xi}}_{\mathbf{D}} \quad (3.118)$$

where \mathbf{D} is called the system dissipation matrix.

Finally, the generalized force due to viscous friction on a rigid body system may be formulated as

$$\mathbf{f}^D = \frac{\partial \mathcal{R}}{\partial \boldsymbol{\xi}} = \mathbf{D} \boldsymbol{\xi} \quad (3.119)$$

3.4.6 Summary

Given a rigid body system subject to inertia, gravity, dissipation and linear springs as discussed in this section, the equation of motion may be derived as follows. The description of the system consists of:

1. the chosen parameterization in the configuration coordinates \mathbf{x} , the velocity coordinates $\boldsymbol{\xi}$ and their relation captured by the kinematics matrix \mathbf{A} .
2. a set of transformation matrices ${}_b^a \mathbf{G}(\mathbf{x})$ that maps the coordinates to the chosen rigid body frames. They must form a connected graph including all body frames and the reference frame.

3. the constitutive parameters merged into the inertia matrices ${}^0_b\mathbf{M}'$, dissipation matrices ${}^a_b\mathbf{D}'$, stiffness matrices ${}^a_b\mathbf{K}'$, their corresponding minimum ${}^a_b\mathbf{G}_R$ and the gravity vector \mathbf{a}_G . It should be stressed that these only depend on the body frames, but are independent of the chosen coordinates.

Given these inputs, there is an algorithm

$$(\mathbf{x}, \boldsymbol{\xi}, \mathbf{A}, {}^a_b\mathbf{G}, {}^0_b\mathbf{M}', {}^a_b\mathbf{D}', {}^a_b\mathbf{K}', {}^a_b\mathbf{G}_R, \mathbf{a}_G) \mapsto (\mathbf{M}, \mathbf{c}, \mathbf{f}^D, \mathbf{f}^K, \mathbf{f}^G) \quad (3.120)$$

that computes the relevant parts of the equation of motion. It may be summarized as

1. compute the body Jacobians for the given configurations:

$${}^a_b\mathbf{J}(\mathbf{x}) = \frac{\partial}{\partial \dot{\mathbf{x}}} \text{vee} \left({}^b_a\mathbf{G}(\mathbf{x}) \frac{d}{dt}({}^a_b\mathbf{G}(\mathbf{x})) \right) \mathbf{A}(\mathbf{x}) \quad (3.121)$$

2. use the group rules to compute the missing configurations and Jacobians

$${}^a_c\mathbf{G} = {}^a_b\mathbf{G} {}^b_c\mathbf{G}, \quad {}^b_a\mathbf{G} = {}^a_b\mathbf{G}^{-1}, \quad (3.122a)$$

$${}^a_c\mathbf{J} = \text{Ad}_{\xi} {}^a_b\mathbf{J} + {}^b_c\mathbf{J}, \quad {}^b_a\mathbf{J} = -\text{Ad}_{\xi} {}^a_b\mathbf{J}, \quad (3.122b)$$

$${}^a_c\dot{\mathbf{J}} = \text{Ad}_{\dot{\xi}} ({}^a_b\dot{\mathbf{J}} + \text{ad}_{\xi} {}^a_b\mathbf{J}) + {}^b_c\dot{\mathbf{J}}, \quad {}^b_a\dot{\mathbf{J}} = -\text{Ad}_{\dot{\xi}} ({}^a_b\dot{\mathbf{J}} + \text{ad}_{\dot{\xi}} {}^a_b\mathbf{J}), \quad (3.122c)$$

3. assemble the system matrices

$$\mathbf{M} = \sum_b {}^0_b\mathbf{J}^\top \text{Vee}({}^0_b\mathbf{M}') {}^0_b\mathbf{J}, \quad (3.123a)$$

$$\mathbf{c} = \sum_b {}^0_b\mathbf{J}^\top \text{vee2} ((\text{wed}({}^0_b\mathbf{J}\xi) + \text{wed}({}^0_b\mathbf{J}\xi)^2) {}^0_b\mathbf{M}') \quad (3.123b)$$

$$\mathbf{D} = \sum_{a,b} {}^a_b\mathbf{J}^\top \text{Vee}({}^a_b\mathbf{D}') {}^a_b\mathbf{J} \quad (3.123c)$$

$$\mathbf{f}^K = \sum_{a,b} {}^a_b\mathbf{J}^\top \text{vee2} ((\mathbf{I}_4 - {}^b_a\mathbf{G} {}^a_b\mathbf{G}_R) {}^a_b\mathbf{K}') \quad (3.123d)$$

$$\mathbf{f}^G = \sum_b {}^0_b\mathbf{J}^\top \text{vee2} ({}^0_b\mathbf{G}^\top \text{wed}(-\boldsymbol{\alpha}_G) {}^0_b\mathbf{M}'), \quad \boldsymbol{\alpha}_G = [\mathbf{a}_G^\top, \mathbf{0}_{1 \times 3}]^\top \quad (3.123e)$$

The explicit equations of motion reads

$$\dot{\mathbf{x}} = \mathbf{A}\boldsymbol{\xi}, \quad (3.124a)$$

$$\dot{\boldsymbol{\xi}} = \mathbf{M}^{-1}(\mathbf{f}^E - \mathbf{c} - \mathbf{D}\boldsymbol{\xi} - \mathbf{f}^K - \mathbf{f}^G). \quad (3.124b)$$

The first step (3.121) requires differentiation, so must be performed symbolically. The remaining steps only require basic linear algebra, so can be preformed numerically. For small systems it might be still reasonable to compute $\mathbf{M}(\mathbf{x})$ symbolically, but for larger systems the explicit expressions can be overwhelming even for contemporary computers.

3.5 Additional general constraints

So far we dealt with geometric constraints and essentially eliminated them by suitable choice of coordinates. This section considers additional constraints that may also depend on velocity and/or even acceleration, but sticks to the chosen coordinates \mathbf{x} and $\boldsymbol{\xi}$.

Types of constraints. Recall that any smooth constraint is equivalent to its derivative supplemented by the appropriate initial condition. We may consider the following types of constraints

- geometric constraint:

$$\begin{aligned} \psi(\mathbf{x}) &= \mathbf{0} \\ \Leftrightarrow \quad \underbrace{\partial_i \psi^\kappa(\mathbf{x})}_{Z_i^\kappa(\mathbf{x})} \dot{\xi}^i &= \underbrace{-\partial_j \partial_i \psi^\kappa(\mathbf{x}) \xi^i \xi^j}_{z^\kappa(\mathbf{x}, \boldsymbol{\xi})}, \quad \psi^\kappa(\mathbf{x}_0) = 0, \quad \partial_i \psi^\kappa(\mathbf{x}_0) \xi_0^i = 0 \end{aligned} \quad (3.125a)$$

- linear kinematic constraint (possibly nonholonomic):

$$\begin{aligned} \mathbf{N}(\mathbf{x}) \dot{\mathbf{x}} &= \underbrace{\mathbf{N}(\mathbf{x}) \mathbf{A}(\mathbf{x}) \boldsymbol{\xi}}_{\mathbf{Z}(\mathbf{x})} = \mathbf{0} \\ \Leftrightarrow \quad Z_i^\kappa(\mathbf{x}) \dot{\xi}^i &= \underbrace{-\partial_j Z_i^\kappa(\mathbf{x}) \xi^i \xi^j}_{z^\kappa(\mathbf{x}, \boldsymbol{\xi})}, \quad Z_i^\kappa(\mathbf{x}_0) \xi_0^\kappa = 0 \end{aligned} \quad (3.125b)$$

- general kinematic constraints

$$\begin{aligned} \eta(\mathbf{x}, \boldsymbol{\xi}, t) &= \mathbf{0} \\ \Leftrightarrow \quad \underbrace{\frac{\partial \eta^\kappa}{\partial \xi^i}(\mathbf{x}, \boldsymbol{\xi}, t)}_{Z_i^\kappa(\mathbf{x}, \boldsymbol{\xi}, t)} \dot{\xi}^i &= \underbrace{-\partial_i \eta^\kappa(\mathbf{x}, \boldsymbol{\xi}, t) \xi^i - \frac{\partial \eta^\kappa}{\partial t}(\mathbf{x}, \boldsymbol{\xi}, t)}_{z^\kappa(\mathbf{x}, \boldsymbol{\xi}, t)}, \quad \eta^\kappa(\mathbf{x}_0, \boldsymbol{\xi}_0, t_0) = 0 \end{aligned} \quad (3.125c)$$

- linear² acceleration constraints.

$$\mathbf{Z}(\mathbf{x}, \boldsymbol{\xi}, t) \dot{\boldsymbol{\xi}} = \mathbf{z}(\mathbf{x}, \boldsymbol{\xi}, t) \quad (3.125d)$$

All these constraints can be formulated as *linear acceleration constraints* $\mathbf{Z} \dot{\boldsymbol{\xi}} = \mathbf{z}$ possibly supplemented by suitable conditions on the initial coordinates $\mathbf{x}_0 = \mathbf{x}(t_0)$ and $\boldsymbol{\xi}_0 = \boldsymbol{\xi}(t_0)$.

Gauss' principle. Let the free system (without these additional constraints) be governed by the acceleration $\dot{\boldsymbol{\xi}} = \mathbf{M}^{-1} \mathbf{b}$. Then Gauss' principle for the system with the additional constraint states

$$\begin{aligned} \min_{\dot{\boldsymbol{\xi}} \in \mathbb{R}^n} \quad \mathcal{G} &= \frac{1}{2} \dot{\boldsymbol{\xi}}^\top \mathbf{M} \dot{\boldsymbol{\xi}} - \dot{\boldsymbol{\xi}}^\top \mathbf{b} + \mathcal{G}_0 \\ \text{s. t.} \quad \mathbf{Z} \dot{\boldsymbol{\xi}} &= \mathbf{z} \end{aligned} \quad (3.126)$$

This is a standard quadratic optimization problem with well established solutions. Let $\text{rank } \mathbf{Z} = c \leq n$ and assume that \mathbf{z} lies in the column space \mathbf{Z} , i.e. the constraint equations is solvable. For $c = n$ the trivial solution is $\boldsymbol{\xi} = \mathbf{Z}^{-1} \mathbf{z}$. For the common case $0 < c < n$ we may consider two solution approaches:

²Nonlinear acceleration constraints could be handled as well, but with a more sophisticated solution than (3.130)

Solution using null space. Similar to the choice of minimal velocity coordinates above [link] we may formulate *all* solution to the constraint equation as $\dot{\boldsymbol{\xi}} = \mathbf{W}\boldsymbol{\alpha} + \mathbf{w}$. The columns of the matrix $\mathbf{W} \in \mathbb{R}^{n \times c}$ span the null space of \mathbf{Z} , i.e. $\mathbf{Z}\mathbf{W} = \mathbf{0}$ and rank $\mathbf{W} = n - c$. The tuple $\mathbf{w} \in \mathbb{R}^n$ is any solution to the constraint equation, i.e. $\mathbf{Z}\mathbf{w} = \mathbf{z}$. The variables $\boldsymbol{\alpha} \in \mathbb{R}^{n-c}$ may be called the *acceleration coordinates*.

As in the previous section, this transforms (3.126) to an unconstrained optimization problem with

$$\mathcal{G} = \frac{1}{2}(\mathbf{W}\boldsymbol{\alpha} + \mathbf{w})^\top \mathbf{M}(\mathbf{W}\boldsymbol{\alpha} + \mathbf{w}) - (\mathbf{W}\boldsymbol{\alpha} + \mathbf{w})^\top \mathbf{b} + \mathcal{G}_0 \quad (3.127)$$

$$= \frac{1}{2}\boldsymbol{\alpha}^\top \underbrace{\mathbf{W}^\top \mathbf{M} \mathbf{W}}_{\mathbf{M}^c} \boldsymbol{\alpha} - \boldsymbol{\alpha}^\top \underbrace{\mathbf{W}^\top (\mathbf{b} - \mathbf{M}\mathbf{w})}_{\mathbf{b}^c} + \underbrace{\mathbf{w}^\top \mathbf{M}\mathbf{w} - \mathbf{w}^\top \mathbf{b} + \mathcal{G}_0}_{\mathcal{G}_0^c} \quad (3.128)$$

with the obvious minimum $\boldsymbol{\alpha} = (\mathbf{M}^c)^{-1}\mathbf{b}^c$. This approach is quite common also for the numerical solution of such problems, see [Gould et al., 2001].

Finally, the equations of motion of the constrained system are

$$\dot{\mathbf{x}} = \mathbf{A}\boldsymbol{\xi}, \quad \dot{\boldsymbol{\xi}} = \mathbf{W}(\mathbf{M}^c)^{-1}\mathbf{b}^c + \mathbf{w}. \quad (3.129)$$

Solution using Lagrange multipliers. Another common solution approach to (3.126) utilizes the concept *Lagrange multipliers* (see e.g. [Luenberger and Ye, 2015, ch. 14]): Define a *Lagrangian* $\mathcal{L} = \mathcal{G} + \boldsymbol{\lambda}^\top (\mathbf{Z}\boldsymbol{\xi} - \mathbf{z})$ with the Lagrange multipliers $\boldsymbol{\lambda} \in \mathbb{R}^c$. Its critical points are solved from

$$\begin{bmatrix} \frac{\partial \mathcal{L}}{\partial \boldsymbol{\xi}} \\ \frac{\partial \mathcal{L}}{\partial \boldsymbol{\lambda}} \end{bmatrix} = \mathbf{0} \quad \Leftrightarrow \quad \begin{bmatrix} \mathbf{M} & \mathbf{Z}^\top \\ \mathbf{Z} & \mathbf{0} \end{bmatrix} \begin{bmatrix} \dot{\boldsymbol{\xi}} \\ \boldsymbol{\lambda} \end{bmatrix} = \begin{bmatrix} \mathbf{b} \\ \mathbf{z} \end{bmatrix}. \quad (3.130)$$

Similar to the section on the principle of constraint release, the term $\mathbf{Z}^\top \boldsymbol{\lambda}$ may be interpreted as the generalized reaction force on the system to enforce the constraint.

If the constraint matrix \mathbf{Z} has full rank, we may use block matrix inversion

$$\begin{bmatrix} \mathbf{M} & \mathbf{Z}^\top \\ \mathbf{Z} & \mathbf{0} \end{bmatrix}^{-1} = \begin{bmatrix} \mathbf{M}^{-1} - \mathbf{M}^{-1}\mathbf{Z}^\top(\mathbf{Z}\mathbf{M}^{-1}\mathbf{Z}^\top)^{-1}\mathbf{Z}\mathbf{M}^{-1} & \mathbf{M}^{-1}\mathbf{Z}^\top(\mathbf{Z}\mathbf{M}^{-1}\mathbf{Z}^\top)^{-1} \\ (\mathbf{Z}\mathbf{M}^{-1}\mathbf{Z}^\top)^{-1}\mathbf{Z}\mathbf{M}^{-1} & -(\mathbf{Z}\mathbf{M}^{-1}\mathbf{Z}^\top)^{-1} \end{bmatrix} \quad (3.131)$$

to eliminate the Lagrange multipliers and obtain the equations of motion as

$$\dot{\mathbf{x}} = \mathbf{A}\boldsymbol{\xi}, \quad \dot{\boldsymbol{\xi}} = \mathbf{M}^{-1}(\mathbf{b} + \mathbf{Z}^\top(\mathbf{Z}\mathbf{M}^{-1}\mathbf{Z}^\top)^{-1}(\mathbf{z} - \mathbf{Z}\mathbf{M}^{-1}\mathbf{b})). \quad (3.132)$$

The possibility of handling such a variety of constraints might put Gauß' principle in a superior position compared to other principles as pointed out in [Hamel, 1949, p. 525]. The Lagrange-d'Alembert principle handles linear kinematic constraints $\mathbf{N}\dot{\mathbf{x}} = \mathbf{0}$ by requiring $\mathbf{N}\delta\mathbf{x} = \mathbf{0}$. However, there are no real world examples of nonlinear nonholonomic constraints [Hamel, 1949, p. 499], [Neimark and Fufaev, 1972, ch. IV], [Roberson and Schwertassek, 1988, p. 96] and none of acceleration constraints [Hamel, 1949, p. 505 & 525], so one should be careful with this context. Note for example that for nonlinear kinematic and acceleration constraints the reaction forces $\boldsymbol{\lambda}$ enter the balance of energy.

Gauß suggested in [Gauß, 1829] also the application to inequality constraints which will not be discussed here. For a contemporary discussion and applications of this see [Pfeiffer and Glocker, 1996, sec. 6.1].

Chapter 4

Tracking control of rigid body systems

This chapter motivates and discusses several approaches for a model based design of a tracking controller for a rigid body system by static feedback.

System model. The previous chapter discussed the equations of motion of rigid body systems: For chosen configuration coordinates $\mathbf{x}(t) \in \mathbb{X}$, velocity coordinates $\boldsymbol{\xi}(t) \in \mathbb{R}^n$ and the control inputs $\mathbf{u}(t) \in \mathbb{R}^p$ these have the form

$$\dot{\mathbf{x}} = \mathbf{A}(\mathbf{x})\boldsymbol{\xi}, \quad \underbrace{\mathbf{M}(\mathbf{x})\dot{\boldsymbol{\xi}} + \mathbf{c}(\mathbf{x}, \boldsymbol{\xi})}_{\mathbf{f}^M(\mathbf{x}, \boldsymbol{\xi}, \dot{\boldsymbol{\xi}})} + \underbrace{\mathbf{D}(\mathbf{x})\boldsymbol{\xi}}_{\mathbf{f}^D(\mathbf{x}, \boldsymbol{\xi})} + \underbrace{\nabla \mathcal{V}(\mathbf{x})}_{\mathbf{f}^K(\mathbf{x})} = \mathbf{B}(\mathbf{x})\mathbf{u}. \quad (4.1)$$

The forces $\mathbf{f}^M, \mathbf{f}^D, \mathbf{f}^K$ may be computed from the rigid body configurations ${}^a_b\mathbf{G}(\mathbf{x})$ and the constitutive parameters ${}^0_b\mathbf{M}, {}^a_b\mathbf{D}, {}^a_b\mathbf{K}$. This structure will be the main inspiration for the design of the controlled system.

However, mathematically, the control approach does not rely on the model having this structure. We may assume any model of the form

$$\dot{\mathbf{x}} = \mathbf{A}(\mathbf{x})\boldsymbol{\xi}, \quad \mathbf{M}(\mathbf{x})\dot{\boldsymbol{\xi}} + \mathbf{b}(\mathbf{x}, \boldsymbol{\xi}) = \mathbf{B}(\mathbf{x})\mathbf{u} \quad (4.2)$$

where $\mathbf{A}(\mathbf{x}) \in \mathbb{R}^{\nu \times n}$ and $\mathbf{B}(\mathbf{x}) \in \mathbb{R}^{n \times p}$ are full rank, the system inertia matrix $\mathbf{M}(\mathbf{x}) \in \text{SYM}^+(n)$ is symmetric, positive definite, and $\mathbf{b}(\mathbf{x}, \boldsymbol{\xi}) \in \mathbb{R}^n$ collects the remaining terms of the kinetic equation. The system is called *fully-actuated* for $p = n$ and *underactuated* for $0 < p < n$. Firstly we will restrict to fully-actuated systems and later try to expand the approach to underactuated systems.

Reference trajectory and tracking controller. Let there be a *reference trajectory* $t \mapsto \mathbf{x}_R(t)$ which is compatible with the model (4.2): It must be feasible, i.e. $\mathbf{x}_R(t) \in \mathbb{X}$, and sufficiently smooth, so we can define the reference velocity $\boldsymbol{\xi}_R = \mathbf{A}^+(\mathbf{x}_R)\dot{\mathbf{x}}_R$ and acceleration $\dot{\boldsymbol{\xi}}_R$. For the underactuated case we also require the kinetic equation $\mathbf{M}(\mathbf{x}_R)\dot{\boldsymbol{\xi}}_R + \mathbf{b}(\mathbf{x}_R, \boldsymbol{\xi}_R) = \mathbf{B}(\mathbf{x}_R)\mathbf{u}_R$ to have a solution for \mathbf{u}_R .

The design task for a *tracking controller* is: Find a function $\mathbf{u} = \mathbf{u}(\mathbf{x}, \boldsymbol{\xi}, \mathbf{x}_R, \boldsymbol{\xi}_R, \dot{\boldsymbol{\xi}}_R)$ (the controller) such that $t \mapsto \mathbf{x}_R(t)$ is a stable and attractive trajectory of the closed loop which is the combination of model (4.2) and controller.

State of the art. This is a pretty general task and may be tackled by various standard approaches from control theory, see e.g. [Spong et al., 2006, chap. 7-10] for some overview. For fully actuated systems a popular approach is *computed torque*, see e.g. [Murray et al., 1994, sec. 4.5.2], also called *inverse dynamics* in [Spong et al., 2006, sec. 8.3]. It can be regarded as a particularly simple case of feedback linearization utilizing the fact that any set of minimal generalized coordinates $\mathbf{q}(t) \in \mathbb{R}^n$ is a *flat output* of a fully actuated mechanical system [Martin et al., 1997, sec. 7.1].

For underactuated systems there is no standard textbook approach. Examples for the flatness-based approach can be found in e.g. [Rathinam and Murray, 1998], [Murray et al., 1995] or [Martin et al., 1997, sec. 7.1]. General Lyapunov designs can be found in [Olfati-Saber, 2001] and a approach called *controlled Lagrangian* is proposed in [Bloch et al., 2000].

Outline for this chapter. With the computed torque method one might consider the topic to be solved for fully actuated systems. However, for system whose configuration space is not isomorph to \mathbb{R}^n it is only local due to the requirement of minimal coordinates $\mathbf{q}(t) \in \mathbb{R}^n$. Furthermore, applying linear dynamics in these coordinates may result in intrinsic singularities for the closed loop. Recalling the satellite example from section 1.2, it should be clear that linear dynamics for the Euler angles would probably not be a good choice, also see [Konz and Rudolph, 2016] for further examples.

If linear dynamics are not a general choice, what *is* a good choice for the closed loop dynamics? This chapter motivates three approaches for designing a closed loop for fully actuated systems which rely on the underlying rigid body structure. In addition, the result will be extended to underactuated systems. Finally the approach will be applied to several example systems including the tricopter (fully-actuated), the quadcopter (underactuated but flat) and the bicopter (underactuated and probably not flat).

4.1 Approach 1: Inspired by particle distribution

4.1.1 Particle system

The basic idea. Consider a system of *free* particles with the equations of motion $\mathfrak{m}_p \ddot{\mathbf{r}}_p = \mathfrak{F}_p^A, p = 1, \dots, \mathfrak{N}$ and the control inputs \mathfrak{F}_p^A . We want the system to track a smooth reference trajectory $t \mapsto (\mathbf{r}_{1R}, \dots, \mathbf{r}_{\mathfrak{N}R})(t)$. Probably the simplest solution is the control law $\mathfrak{F}_p^A = \mathfrak{m}_p \ddot{\mathbf{r}}_{pR} - \bar{\mathfrak{d}}_p \dot{\mathbf{r}}_{pE} - \bar{\mathfrak{k}}_p \mathbf{r}_{pE}$ with the position error $\mathbf{r}_{pE} = \mathbf{r}_p - \mathbf{r}_{pR}$ and the design parameters $\bar{\mathfrak{k}}_p, \bar{\mathfrak{d}}_p \in \mathbb{R} > 0$. The resulting closed loop is

$$\mathfrak{m}_p \ddot{\mathbf{r}}_{pE} + \bar{\mathfrak{d}}_p \dot{\mathbf{r}}_{pE} + \bar{\mathfrak{k}}_p \mathbf{r}_{pE} = \mathbf{0}, \quad p = 1 \dots \mathfrak{N}. \quad (4.3)$$

It is clearly exponentially stable and the *desired stiffness* $\bar{\mathfrak{k}}_p$ and *desired damping* $\bar{\mathfrak{d}}_p$ are intuitive tuning parameters.

For a system of particles with geometric constraints $\mathbf{c}(\mathbf{r}_1, \dots, \mathbf{r}_{\mathfrak{N}}) = \mathbf{0}$ we cannot achieve (4.3) in general. As the next best thing we can get as close as possible by formulation of

the following constrained optimization problem

$$\begin{aligned} \text{minimize}_{\ddot{\mathbf{r}} \in \mathbb{R}^{3\mathfrak{N}}} \quad & \bar{\mathcal{G}} = \frac{1}{2} \sum_p \frac{1}{\bar{\mathbf{m}}_p} \|\bar{\mathbf{m}}_p \ddot{\mathbf{r}}_{pE} + \bar{\mathbf{d}}_p \dot{\mathbf{r}}_{pE} + \bar{\mathbf{k}}_p \mathbf{r}_{pE}\|^2 \\ \text{subject to} \quad & \mathbf{c}(\mathbf{r}_1, \dots, \mathbf{r}_{\mathfrak{N}}) = \mathbf{0} \end{aligned} \quad (4.4)$$

Note that we also replaced the particle masses \mathbf{m}_p by *desired masses* $\bar{\mathbf{m}}_p$ as additional design parameters. This will turn out crucial for control of underactuated systems.

The controlled system. The constrained problem (4.4) can be transformed to an unconstrained one by formulating the particle accelerations $\ddot{\mathbf{r}}_p = \ddot{\mathbf{r}}_p(\mathbf{x}, \boldsymbol{\xi}, \dot{\boldsymbol{\xi}})$, $p = 1 \dots \mathfrak{N}$ in terms of minimal acceleration coordinates $\dot{\boldsymbol{\xi}}$. Analogous, let the reference particle positions be formulated in terms of the reference coordinates $\mathbf{x}_R, \boldsymbol{\xi}_R, \dot{\boldsymbol{\xi}}_R$, i.e. $\mathbf{r}_{pR} = \mathbf{r}_p(\mathbf{x}_R)$, $\dot{\mathbf{r}}_{pR} = \dot{\mathbf{r}}_p(\mathbf{x}_R, \boldsymbol{\xi}_R)$, $\ddot{\mathbf{r}}_{pR} = \ddot{\mathbf{r}}_p(\mathbf{x}_R, \boldsymbol{\xi}_R, \dot{\boldsymbol{\xi}}_R)$, and the position error $\mathbf{r}_{pE} = \mathbf{r}_{pE}(\mathbf{x}, \mathbf{x}_R) = \mathbf{r}_p(\mathbf{x}) - \mathbf{r}_p(\mathbf{x}_R)$, etc.. With this, the solution of (4.4) can be computed from

$$\begin{aligned} \frac{\partial \bar{\mathcal{G}}}{\partial \dot{\boldsymbol{\xi}}^i} &= \sum_p \langle \bar{\mathbf{m}}_p \ddot{\mathbf{r}}_{pE} + \bar{\mathbf{d}}_p \dot{\mathbf{r}}_{pE} + \bar{\mathbf{k}}_p \mathbf{r}_{pE}, \frac{\partial \ddot{\mathbf{r}}_p}{\partial \dot{\boldsymbol{\xi}}^i} \rangle \\ &= \sum_p \bar{\mathbf{m}}_p \langle \ddot{\mathbf{r}}_{pE}, \frac{\partial \ddot{\mathbf{r}}_p}{\partial \dot{\boldsymbol{\xi}}^i} \rangle + \sum_p \bar{\mathbf{d}}_p \langle \dot{\mathbf{r}}_{pE}, \frac{\partial \ddot{\mathbf{r}}_p}{\partial \dot{\boldsymbol{\xi}}^i} \rangle + \sum_p \bar{\mathbf{k}}_p \langle \mathbf{r}_{pE}, \partial_i \mathbf{r}_p \rangle \\ &= \underbrace{\frac{\partial}{\partial \dot{\boldsymbol{\xi}}^i} \sum_p \frac{1}{2} \bar{\mathbf{m}}_p \|\ddot{\mathbf{r}}_{pE}\|^2}_{\bar{\mathcal{S}}} + \underbrace{\frac{\partial}{\partial \dot{\boldsymbol{\xi}}^i} \sum_p \frac{1}{2} \bar{\mathbf{d}}_p \|\dot{\mathbf{r}}_{pE}\|^2}_{\bar{\mathcal{R}}} + \underbrace{\partial_i \sum_p \frac{1}{2} \bar{\mathbf{k}}_p \|\mathbf{r}_{pE}\|^2}_{\bar{\mathcal{V}}} = 0, \quad i = 1, \dots, n. \\ &\underbrace{\bar{\mathcal{S}}}_{\bar{f}_i^M} \quad \underbrace{\bar{\mathcal{R}}}_{\bar{f}_i^D} \quad \underbrace{\bar{\mathcal{V}}}_{\bar{f}_i^K} \end{aligned} \quad (4.5)$$

Here we introduced formulations for the *controlled acceleration energy* $\bar{\mathcal{S}}(\mathbf{x}, \boldsymbol{\xi}, \dot{\boldsymbol{\xi}}, \mathbf{x}_R, \boldsymbol{\xi}_R, \dot{\boldsymbol{\xi}}_R)$, the *controlled dissipation function* $\bar{\mathcal{R}}(\mathbf{x}, \boldsymbol{\xi}, \mathbf{x}_R, \boldsymbol{\xi}_R)$ and the *controlled potential energy* $\bar{\mathcal{V}}(\mathbf{x}, \mathbf{x}_R)$. It is worth noting that the inertia force $\bar{\mathbf{f}}^M$ could also be derived from the *controlled kinetic energy* $\bar{\mathcal{T}}(\mathbf{x}, \boldsymbol{\xi}, \mathbf{x}_R, \boldsymbol{\xi}_R)$ as

$$\bar{f}_i^M = \frac{d}{dt} \frac{\partial \bar{\mathcal{T}}}{\partial \dot{\boldsymbol{\xi}}^i} + \gamma_{ij}^k \xi^j \frac{\partial \bar{\mathcal{T}}}{\partial \xi^k} - \partial_i \bar{\mathcal{T}}, \quad \bar{\mathcal{T}} = \frac{1}{2} \sum_p \bar{\mathbf{m}}_p \|\dot{\mathbf{r}}_{pE}\|^2. \quad (4.6)$$

Also note that all the defined “energies” are symmetric in the sense that $\mathcal{V}(\mathbf{x}, \mathbf{x}_R) = \mathcal{V}(\mathbf{x}_R, \mathbf{x})$, etc..

The corresponding forces expressed more explicitly are

$$\begin{aligned} \bar{f}_i^M &= \frac{\partial \bar{\mathcal{S}}}{\partial \dot{\boldsymbol{\xi}}^i} = \underbrace{\sum_p \bar{\mathbf{m}}_p \langle \partial_i \mathbf{r}_p(\mathbf{x}), \partial_j \mathbf{r}_p(\mathbf{x}) \rangle \dot{\xi}^j}_{\bar{M}_{ij}(\mathbf{x})} + \underbrace{\sum_p \bar{\mathbf{m}}_p \langle \partial_i \mathbf{r}_p(\mathbf{x}), \partial_k \partial_j \mathbf{r}_p(\mathbf{x}) \rangle \xi^j \xi^k}_{\bar{\Gamma}_{ijk}(\mathbf{x})} \\ &\quad - \underbrace{\sum_p \bar{\mathbf{m}}_p \langle \partial_i \mathbf{r}_p(\mathbf{x}), \partial_j \mathbf{r}_p(\mathbf{x}_R) \rangle \dot{\xi}_R^j}_{\bar{M}'_{ij}(\mathbf{x}, \mathbf{x}_R)} - \underbrace{\sum_p \bar{\mathbf{m}}_p \langle \partial_i \mathbf{r}_p(\mathbf{x}), \partial_k \partial_j \mathbf{r}_p(\mathbf{x}_R) \rangle \xi_R^j \xi_R^k}_{\bar{\Gamma}'_{ijk}(\mathbf{x}, \mathbf{x}_R)}, \end{aligned} \quad (4.7a)$$

$$\bar{f}_i^D = \frac{\partial \bar{\mathcal{R}}}{\partial \dot{\boldsymbol{\xi}}^i} = \underbrace{\sum_p \bar{\mathbf{d}}_p \langle \partial_i \mathbf{r}_p(\mathbf{x}), \partial_j \mathbf{r}_p(\mathbf{x}) \rangle \xi^j}_{\bar{D}_{ij}(\mathbf{x})} - \underbrace{\sum_p \bar{\mathbf{d}}_p \langle \partial_i \mathbf{r}_p(\mathbf{x}), \partial_j \mathbf{r}_p(\mathbf{x}_R) \rangle \xi_R^j}_{\bar{D}'_{ij}(\mathbf{x}, \mathbf{x}_R)}, \quad (4.7b)$$

$$\bar{f}_i^K = \partial_i \bar{\mathcal{V}} = \sum_p \bar{\mathbf{k}}_p \langle \partial_i \mathbf{r}_p(\mathbf{x}), \mathbf{r}_p(\mathbf{x}) - \mathbf{r}_p(\mathbf{x}_R) \rangle. \quad (4.7c)$$

So we can rewrite (4.5) as

$$\begin{aligned} \bar{M}_{ij}(\mathbf{x})\dot{\xi}^j - \bar{M}'_{ij}(\mathbf{x}, \mathbf{x}_R)\dot{\xi}_R^j + \bar{\Gamma}_{ijk}(\mathbf{x})\xi^j\xi^k - \bar{\Gamma}'_{ijk}(\mathbf{x}, \mathbf{x}_R)\xi_R^j\xi_R^k \\ + \bar{D}_{ij}(\mathbf{x})\xi^j - \bar{D}'_{ij}(\mathbf{x}, \mathbf{x}_R)\xi_R^j + \partial_i \bar{\mathcal{V}}(\mathbf{x}, \mathbf{x}_R) = 0, \quad i = 1, \dots, n. \end{aligned} \quad (4.8)$$

Total energy. Having a definition for a kinetic energy $\bar{\mathcal{T}}$ and a potential energy $\bar{\mathcal{V}}$ it is worth investigating the total energy $\bar{\mathcal{W}} = \bar{\mathcal{T}} + \bar{\mathcal{V}}$ and its change along the solutions of closed loop (4.8). Using the substitutions defined in (4.7) and $\Psi(\mathbf{x}, \mathbf{x}_R) \in \mathbb{R}^{n \times n}$ defined through $\bar{M}'_{ij}(\mathbf{x}, \mathbf{x}_R) = \Psi_i^s(\mathbf{x}, \mathbf{x}_R)\bar{M}_{sj}(\mathbf{x})$ we have

$$\bar{\mathcal{W}} = \overbrace{\frac{1}{2}\bar{M}_{ij}(\mathbf{x})\xi^i\xi^j - \bar{M}'_{ij}(\mathbf{x}, \mathbf{x}_R)\xi^i\xi_R^j + \frac{1}{2}\bar{M}_{ij}(\mathbf{x}_R)\xi_R^i\xi_R^j}^{\bar{\mathcal{T}}(\mathbf{x}, \xi, \mathbf{x}_R, \xi_R)} + \bar{\mathcal{V}}(\mathbf{x}, \mathbf{x}_R) \quad (4.9)$$

$$\begin{aligned} \dot{\bar{\mathcal{W}}} &= \xi^i(\bar{M}_{ij}(\mathbf{x})\dot{\xi}^j + \bar{\Gamma}_{ijk}(\mathbf{x})\xi^j\xi^k - \bar{M}'_{ij}(\mathbf{x}, \mathbf{x}_R)\dot{\xi}_R^j - \bar{\Gamma}'_{ijk}(\mathbf{x}, \mathbf{x}_R)\xi_R^j\xi_R^k + \partial_i \bar{\mathcal{V}}(\mathbf{x}, \mathbf{x}_R)) \\ &\quad + \xi_R^i(\bar{M}_{ij}(\mathbf{x}_R)\dot{\xi}_R^j + \bar{\Gamma}_{ijk}(\mathbf{x}_R)\xi_R^j\xi_R^k - \bar{M}'_{ij}(\mathbf{x}_R, \mathbf{x})\dot{\xi}^j - \bar{\Gamma}'_{ijk}(\mathbf{x}_R, \mathbf{x})\xi^j\xi^k + \partial_i \bar{\mathcal{V}}(\mathbf{x}_R, \mathbf{x})) \\ &\stackrel{(4.8)}{=} -(\xi^i - \Psi_s^i(\mathbf{x}, \mathbf{x}_R)\xi_R^s)(\bar{D}_{ij}(\mathbf{x})\xi^j - \bar{D}'_{ij}(\mathbf{x}, \mathbf{x}_R)\xi_R^j) \\ &\quad + \xi_R^i(\partial_i \bar{\mathcal{V}}(\mathbf{x}_R, \mathbf{x}) + \Psi_i^s(\mathbf{x}, \mathbf{x}_R)\partial_s \bar{\mathcal{V}}(\mathbf{x}, \mathbf{x}_R) + (\bar{M}_{ij}(\mathbf{x}_R) - \Psi_i^s(\mathbf{x}, \mathbf{x}_R)\bar{M}'_{sj}(\mathbf{x}, \mathbf{x}_R))\dot{\xi}_R^j \\ &\quad + (\bar{\Gamma}_{ijk}(\mathbf{x}_R) - \Psi_i^s(\mathbf{x}, \mathbf{x}_R)\bar{\Gamma}'_{sjk}(\mathbf{x}, \mathbf{x}_R))\xi_R^j\xi_R^k - (\bar{\Gamma}'_{ijk}(\mathbf{x}_R, \mathbf{x}) - \Psi_i^s(\mathbf{x}, \mathbf{x}_R)\bar{\Gamma}_{sjk}(\mathbf{x}))\xi^j\xi^k) \end{aligned} \quad (4.10)$$

Obviously the total energy $\bar{\mathcal{W}}$ is not a Lyapunov function for a general reference trajectory. It is, however, for the very special case of $\xi_R = \mathbf{0}$, i.e. proves stability for a constant reference configuration $\mathbf{x}_R = const..$

4.1.2 Free rigid body

Consider the free rigid body discussed in section 3.3 as a special case of a particle system. As motivated there we use the position $\mathbf{r}(t) \in \mathbb{R}^3$ and orientation matrix $\mathbf{R}(t) \in \text{SO}(3)$ merged into the configuration matrix $\mathbf{G}(t) = [\begin{smallmatrix} \mathbf{R}(t) & \mathbf{r}(t) \\ \mathbf{0} & 1 \end{smallmatrix}] \in \text{SE}(3)$ as configuration coordinates. Expressing the particle positions as $\mathbf{r}_p = \mathbf{r} + \mathbf{R}\mathbf{h}_p$ and applying the same calculations as in (3.88) we can write the energies from (4.5) as

$$\bar{\mathcal{V}} = \sum_p \frac{1}{2}\bar{\mathfrak{k}}_p \|\mathbf{r}_p - \mathbf{r}_{pR}\|^2 = \frac{1}{2}\|(\mathbf{G} - \mathbf{G}_R)^\top\|_{\mathbf{K}'}^2 \quad (4.11a)$$

$$\bar{\mathcal{R}} = \sum_p \frac{1}{2}\bar{\mathfrak{d}}_p \|\dot{\mathbf{r}}_p - \dot{\mathbf{r}}_{pR}\|^2 = \frac{1}{2}\|(\dot{\mathbf{G}} - \dot{\mathbf{G}}_R)^\top\|_{\mathbf{D}'}^2 \quad (4.11b)$$

$$\bar{\mathcal{S}} = \sum_p \frac{1}{2}\bar{\mathfrak{m}}_p \|\ddot{\mathbf{r}}_p - \ddot{\mathbf{r}}_{pR}\|^2 = \frac{1}{2}\|(\ddot{\mathbf{G}} - \ddot{\mathbf{G}}_R)^\top\|_{\mathbf{M}'}^2 \quad (4.11c)$$

$$\bar{\mathcal{T}} = \sum_p \frac{1}{2}\bar{\mathfrak{m}}_p \|\dot{\mathbf{r}}_p - \dot{\mathbf{r}}_{pR}\|^2 = \frac{1}{2}\|(\dot{\mathbf{G}} - \dot{\mathbf{G}}_R)^\top\|_{\mathbf{M}'}^2 \quad (4.11d)$$

where

$$\bar{\mathbf{K}}' = \sum_p \bar{\mathbf{k}}_p \begin{bmatrix} \mathbf{h}_p \mathbf{h}_p^\top & \mathbf{h}_p^\top \\ \mathbf{h}_p & 1 \end{bmatrix} = \begin{bmatrix} \bar{\mathbf{H}}' & \bar{k} \bar{\mathbf{h}} \\ \bar{k} \bar{\mathbf{h}}^\top & \bar{k} \end{bmatrix}, \quad (4.12a)$$

$$\bar{\mathbf{D}}' = \sum_p \bar{\mathbf{d}}_p \begin{bmatrix} \mathbf{h}_p \mathbf{h}_p^\top & \mathbf{h}_p^\top \\ \mathbf{h}_p & 1 \end{bmatrix} = \begin{bmatrix} \bar{\mathbf{Y}}' & \bar{d} \bar{\mathbf{l}} \\ \bar{d} \bar{\mathbf{l}}^\top & \bar{d} \end{bmatrix}, \quad (4.12b)$$

$$\bar{\mathbf{M}}' = \sum_p \bar{\mathbf{m}}_p \begin{bmatrix} \mathbf{h}_p \mathbf{h}_p^\top & \mathbf{h}_p^\top \\ \mathbf{h}_p & 1 \end{bmatrix} = \begin{bmatrix} \bar{\Theta}' & \bar{m} \bar{\mathbf{s}} \\ \bar{m} \bar{\mathbf{s}}^\top & \bar{m} \end{bmatrix}. \quad (4.12c)$$

As before we can interpret the entries of the *desired inertia matrix* $\bar{\mathbf{M}} = \text{Vee}(\bar{\mathbf{M}}')$ as the *desired total mass* \bar{m} , *desired center of mass* $\bar{\mathbf{s}}$ and the *desired moment of inertia* $\bar{\Theta} = \text{Vee}(\bar{\Theta}')$. The analog holds for the entries of the *desired damping matrix* $\bar{\mathbf{D}} = \text{Vee}(\bar{\mathbf{D}}')$ and the *desired stiffness matrix* $\bar{\mathbf{K}} = \text{Vee}(\bar{\mathbf{K}}')$.

Introduce the translational $\mathbf{v}(t) \in \mathbb{R}^3$ and angular velocity $\boldsymbol{\omega}(t) \in \mathbb{R}^3$ merged into $\boldsymbol{\xi} = [\mathbf{v}^\top, \boldsymbol{\omega}^\top]^\top = \text{vee}(\mathbf{G}^{-1} \mathbf{G})$ as velocity coordinates. Furthermore, we introduce the *configuration error* $\mathbf{G}_E = \mathbf{G}_R^{-1} \mathbf{G}$ and exploit the invariance of the norm to left translation of the argument to express the desired energies (4.11) as

$$\bar{\mathcal{V}} = \frac{1}{2} \| (\mathbf{I}_4 - \mathbf{G}_E^{-1})^\top \|_{\bar{\mathbf{K}}'}^2 \quad (4.13a)$$

$$\bar{\mathcal{R}} = \frac{1}{2} \| (\text{wed}(\boldsymbol{\xi}) - \mathbf{G}_E^{-1} \text{wed}(\boldsymbol{\xi}_R))^\top \|_{\bar{\mathbf{D}}'}^2 \quad (4.13b)$$

$$\bar{\mathcal{S}} = \frac{1}{2} \| (\text{wed}(\dot{\boldsymbol{\xi}}) + \text{wed}(\boldsymbol{\xi})^2 - \mathbf{G}_E^{-1} (\text{wed}(\dot{\boldsymbol{\xi}}_R) + \text{wed}(\boldsymbol{\xi}_R)^2))^\top \|_{\bar{\mathbf{M}}'}^2 \quad (4.13c)$$

$$\bar{\mathcal{T}} = \frac{1}{2} \| (\text{wed}(\boldsymbol{\xi}) - \mathbf{G}_E^{-1} \text{wed}(\boldsymbol{\xi}_R))^\top \|_{\bar{\mathbf{M}}'}^2. \quad (4.13d)$$

The resulting forces can be expressed as

$$\bar{\mathbf{f}}^K = \nabla \bar{\mathcal{V}} = \text{vee2} ((\mathbf{I}_4 - \mathbf{G}_E^{-1}) \bar{\mathbf{K}}'), \quad (4.14a)$$

$$\bar{\mathbf{f}}^D = \frac{\partial \bar{\mathcal{R}}}{\partial \boldsymbol{\xi}} = \text{vee2} ((\text{wed}(\boldsymbol{\xi}) - \mathbf{G}_E^{-1} \text{wed}(\boldsymbol{\xi}_R)) \bar{\mathbf{D}}'), \quad (4.14b)$$

$$\bar{\mathbf{f}}^M = \frac{\partial \bar{\mathcal{S}}}{\partial \dot{\boldsymbol{\xi}}} = \text{vee2} ((\text{wed}(\dot{\boldsymbol{\xi}}) + \text{wed}(\boldsymbol{\xi})^2 - \mathbf{G}_E^{-1} (\text{wed}(\dot{\boldsymbol{\xi}}_R) + \text{wed}(\boldsymbol{\xi}_R)^2)) \bar{\mathbf{M}}') \quad (4.14c)$$

or more explicitly

$$\bar{\mathbf{f}}^K = \begin{bmatrix} \bar{k} \mathbf{R}_E^\top (\mathbf{r}_E + (\mathbf{R}_E - \mathbf{I}_3) \bar{\mathbf{h}}) \\ \bar{k} \text{wed}(\bar{\mathbf{h}}) \mathbf{R}_E^\top \mathbf{r}_E + \text{vee2} (\text{Vee}(\bar{\mathbf{H}})(\mathbf{R}_E - \mathbf{I}_3)) \end{bmatrix} \quad (4.15a)$$

$$\bar{\mathbf{f}}^D = \underbrace{\begin{bmatrix} \bar{d} \mathbf{I}_3 & \bar{d} \text{wed}(\bar{\mathbf{l}})^\top \\ \bar{d} \text{wed}(\bar{\mathbf{l}}) & \bar{\mathbf{Y}} \end{bmatrix}}_{\bar{\mathbf{D}}} \underbrace{\begin{bmatrix} \mathbf{v} \\ \boldsymbol{\omega} \end{bmatrix}}_{\boldsymbol{\xi}} - \underbrace{\begin{bmatrix} \bar{d} \mathbf{R}_E^\top & \mathbf{R}_E^\top \bar{d} \text{wed}(\bar{\mathbf{l}})^\top \\ \bar{d} \text{wed}(\bar{\mathbf{l}}) \mathbf{R}_E^\top & \text{Wed}(\mathbf{R}_E^\top \text{Vee}(\bar{\mathbf{Y}})) \mathbf{R}_E^\top \end{bmatrix}}_{\boldsymbol{\xi}_R} \underbrace{\begin{bmatrix} \mathbf{v}_R \\ \boldsymbol{\omega}_R \end{bmatrix}}_{\boldsymbol{\xi}_R} \quad (4.15b)$$

$$\begin{aligned} \bar{\mathbf{f}}^M = & \underbrace{\begin{bmatrix} \bar{m} \mathbf{I}_3 & \bar{m} \text{wed}(\bar{\mathbf{s}})^\top \\ \bar{m} \text{wed}(\bar{\mathbf{s}}) & \bar{\Theta} \end{bmatrix}}_{\bar{\mathbf{M}}} \underbrace{\begin{bmatrix} \dot{\mathbf{v}} \\ \dot{\boldsymbol{\omega}} \end{bmatrix}}_{\dot{\boldsymbol{\xi}}} + \begin{bmatrix} \bar{m} \text{wed}(\boldsymbol{\omega}) & -\bar{m} \text{wed}(\boldsymbol{\omega}) \text{wed}(\bar{\mathbf{s}}) \\ \bar{m} \text{wed}(\bar{\mathbf{s}}) \text{wed}(\boldsymbol{\omega}) & \text{wed}(\text{Vee}(\bar{\Theta})) \boldsymbol{\omega} \end{bmatrix} \begin{bmatrix} \mathbf{v} \\ \boldsymbol{\omega} \end{bmatrix} \\ & - \begin{bmatrix} \bar{m} \mathbf{R}_E^\top & \mathbf{R}_E^\top \bar{m} \text{wed}(\bar{\mathbf{s}})^\top \\ \bar{m} \text{wed}(\bar{\mathbf{s}}) \mathbf{R}_E^\top & \text{Wed}(\mathbf{R}_E^\top \text{Vee}(\bar{\Theta})) \mathbf{R}_E^\top \end{bmatrix} \begin{bmatrix} \dot{\mathbf{v}}_R \\ \dot{\boldsymbol{\omega}}_R \end{bmatrix} \\ & - \begin{bmatrix} \bar{m} \mathbf{R}_E^\top \text{wed}(\boldsymbol{\omega}_R) & -\bar{m} \mathbf{R}_E^\top \text{wed}(\boldsymbol{\omega}_R) \text{wed}(\bar{\mathbf{s}}) \\ \bar{m} \text{wed}(\bar{\mathbf{s}}) \mathbf{R}_E^\top \text{wed}(\boldsymbol{\omega}_R) & \text{Wed}(\mathbf{R}_E^\top \text{wed}(\boldsymbol{\omega}_R) \text{Vee}(\bar{\Theta})) \mathbf{R}_E^\top \end{bmatrix} \begin{bmatrix} \mathbf{v}_R \\ \boldsymbol{\omega}_R \end{bmatrix} \end{aligned} \quad (4.15c)$$

The closed loop kinetic equation $\bar{\mathbf{f}}^M + \bar{\mathbf{f}}^D + \bar{\mathbf{f}}^K = \mathbf{0}$ contains 30 tuning parameters within the matrices $\bar{\mathbf{M}}'$, $\bar{\mathbf{D}}'$, $\bar{\mathbf{K}}' \in \text{SYM}^+(4)$. The characteristic polynomial of the first order approximation of the system about any constant configuration $\mathbf{x}_R = \text{const.}$ is $\det(\bar{\mathbf{M}}\lambda^2 + \bar{\mathbf{D}}\lambda + \bar{\mathbf{K}})$ where $\bar{\mathbf{M}} = \text{Vee}(\bar{\mathbf{M}}')$, etc..

blah

In contrast to this, the characteristic polynomial resulting from the computed torque method (see [sec:ComputedTorque](#)) for this system is $\det(\mathbf{I}_6\lambda^2 + \mathbf{K}_1\lambda + \mathbf{K}_2)$, which has $n(n+1) = 42$ tuning parameters within the matrixes $\mathbf{K}_1, \mathbf{K}_2 \in \text{SYM}^+(6)$.

blah

A possible generalization of the rigid body potential $\bar{\mathcal{V}}$ which works with all $\frac{1}{2}n(n+1) = 21$ tuning parameters in a matrix $\bar{\mathbf{K}} \in \text{SYM}^+(6)$ is given in [sec:GenRigidBodyPotential](#).

4.1.3 Rigid body systems

Let the particles belong to a system of N rigid bodies with the body configurations ${}_b^a\mathbf{G}$ as discussed in section 3.4. The potential energy from (4.5) may be formulated as $\bar{\mathcal{V}} = \sum_{b=1}^N \frac{1}{2} \|({}^0_b\mathbf{G} - {}^0_b\mathbf{G}_R)^\top\|_{b\bar{\mathbf{K}}}^2$, with a body stiffness matrix ${}^0_b\bar{\mathbf{K}}'$ resulting from (4.12) for each body. This potential only captures stiffness w.r.t. the absolute configurations ${}^0_b\mathbf{G}$. Depending on the control objective it may be equally reasonable to consider a stiffness associated with the relative configurations ${}^a\mathbf{G}$ as illustrated in Figure 4.1. Considering

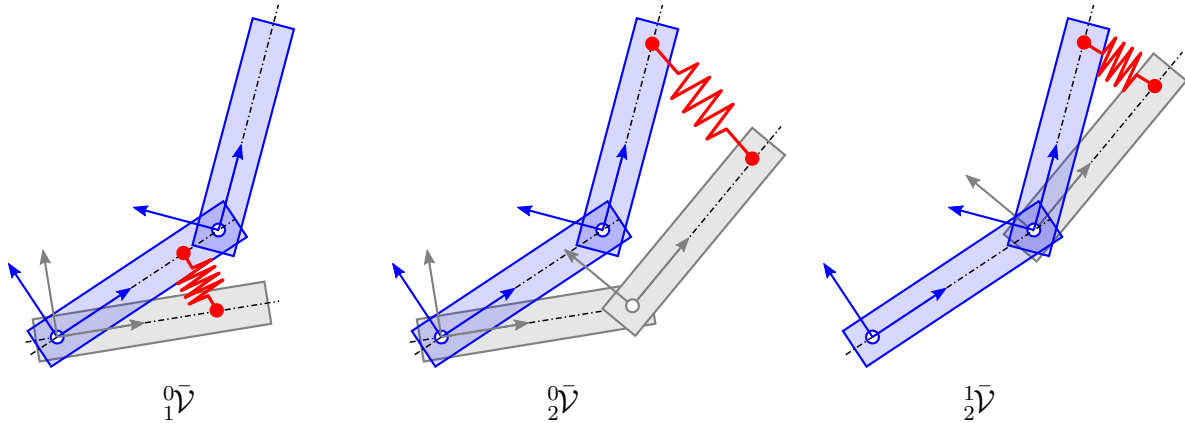


Figure 4.1: Different parts of the potential $\bar{\mathcal{V}}$ for a double pendulum

the same argument for damping and inertia, we propose the following energies for the

control of a rigid body system:

$$\bar{\mathcal{V}} = \sum_{a,b=0}^N \overbrace{\frac{1}{2} \| ({}^a_b \mathbf{G} - {}^a_b \mathbf{G}_R)^\top \|_{{}^a_b \bar{\mathbf{K}}'}^2}^{{}^a_b \bar{\mathcal{V}}}, \quad {}^a_b \bar{\mathbf{K}}' \in \mathbb{SYM}_0^+(4) \quad (4.16a)$$

$$\bar{\mathcal{R}} = \sum_{a,b=0}^N \overbrace{\frac{1}{2} \| ({}^a_b \dot{\mathbf{G}} - {}^a_b \dot{\mathbf{G}}_R)^\top \|_{{}^a_b \bar{\mathbf{D}}'}^2}^{{}^a_b \bar{\mathcal{R}}}, \quad {}^a_b \bar{\mathbf{D}}' \in \mathbb{SYM}_0^+(4) \quad (4.16b)$$

$$\bar{\mathcal{S}} = \sum_{a,b=0}^N \overbrace{\frac{1}{2} \| ({}^a_b \ddot{\mathbf{G}} - {}^a_b \ddot{\mathbf{G}}_R)^\top \|_{{}^a_b \bar{\mathbf{M}}'}^2}^{{}^a_b \bar{\mathcal{S}}}, \quad {}^a_b \bar{\mathbf{M}}' \in \mathbb{SYM}_0^+(4) \quad (4.16c)$$

$$\bar{\mathcal{T}} = \sum_{a,b=0}^N \overbrace{\frac{1}{2} \| ({}^a_b \dot{\mathbf{G}} - {}^a_b \dot{\mathbf{G}}_R)^\top \|_{{}^a_b \bar{\mathbf{M}}'}^2}^{{}^a_b \bar{\mathcal{T}}}. \quad (4.16d)$$

Note that ${}^a_b \bar{\mathbf{K}}' = {}^b_a \bar{\mathbf{K}}'$ implies ${}^b_a \bar{\mathcal{V}} = {}^a_b \bar{\mathcal{V}}$ and ${}^a_a \bar{\mathcal{V}} = 0$ since ${}^a_b \mathbf{G} = {}^a_a \mathbf{G}_R = \mathbf{I}_4$ and analog for damping and inertia.

Let the body configurations ${}^b_a \mathbf{G}(\mathbf{x})$ and the body velocities ${}^b_a \xi = {}^b_a \mathbf{J}(\mathbf{x})\xi$ be formulated in terms of suitable system coordinates \mathbf{x} and ξ , as discussed in section 3.4. With the shorthand notations ${}^a_b \mathbf{G}_E = {}^a_b \mathbf{G}_E(\mathbf{x}, \mathbf{x}_R) = {}^a_b \mathbf{G}^{-1}(\mathbf{x}_R) {}^a_b \mathbf{G}(\mathbf{x})$ and ${}^a_b \mathbf{J} = {}^a_b \mathbf{J}(\mathbf{x})$, ${}^a_b \mathbf{J}_R = {}^a_b \mathbf{J}(\mathbf{x}_R)$ we can express (4.16) as

$$\bar{\mathcal{V}} = \sum_{a,b} \frac{1}{2} \| (\mathbf{I}_4 - {}^a_b \mathbf{G}_E^{-1})^\top \|_{{}^a_b \bar{\mathbf{K}}'}^2, \quad (4.17a)$$

$$\bar{\mathcal{R}} = \sum_{a,b} \frac{1}{2} \| (\text{wed}({}^a_b \mathbf{J} \xi) - {}^a_b \mathbf{G}_E^{-1} \text{wed}({}^a_b \mathbf{J}_R \xi_R))^\top \|_{{}^a_b \bar{\mathbf{D}}'}^2, \quad (4.17b)$$

$$\begin{aligned} \bar{\mathcal{S}} = \sum_{a,b} \frac{1}{2} & \| (\text{wed}({}^a_b \mathbf{J} \dot{\xi} + {}^a_b \dot{\mathbf{J}} \xi) + \text{wed}({}^a_b \mathbf{J} \xi)^2 \\ & - {}^a_b \mathbf{G}_E^{-1} (\text{wed}({}^a_b \mathbf{J}_R \dot{\xi}_R + {}^a_b \dot{\mathbf{J}}_R \xi_R) + \text{wed}({}^a_b \mathbf{J}_R \xi_R)^2))^\top \|_{{}^a_b \bar{\mathbf{M}}'}^2 \end{aligned} \quad (4.17c)$$

$$\bar{\mathcal{T}} = \sum_{a,b} \frac{1}{2} \| (\text{wed}({}^a_b \mathbf{J} \xi) - {}^a_b \mathbf{G}_E^{-1} \text{wed}({}^a_b \mathbf{J}_R \xi_R))^\top \|_{{}^a_b \bar{\mathbf{M}}'}^2. \quad (4.17d)$$

Plugging this into the original definition of the closed loop (4.7) we find:

The desired closed loop system for the particle based approach is given by

$$\bar{\mathbf{f}}^M + \bar{\mathbf{f}}^D + \bar{\mathbf{f}}^K = \mathbf{0} \quad (4.18a)$$

where

$$\bar{\mathbf{f}}^K = \nabla \bar{\mathcal{V}} = \sum_{a,b} {}^a_b \mathbf{J}^\top \text{vee2} ((\mathbf{I}_4 - {}^a_b \mathbf{G}_E^{-1}) {}^a_b \bar{\mathbf{K}}') \quad (4.18b)$$

$$\bar{\mathbf{f}}^D = \frac{\partial \bar{\mathcal{R}}}{\partial \xi} = \sum_{a,b} {}^a_b \mathbf{J}^\top \text{vee2} ((\text{wed}({}^a_b \mathbf{J} \xi) - {}^a_b \mathbf{G}_E^{-1} \text{wed}({}^a_b \mathbf{J}_R \xi_R)) {}^a_b \bar{\mathbf{D}}') \quad (4.18c)$$

$$\begin{aligned} \bar{\mathbf{f}}^M = \frac{\partial \bar{\mathcal{S}}}{\partial \dot{\xi}} = \sum_{a,b} & {}^a_b \mathbf{J}^\top \text{vee2} ((\text{wed}({}^a_b \mathbf{J} \dot{\xi} + {}^a_b \dot{\mathbf{J}} \xi) + \text{wed}({}^a_b \mathbf{J} \xi)^2 \\ & - {}^a_b \mathbf{G}_E^{-1} (\text{wed}({}^a_b \mathbf{J}_R \dot{\xi}_R + {}^a_b \dot{\mathbf{J}}_R \xi_R) + \text{wed}({}^a_b \mathbf{J}_R \xi_R)^2)) {}^a_b \bar{\mathbf{M}}') \end{aligned} \quad (4.18d)$$

The system inertia matrix $\bar{\mathbf{M}}$ can be recovered from the first term in (4.18d):

$$\sum_{a,b} {}^a_b \mathbf{J}^\top \text{vee2} \left(\text{wed}({}^a_b \mathbf{J} \dot{\boldsymbol{\xi}}) {}^a_b \bar{\mathbf{M}}' \right) = \underbrace{\sum_{a,b} {}^a_b \mathbf{J}^\top \text{Wed}({}^a_b \bar{\mathbf{M}}') {}^a_b \mathbf{J} \dot{\boldsymbol{\xi}}}_{\bar{\mathbf{M}}} = \frac{\partial^2 \bar{\mathcal{S}}}{\partial \dot{\boldsymbol{\xi}} \partial \dot{\boldsymbol{\xi}}} = \frac{\partial^2 \bar{\mathcal{T}}}{\partial \boldsymbol{\xi} \partial \boldsymbol{\xi}} \quad (4.19)$$

Though the body inertia matrices ${}^a_b \bar{\mathbf{M}}' \in \mathbb{SYM}_0^+(4)$ from (4.16c) are only required to be positive semi-definite, the resulting system inertia matrix $\bar{\mathbf{M}}(\mathbf{x}) \in \mathbb{SYM}^+(n)$ is required to be positive definite for the closed loop to be solvable.

4.2 Approach 2: Body based approach

The previous approach for the design of a closed loop has a vivid interpretation for the control energies and parameters. However, the total energy \mathcal{W} does not, in general, serve as a Lyapunov function. In this section we attempt to modify the energies to account for this.

4.2.1 Free rigid body

Using the configuration error $\mathbf{G}_E = \mathbf{G}_R^{-1} \mathbf{G}$ and its velocity $\dot{\boldsymbol{\xi}}_E = \mathbf{G}_E^{-1} \dot{\mathbf{G}}_E = \dot{\boldsymbol{\xi}} - \text{Ad}_{\mathbf{G}_E}^{-1} \dot{\boldsymbol{\xi}}_R$ we modify the energies from section 4.1 to

$$\bar{\mathcal{V}} = \frac{1}{2} \|(\mathbf{G}_E - \mathbf{I}_4)^\top\|_{\bar{\mathbf{K}}}^2, \quad \bar{\mathbf{K}}' \in \mathbb{SYM}^+(4), \quad (4.20a)$$

$$\bar{\mathcal{R}} = \frac{1}{2} \|\dot{\mathbf{G}}_E^\top\|_{\bar{\mathbf{D}}'}^2 = \frac{1}{2} \|\text{wed}(\dot{\boldsymbol{\xi}}_E)^\top\|_{\bar{\mathbf{D}}'}^2 = \frac{1}{2} \dot{\boldsymbol{\xi}}_E^\top \bar{\mathbf{D}} \dot{\boldsymbol{\xi}}_E, \quad \bar{\mathbf{D}}' \in \mathbb{SYM}^+(4), \quad (4.20b)$$

$$\bar{\mathcal{S}} = \frac{1}{2} \|\ddot{\mathbf{G}}_E^\top\|_{\bar{\mathbf{M}}'}^2 = \frac{1}{2} \|(\text{wed}(\dot{\boldsymbol{\xi}}_E) + \text{wed}(\boldsymbol{\xi}_E)^2)^\top\|_{\bar{\mathbf{M}}'}^2, \quad \bar{\mathbf{M}}' \in \mathbb{SYM}^+(4), \quad (4.20c)$$

$$\bar{\mathcal{T}} = \frac{1}{2} \|\dot{\mathbf{G}}_E^\top\|_{\bar{\mathbf{M}}'}^2 = \frac{1}{2} \|\text{wed}(\dot{\boldsymbol{\xi}}_E)^\top\|_{\bar{\mathbf{M}}'}^2 = \frac{1}{2} \dot{\boldsymbol{\xi}}_E^\top \bar{\mathbf{M}} \dot{\boldsymbol{\xi}}_E \quad (4.20d)$$

with usual substitution $\bar{\mathbf{M}} = \text{Vee}(\bar{\mathbf{M}}')$. The closed loop forces are again defined as the derivatives of their corresponding energies. Using $\partial \boldsymbol{\xi}_E / \partial \boldsymbol{\xi} = \mathbf{I}_6$ we have

$$\bar{\mathbf{f}}^K = \nabla \bar{\mathcal{V}} = \text{vee2} ((\mathbf{I}_4 - \mathbf{G}_E^{-1}) \bar{\mathbf{K}}') \quad (4.21a)$$

$$\bar{\mathbf{f}}^D = \frac{\partial \bar{\mathcal{R}}}{\partial \boldsymbol{\xi}} = \text{vee2} (\text{wed}(\dot{\boldsymbol{\xi}}_E) \bar{\mathbf{D}}') = \bar{\mathbf{D}} \dot{\boldsymbol{\xi}}_E \quad (4.21b)$$

$$\bar{\mathbf{f}}^M = \frac{\partial \bar{\mathcal{S}}}{\partial \dot{\boldsymbol{\xi}}} = \text{vee2} ((\text{wed}(\dot{\boldsymbol{\xi}}_E) + \text{wed}(\boldsymbol{\xi}_E)^2) \bar{\mathbf{M}}') = \bar{\mathbf{M}} \dot{\boldsymbol{\xi}}_E - \text{ad}_{\dot{\boldsymbol{\xi}}_E}^\top \bar{\mathbf{M}} \dot{\boldsymbol{\xi}}_E \quad (4.21c)$$

A crucial result of this approach is that the resulting closed loop equations can be written as *autonomous* equations for the configuration \mathbf{G}_E and velocity error $\dot{\boldsymbol{\xi}}_E$ as

$$\dot{\mathbf{G}}_E = \mathbf{G} \text{wed}(\boldsymbol{\xi}_E), \quad \bar{\mathbf{M}} \dot{\boldsymbol{\xi}}_E - \text{ad}_{\dot{\boldsymbol{\xi}}_E}^\top \bar{\mathbf{M}} \dot{\boldsymbol{\xi}}_E + \bar{\mathbf{D}} \dot{\boldsymbol{\xi}}_E + \text{vee2} ((\mathbf{I}_4 - \mathbf{G}_E^{-1}) \bar{\mathbf{K}}') = \mathbf{0}. \quad (4.22)$$

A quite similar (though restricted to $\mathbf{s} = \mathbf{l} = \mathbf{h} = \mathbf{0}$) closed loop for the free rigid body is proposed in [Koditschek, 1989], though motivated from a Lie group point of view.

Total energy. The change of the total energy $\bar{\mathcal{W}} = \bar{\mathcal{T}} + \bar{\mathcal{V}}$ along the solutions of the closed loop (4.22) is

$$\dot{\bar{\mathcal{W}}} = \xi_E^\top (\bar{\mathbf{M}} \dot{\xi}_E + \text{vee2}((\mathbf{I}_4 - \mathbf{G}_E^{-1}) \bar{\mathbf{K}}')) = \underbrace{\xi_E^\top \text{ad}_{\xi_E}^\top \bar{\mathbf{M}} \xi_E}_{=0} - \xi_E^\top \bar{\mathbf{D}} \xi_E = -2\bar{\mathcal{R}}. \quad (4.23)$$

Note that $\bar{\mathbf{K}}', \bar{\mathbf{D}}', \bar{\mathbf{M}}' \in \mathbb{S}\mathbb{Y}\mathbb{M}^+(4)$ imply the positive definiteness of the total energy $\bar{\mathcal{W}}$ and the dissipation function $\bar{\mathcal{R}}$. Using this with the techniques from [Koditschek, 1989], one can show that “almost” all solutions of (4.22) converge to $\mathbf{G}_E = \mathbf{I}_4$ and $\xi_E = \mathbf{0}$. The remaining solutions are the constant ($\xi_E = \mathbf{0}$) configurations $\mathbf{G}_E \neq \mathbf{I}_4$ which are critical points of the potential $\bar{\mathcal{V}}$, see subsection 3.3.4. Roughly speaking, the configuration in which the body is 180° rotated to its reference.

4.2.2 Rigid body systems

For a rigid body system, let the body configurations ${}^a_b \mathbf{G} = {}^a_b \mathbf{G}(\mathbf{x})$ and the body velocities ${}^a_b \dot{\xi} = {}^a_b \mathbf{J}(\mathbf{x}) \xi$ be parameterized by the configuration \mathbf{x} and velocity coordinates ξ . So the body configuration errors ${}^a_b \mathbf{G}_E$ and body velocity errors ${}^a_b \dot{\xi}_E$ may be expressed as

$${}^a_b \mathbf{G}_E(\mathbf{x}, \mathbf{x}_R) = {}^a_b \mathbf{G}^{-1}(\mathbf{x}_R) {}^a_b \mathbf{G}(\mathbf{x}), \quad (4.24a)$$

$${}^a_b \dot{\xi}_E(\mathbf{x}, \xi, \mathbf{x}_R, \xi_R) = {}^a_b \mathbf{J}(\mathbf{x}) \xi - \text{Ad}_{{}^a_b \mathbf{G}_E(\mathbf{x}, \mathbf{x}_R)}^{-1} {}^a_b \mathbf{J}_R(\mathbf{x}_R) \xi_R. \quad (4.24b)$$

As done in subsection 4.1.3, the system energies are simply the sum over the energies associated with the absolute and relative body configurations:

$$\bar{\mathcal{V}} = \sum_{a,b} \frac{1}{2} \|({}^a_b \mathbf{G}_E - \mathbf{I}_4)^\top\|_{{}^a_b \bar{\mathbf{K}}'}^2, \quad (4.25a)$$

$$\bar{\mathcal{R}} = \sum_{a,b} \frac{1}{2} \|\text{wed}({}^a_b \dot{\xi}_E)^\top\|_{{}^a_b \bar{\mathbf{D}}'}^2, \quad (4.25b)$$

$$\bar{\mathcal{S}} = \sum_{a,b} \frac{1}{2} \|(\text{wed}({}^a_b \dot{\xi}_E) + \text{wed}({}^a_b \dot{\xi}_E)^2)^\top\|_{{}^a_b \bar{\mathbf{M}}'}^2, \quad (4.25c)$$

$$\bar{\mathcal{T}} = \sum_{a,b} \frac{1}{2} \|\text{wed}({}^a_b \dot{\xi}_E)^\top\|_{{}^a_b \bar{\mathbf{M}}'}^2. \quad (4.25d)$$

Overall, the desired controlled system for the body based approach takes the form

$$\bar{\mathbf{f}}^M + \bar{\mathbf{f}}^D + \bar{\mathbf{f}}^K = \mathbf{0} \quad (4.26a)$$

where

$$\bar{\mathbf{f}}^K = \nabla \bar{\mathcal{V}} = \sum_{a,b} {}^a_b \mathbf{J}^\top \text{vee2}((\mathbf{I}_4 - {}^a_b \mathbf{G}_E^{-1}) {}^a_b \bar{\mathbf{K}}'), \quad (4.26b)$$

$$\bar{\mathbf{f}}^D = \frac{\partial \bar{\mathcal{R}}}{\partial \xi} = \sum_{a,b} {}^a_b \mathbf{J}^\top {}^a_b \bar{\mathbf{D}} {}^a_b \dot{\xi}_E \quad (4.26c)$$

$$\bar{\mathbf{f}}^M = \frac{\partial \bar{\mathcal{S}}}{\partial \dot{\xi}} = \sum_{a,b} {}^a_b \mathbf{J}^\top ({}^a_b \bar{\mathbf{M}} {}^a_b \dot{\xi}_E - \text{ad}_{{}^a_b \dot{\xi}_E}^\top {}^a_b \bar{\mathbf{M}} {}^a_b \dot{\xi}_E) \quad (4.26d)$$

The change of the total energy $\bar{\mathcal{W}} = \bar{\mathcal{T}} + \bar{\mathcal{V}}$ along the solutions of (4.26) does *not* take a similar form to (4.23). Consequently there is no simple conclusion about stability.

4.3 Approach 3: Inspired by total energy

The previous approaches for the design of a closed loop also motived a total energy $\bar{\mathcal{W}}$. Unfortunately, it did, in general, not turn out to be useful for stability analysis. In this section we like to motivate yet another approach for the design of a closed loop dynamics for the tracking problem which is based on the total energy as Lyapunov function.

4.3.1 Overall structure

The general structure of this approach follows [Bullo and Murray, 1999].

Total energy. Initially we drop the rigid body structure of the system and only consider the coordinates $\mathbf{x}, \boldsymbol{\xi}$ and their kinematic relation $\dot{\mathbf{x}} = \mathbf{A}(\mathbf{x})\boldsymbol{\xi}$. Define the “total error energy” as

$$\bar{\mathcal{W}}(\mathbf{x}, \boldsymbol{\xi}, \mathbf{x}_R, \boldsymbol{\xi}_R) = \underbrace{\frac{1}{2} \|\boldsymbol{\xi} - \mathbf{Q}(\mathbf{x}, \mathbf{x}_R)\boldsymbol{\xi}_R\|_{\bar{\mathbf{M}}(\mathbf{x})}^2}_{\bar{\tau}} + \bar{\mathcal{V}}(\mathbf{x}, \mathbf{x}_R) \quad (4.27)$$

with the positive definite error potential $\bar{\mathcal{V}} : \mathbb{X} \times \mathbb{X} \rightarrow \mathbb{R}^+$, $\bar{\mathcal{V}}(\mathbf{x}, \mathbf{x}_R) = 0 \Leftrightarrow \mathbf{x} = \mathbf{x}_R$ and the positive definite inertia matrix $\bar{\mathbf{M}}(\mathbf{x}) \in \text{SYM}^+(n)$. So far the transport map $\mathbf{Q} : \mathbb{X} \times \mathbb{X} \rightarrow \mathbb{R}^{n \times n}$ may be any regular matrix with $\mathbf{Q}(\mathbf{x}, \mathbf{x}) = \mathbf{I}_n$. Combination of these requirements yields the positive definiteness of the total energy, i.e.

$$\bar{\mathcal{W}}(\mathbf{x}, \boldsymbol{\xi}, \mathbf{x}_R, \boldsymbol{\xi}_R) \geq 0, \quad \bar{\mathcal{W}}(\mathbf{x}, \boldsymbol{\xi}, \mathbf{x}_R, \boldsymbol{\xi}_R) = 0 \Leftrightarrow \mathbf{x} = \mathbf{x}_R, \boldsymbol{\xi} = \boldsymbol{\xi}_R. \quad (4.28)$$

Change of total energy. The time derivative of the total energy is

$$\begin{aligned} \dot{\bar{\mathcal{W}}} &= \boldsymbol{\xi}_E^\top (\bar{\mathbf{M}} \dot{\boldsymbol{\xi}}_E + \frac{1}{2} \dot{\bar{\mathbf{M}}} \boldsymbol{\xi}_E) + \boldsymbol{\xi}^\top \nabla \bar{\mathcal{V}} + \boldsymbol{\xi}_R^\top \nabla_R \bar{\mathcal{V}} \\ &= \boldsymbol{\xi}_E^\top (\bar{\mathbf{M}} \dot{\boldsymbol{\xi}}_E + \frac{1}{2} \dot{\bar{\mathbf{M}}} \boldsymbol{\xi}_E + \nabla \bar{\mathcal{V}}) + \boldsymbol{\xi}_R^\top (\nabla_R \bar{\mathcal{V}} + \mathbf{Q}^\top \nabla \bar{\mathcal{V}}). \end{aligned} \quad (4.29)$$

where $\nabla_R = \mathbf{A}^\top(\mathbf{x}_R) \frac{\partial}{\partial \mathbf{x}_R}$. The second term vanishes if we require the transport map \mathbf{Q} to fulfill

$$\nabla_R \bar{\mathcal{V}} = -\mathbf{Q}^\top \nabla \bar{\mathcal{V}}. \quad (4.30)$$

With a positive definite damping matrix $\bar{\mathbf{D}} \in \text{SYM}^+(n)$ and a yet to define skew symmetric matrix $\bar{\mathbf{S}} = -\bar{\mathbf{S}}^\top \in \mathbb{R}^{n \times n}$ we set the closed loop kinetics as

$$\bar{\mathbf{M}} \dot{\boldsymbol{\xi}}_E + \frac{1}{2} \dot{\bar{\mathbf{M}}} \boldsymbol{\xi}_E + \nabla \bar{\mathcal{V}} = -(\bar{\mathbf{D}} + \bar{\mathbf{S}}) \boldsymbol{\xi}_E. \quad (4.31)$$

Plugging the closed loop kinetics (4.31) and the requirement on the transport map (4.30) into the change of energy (4.29) we obtain

$$\dot{\bar{\mathcal{W}}} = -\boldsymbol{\xi}_E^\top \bar{\mathbf{D}} \boldsymbol{\xi}_E = -\|\boldsymbol{\xi}_E\|_{\bar{\mathbf{D}}}^2. \quad (4.32)$$

Since $\frac{d}{dt} \bar{\mathcal{W}}$ is only negative semidefinite, we can only conclude stability but not attractiveness. One can pursue the prove of attractiveness by adding a cross term as done in [Bullo and Murray, 1999, sec. 4.2].

Covariance of the closed loop. The skew symmetric matrix $\bar{\mathbf{S}}$ cancels out in the balance of energy, so is of no interest for tuning purposes. Instead it is used to ensure that the closed loop (4.31) is *covariant*, i.e. its definition is unchanged under a change of coordinates. While the stiffness force $\bar{f}_i^K = \partial_i \bar{\mathcal{V}}$ and the dissipative force $\bar{f}_i^D = \bar{D}_{ij} \xi_E^j$ are tensors, the inertia force $\bar{f}_i^M = \bar{M}_{ij} \dot{\xi}_E^j + \frac{1}{2} \partial_k \bar{M}_{ij} \xi_E^k \xi_E^j + \bar{S}_{ij} \xi_E^j$ is not. A universal way is to derive a transformation law and put it as an additional requirement for the closed loop. This would still not lead to a unique definition for $\bar{\mathbf{S}}$.

However, regarding \bar{M}_{ij} as the coefficients of a Riemannian metric, there are the coefficients of the unique Levi Civita connection already encountered in (3.31):

$$\bar{\Gamma}_{ijk} = \frac{1}{2} (\partial_k \bar{M}_{ij} + \partial_j \bar{M}_{ik} - \partial_i \bar{M}_{jk} + \gamma_{ij}^s \bar{M}_{sk} + \gamma_{ik}^s \bar{M}_{sj} - \gamma_{jk}^s \bar{M}_{si}), \quad i, j, k = 1, \dots, n. \quad (4.33)$$

This motivates the inertia force in the clearly covariant form

$$\bar{f}_i^M = \bar{M}_{ij} \dot{\xi}_E^j + \bar{\Gamma}_{ijk} \xi_E^k \xi_E^j. \quad (4.34)$$

It may be realized by setting $\bar{S}_{ij} = \bar{\Gamma}_{ijk} \xi_E^k - \frac{1}{2} \dot{\bar{M}}_{ij} = \frac{1}{2} (\bar{\Gamma}_{ijk} - \bar{\Gamma}_{jik}) \xi_E^k = -\bar{S}_{ji}$ in (4.31).

4.3.2 Special cases

Euclidean space. The existing literature on control of mechanical systems uses almost exclusively minimal generalized coordinates $\mathbf{q} \in \mathbb{R}^n$ and the velocity coordinates $\dot{\mathbf{q}}$. Then the model can we written as

$$\mathbf{M}(\mathbf{q}) \ddot{\mathbf{q}} + \mathbf{C}(\mathbf{q}, \dot{\mathbf{q}}) \dot{\mathbf{q}} = \mathbf{f}^A \quad (4.35)$$

where $C_{ij} = \Gamma_{ijk} \xi_E^k$ and \mathbf{f}^A collects the remaining forces. For a fully actuated system there exists an input transformation such that \mathbf{f}^A can be regarded as virtual inputs.

On the Euclidean space \mathbb{R}^n it is reasonable to introduce error coordinates $\mathbf{q}_E = \mathbf{q} - \mathbf{q}_R$ and to use a quadratic error potential

$$\bar{\mathcal{V}} = \frac{1}{2} \mathbf{q}_E^\top \bar{\mathbf{K}} \mathbf{q}_E, \quad \bar{\mathbf{K}} \in \text{SYM}^+(n). \quad (4.36)$$

This error potential obviously has the transport map $\mathbf{Q} = \mathbf{I}_n$ and the resulting error velocity $\xi_E = \dot{\mathbf{q}}_E = \dot{\mathbf{q}} - \dot{\mathbf{q}}_R$. Furthermore it is reasonable to choose a constant dissipation matrix $\bar{\mathbf{D}} \in \text{SYM}^+(n)$.

Joint PD-Control. Choosing the desired inertia identical to the model inertia $\bar{\mathbf{M}} = \mathbf{M}$, which also implies $\bar{\mathbf{C}} = \mathbf{C}$, yields the closed loop kinetics

$$\mathbf{M}(\mathbf{q}) \ddot{\mathbf{q}}_E + \mathbf{C}(\mathbf{q}, \dot{\mathbf{q}}) \dot{\mathbf{q}}_E + \bar{\mathbf{D}} \dot{\mathbf{q}}_E + \bar{\mathbf{K}} \mathbf{q}_E = \mathbf{0}. \quad (4.37)$$

The resulting control law is

$$\mathbf{f}^A = \mathbf{M}(\mathbf{q}) \ddot{\mathbf{q}}_R + \mathbf{C}(\mathbf{q}, \dot{\mathbf{q}}) \dot{\mathbf{q}}_R - \bar{\mathbf{D}} \dot{\mathbf{q}}_E - \bar{\mathbf{K}} \mathbf{q}_E. \quad (4.38)$$

This approach is commonly called *joint proportional derivative controller* [Slotine and Li, 1991, sec. 9.1.1] or *augmented PD control law* [Murray et al., 1994, sec. 4.5.3], [Spong et al., 2006, sec. 8.2].

Computed torque. Choosing the desired inertia as $\bar{\mathbf{M}} = \mathbf{I}_n$, which implies $\bar{\mathbf{C}} = \mathbf{0}$ leads to the closed loop kinetics

$$\ddot{\mathbf{q}}_{\text{E}} + \bar{\mathbf{D}}\dot{\mathbf{q}}_{\text{E}} + \bar{\mathbf{K}}\mathbf{q}_{\text{E}} = \mathbf{0}. \quad (4.39)$$

The resulting control law is

$$\mathbf{f}^{\text{A}} = \mathbf{M}(\mathbf{q})(\ddot{\mathbf{q}}_{\text{R}} - \bar{\mathbf{D}}\dot{\mathbf{q}}_{\text{E}} - \bar{\mathbf{K}}\mathbf{q}_{\text{E}}) + \mathbf{C}(\mathbf{q}, \dot{\mathbf{q}})\dot{\mathbf{q}}. \quad (4.40)$$

This approach is commonly called *computed torque* [Murray et al., 1994, sec. 4.5.2], [Slotine and Li, 1991, sec. 9.1.2] or *inverse dynamics control* [Spong et al., 2006, sec. 8.3].

These well established approaches are contained within the derived framework. However, as argued in the introduction of this chapter, the use of the Euclidean metric (4.36) only makes sense if the configuration space is indeed an Euclidean space. Application of this approach to e.g. the rigid body orientation would lead to quite awkward motion.

4.3.3 Free rigid body

Consider a single free rigid body as extensively discussed in section 3.3. We use the position \mathbf{r} and orientation \mathbf{R} combined in the matrix $\mathbf{G} \in \mathbb{SE}(3)$ as configuration coordinates and the linear velocity $\mathbf{v} = \mathbf{R}^T \dot{\mathbf{r}}$ and angular velocity $\boldsymbol{\omega} = \text{vee}(\mathbf{R}^T \dot{\mathbf{R}})$ combined in $[\mathbf{v}^T, \boldsymbol{\omega}^T]^T = \boldsymbol{\xi} = \text{vee}(\mathbf{G}^{-1} \dot{\mathbf{G}})$ as velocity coordinates.

Potential and transport map. As for the previous approaches, a reasonable choice (motivated from linear springs in subsection 3.3.4) for the potential energy for a rigid body is

$$\bar{\mathcal{V}} = \frac{1}{2} \|(\mathbf{G} - \mathbf{G}_{\text{R}})^T\|_{\mathbf{K}'}^2, \quad \bar{\mathbf{K}}' \in \mathbb{SYM}^+(4). \quad (4.41)$$

The time derivative of the potential is

$$\begin{aligned} \dot{\bar{\mathcal{V}}} &= \text{tr}((\mathbf{G} - \mathbf{G}_{\text{R}})\bar{\mathbf{K}}'(\mathbf{G} \text{ wed}(\boldsymbol{\xi}) - \mathbf{G}_{\text{R}} \text{ wed}(\boldsymbol{\xi}_{\text{R}}))^T) \\ &= \text{tr}((\mathbf{I}_4 - \mathbf{G}^{-1}\mathbf{G}_{\text{R}})\bar{\mathbf{K}}' \text{ wed}(\boldsymbol{\xi} - \text{Ad}_{\mathbf{G}^{-1}\mathbf{G}_{\text{R}}}\boldsymbol{\xi}_{\text{R}})^T) \\ &= \underbrace{(\boldsymbol{\xi} - \text{Ad}_{\mathbf{G}^{-1}\mathbf{G}_{\text{R}}}\boldsymbol{\xi}_{\text{R}})}_{\boldsymbol{\xi}_{\text{E}}}^T \underbrace{\text{vee}2((\mathbf{I}_4 - \mathbf{G}^{-1}\mathbf{G}_{\text{R}})\bar{\mathbf{K}}')}_{\nabla \bar{\mathcal{V}}}. \end{aligned} \quad (4.42)$$

Recalling the identity $\nabla \bar{\mathcal{V}} = \partial \dot{\bar{\mathcal{V}}} / \partial \boldsymbol{\xi}$, it is evident that $\mathbf{Q} = \text{Ad}_{\mathbf{G}^{-1}\mathbf{G}_{\text{R}}}$ is a transport map for this potential¹. The potential $\bar{\mathcal{V}}$ and the resulting force $\bar{\mathbf{f}}^{\text{K}} = \nabla \bar{\mathcal{V}}$ coincides with the ones given for the previous approaches, already explicitly stated in (4.14a).

¹It should be noted that the transport map given in (4.42) is not unique. One can check by direct calculation that the following matrix also fulfills the required relation (4.30):

$$\mathbf{Q} = \begin{bmatrix} \mathbf{R}^T \mathbf{R}_{\text{R}} & \text{wed} \bar{\mathbf{h}} \mathbf{R}^T \mathbf{R}_{\text{R}} - \mathbf{R}^T \mathbf{R}_{\text{R}} \text{ wed} \bar{\mathbf{h}} \\ \mathbf{0} & \mathbf{R}^T \mathbf{R}_{\text{R}} \end{bmatrix}. \quad (4.43)$$

Damping. Using the same damping matrix $\bar{\mathbf{D}} = \text{Vee}(\bar{\mathbf{D}}')$ with $\bar{\mathbf{D}}' \in \mathbb{SYM}^+(4)$ as with the body based approach, we find the same damping force (4.21b).

Inertia. Using the same inertia matrix as for the body based approach $\bar{\mathbf{M}} = \text{Vee}(\bar{\mathbf{M}}')$ with $\bar{\mathbf{M}}' \in \mathbb{SYM}^+(4)$ we find the controlled inertial force $\bar{\mathbf{f}}^M$ as

$$\bar{\mathbf{f}}^M = \underbrace{\begin{bmatrix} \bar{m}\mathbf{I}_3 & \bar{m}(\text{wed } \bar{\mathbf{s}})^\top \\ \bar{m} \text{ wed } \bar{\mathbf{s}} & \bar{\Theta} \end{bmatrix}}_{\bar{\mathbf{M}}} \underbrace{\begin{bmatrix} \dot{\mathbf{v}}_E \\ \dot{\boldsymbol{\omega}}_E \end{bmatrix}}_{\dot{\boldsymbol{\xi}}_E} + \underbrace{\begin{bmatrix} \bar{m} \text{ wed } \boldsymbol{\omega} & -\bar{m} \text{ wed } \boldsymbol{\omega} \text{ wed } \bar{\mathbf{s}} \\ \bar{m} \text{ wed } \bar{\mathbf{s}} \text{ wed } \boldsymbol{\omega} & \text{wed}(\text{Wed } \bar{\Theta} \boldsymbol{\omega}) \end{bmatrix}}_{\bar{C}(\boldsymbol{\xi}) = -\bar{C}^\top(\boldsymbol{\xi})} \underbrace{\begin{bmatrix} \mathbf{v}_E \\ \boldsymbol{\omega}_E \end{bmatrix}}_{\boldsymbol{\xi}_E}. \quad (4.44)$$

This result is similar to the previous body based approach (4.22), only differing by replacing $\bar{C}(\boldsymbol{\xi})$ with $\bar{C}(\boldsymbol{\xi}_E)$. Consequently with this approach the closed loop dynamics are not autonomous.

4.3.4 Rigid body systems

As for the previous approaches we use the rigid body structure, i.e. the configurations ${}_b^a\mathbf{G}(\mathbf{x})$ and velocities ${}_b^a\boldsymbol{\xi}(\mathbf{x}, \boldsymbol{\xi}) = {}_b^a\mathbf{J}(\mathbf{x})\boldsymbol{\xi}$, as inspiration for controlled kinetics. Assigning stiffness, damping and inertia ${}_b^a\bar{\mathbf{K}}', {}_b^a\bar{\mathbf{D}}', {}_b^a\bar{\mathbf{M}}' \in \mathbb{SYM}_0^+(4)$ to each absolute and relative configuration leads to the following potential energy $\bar{\mathcal{V}}$, damping $\bar{\mathbf{D}}$ and inertia matrix $\bar{\mathbf{M}}$:

$$\bar{\mathcal{V}}(\mathbf{x}, \mathbf{x}_R) = \sum_{a,b} \frac{1}{2} \|({}_b^a\mathbf{G}(\mathbf{x}) - {}_b^a\mathbf{G}(\mathbf{x}_R))^\top\|_{{}_b^a\bar{\mathbf{K}}'}^2, \quad {}_b^a\bar{\mathbf{K}}' \in \mathbb{SYM}_0^+(4) \quad (4.45a)$$

$$\bar{\mathbf{D}}(\mathbf{x}) = \sum_{a,b} {}_b^a\mathbf{J}^\top(\mathbf{x}) \text{Vee}({}_b^a\bar{\mathbf{D}}') {}_b^a\mathbf{J}(\mathbf{x}), \quad {}_b^a\bar{\mathbf{D}}' \in \mathbb{SYM}_0^+(4) \quad (4.45b)$$

$$\bar{\mathbf{M}}(\mathbf{x}) = \sum_{a,b} {}_b^a\mathbf{J}^\top(\mathbf{x}) \text{Vee}({}_b^a\bar{\mathbf{M}}') {}_b^a\mathbf{J}(\mathbf{x}), \quad {}_b^a\bar{\mathbf{M}}' \in \mathbb{SYM}_0^+(4) \quad (4.45c)$$

Note that the body matrices do not have to be positive definite, only the resulting system matrices and the potential have to be positive definite to ensure stability.

Transport map. The potential $\bar{\mathcal{V}}$ and the resulting force $\nabla \bar{\mathcal{V}}$ are identical to the previous approaches, see e.g. (4.18b). For this energy based approach we require the existence of a transport map. The condition (4.30) for the transport map \mathbf{Q} with the given potential (4.45a) may be expanded to

$$\sum_{a,b} ({}^a_b\mathbf{J}\mathbf{Q} - \text{Ad}_{{}^a_b\mathbf{G}_E^{-1}} {}^a_b\mathbf{J}_R)^\top \text{vee2}((\mathbf{I}_4 - {}^a_b\mathbf{G}_E^{-1}) {}^a_b\bar{\mathbf{K}}') = \mathbf{0}. \quad (4.46)$$

with the shorthand notation ${}_b^a\mathbf{G}_E = {}_b^a\mathbf{G}^{-1}(\mathbf{x}_R) {}^a_b\mathbf{G}(\mathbf{x})$ and ${}_b^a\mathbf{J}_R = {}^a_b\mathbf{J}(\mathbf{x}_R)$. There is no general solution for this, the transport map \mathbf{Q} has to be computed for each example individually. A major caveat of this approach is that there is no general guaranty on the existence of a transport map.

4.4 Constant reference and linearization

Constant reference. For a constant reference configuration $\mathbf{x}_R = const. \Rightarrow \xi_R, \dot{\xi}_R = \mathbf{0}$, the three proposed control templates lead to the same system

$$\dot{\mathbf{x}} = \mathbf{A}(\mathbf{x})\xi, \quad \bar{\mathbf{M}}(\mathbf{x})\dot{\xi} + \bar{\mathbf{c}}(\mathbf{x}, \xi) + \bar{\mathbf{D}}(\mathbf{x})\xi + \nabla\bar{\mathcal{V}}(\mathbf{x}, \mathbf{x}_R) = \mathbf{0} \quad (4.47a)$$

where

$$\bar{\mathbf{M}}(\mathbf{x}) = \sum_{a,b} \left({}^a_b \mathbf{J}(\mathbf{x}) \right)^\top {}^a_b \bar{\mathbf{M}} {}^a_b \mathbf{J}(\mathbf{x}), \quad (4.47b)$$

$$\bar{\mathbf{c}}(\mathbf{x}, \xi) = \sum_{a,b} \left({}^a_b \mathbf{J}(\mathbf{x}) \right)^\top \left({}^a_b \bar{\mathbf{M}} {}^a_b \mathbf{J}(\mathbf{x}, \xi) - \text{ad}_{{}^a_b \mathbf{J}(\mathbf{x})}^\top {}^a_b \bar{\mathbf{M}} {}^a_b \mathbf{J}(\mathbf{x}) \right) \xi \quad (4.47c)$$

$$\bar{\mathbf{D}}(\mathbf{x}) = \sum_{a,b} \left({}^a_b \mathbf{J}(\mathbf{x}) \right)^\top {}^a_b \bar{\mathbf{D}} {}^a_b \mathbf{J}(\mathbf{x}), \quad (4.47d)$$

$$\nabla\bar{\mathcal{V}}(\mathbf{x}, \mathbf{x}_R) = \sum_{a,b} \left({}^a_b \mathbf{J}(\mathbf{x}) \right)^\top \text{vee2} \left((\mathbf{I}_4 - {}^a_b \mathbf{G}_E^{-1}(\mathbf{x}, \mathbf{x}_R)) {}^a_b \bar{\mathbf{K}}' \right) \quad (4.47e)$$

The total energy $\bar{\mathcal{W}} = \frac{1}{2}\xi^\top \bar{\mathbf{M}}\xi + \bar{\mathcal{V}}$ is a Lyapunov function for this system if the system inertia matrix $\bar{\mathbf{M}}$ and the potential energy $\bar{\mathcal{V}}$ are positive definite, and the system dissipation matrix $\bar{\mathbf{D}}$ is positive semi-definite.

Linearization. Assuming that the configuration of the system is close to its reference, i.e. $\mathbf{x} \approx \mathbf{x}_R$. The first order approximation (see subsection 2.2.3) of (4.47) with $\boldsymbol{\varepsilon} = \mathbf{A}^+(\mathbf{x}_R)(\mathbf{x} - \mathbf{x}_R)$ is

$$\bar{\mathbf{M}}_0 \ddot{\boldsymbol{\varepsilon}} + \bar{\mathbf{D}}_0 \dot{\boldsymbol{\varepsilon}} + \bar{\mathbf{K}}_0 \boldsymbol{\varepsilon} = \mathbf{0} \quad (4.48a)$$

where

$$\bar{\mathbf{M}}_0 = \bar{\mathbf{M}}(\mathbf{x}_R) = \sum_{a,b} \left({}^a_b \mathbf{J}(\mathbf{x}_R) \right)^\top {}^a_b \bar{\mathbf{M}} {}^a_b \mathbf{J}(\mathbf{x}_R), \quad (4.48b)$$

$$\bar{\mathbf{D}}_0 = \bar{\mathbf{D}}(\mathbf{x}_R) = \sum_{a,b} \left({}^a_b \mathbf{J}(\mathbf{x}_R) \right)^\top {}^a_b \bar{\mathbf{D}} {}^a_b \mathbf{J}(\mathbf{x}_R), \quad (4.48c)$$

$$\bar{\mathbf{K}}_0 = \nabla^2 \bar{\mathcal{V}}(\mathbf{x}_R, \mathbf{x}_R) = \sum_{a,b} \left({}^a_b \mathbf{J}(\mathbf{x}_R) \right)^\top {}^a_b \bar{\mathbf{K}} {}^a_b \mathbf{J}(\mathbf{x}_R) \quad (4.48d)$$

4.5 Underactuated systems

The first three sections of this chapter motivated different desired closed loop dynamics which share the structure

$$\dot{\mathbf{x}} = \mathbf{A}(\mathbf{x})\xi, \quad \bar{\mathbf{M}}(\mathbf{x})\dot{\xi} + \bar{\mathbf{b}}(\mathbf{x}, \xi, \mathbf{x}_R, \xi_R, \dot{\xi}_R) = \mathbf{0}. \quad (4.49)$$

The system model with the available control input \mathbf{u} has the form of (4.1):

$$\dot{\mathbf{x}} = \mathbf{A}(\mathbf{x})\xi, \quad \mathbf{M}(\mathbf{x})\dot{\xi} + \mathbf{b}(\mathbf{x}, \xi) = \mathbf{B}(\mathbf{x})\mathbf{u}. \quad (4.50)$$

For a fully actuated system, i.e. $\text{rank } \mathbf{B} = n$, the combination of (4.49) and (4.50) can be solved for the system input \mathbf{u} yielding the required control law:

$$\mathbf{u} = \mathbf{B}^{-1}(\mathbf{b} - \mathbf{M}\bar{\mathbf{M}}^{-1}\bar{\mathbf{b}}). \quad (4.51)$$

For an underactuated system, i.e. $\text{rank } \mathbf{B} = p < n$, this is generally not possible.

4.5.1 Control law through static optimization

The idea. If the desired closed loop dynamics (4.49) cannot be achieved exactly, the next best thing is to get “as close as possible” while still obeying the model dynamics (4.50). In order to formalize the “as close as possible” we take again inspiration from mechanics, more precisely from Gauss’ principle of least constraint, previously discussed in section 3.2: The free motion is the solution of the desired closed loop (4.49), the optimization metric is the desired closed loop inertia $\bar{\mathbf{M}}$ and the constraints are the model kinetics (4.50). Then the control law is the solution of the static optimization problem

$$\begin{aligned} & \text{minimize } \bar{\mathcal{G}} = \frac{1}{2} \|\dot{\boldsymbol{\xi}} + \bar{\mathbf{M}}^{-1} \bar{\mathbf{b}}\|_{\bar{\mathbf{M}}}^2 \\ & \text{subject to } \mathbf{M}\dot{\boldsymbol{\xi}} + \mathbf{b} = \mathbf{B}\mathbf{u}, \mathbf{u} \in \mathbb{R}^p \end{aligned} \quad (4.52)$$

Explicit control law. Elimination of the acceleration $\dot{\boldsymbol{\xi}} = \mathbf{M}^{-1}(\mathbf{B}\mathbf{u} - \mathbf{b})$ from (4.52) leads to

$$\begin{aligned} \bar{\mathcal{G}} &= \frac{1}{2} \|\mathbf{M}^{-1}\mathbf{B}\mathbf{u} - \underbrace{(\mathbf{M}^{-1}\mathbf{b} - \bar{\mathbf{M}}^{-1}\bar{\mathbf{b}})}_{\tilde{\mathbf{a}}}\|_{\bar{\mathbf{M}}}^2 \\ &= \frac{1}{2} \mathbf{u}^\top \underbrace{\mathbf{B}^\top \mathbf{M}^{-1} \bar{\mathbf{M}} \mathbf{M}^{-1} \mathbf{B}}_{\mathbf{H}} \mathbf{u} - \mathbf{u}^\top \mathbf{B}^\top \mathbf{M}^{-1} \bar{\mathbf{M}} \tilde{\mathbf{a}} + \frac{1}{2} \tilde{\mathbf{a}}^\top \bar{\mathbf{M}} \tilde{\mathbf{a}} \\ &= \frac{1}{2} (\mathbf{u} - \underbrace{\mathbf{H}^{-1} \mathbf{B}^\top \mathbf{M}^{-1} \bar{\mathbf{M}} \tilde{\mathbf{a}}}_{\mathbf{u}_0})^\top \mathbf{H} (\mathbf{u} - \underbrace{\mathbf{H}^{-1} \mathbf{B}^\top \mathbf{M}^{-1} \bar{\mathbf{M}} \tilde{\mathbf{a}}}_{\mathbf{u}_0}) \\ &\quad + \frac{1}{2} \tilde{\mathbf{a}}^\top \bar{\mathbf{M}} \underbrace{(\mathbf{I}_n - \mathbf{M}^{-1} \mathbf{B} \mathbf{H}^{-1} \mathbf{B}^\top \mathbf{M}^{-1} \bar{\mathbf{M}})}_{\mathbf{P}^\perp} \tilde{\mathbf{a}} \\ &= \frac{1}{2} \|\mathbf{u} - \mathbf{u}_0\|_{\mathbf{H}}^2 + \underbrace{\frac{1}{2} \|\mathbf{P}^\perp \tilde{\mathbf{a}}\|_{\bar{\mathbf{M}}}^2}_{\bar{\mathcal{G}}_0}. \end{aligned} \quad (4.53)$$

The control law, i.e. the solution of the minimization problem, is obviously $\mathbf{u} = \mathbf{u}_0$.

For the special case of a fully actuated system, i.e. \mathbf{B} is invertible, the control law simplifies to $\mathbf{u}_0 = \mathbf{B}^{-1}(\mathbf{b} - \mathbf{M}\bar{\mathbf{M}}^{-1}\bar{\mathbf{b}})$ as already stated above. Furthermore, for this case, we have $\mathbf{P}^\perp = \mathbf{0}$ and consequently $\bar{\mathcal{G}}_0 = 0$.

Feasible closed loop kinetics. Plugging $\mathbf{u} = \mathbf{u}_0$ into the model (4.50) we obtain the actual closed loop kinetics:

$$\begin{aligned} \mathbf{M}\dot{\boldsymbol{\xi}} + \mathbf{b} &= \mathbf{B} \underbrace{\mathbf{H}^{-1} \mathbf{B}^\top \mathbf{M}^{-1} \bar{\mathbf{M}} (\mathbf{M}^{-1}\mathbf{b} - \bar{\mathbf{M}}^{-1}\bar{\mathbf{b}})}_{\mathbf{u}_0} \\ \Leftrightarrow \dot{\boldsymbol{\xi}} &= \mathbf{M}^{-1} \mathbf{B} \mathbf{H}^{-1} \mathbf{B}^\top \mathbf{M}^{-1} \bar{\mathbf{M}} (\mathbf{M}^{-1}\mathbf{b} - \bar{\mathbf{M}}^{-1}\bar{\mathbf{b}}) - \mathbf{M}^{-1}\mathbf{b} \\ \Leftrightarrow \bar{\mathbf{M}}\dot{\boldsymbol{\xi}} + \bar{\mathbf{b}} &= \underbrace{\bar{\mathbf{M}} \mathbf{P}^\perp (\bar{\mathbf{M}}^{-1}\bar{\mathbf{b}} - \mathbf{M}^{-1}\mathbf{b})}_{\tilde{\mathbf{b}}}. \end{aligned} \quad (4.54)$$

We may interpret this additional vector² $\tilde{\mathbf{b}}(\mathbf{x}, \dot{\boldsymbol{\xi}}, \mathbf{x}_R, \dot{\boldsymbol{\xi}}_R) \in \mathbb{R}^n$ as a force that makes the closed loop kinetics feasible, i.e. realizable with the available controls. The residual Gaussian constraint is $\bar{\mathcal{G}}_0 = \frac{1}{2}\|\tilde{\mathbf{b}}\|_{\bar{\mathbf{M}}}^2$.

In general, the value $\bar{\mathcal{G}}_0$ is a measure of how much the resulting closed loop differs from the original desired system (4.49). One main goal when parameterizing the controller is to make $\bar{\mathcal{G}}_0$ as small as possible. Unfortunately the form of $\bar{\mathcal{G}}_0$ in (4.54) is not handy, mainly due to rank $\mathbf{P}^\perp = n - p$. In the following we like to find a more handy formulation.

4.5.2 Matching condition

Instead of eliminating the accelerations $\dot{\boldsymbol{\xi}}$ we may also eliminate the controls \mathbf{u} from (4.52). Let $\mathbf{B}^\perp \in \mathbb{R}^{n \times (n-p)}$ be any orthogonal complement to \mathbf{B} , i.e. rank $\mathbf{B}^\perp = n - p$ and $\mathbf{B}^\top \mathbf{B}^\perp = \mathbf{0}$. With this (4.52) is equivalent to

$$\begin{aligned} & \text{minimize } \bar{\mathcal{G}} = \frac{1}{2}\|\dot{\boldsymbol{\xi}} + \bar{\mathbf{M}}^{-1}\bar{\mathbf{b}}\|_{\bar{\mathbf{M}}}^2 \\ & \text{subject to } (\mathbf{B}^\perp)^\top(\mathbf{M}\dot{\boldsymbol{\xi}} + \mathbf{b}) = \mathbf{0} \end{aligned} \quad (4.55)$$

Using the method of Lagrangian multipliers with $\mathcal{L} = \bar{\mathcal{G}} + \boldsymbol{\mu}^\top(\mathbf{B}^\perp)^\top(\mathbf{M}\dot{\boldsymbol{\xi}} + \mathbf{b})$ leads to the necessary condition

$$\begin{bmatrix} \frac{\partial \mathcal{L}}{\partial \dot{\boldsymbol{\xi}}} \\ \frac{\partial \mathcal{L}}{\partial \boldsymbol{\mu}} \end{bmatrix} = \begin{bmatrix} \bar{\mathbf{M}} & \mathbf{M}\mathbf{B}^\perp \\ (\mathbf{M}\mathbf{B}^\perp)^\top & \mathbf{0} \end{bmatrix} \begin{bmatrix} \dot{\boldsymbol{\xi}} \\ \boldsymbol{\mu} \end{bmatrix} + \begin{bmatrix} \bar{\mathbf{b}} \\ (\mathbf{B}^\perp)^\top \mathbf{b} \end{bmatrix} = \mathbf{0} \quad (4.56)$$

Using blockwise inversion we may solve

$$-\boldsymbol{\mu} = \underbrace{((\mathbf{M}\mathbf{B}^\perp)^\top \bar{\mathbf{M}}^{-1} \mathbf{M}\mathbf{B}^\perp)^{-1}}_S \underbrace{(\mathbf{B}^\perp)^\top(\mathbf{M}\bar{\mathbf{M}}^{-1}\bar{\mathbf{b}} - \mathbf{b})}_\lambda. \quad (4.57)$$

With this, the feasible closed loop kinetics and the residual Gaussian constraint may be expressed by

$$\bar{\mathbf{M}}\dot{\boldsymbol{\xi}} + \bar{\mathbf{b}} = \underbrace{\mathbf{M}\mathbf{B}^\perp \mathbf{S} \boldsymbol{\lambda}}_{\tilde{\mathbf{b}}}, \quad \bar{\mathcal{G}}_0 = \frac{1}{2}\|\boldsymbol{\lambda}\|_S^2. \quad (4.58)$$

It is much simpler to analyze $\boldsymbol{\lambda}$ which has only the dimension of the underactuation $n - p$ instead of $\tilde{\mathbf{b}}$ which has the full dimension n of the configuration space. Though it should be stressed that the values of $\bar{\mathcal{G}}_0$ and $\tilde{\mathbf{b}}$ are, as derived above, independent of the choice of \mathbf{B}^\perp .

The best case is, of course, if we achieve

$$\boldsymbol{\lambda} = (\mathbf{B}^\perp)^\top(\mathbf{M}\bar{\mathbf{M}}^{-1}\bar{\mathbf{b}} - \mathbf{b}) = \mathbf{0} \quad \Rightarrow \quad \tilde{\mathbf{b}} = \mathbf{0}, \quad \bar{\mathcal{G}}_0 = 0 \quad (4.59)$$

i.e. the desired closed loop is realized exactly. An approach based on this is discussed in [Bloch et al., 2000]. A condition similar to (4.59) is therein called the *the matching condition* and is required to be fulfilled exactly. However, the examples for which this approach is demonstrated restricts to stabilization tasks $\boldsymbol{\xi}_R = \mathbf{0}$ for small academic systems.

²The coefficients $\tilde{\mathbf{b}}$ do indeed transform like a tensor, even though \mathbf{b} and $\bar{\mathbf{b}}$ do not.

An advantage of the presented approach is that the control law $\mathbf{u} = \mathbf{u}_0$ is defined independently of whether the matching condition is fulfilled or not. Instead the quantity $\boldsymbol{\lambda}$, which we will call the *matching force* in the following, ensures that the control law is realizable.

4.5.3 Approximations

The matching force (4.59) may become very cumbersome for complex systems and might even be impossible to vanish with the given parameters. It might be instructive to analyze it for particular situations.

Zero error. Assume that the controller tracks the reference perfectly, i.e. $\mathbf{x} = \mathbf{x}_R$ and $\boldsymbol{\xi} = \boldsymbol{\xi}_R$. One may check that for this case the three approaches all yield $\bar{\mathbf{b}} = \bar{\mathbf{M}}\boldsymbol{\xi}_R$. The resulting matching force $\boldsymbol{\lambda}^{\text{ZeroError}}$ for this special case is

$$\boldsymbol{\lambda}^{\text{ZeroError}} = (\mathbf{B}^\perp(\mathbf{x}_R))^\top (\mathbf{M}(\mathbf{x}_R)\dot{\boldsymbol{\xi}}_R - \mathbf{b}(\mathbf{x}_R, \boldsymbol{\xi}_R)) \quad (4.60)$$

Evidently, this is independent of the closed loop parameters, and should rather be regarded as a constraint on the *reference trajectory* $t \mapsto \mathbf{x}_R(t)$. The condition $\boldsymbol{\lambda}^{\text{ZeroError}} = \mathbf{0}$ is essentially the model equation after elimination of the control inputs.

A very useful approach here is to formulate the reference trajectory in terms of a *flat output* [Fliess et al., 1995] of the model. The first step for a systematic construction of a flat output is commonly the elimination of the control inputs (see e.g. [Schlacher and Schöberl, 2007]) i.e. $\boldsymbol{\lambda}^{\text{ZeroError}} = \mathbf{0}$.

Small error. Assume that we a small error $\boldsymbol{\varepsilon} = \mathbf{A}^+(\mathbf{x}_R)(\mathbf{x} - \mathbf{x}_R)$ to a constant reference $\boldsymbol{\xi}_R = \mathbf{0}$ as already considered in section 4.4. Then the model and the closed loop template may be approximated by

$$\mathbf{M}_0\ddot{\boldsymbol{\varepsilon}} + \mathbf{D}_0\dot{\boldsymbol{\varepsilon}} + \mathbf{K}_0\boldsymbol{\varepsilon} = \mathbf{B}(\mathbf{x}_R)\Delta\mathbf{u}, \quad (4.61a)$$

$$\bar{\mathbf{M}}_0\ddot{\boldsymbol{\varepsilon}} + \bar{\mathbf{D}}_0\dot{\boldsymbol{\varepsilon}} + \bar{\mathbf{K}}_0\boldsymbol{\varepsilon} = \mathbf{0} \quad (4.61b)$$

and the matching force $\boldsymbol{\lambda}^{\text{SmallError}}$ for this special case is

$$\begin{aligned} \boldsymbol{\lambda}^{\text{SmallError}} &= (\mathbf{B}^\perp(\mathbf{x}_R))^\top (\mathbf{M}_0\bar{\mathbf{M}}_0^{-1}(\bar{\mathbf{D}}_0\dot{\boldsymbol{\varepsilon}} + \bar{\mathbf{K}}_0\boldsymbol{\varepsilon}) - (\mathbf{D}_0\dot{\boldsymbol{\varepsilon}} + \mathbf{K}_0\boldsymbol{\varepsilon})) \\ &= \underbrace{(\mathbf{B}^\perp(\mathbf{x}_R))^\top (\mathbf{M}_0\bar{\mathbf{M}}_0^{-1}\bar{\mathbf{D}}_0 - \mathbf{D}_0)}_{\boldsymbol{\Lambda}_D} \dot{\boldsymbol{\varepsilon}} + \underbrace{(\mathbf{B}^\perp(\mathbf{x}_R))^\top (\mathbf{M}_0\bar{\mathbf{M}}_0^{-1}\bar{\mathbf{K}}_0 - \mathbf{K}_0)}_{\boldsymbol{\Lambda}_K} \boldsymbol{\varepsilon} \end{aligned} \quad (4.62)$$

As $\boldsymbol{\varepsilon}$ and $\dot{\boldsymbol{\varepsilon}}$ can be arbitrary, the matrices $\boldsymbol{\Lambda}_K$ and $\boldsymbol{\Lambda}_D$ have to vanish, for $\boldsymbol{\lambda}^{\text{SmallError}}$ to vanish. For the following examples it will turn out that we can always find suitable parameters within $\bar{\mathbf{M}}_0$, $\bar{\mathbf{D}}_0$ and $\bar{\mathbf{K}}_0$ such that $\boldsymbol{\Lambda}_K = \boldsymbol{\Lambda}_D = \mathbf{0}$. Thus ensuring that at least the first order approximation of the actual matching force $\boldsymbol{\lambda}$ vanishes.

4.5.4 Systems with input constraints

In most control systems the control inputs \mathbf{u} can not take arbitrary values, but due to practical limitations are required to be e.g. $u_a \in [-u_a^{\max}, u_a^{\max}], a = 1, \dots, p$. More generally we assume that the constraints can be written as $\mathbf{W}\mathbf{u} \leq \mathbf{l}$ where the inequality is understood componentwise. Adding this constraint to the original problem (4.52) is

$$\begin{aligned} & \text{minimize } \bar{\mathcal{G}} = \frac{1}{2} \|\dot{\boldsymbol{\xi}} + \bar{\mathbf{M}}^{-1} \bar{\mathbf{b}}\|_{\bar{\mathbf{M}}}^2 \\ & \text{subject to } \mathbf{M}\dot{\boldsymbol{\xi}} + \mathbf{b} = \mathbf{B}\mathbf{u}, \quad \mathbf{W}\mathbf{u} \leq \mathbf{l}, \quad \mathbf{u} \in \mathbb{R}^p \end{aligned} \quad (4.63)$$

With the elimination of $\dot{\boldsymbol{\xi}}$ as done in subsection 4.5.1 this is equivalent to

$$\begin{aligned} & \text{minimize } \bar{\mathcal{G}} = \frac{1}{2} \|\mathbf{u} - \mathbf{u}_0\|_{\mathbf{H}}^2 \\ & \text{subject to } \mathbf{W}\mathbf{u} \leq \mathbf{l}, \quad \mathbf{u} \in \mathbb{R}^p \end{aligned} \quad (4.64)$$

with \mathbf{H} and \mathbf{u}_0 defined in (4.53).

Given that $\mathbf{H} \in \mathbb{S}\mathbb{Y}\mathbb{M}^+(p)$ by construction and the feasible set $\mathbb{U} = \{\mathbf{u} \in \mathbb{R}^p \mid \mathbf{W}\mathbf{u} \leq \mathbf{l}\}$ is convex, this problem has a unique solution, though it usually has to be computed numerically. For the following simulation results the MATLAB function `quadprog` was used and a C++ implementation of the Active-Set algorithm from [Nocedal and Wright, 2006, Algorithm 16.3] was used for the real-time implementation on the Multicopters.

If $\mathbf{u}_0 \in \mathbb{U}$ the solution is obviously $\mathbf{u} = \mathbf{u}_0$ and is independent of \mathbf{H} . If this is not the case the matrix \mathbf{H} determines which components of \mathbf{u} are prioritized. It is crucial to notice that \mathbf{H} is not the tuning parameter here, but is computed from the desired system inertia $\bar{\mathbf{M}}$ and the model matrices, see (4.53). As evident from (4.63), the actual tuning parameter here is the desired closed loop inertia matrix $\bar{\mathbf{M}}$ which determines how the components of the system acceleration $\dot{\boldsymbol{\xi}}$ are prioritized when computing a feasible control force.

4.6 Summary and recipe

We have proposed three approaches for a control law for rigid body systems. Each of them formulated a slightly different template for the desired closed loop dynamics. The actual control law results from its combination with the model dynamics. For a fully actuated system the desired closed loop is achieved exactly. For an underactuated system or in the presence of input constraints one achieves closed loop dynamics that are “as close as possible” to the desired dynamics in the sense that the resulting acceleration differs the least.

The implementation of the controller is determined by the rigid body parameterization ${}^g\mathbf{G}(\mathbf{x})$, the kinematics $\dot{\mathbf{x}} = \mathbf{A}(\mathbf{x})\boldsymbol{\xi}$ and the *desired* constitutive parameters ${}^b\bar{\mathbf{M}}, {}^b\bar{\mathbf{D}}, {}^b\bar{\mathbf{K}}$. It is crucial to note that the resulting controlled system is invariant to the chosen coordinates $\mathbf{x}, \boldsymbol{\xi}$ in the same way as the system model: Though the describing equations depend explicitly on the coordinates, the resulting motion of the closed loop system is the same for any choice of coordinates. This can be validated by checking the covariance of the closed loop equations.

What does affect the motion of the controlled system are the constitutive parameters, i.e. the values within ${}^a_b\bar{\mathbf{M}}$, ${}^a_b\bar{\mathbf{D}}$, ${}^a_b\bar{\mathbf{K}}$. These are associated with the rigid bodies and are completely independent of the system coordinates. For the energy based approach, the choice of a transport map might not be unique and consequently might also affect the motion.

THE recipe:

- Modeling: A recipe for the derivation of the equations of motion of a rigid body system was given in subsection 3.4.6:

- Choose a set of (possibly redundant) configuration coordinates $\mathbf{x}(t) \in \mathbb{X} = \{\mathbf{x} \in \mathbb{R}^\nu \mid \phi(\mathbf{x}) = \mathbf{0}\}$ and minimal velocity coordinates $\boldsymbol{\xi}(t) \in \mathbb{R}^n$, $n = \dim \mathbb{X}$ that are related by the kinematics matrix $\mathbf{A}(\mathbf{x}) \in \mathbb{R}^{\nu \times n}$:

$$\dot{\mathbf{x}} = \mathbf{A}\boldsymbol{\xi} \quad (4.65a)$$

- Formulate the rigid body configurations ${}^a_b\mathbf{G}(\mathbf{x}) \in \mathbb{SE}(3)$, $a, b = 0, \dots, N$ in terms of the chosen coordinates. This determines the body Jacobians

$${}^a_b\mathbf{J} = \frac{\partial}{\partial \dot{\mathbf{x}}} \text{vee}({}^a_b\mathbf{G}^{-1} {}^a_b\dot{\mathbf{G}}) \mathbf{A} \quad (4.65b)$$

- Compute the model inertia force $\mathbf{f}^M = \mathbf{M}\dot{\boldsymbol{\xi}} + \mathbf{c}$ from the body inertias ${}^0_b\mathbf{M}'$ (see subsection 3.4.2)

$$\mathbf{M} = \sum_b {}^0_b\mathbf{J}^\top \text{Vee}({}^0_b\mathbf{M}') {}^0_b\mathbf{J}, \quad \mathbf{c} = \sum_b {}^0_b\mathbf{J}^\top (\text{Vee}({}^0_b\mathbf{M}') {}^0_b\dot{\mathbf{J}} - \text{ad}_{{}^0_b\mathbf{J}\boldsymbol{\xi}}^\top \text{Vee}({}^0_b\mathbf{M}') {}^0_b\mathbf{J}) \boldsymbol{\xi} \quad (4.65c)$$

- The model kinetics are the balance of the inertia force \mathbf{f}^M , the force of control inputs $\mathbf{B}\mathbf{u}$ and whatever other forces \mathbf{f}^A may act on the system

$$\mathbf{M}\dot{\boldsymbol{\xi}} + \underbrace{\mathbf{c} + \mathbf{f}^A}_{b} = \mathbf{B}\mathbf{u} \quad (4.65d)$$

- Closed loop template

- The template is computed from the body configurations ${}^a_b\mathbf{G}$, the body Jacobians ${}^a_b\mathbf{J}$ and the control parameters ${}^a_b\bar{\mathbf{K}}'$, ${}^a_b\bar{\mathbf{D}}'$, ${}^a_b\bar{\mathbf{M}}'$:

$$\bar{\mathbf{M}} = \sum_{a,b} {}^a_b\mathbf{J}^\top \text{Vee}({}^a_b\bar{\mathbf{M}}') {}^a_b\mathbf{J} \quad (4.66a)$$

$$\bar{\mathbf{f}}^K = \sum_{a,b} {}^a_b\mathbf{J}^\top \text{vee2}((\mathbf{I}_4 - {}^a_b\mathbf{G}_E^{-1}) {}^a_b\bar{\mathbf{K}}') \quad (4.66b)$$

- particle-based approach (see subsection 4.1.3)

$$\bar{\mathbf{f}}^D = \sum_{a,b} {}^a_b\mathbf{J}^\top \text{vee2}((\text{wed}({}^a_b\mathbf{J}(\mathbf{x})\boldsymbol{\xi}) - {}^a_b\mathbf{G}_E^{-1} \text{wed}({}^a_b\mathbf{J}(\mathbf{x}_R)\boldsymbol{\xi}_R)) {}^a_b\bar{\mathbf{D}}') \quad (4.66c)$$

$$\begin{aligned} \bar{\mathbf{c}} = & \sum_{a,b} {}^a_b\mathbf{J}^\top \text{vee2}((\text{wed}({}^a_b\dot{\mathbf{J}}\boldsymbol{\xi}) + \text{wed}({}^a_b\mathbf{J}\boldsymbol{\xi})^2 \\ & - {}^a_b\mathbf{G}_E^{-1}(\text{wed}({}^a_b\mathbf{J}_R\dot{\boldsymbol{\xi}}_R + {}^a_b\dot{\mathbf{J}}_R\boldsymbol{\xi}_R) + \text{wed}({}^a_b\mathbf{J}_R\boldsymbol{\xi}_R)^2)) {}^a_b\bar{\mathbf{M}}') \end{aligned} \quad (4.66d)$$

- body-based approach (see subsection 4.2.2)

$$\bar{\mathbf{f}}^D = \sum_{a,b} {}^a_b \mathbf{J}^\top \text{Vee}({}^a_b \bar{\mathbf{D}}') {}^a_b \xi_E, \quad {}^a_b \dot{\xi}_E = {}^a_b \mathbf{J} \xi - \text{Ad}_{{}^a_b \mathbf{G}_E^{-1}} {}^a_b \mathbf{J}_R \xi_R, \quad (4.66e)$$

$$\begin{aligned} \bar{\mathbf{c}} = \sum_{a,b} {}^a_b \mathbf{J}^\top & \left({}^a_b \bar{\mathbf{M}} ({}^a_b \dot{\mathbf{J}} \xi - \text{Ad}_{{}^a_b \mathbf{G}_E^{-1}} ({}^a_b \mathbf{J}_R \dot{\xi}_R + {}^a_b \dot{\mathbf{J}}_R \xi_R) + \text{ad}_{{}^a_b \xi_E} \text{Ad}_{{}^a_b \mathbf{G}_E^{-1}} {}^a_b \mathbf{J}_R \xi_R) \right. \\ & \left. - \text{ad}_{{}^a_b \xi_E}^\top {}^a_b \bar{\mathbf{M}} {}^a_b \xi_E \right), \end{aligned} \quad (4.66f)$$

- energy-based approach (see subsection 4.3.4, requires the choice of a transport map \mathbf{Q})

$$\bar{\mathbf{f}}^D = \bar{\mathbf{D}} \xi_E, \quad \bar{\mathbf{D}} = \sum_{a,b} {}^a_b \mathbf{J}^\top \text{Vee}({}^a_b \bar{\mathbf{D}}') {}^a_b \mathbf{J}, \quad \xi_E = \xi - \mathbf{Q} \xi_R \quad (4.66g)$$

$$\bar{\mathbf{C}} = \sum_{a,b} {}^a_b \mathbf{J}^\top (\text{Vee}({}^a_b \bar{\mathbf{M}}') {}^a_b \dot{\mathbf{J}} + {}^a_b \bar{\mathbf{C}} {}^a_b \mathbf{J}), \quad {}^a_b \bar{\mathbf{C}}_{pq} = \Gamma_{pqr}({}^a_b \bar{\mathbf{M}}') {}^a_b J_k^r \xi^k \quad (4.66h)$$

$$\bar{\mathbf{c}} = \bar{\mathbf{C}} \xi_E - \bar{\mathbf{M}}(\mathbf{Q} \dot{\xi}_R + \dot{\mathbf{Q}} \xi_R), \quad (4.66i)$$

- The desired closed loop kinetics are

$$\bar{\mathbf{M}} \dot{\xi} + \underbrace{\bar{\mathbf{c}} + \bar{\mathbf{f}}^D + \bar{\mathbf{f}}^K}_{\bar{\mathbf{b}}} = \mathbf{0} \quad (4.66j)$$

- Control law:

- For the fully actuated case, the desired closed loop is realized by

$$\mathbf{u} = \mathbf{B}^{-1}(\mathbf{b} - \bar{\mathbf{M}} \bar{\mathbf{M}}^{-1} \bar{\mathbf{b}}) \quad (4.67a)$$

- In the underactuated case, the acceleration error measured by the Gaussian constraint, is minimized by (see subsection 4.5.1)

$$\mathbf{u} = (\mathbf{B}^\top \mathbf{M}^{-1} \bar{\mathbf{M}} \mathbf{M}^{-1} \mathbf{B})^{-1} \mathbf{B}^\top \mathbf{M}^{-1} (\bar{\mathbf{M}} \mathbf{M}^{-1} \mathbf{b} - \bar{\mathbf{b}}) \quad (4.67b)$$

Choosing an orthogonal complement \mathbf{B}^\perp to the input matrix \mathbf{B} , i.e. $\text{rank } \mathbf{B}^\perp = n - p$ and $\mathbf{B}^\top \mathbf{B}^\perp = \mathbf{0}$, the residual acceleration error can be written as $\bar{\mathcal{G}}_0 = \frac{1}{2} \|\boldsymbol{\lambda}\|_S^2$ where (see subsection 4.5.2)

$$\boldsymbol{\lambda} = (\mathbf{B}^\perp)^\top (\bar{\mathbf{M}} \mathbf{M}^{-1} \bar{\mathbf{b}} - \mathbf{b}) = \mathbf{0}, \quad \mathbf{S} = ((\mathbf{B}^\perp)^\top \bar{\mathbf{M}} \mathbf{M}^{-1} \bar{\mathbf{M}} \mathbf{B}^\perp)^{-1} \quad (4.67c)$$

By adjusting the control parameters within $\bar{\mathbf{M}}$ and $\bar{\mathbf{b}}$ one may try to minimize $\bar{\mathcal{G}}_0$.

4.7 Examples of fully actuated systems

4.7.1 Prismatic joint

Model. Probably the simplest example of a rigid body system is a single body moving in a prismatic joint, i.e. can only translate on one axis as illustrated on the left of Figure 4.2.

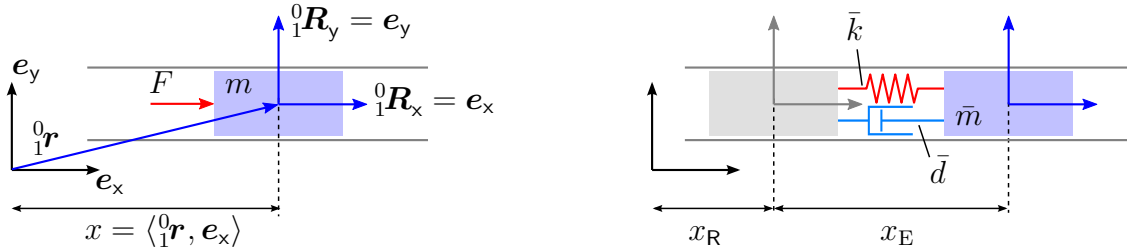


Figure 4.2: Model of a prismatic joint (left) and the closed loop (right)

The corresponding rigid body transformation is simply

$${}^0\mathbf{G} = \begin{bmatrix} 1 & 0 & 0 & x \\ 0 & 1 & 0 & 0 \\ 0 & 0 & 1 & 0 \\ 0 & 0 & 0 & 1 \end{bmatrix}. \quad (4.68)$$

With the trivial choice of the velocity coordinate $\xi = \dot{x}$, i.e. $\mathbf{A} = 1$, the equation of motion is

$$m\ddot{x} = F. \quad (4.69)$$

Closed loop. Due to the geometry of the model, only the controlled total mass 0m within the controlled body inertia matrix ${}^0\mathbf{M}$ contributes to the controlled kinetics and analog for the dissipation and stiffness. For the sake of readability we drop the body indices for the following examples of single bodies. So the only parameters contributing to the controlled kinetics are $\bar{m}, \bar{d}, \bar{k} \in \mathbb{R} > 0$.

For this example all three proposed control approaches are identical. With the displacement error $x_E = x - x_R$ the resulting energies are

$$\bar{\mathcal{V}} = \frac{1}{2}\bar{k}x_E^2, \quad \bar{\mathcal{R}} = \frac{1}{2}\bar{d}\dot{x}_E^2, \quad \bar{\mathcal{T}} = \frac{1}{2}\bar{m}\ddot{x}_E^2, \quad \bar{\mathcal{S}} = \frac{1}{2}\bar{m}\ddot{x}_E^2. \quad (4.70)$$

The potential has the obvious transport map $\mathbf{Q} = 1$ and the resulting closed loop kinetics are

$$\bar{m}\ddot{x}_E + \bar{d}\dot{x}_E + \bar{k}x_E = 0. \quad (4.71)$$

The corresponding explicit control law is

$$F = m\ddot{x}_R - \frac{m\bar{d}}{\bar{m}}\dot{x}_E - \frac{m\bar{k}}{\bar{m}}x_E. \quad (4.72)$$

An interpretation of the closed loop is given on the right side of Figure 4.2: The controlled body can be thought as being connected by a spring (stiffness \bar{k}) and a damper (viscosity \bar{d}) to its reference position x_R . The inertial force $\bar{m}\ddot{x}_E$ reacts to the error acceleration, i.e. to the acceleration of the body relative to its reference acceleration \ddot{x}_R . One could say the body has an inertia w.r.t. its reference.

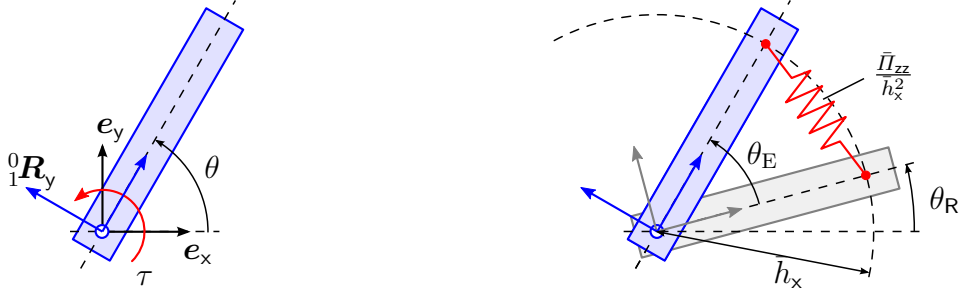


Figure 4.3: Revolute joint: rigid body constrained to rotate about an axis

4.7.2 Revolute joint

Model. Another elemental case is the revolute joint, i.e. a rigid body constrained to rotate about an axis as illustrated on the left side of Figure 4.3. With the joint angle θ the rigid body configuration may be written as

$${}^0\mathbf{G} = \begin{bmatrix} \cos \theta & -\sin \theta & 0 & 0 \\ \sin \theta & \cos \theta & 0 & 0 \\ 0 & 0 & 1 & 0 \\ 0 & 0 & 0 & 1 \end{bmatrix}. \quad (4.73)$$

With the velocity coordinate $\xi = \dot{\theta}$ the equation of motion is

$$\bar{\Theta}_{zz}\ddot{\theta} = \tau. \quad (4.74)$$

Potential energy. Due to the geometry of the model, only the control parameters $\bar{\Theta}_{zz}, \bar{\Upsilon}_{zz}, \bar{\Pi}_{zz} \in \mathbb{R} > 0$ contribute to the closed loop kinetics. With the angle error $\theta_E = \theta - \theta_R$ the potential may be written as

$$\bar{\mathcal{V}} = \bar{\Pi}_{zz}(1 - \cos \theta_E). \quad (4.75)$$

It has the obvious transport map $\mathbf{Q} = 1$. The potential could be realized by attaching a single linear spring with stiffness $\bar{\Pi}_{zz}/\bar{h}_z^2$ between desired configuration and actual configuration at a distance \bar{h}_z as illustrated on the right side of Figure 4.3. This also gives a vivid interpretation of the maximum on the potential at $\theta_E = \pm\pi$.

Approach 1. The particle based approach leads to the following closed loop kinetics

$$\bar{\Theta}_{zz}(\ddot{\theta} - \ddot{\theta}_R \cos \theta_E - \dot{\theta}_R^2 \sin \theta_E) + \bar{\Upsilon}_{zz}(\dot{\theta} - \dot{\theta}_R \cos \theta_E) + \bar{\Pi}_{zz} \sin \theta_E = 0. \quad (4.76)$$

The total energy $\bar{\mathcal{W}}$ and its time derivative are

$$\bar{\mathcal{W}} = \frac{1}{2}\bar{\Theta}_z(\dot{\theta}^2 - 2\dot{\theta}\dot{\theta}_R \cos \theta_E + \dot{\theta}_R^2) + \bar{\Pi}_z(1 - \cos \theta_E), \quad (4.77a)$$

$$\begin{aligned} \frac{d}{dt}\bar{\mathcal{W}} = & -\bar{\Upsilon}_z(\dot{\theta} - \dot{\theta}_R \cos \theta_E)^2 + \bar{\Pi}_z \dot{\theta}_R \sin \theta_E (\cos \theta_E - 1) \\ & + \bar{\Theta}_z \dot{\theta}_R (\ddot{\theta}_R(1 - \cos^2 \theta_E) + (\dot{\theta}^2 - \dot{\theta}_R^2 \cos \theta_E) \sin \theta_E) \end{aligned} \quad (4.77b)$$

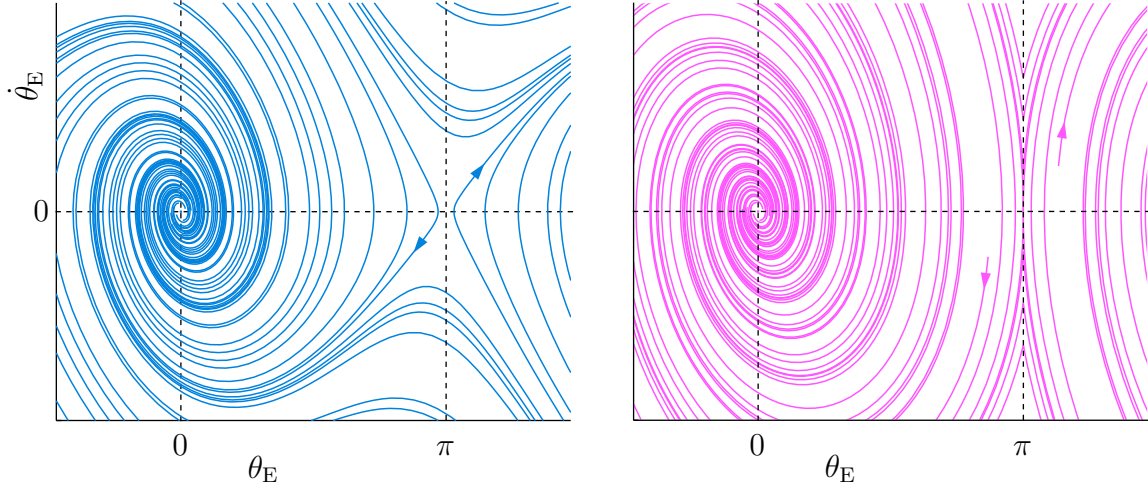


Figure 4.4: Phase plot for (4.79), left, and for (4.80), right

Without further assumptions on the reference trajectory $t \mapsto \theta_R(t)$ the total energy is *not* a Lyapunov function for the closed loop. The linear approximation $\theta \approx \theta_R$ of (4.76) has the characteristic polynomial

$$\lambda^2 + \frac{\bar{r}_z}{\bar{\theta}_z} \lambda + \left(\frac{\bar{\Pi}_z}{\bar{\theta}_z} - \dot{\theta}_R^2 \right). \quad (4.78)$$

So even for the special case of constant reference velocity $\ddot{\theta}_R(t) = 0$, we need $\frac{\bar{\Pi}_z}{\bar{\theta}_z} > \dot{\theta}_R^2$ to ensure local stability.

Approach 2 & 3. For this example the body-based and energy-based approaches lead to identical energies and closed loop kinetics:

$$\bar{\mathcal{R}} = \frac{1}{2} \bar{\mathcal{T}}_{zz} \dot{\theta}_E^2, \quad \bar{\mathcal{T}} = \frac{1}{2} \bar{\Theta}_{zz} \dot{\theta}_E^2, \quad \bar{\Theta}_{zz} \ddot{\theta}_E + \bar{\mathcal{T}}_{zz} \dot{\theta}_E + \bar{\Pi}_{zz} \sin \theta_E = 0. \quad (4.79)$$

The total energy $\bar{\mathcal{W}} = \bar{\mathcal{T}} + \bar{\mathcal{V}}$, $\dot{\bar{\mathcal{W}}} = -2\bar{\mathcal{R}}$ can be used to conclude that the system converges for *almost* all initial conditions $(\theta_E(0), \dot{\theta}_E(0))$. The remaining initial condition $\theta_E(0) = \pm\pi$ and $\dot{\theta}_E(0) = 0$ is unstable, see Figure 4.4. As a physical interpretation: the controlled dynamics coincide with the dynamics of a damped physical pendulum.

Linear control. Since the model (4.74) is a linear differential equation, the following linear closed loop equation might also be reasonable

$$\bar{\Theta}_{zz} \ddot{\theta}_E + \bar{\mathcal{T}}_{zz} \dot{\theta}_E + \bar{\Pi}_{zz} \theta_E = 0. \quad (4.80)$$

The difference between the closed loop (4.79) and (4.80) may be visualized by the corresponding phase plots, see Figure 4.4: The linear control law leads to non-smooth phase curves at $\theta = \pm\pi$, which is the consequence of the linear design for a system whose configuration space is actually $\mathbb{S}^1 \not\cong \mathbb{R}$. See [Konz and Rudolph, 2016, sec. 1.2] for a deeper discussion.

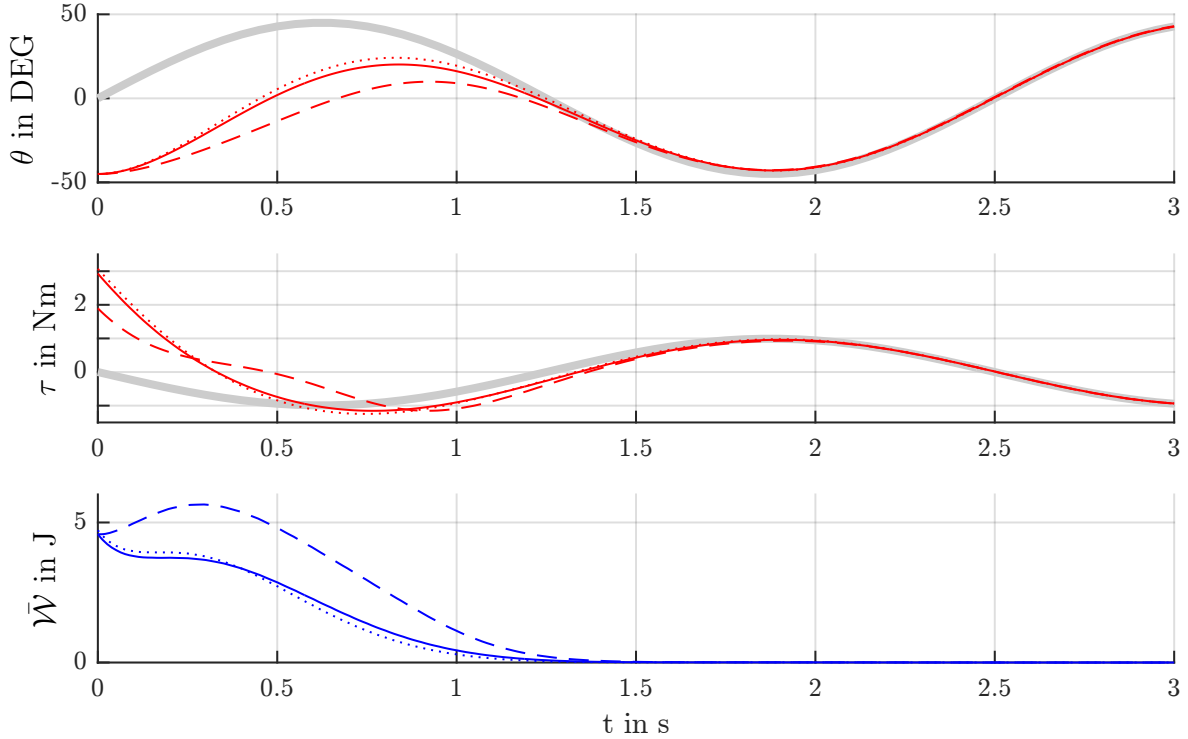


Figure 4.5: Simulation result for the revolute joint: gray line: reference, dashed line: particle-based approach, solid line: energy-based approach, dotted line: linear approach

Simulation results. Figure 4.5 shows simulation results comparing the three different approaches (4.76), (4.79) and (4.80) tracking a reference $\theta_R(t) = \frac{\pi}{2} \sin(\frac{2\pi}{2.5}t)$. Evidently, all approaches fulfill the control objective, i.e. the joint angle θ converges to its reference θ_R .

4.7.3 Rigid body orientation

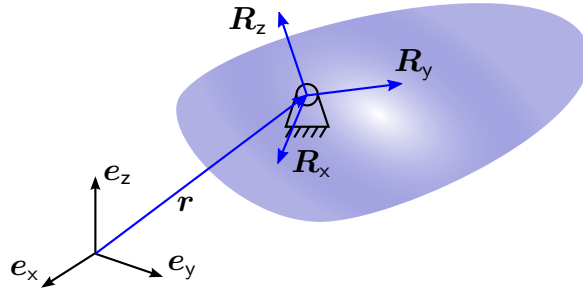


Figure 4.6: rigid body fixed at one point

Model. Consider a rigid body fixed at one point $\mathbf{r} = \text{const.}$ as illustrated in Figure 4.6. Its orientation may be parameterized by the coefficients of the rotation matrix $\mathbf{R} = [\mathbf{R}_x, \mathbf{R}_y, \mathbf{R}_z] \in \mathbb{SO}(3)$. With the angular velocity $\boldsymbol{\omega} = \text{Vee}(\mathbf{R}^\top \dot{\mathbf{R}})$ as velocity coordinates,

the inertia matrix Θ and the control torques τ about the body fixed axes, the equations of motion may be written as

$$\dot{\mathbf{R}} = \mathbf{R} \text{wed}(\boldsymbol{\omega}) \quad \Theta \dot{\boldsymbol{\omega}} + \text{wed}(\boldsymbol{\omega}) \Theta \boldsymbol{\omega} = \boldsymbol{\tau}. \quad (4.81)$$

Potential energy. Only the parameters $\bar{\Theta}$, $\bar{\Upsilon}$ and $\bar{\Pi}$ contribute to the closed loop kinetics. Using the attitude error $\mathbf{R}_E = \mathbf{R}_R^\top \mathbf{R}$ the error potential, its differential and Hessian are

$$\bar{\mathcal{V}} = \text{tr} (\text{Wed}(\bar{\Pi})(\mathbf{I}_3 - \mathbf{R}_E)), \quad (4.82a)$$

$$\bar{\mathbf{f}}^K = \nabla \bar{\mathcal{V}} = \text{vee2}(\text{Wed}(\bar{\Pi}) \mathbf{R}_E), \quad (4.82b)$$

$$(\nabla^2 \bar{\mathcal{V}})|_{\mathbf{R}=\mathbf{R}_R} = \bar{\Pi}. \quad (4.82c)$$

The potential has the transport map $\mathbf{Q} = \mathbf{R}_E^\top$, so the velocity error for the energy based approach is $\boldsymbol{\omega}_E = \boldsymbol{\omega} - \mathbf{R}_E^\top \boldsymbol{\omega}_R$ which coincides with the body velocity error.

Particle-based approach. The particle-based approach (4.18) leads to

$$\begin{aligned} \bar{\mathbf{f}}^M &= \bar{\Theta} \dot{\boldsymbol{\omega}} - \text{Vee}(\mathbf{R}_E^\top \text{Wed}(\bar{\Theta})) \mathbf{R}_E^\top \dot{\boldsymbol{\omega}}_R \\ &\quad + \text{wed}(\boldsymbol{\omega}) \bar{\Theta} \boldsymbol{\omega} + \text{vee2}(\text{Wed}(\bar{\Theta}) \text{wed}(\boldsymbol{\omega}_R)^2 \mathbf{R}_E) \end{aligned} \quad (4.83a)$$

$$\bar{\mathbf{f}}^D = \bar{\Upsilon} \boldsymbol{\omega} - \text{Vee}(\mathbf{R}_E^\top \text{Wed}(\bar{\Upsilon})) \mathbf{R}_E^\top \boldsymbol{\omega}_R \quad (4.83b)$$

Body-based approach. The body-based approach (4.26) leads to

$$\bar{\mathbf{f}}^M = \bar{\Theta} \dot{\boldsymbol{\omega}}_E + \text{wed}(\boldsymbol{\omega}_E) \bar{\Theta} \boldsymbol{\omega}_E \quad (4.84a)$$

$$\bar{\mathbf{f}}^D = \bar{\Upsilon} \boldsymbol{\omega}_E. \quad (4.84b)$$

The corresponding control law coincides with the one proposed in [Koditschek, 1989]. The total energy $\bar{\mathcal{W}} = \frac{1}{2} \boldsymbol{\omega}_E^\top \bar{\Theta} \boldsymbol{\omega}_E + \bar{\mathcal{V}}$ with $\dot{\bar{\mathcal{W}}} = -\boldsymbol{\omega}_E^\top \bar{\Upsilon} \boldsymbol{\omega}_E$ serves as a Lyapunov function for the closed loop.

Energy-based approach. For the energy-based approach (4.31) leads to

$$\bar{\mathbf{f}}^M = \bar{\Theta} \dot{\boldsymbol{\omega}}_E + \text{wed}(\text{Wed}(\bar{\Theta}) \boldsymbol{\omega}) \boldsymbol{\omega}_E \quad (4.85a)$$

$$\bar{\mathbf{f}}^D = \bar{\Upsilon} \boldsymbol{\omega}_E. \quad (4.85b)$$

The corresponding control law coincides with one proposed in [Bullo and Murray, 1999]. The total energy is the same as the one for the body based approach. The two approaches only differ in the gyroscopic terms.

Linearization. For a small error to the reference we have

$$\mathbf{R} = \mathbf{R}_R + \mathbf{R}_R \text{wed}(\boldsymbol{\varepsilon}), \quad \boldsymbol{\omega} = \boldsymbol{\omega}_R + \dot{\boldsymbol{\varepsilon}}, \quad \bar{\Theta} \ddot{\boldsymbol{\varepsilon}} + \bar{\Upsilon} \dot{\boldsymbol{\varepsilon}} + \bar{\Pi} \boldsymbol{\varepsilon} = 0. \quad (4.86)$$

4.7.4 Planar rigid body

A planar rigid body is a free rigid body in two dimensional space, i.e. it can translate in two dimensions and rotate about an perpendicular axis as illustrated in Figure 4.7. The model equations as well as the closed loop equations could be directly derived from the three dimensional rigid body by setting e.g. $v_z = 0$, $\omega_x = \omega_y = 0$ and removing the trivial equations. However it might be still instructive to display the resulting equations.

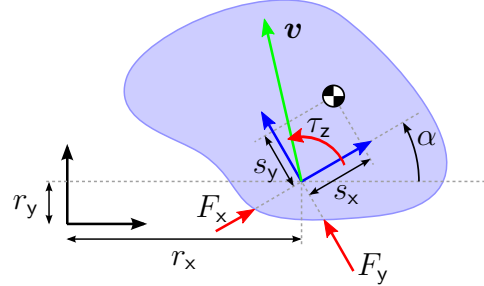


Figure 4.7: model of the planar rigid body

Coordinates and kinematics. As configuration coordinates \boldsymbol{x} we use the position r_x, r_y and the sine s_α and cosine c_α of the angle α . Consequently we have to impose the constraint $c_\alpha^2 + s_\alpha^2 - 1 = 0$ on the configuration coordinates. As velocity coordinates $\boldsymbol{\xi}$ we use the components v_x, v_y of the translational velocity w.r.t. the body fixed frame as illustrated in Figure 4.7 and the angular velocity $\omega_z = \dot{\alpha}$. This kinematic relation is

$$\frac{d}{dt} \underbrace{\begin{bmatrix} r_x \\ r_y \\ s_\alpha \\ c_\alpha \end{bmatrix}}_{\boldsymbol{x}} = \underbrace{\begin{bmatrix} c_\alpha & -s_\alpha & 0 \\ s_\alpha & c_\alpha & 0 \\ 0 & 0 & c_\alpha \\ 0 & 0 & -s_\alpha \end{bmatrix}}_{\boldsymbol{A}} \underbrace{\begin{bmatrix} v_x \\ v_y \\ \omega_z \end{bmatrix}}_{\boldsymbol{\xi}} \quad (4.87)$$

The rigid body configuration ${}^0_1\mathbf{G}$ and the resulting body Jacobian ${}^0_1\mathbf{J}$ w.r.t. the chosen velocity coordinates are

$${}^0_1\mathbf{G} = \begin{bmatrix} c_\alpha & -s_\alpha & 0 & r_x \\ s_\alpha & c_\alpha & 0 & r_y \\ 0 & 0 & 1 & 0 \\ 0 & 0 & 0 & 1 \end{bmatrix}, \quad {}^0_1\mathbf{J} = \begin{bmatrix} 1 & 0 & 0 \\ 0 & 1 & 0 \\ 0 & 0 & 0 \\ 0 & 0 & 0 \\ 0 & 0 & 0 \\ 0 & 0 & 1 \end{bmatrix} \quad (4.88)$$

Kinetic equation. Let the rigid body have the total mass m , the moment of inertia Θ_z and the coordinates s_x, s_y of the center of mass w.r.t. the body fixed frame. As control input consider the forces F_x, F_y and the torque τ_z as displayed in Figure 4.7. The resulting

kinetic equation is

$$\underbrace{\begin{bmatrix} m & 0 & -ms_y \\ 0 & m & ms_x \\ -ms_y & ms_x & \Theta_z \end{bmatrix}}_M \underbrace{\begin{bmatrix} \dot{v}_x \\ \dot{v}_y \\ \dot{\omega}_z \end{bmatrix}}_{\dot{\xi}} + \begin{bmatrix} -m(v_y + s_x \omega_z) \omega_z \\ m(v_x - s_y \omega_z) \omega_z \\ m(s_x v_x + s_y v_y) \omega_z \end{bmatrix} = \underbrace{\begin{bmatrix} F_x \\ F_y \\ \tau_z \end{bmatrix}}_u. \quad (4.89)$$

Control parameters. For the controlled kinetics we chose the following non-zero parameters

$${}^0\bar{m}, {}^0d, {}^0k \in \mathbb{R}^+, \quad {}^0\bar{s}_x, {}^0\bar{s}_y, {}^0\bar{l}_x, {}^0\bar{l}_y, {}^0\bar{h}_x, {}^0\bar{h}_y \in \mathbb{R}, \quad {}^0\bar{\Theta}_z, {}^0\bar{\Upsilon}_z, {}^0\bar{\Pi}_z \in \mathbb{R}^+. \quad (4.90)$$

Since all parameters are associated with the configuration ${}^0\mathbf{G}$, we drop the indices in the following, i.e. $\bar{m} = {}^0\bar{m}$.

Potential. The potential, resulting from the chosen parameters (4.90), and its derivatives are

$$\begin{aligned} \bar{\mathcal{V}} = & \frac{1}{2}\bar{k}(r_x - r_{xR})^2 + \frac{1}{2}\bar{k}(r_y - r_{yR})^2 + \bar{\Pi}_z(1 - c_{\alpha_E}) \\ & + \bar{k}\bar{h}_x(c_\alpha - c_{\alpha_R})(r_x - r_{xR}) - \bar{k}\bar{h}_y(s_\alpha - s_{\alpha_R})(r_x - r_{xR}) \\ & + \bar{k}\bar{h}_y(c_\alpha - c_{\alpha_R})(r_y - r_{yR}) - \bar{k}\bar{h}_x(s_\alpha - s_{\alpha_R})(r_y - r_{yR}) \end{aligned} \quad (4.91a)$$

$$\nabla \bar{\mathcal{V}} = \begin{bmatrix} \bar{k}(c_\alpha(r_x - r_{xR}) + s_\alpha(r_y - r_{yR}) + \bar{h}_x(1 - c_{\alpha_E}) - \bar{h}_y s_{\alpha_E}) \\ \bar{k}(-s_\alpha(r_x - r_{xR}) + c_\alpha(r_y - r_{yR}) + \bar{h}_x s_{\alpha_E} + \bar{h}_y(1 - c_{\alpha_E})) \\ \bar{k}((\bar{h}_x c_\alpha + \bar{h}_y s_\alpha)(r_y - r_{yR}) - (\bar{h}_y c_\alpha + \bar{h}_x s_\alpha)(r_x - r_{xR})) + \bar{\Pi}_z s_{\alpha_E} \end{bmatrix} \quad (4.91b)$$

$$\nabla^2 \bar{\mathcal{V}}|_R = \begin{bmatrix} \bar{k} & 0 & -\bar{k}\bar{h}_y \\ 0 & \bar{k} & \bar{k}\bar{h}_x \\ -\bar{k}\bar{h}_y & \bar{k}\bar{h}_x & \bar{\Pi}_z \end{bmatrix} \quad (4.91c)$$

The sine and cosine of the angle error $\alpha - \alpha_R$ are introduced just for readability

$$c_{\alpha_E} = c_\alpha c_{\alpha_R} + s_\alpha s_{\alpha_R} = \cos(\alpha - \alpha_R), \quad s_{\alpha_E} = s_\alpha c_{\alpha_R} - c_\alpha s_{\alpha_R} = \sin(\alpha - \alpha_R). \quad (4.92)$$

From the Hessian $\nabla^2 \bar{\mathcal{V}}|_R$ at the critical point $\mathbf{x} = \mathbf{x}_R$ one can see that (local) positive definiteness requires $\bar{\Pi}_z > \bar{k}(\bar{h}_x^2 + \bar{h}_y^2)$. We will encounter the analog requirement for the controlled moment of inertia $\bar{\Theta}_z$ and damping $\bar{\Upsilon}_z$.

A transport map for (4.91a) is given by³

$$\underbrace{\begin{bmatrix} v_{xE} \\ v_{yE} \\ \omega_{zE} \end{bmatrix}}_{\xi_E} = \underbrace{\begin{bmatrix} v_x \\ v_y \\ \omega_z \end{bmatrix}}_{\xi} - \underbrace{\begin{bmatrix} c_{\alpha_E} & s_{\alpha_E} & s_\alpha(r_x - r_{xR}) - c_\alpha(r_y - r_{yR}) \\ -s_{\alpha_E} & c_{\alpha_E} & c_\alpha(r_x - r_{xR}) + s_\alpha(r_y - r_{yR}) \\ 0 & 0 & 1 \end{bmatrix}}_Q \underbrace{\begin{bmatrix} v_{xR} \\ v_{yR} \\ \omega_{zR} \end{bmatrix}}_{\xi_R}. \quad (4.93)$$

³An alternative transport map corresponding to (4.43) is

$$Q = \begin{bmatrix} c_{\alpha_E} & s_{\alpha_E} & \bar{h}_x s_{\alpha_E} - \bar{h}_y(c_{\alpha_E} - 1) \\ -s_{\alpha_E} & c_{\alpha_E} & \bar{h}_x(c_{\alpha_E} - 1) + \bar{h}_y s_{\alpha_E} \\ 0 & 0 & 1 \end{bmatrix}. \quad (4.94)$$

Particle-based approach. The damping and inertia force using the particle based approach are:

$$\bar{\mathbf{f}}^D = \underbrace{\begin{bmatrix} \bar{d} & 0 & -\bar{d}\bar{l}_y \\ 0 & \bar{d} & \bar{d}\bar{l}_x \\ -\bar{d}\bar{l}_y & \bar{d}\bar{l}_x & \bar{\Upsilon}_z \end{bmatrix}}_D \underbrace{\begin{bmatrix} v_x \\ v_y \\ \omega_z \end{bmatrix}}_{\xi} - \underbrace{\begin{bmatrix} \bar{d}c_{\alpha_E} & \bar{d}s_{\alpha_E} & \bar{d}(\bar{l}_x s_{\alpha_E} - \bar{l}_y c_{\alpha_E}) \\ -\bar{d}s_{\alpha_E} & \bar{d}c_{\alpha_E} & \bar{d}(\bar{l}_x c_{\alpha_E} + \bar{l}_y s_{\alpha_E}) \\ -\bar{d}(\bar{l}_x s_{\alpha_E} + \bar{l}_y c_{\alpha_E}) & \bar{d}(\bar{l}_x c_{\alpha_E} - \bar{l}_y s_{\alpha_E}) & \bar{\Upsilon}_z c_{\alpha_E} \end{bmatrix}}_{\xi_R} \underbrace{\begin{bmatrix} v_{xR} \\ v_{yR} \\ \omega_{zR} \end{bmatrix}}_{\dot{\xi}_R}, \quad (4.95a)$$

$$\bar{\mathbf{f}}^M = \underbrace{\begin{bmatrix} \bar{m} & 0 & -\bar{m}\bar{s}_y \\ 0 & \bar{m} & \bar{m}\bar{s}_x \\ -\bar{m}\bar{s}_y & \bar{m}\bar{s}_x & \bar{\Upsilon}_z \end{bmatrix}}_M \underbrace{\begin{bmatrix} \dot{v}_x \\ \dot{v}_y \\ \dot{\omega}_z \end{bmatrix}}_{\dot{\xi}} + \underbrace{\begin{bmatrix} -\bar{m}(v_y + \bar{s}_x \omega_z) \omega_z \\ \bar{m}(v_x - \bar{s}_y \omega_z) \omega_z \\ \bar{m}(\bar{s}_x v_x + \bar{s}_y v_y) \omega_z \end{bmatrix}}_{\ddot{\xi}} - \underbrace{\begin{bmatrix} \bar{m}c_{\alpha_E} & \bar{m}s_{\alpha_E} & \bar{m}(\bar{s}_x s_{\alpha_E} - \bar{s}_y c_{\alpha_E}) \\ -\bar{m}s_{\alpha_E} & \bar{m}c_{\alpha_E} & \bar{m}(\bar{s}_x c_{\alpha_E} + \bar{s}_y s_{\alpha_E}) \\ -\bar{m}(\bar{s}_x s_{\alpha_E} + \bar{s}_y c_{\alpha_E}) & \bar{m}(\bar{s}_x c_{\alpha_E} - \bar{s}_y s_{\alpha_E}) & \bar{\Upsilon}_z c_{\alpha_E} \end{bmatrix}}_{\ddot{\xi}_R} \underbrace{\begin{bmatrix} \dot{v}_{xR} \\ \dot{v}_{yR} \\ \dot{\omega}_{zR} \end{bmatrix}}_{\dot{\dot{\xi}}_R} - \underbrace{\begin{bmatrix} -\bar{m}((v_{yR} + \bar{s}_x \omega_{zR}) c_{\alpha_E} - (v_{xR} - \bar{s}_y \omega_{zR}) s_{\alpha_E}) \omega_{zR} \\ \bar{m}((v_{yR} + \bar{s}_x \omega_{zR}) s_{\alpha_E} + (v_{xR} - \bar{s}_y \omega_{zR}) c_{\alpha_E}) \omega_{zR} \\ \bar{m}((\bar{s}_x v_{xR} + \bar{s}_y v_{yR}) c_{\alpha_E} - (\bar{s}_y v_{xR} - \bar{s}_x v_{yR}) s_{\alpha_E}) \omega_{zR} + \bar{\Theta}_z s_{\alpha_E} \omega_{zR}^2 \end{bmatrix}}_{\ddot{\xi}_R}. \quad (4.95b)$$

The corresponding total energy as defined in (4.5), is not a Lyapunov function for the closed loop.

Body-based approach. The damping and inertia force using the body-based approach are:

$$\bar{\mathbf{f}}^D = \underbrace{\begin{bmatrix} \bar{d} & 0 & -\bar{d}\bar{l}_y \\ 0 & \bar{d} & \bar{d}\bar{l}_x \\ -\bar{d}\bar{l}_y & \bar{d}\bar{l}_x & \bar{\Upsilon}_z \end{bmatrix}}_D \underbrace{\begin{bmatrix} v_{xE} \\ v_{yE} \\ \omega_{zE} \end{bmatrix}}_{\xi_E} \quad (4.96a)$$

$$\bar{\mathbf{f}}^M = \underbrace{\begin{bmatrix} \bar{m} & 0 & -\bar{m}\bar{s}_y \\ 0 & \bar{m} & \bar{m}\bar{s}_x \\ -\bar{m}\bar{s}_y & \bar{m}\bar{s}_x & \bar{\Theta}_z \end{bmatrix}}_M \underbrace{\begin{bmatrix} \dot{v}_{xE} \\ \dot{v}_{yE} \\ \dot{\omega}_{zE} \end{bmatrix}}_{\dot{\xi}_E} + \underbrace{\begin{bmatrix} 0 & -\bar{m}\omega_{zE} & -\bar{m}\bar{s}_x \omega_{zE} \\ \bar{m}\omega_{zE} & 0 & -\bar{m}\bar{s}_y \omega_{zE} \\ \bar{m}\bar{s}_x \omega_{zE} & \bar{m}\bar{s}_y \omega_{zE} & 0 \end{bmatrix}}_{\ddot{\xi}_E} \underbrace{\begin{bmatrix} v_{xE} \\ v_{yE} \\ \omega_{zE} \end{bmatrix}}_{\dot{\dot{\xi}}_E} \quad (4.96b)$$

where the velocity error ξ_E was defined in (4.93). The total energy $\bar{\mathcal{W}} = \frac{1}{2}\xi_E^\top \mathbf{M} \xi_E + \bar{\mathcal{V}}$ is a Lyapunov function for the closed loop.

Energy-based approach. The damping and inertia forces using the energy-based approach are:

$$\bar{\mathbf{f}}^D = \underbrace{\begin{bmatrix} \bar{d} & 0 & -\bar{d}\bar{l}_y \\ 0 & \bar{d} & \bar{d}\bar{l}_x \\ -\bar{d}\bar{l}_y & \bar{d}\bar{l}_x & \bar{\gamma}_z \end{bmatrix}}_{\mathbf{D}} \underbrace{\begin{bmatrix} v_{xE} \\ v_{yE} \\ \omega_{zE} \end{bmatrix}}_{\boldsymbol{\xi}_E}, \quad (4.97a)$$

$$\bar{\mathbf{f}}^M = \underbrace{\begin{bmatrix} \bar{m} & 0 & -\bar{m}\bar{s}_y \\ 0 & \bar{m} & \bar{m}\bar{s}_x \\ -\bar{m}\bar{s}_y & \bar{m}\bar{s}_x & \bar{\theta}_z \end{bmatrix}}_{\mathbf{M}} \underbrace{\begin{bmatrix} \dot{v}_{xE} \\ \dot{v}_{yE} \\ \dot{\omega}_{zE} \end{bmatrix}}_{\dot{\boldsymbol{\xi}}_E} + \begin{bmatrix} 0 & -\bar{m}\omega_z & -\bar{m}\bar{s}_x\omega_z \\ \bar{m}\omega_z & 0 & -\bar{m}\bar{s}_y\omega_z \\ \bar{m}\bar{s}_x\omega_z & \bar{m}\bar{s}_y\omega_z & 0 \end{bmatrix} \begin{bmatrix} v_{xE} \\ v_{yE} \\ \omega_{zE} \end{bmatrix}. \quad (4.97b)$$

The total energy $\bar{\mathcal{W}} = \frac{1}{2}\boldsymbol{\xi}_E^\top \mathbf{M} \boldsymbol{\xi}_E + \bar{\mathcal{V}}$ coincides with the total energy for the body-based approach and is a Lyapunov function for this closed loop as well. Note that the two approaches do differ in the gyroscopic terms, so do lead to different solutions of the closed loop dynamics.

Simulation result. In subsection 4.7.5 we will give and discuss a simulation result for the special parameter choice $\bar{s}_x = \bar{l}_x = \bar{h}_x = 0$ and $\bar{s}_y = \bar{l}_y = \bar{h}_y = 0$.

4.7.5 Free rigid body: decoupling of translational and rotational motion

The closed loop equations for a (free) three dimensional rigid body were given in subsection 4.1.2, subsection 4.2.1 and subsection 4.3.3. The reduced equations for the planar case were given in subsection 4.7.4. For most applications we like to *decouple* the translational and the rotational motion of the body.

Observing the closed loop equations one can see immediately that the coupling terms vanish if $\bar{s} = \bar{l} = \bar{h} = \mathbf{0}$, i.e. the chosen body fixed point \mathbf{r} coincides with the center of mass, damping and stiffness. Then the rotational dynamics are identical to the closed loop given in subsection 4.7.3 (subsection 4.7.2 for the planar case), so are indeed decoupled/independent from the translational motion.

Translational dynamics. For the translational dynamics the situation is more difficult: Introduce $\mathbf{e} = \mathbf{r} - \mathbf{r}_R$ as the components of the position error w.r.t. the inertial frame and $\mathbf{r}_E = \mathbf{R}_R^\top(\mathbf{r} - \mathbf{r}_R)$ as the components w.r.t. the reference frame. The translational dynamics for the different approaches and given transport map are equivalent to

$$\text{particle-based:} \quad \bar{m}\ddot{\mathbf{e}} + \bar{d}\dot{\mathbf{e}} + \bar{k}\mathbf{e} = \mathbf{0} \quad (4.98a)$$

$$\text{body-based:} \quad \bar{m}\ddot{\mathbf{r}}_E + \bar{d}\dot{\mathbf{r}}_E + \bar{k}\mathbf{r}_E = \mathbf{0} \quad (4.98b)$$

$$\text{energy-based:} \quad \bar{m}(\ddot{\mathbf{r}}_E + \text{wed}(\boldsymbol{\omega}_R)\dot{\mathbf{r}}_E) + \bar{d}\dot{\mathbf{r}}_E + \bar{k}\mathbf{r}_E = \mathbf{0} \quad (4.98c)$$

Translational energy. For the rigid body we can split the total energy $\bar{\mathcal{W}} = \bar{\mathcal{W}}_r + \bar{\mathcal{W}}_R$ into a part associated with the position $\bar{\mathcal{W}}_r$ and one associated with the orientation $\bar{\mathcal{W}}_R$. The rotational energies for the corresponding approaches coincide with the ones given in subsection 4.7.3 (subsection 4.7.2 for the planar case). The translational energies and their change along the solutions of (4.98) are

$$\text{particle-based: } \bar{\mathcal{W}}_r = \frac{1}{2}\bar{k}\|\mathbf{e}\|^2 + \frac{1}{2}\bar{m}\|\dot{\mathbf{e}}\|^2, \quad \dot{\bar{\mathcal{W}}}_r = -\bar{d}\|\dot{\mathbf{e}}\|^2 \quad (4.99a)$$

$$\text{body-based: } \bar{\mathcal{W}}_r = \frac{1}{2}\bar{k}\|\mathbf{r}_E\|^2 + \frac{1}{2}\bar{m}\|\dot{\mathbf{r}}_E\|^2, \quad \dot{\bar{\mathcal{W}}}_r = -\bar{d}\|\dot{\mathbf{r}}_E\|^2 \quad (4.99b)$$

$$\text{energy-based: } \bar{\mathcal{W}}_r = \frac{1}{2}\bar{k}\|\mathbf{r}_E\|^2 + \frac{1}{2}\bar{m}\|\dot{\mathbf{r}}_E\|^2, \quad \dot{\bar{\mathcal{W}}}_r = -\bar{d}\|\dot{\mathbf{r}}_E\|^2 \quad (4.99c)$$

For their comparison note that

$$\|\mathbf{e}\| = \|\mathbf{r}_E\|, \quad \|\dot{\mathbf{e}}\| = \|\dot{\mathbf{r}}_E + \text{wed}(\boldsymbol{\omega}_R)\mathbf{r}_E\|. \quad (4.100)$$

The crucial observation is that for all approaches the translational dynamics and energy are indeed independent of the actual orientation \mathbf{R} and its velocity $\boldsymbol{\omega}$, but for some approaches they depend on their *reference* \mathbf{R}_R and $\boldsymbol{\omega}_R$. For a constant reference orientation $\mathbf{R}_R = \text{const.}$ and consequently $\boldsymbol{\omega}_R = \mathbf{0}$ all four approaches are equivalent. Furthermore it is worth noting that the error dynamics as well as the energies are invariant to the reference trajectory $t \mapsto \mathbf{r}_R(t)$ for the position.

Simulation. The difference between these cases will be discussed on simulation results for the simpler, yet as illustrative, example of a planar rigid body: The reference configuration is $r_{xR}(t) = r_{yR}(t) = 0$ and $\alpha_R(t) = \pi t$ which yields the constant reference velocity $\boldsymbol{\xi}_R(t) = [0, 0, \pi]$. The control parameters are set to $\bar{m} = 1$, $\bar{d} = 4$, $\bar{k} = 4$ (neglecting the units). The roots of the characteristic polynomial of (4.98c) are $\lambda \approx \{-0.5 \pm 0.6i, -3.5 \pm 3.7i\}$, resulting from the control parameters as well as the constant angular velocity $\omega_{zR} = \pi$. The characteristic polynomial for the other approaches is independent of the reference trajectory and has a quadruple root at $\lambda = -2$.

Figure 4.8 shows the simulation result for the initial conditions $r_x(0) = 0, r_y(0) = 1, \alpha(0) = 0$ and $\boldsymbol{\xi}(0) = \mathbf{0}$. Observing from the inertial frame, top left of Figure 4.8, for approach 2 the body follows a straight line to its reference position, whereas for the other approaches spiral around it. Observing from the reference frame, top right of Figure 4.8, for approach 3 the body follows a direct path, given the initial velocity. The middle graph in Figure 4.8 shows the evolution of the translational energy $\bar{\mathcal{W}}_r$. The difference in the initial values results from $\dot{\mathbf{e}}(0) = \mathbf{0}$, but $\dot{\mathbf{r}}_E(0) \neq \mathbf{0}$. The bottom graph in Figure 4.8 shows the evolution of the euclidean distance $\|\mathbf{e}\| = \|\mathbf{r}_E\|$. The rate of convergence for approach 2 and 3 are the same as could be expected from having the same characteristic polynomial.

Even though the energy based approach with the transport map from (4.42) might be mathematically the most elegant solution, its simulation result is not intuitive. Which approach is most desirable, depends given application. For indoor robots (like the multicopters discussed in the next chapter) it is probably most desirable if it corrects its position error following a straight line in the inertial frame.

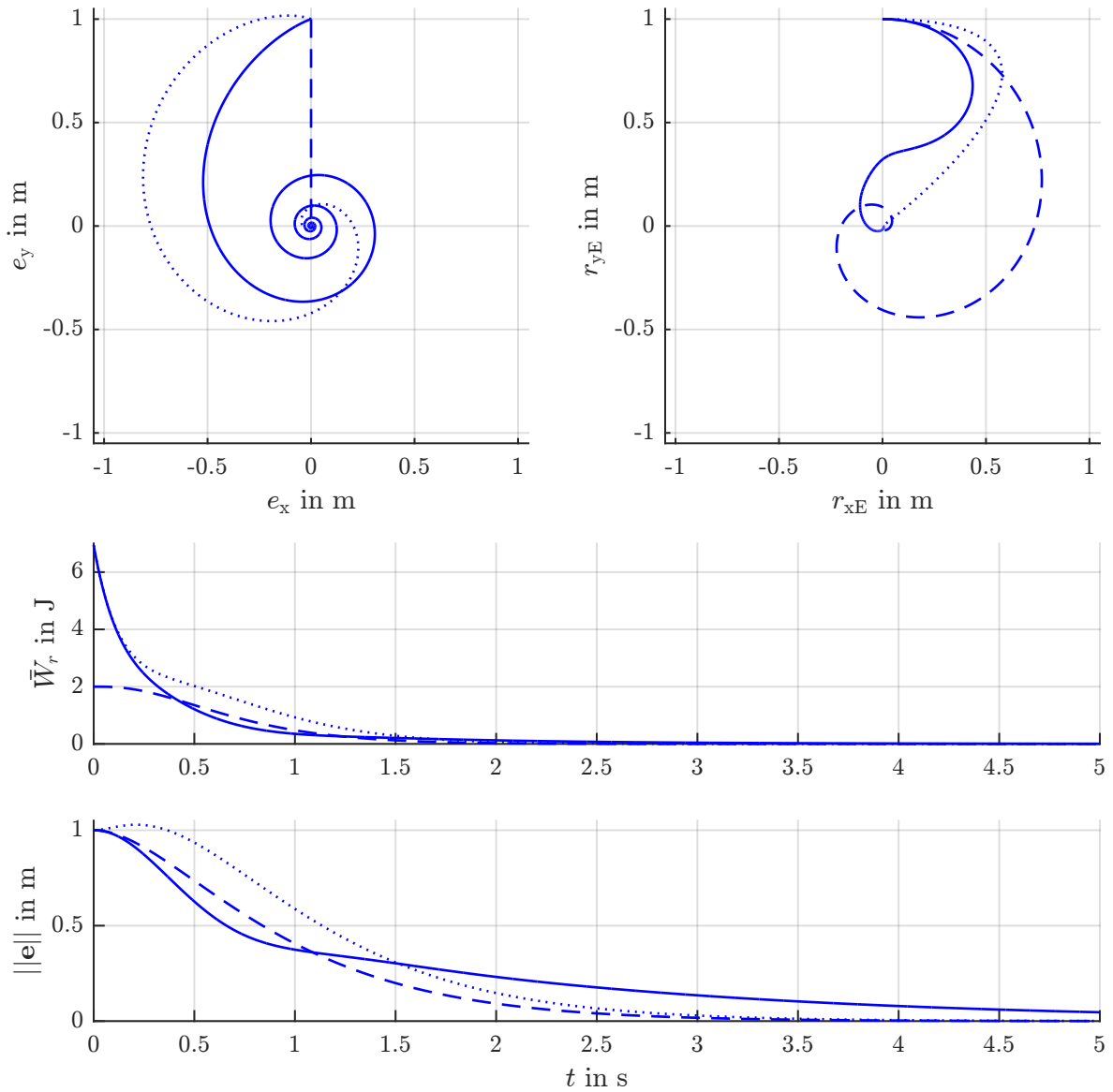


Figure 4.8: Simulation result for the planar rigid body. The solid line: energy-based approach with $\mathbf{Q} = \text{Ad}_{\mathbf{G}^{-1}\mathbf{G}_R}$, dashed line: particle-based approach, dotted line: body-based approach.

4.7.6 SCARA robot

As a simple example of a multi-body system we consider a SCARA robot as displayed in Figure 4.9. For the sake of demonstration we neglect the vertical axis and the tool orientation. The remaining two axis are sufficient to position a tool (red point in Figure 4.9) in the workspace (green shaded area).

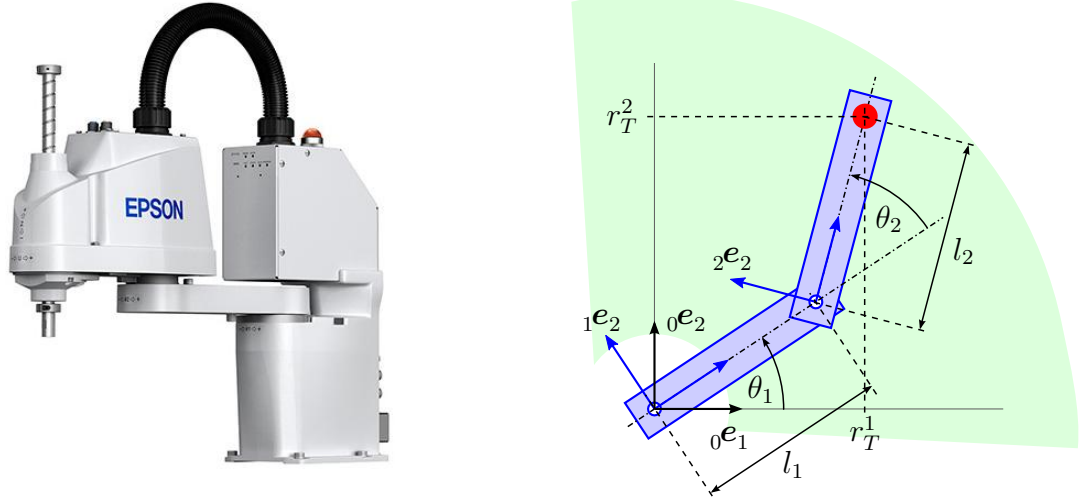


Figure 4.9: A Scara robot and its mechanical model (image www.epson.com)

Model. The model consists of two rigid bodies constraint by two revolute joints. A reasonable choice of coordinates are the relative joint angles $\boldsymbol{x} = [\theta_1, \theta_2]^\top$ and their derivatives $\boldsymbol{\xi} = [\dot{\theta}_1, \dot{\theta}_2]^\top$. The rigid body configurations are

$${}^0\mathbf{G} = \begin{bmatrix} \cos \theta_1 & -\sin \theta_1 & 0 & 0 \\ \sin \theta_1 & \cos \theta_1 & 0 & 0 \\ 0 & 0 & 1 & 0 \\ 0 & 0 & 0 & 1 \end{bmatrix}, \quad {}^0\mathbf{J} = \begin{bmatrix} 0 & 0 \\ 0 & 0 \\ 0 & 0 \\ 0 & 0 \\ 1 & 0 \end{bmatrix} \quad (4.101a)$$

$${}^1\mathbf{G} = \begin{bmatrix} \cos \theta_2 & -\sin \theta_2 & 0 & l_1 \\ \sin \theta_2 & \cos \theta_2 & 0 & 0 \\ 0 & 0 & 1 & 0 \\ 0 & 0 & 0 & 1 \end{bmatrix}, \quad {}^1\mathbf{J} = \begin{bmatrix} 0 & 0 \\ 0 & 0 \\ 0 & 0 \\ 0 & 0 \\ 0 & 1 \end{bmatrix}. \quad (4.101b)$$

Let ${}_1\Theta_z$ be the moment of inertia of the first body about the first joint and l_1 be the distance between the two joints. The second body has the mass ${}_2m$, the center of mass (${}_2s_x, {}_2s_y$) and the moment of inertia ${}_2\Theta_z$ about the second joint. The control forces are the joint torques $\mathbf{u} = [\tau_1, \tau_2]^\top$. Overall, the equations of motion for the SCARA robot are

$$\begin{bmatrix} {}_1\Theta_z + {}_2\Theta_z + {}_2ml_1^2 + 2a(\theta_2) & {}_2\Theta_z + a(\theta_2) \\ {}_2\Theta_z + a(\theta_2) & {}_2\Theta_z \end{bmatrix} \begin{bmatrix} \ddot{\theta}_1 \\ \ddot{\theta}_2 \end{bmatrix} + \begin{bmatrix} a'(\theta_2)(2\dot{\theta}_1\dot{\theta}_2 + \dot{\theta}_2^2) \\ -a'(\theta_2)\dot{\theta}_1^2 \end{bmatrix} = \begin{bmatrix} \tau_1 \\ \tau_2 \end{bmatrix} \quad (4.102)$$

where

$$a(\theta_2) = {}_2ml_1({}_2s_x \cos \theta_2 - {}_2s_y \sin \theta_2), \quad a'(\theta_2) = -{}_2ml_1({}_2s_x \sin \theta_2 + {}_2s_y \cos \theta_2). \quad (4.103)$$

Controller parameterization 1. In the following we will discuss two different controller parameterizations for the SCARA. For the first parameterization the non-zero parameters are

$${}^0_1\bar{\Pi}_z, {}^0_1\bar{\Upsilon}_z, {}^0_1\bar{\Theta}_z, {}^1_2\bar{\Pi}_z, {}^1_2\bar{\Upsilon}_z, {}^1_2\bar{\Theta}_z \in \mathbb{R} > 0. \quad (4.104)$$

These parameters are directly associated with the errors $\theta_{iE} = \theta_i - \theta_{iR}$, $i = 1, 2$ of the joint angles. The resulting potential is

$$\bar{\mathcal{V}} = {}^0_1\bar{\Pi}_z(1 - \cos \theta_{1E}) + {}^1_2\bar{\Pi}_z(1 - \cos \theta_{2E}). \quad (4.105)$$

and obeys the transport map $\mathbf{Q} = \mathbf{I}_2$.

The resulting controlled kinetics for the body and energy-based approach are

$${}^{i-1}_i\bar{\Theta}_z \ddot{\theta}_{iE} + {}^{i-1}_i\bar{\Upsilon}_z \dot{\theta}_{iE} + {}^{i-1}_i\bar{\Pi}_z \sin \theta_{iE} = 0, \quad i = 1, 2. \quad (4.106)$$

The controlled kinetics for the particle based approach yield

$${}^{i-1}_i\bar{\Theta}_z (\ddot{\theta}_i - \ddot{\theta}_{iR} \cos \theta_{iE} - \dot{\theta}_{iR}^2 \sin \theta_{iE}) + {}^{i-1}_i\bar{\Upsilon}_z (\dot{\theta}_i - \dot{\theta}_{iR} \cos \theta_{iE}) + {}^{i-1}_i\bar{\Pi}_z \sin \theta_{iE} = 0, \quad i = 1, 2. \quad (4.107)$$

With this parameterization the controlled kinetics coincide with two copies of the kinetics of the revolute joint discussed in subsection 4.7.2.

Controller parameterization 2. The non-zero parameters for another interesting parameterization of the controller are

$${}^0_2\bar{k}, {}^0_2\bar{d}, {}^0_2\bar{m} \in \mathbb{R} > 0, \quad {}^0_2\bar{h}_x = {}^0_2\bar{l}_x = {}^0_2\bar{s}_x = l_2. \quad (4.108)$$

The resulting potential can be written as

$$\bar{\mathcal{V}}(\mathbf{x}, \mathbf{x}_R) = \frac{1}{2} {}^0_2\bar{k} \|\mathbf{r}_T(\mathbf{x}) - \mathbf{r}_T(\mathbf{x}_R)\|^2 \quad \mathbf{r}_T(\mathbf{x}) = \begin{bmatrix} l_1 \cos \theta_1 + l_2 \cos(\theta_1 + \theta_2) \\ l_1 \sin \theta_1 + l_2 \sin(\theta_1 + \theta_2) \end{bmatrix}, \quad (4.109)$$

where \mathbf{r}_T is the position of the tool as illustrated in Figure 4.9. Using the *tool position error* $\mathbf{e}(\mathbf{x}, \mathbf{x}_R) = \mathbf{r}_T(\mathbf{x}) - \mathbf{r}_T(\mathbf{x}_R)$ as error coordinates, we can apply the rule from (A.8) to compute the transport map as

$$\mathbf{Q}(\mathbf{x}, \mathbf{x}_R) = (\nabla \mathbf{r}_T(\mathbf{x}))^{-1} \nabla \mathbf{r}_T(\mathbf{x}_R). \quad (4.110)$$

The determinant of the differential $\det \nabla \mathbf{r}_T(\mathbf{x}) = \sin \theta_2$ reflects the well known singularity of the SCARA inverse kinematics, see e.g. [Murray et al., 1994, example 3.6].

The closed loop kinetics for the particle and energy-based approach in terms of the model coordinates \boldsymbol{x} and the error velocity $\boldsymbol{\xi}_E = \boldsymbol{\xi} - \mathbf{Q}\boldsymbol{\xi}_R$ are

$$\underbrace{\begin{bmatrix} l_1^2 + 2l_1l_2 \cos \theta_2 + l_2^2 & l_1l_2 \cos \theta_2 + l_2^2 \\ l_1l_2 \cos \theta_2 + l_2^2 & l_2^2 \end{bmatrix}}_{\bar{\mathbf{M}}} \dot{\boldsymbol{\xi}}_E + \underbrace{\begin{bmatrix} -\dot{\theta}_2 & -\dot{\theta}_1 - \dot{\theta}_2 \\ \dot{\theta}_1 & 0 \end{bmatrix}}_{\frac{1}{2}\bar{m}l_1l_2 \sin \theta_2} \boldsymbol{\xi}_E + \underbrace{\begin{bmatrix} l_1^2 + 2l_1l_2 \cos \theta_2 + l_2^2 & l_1l_2 \cos \theta_2 + l_2^2 \\ l_1l_2 \cos \theta_2 + l_2^2 & l_2^2 \end{bmatrix}}_{\bar{\mathbf{D}}} \boldsymbol{\xi}_E + \underbrace{\begin{bmatrix} l_1^2 \sin \theta_{1E} + l_1l_2(\sin(\theta_{1E} - \theta_{2R}) + \sin(\theta_{1E} + \theta_2)) + l_2^2 \sin(\theta_{1E} + \theta_{2E}) \\ l_1l_2(\sin(\theta_{1E} + \theta_2) - \sin(\theta_2)) + l_2^2 \sin(\theta_{1E} + \theta_{2E}) \end{bmatrix}}_{\nabla \bar{\mathcal{V}}} = \mathbf{0}. \quad (4.111a)$$

In terms of the tool position error \boldsymbol{e} this is equivalent to the much simpler equation

$$\frac{1}{2}\bar{m}\ddot{\boldsymbol{e}} + \frac{1}{2}\bar{d}\dot{\boldsymbol{e}} + \frac{1}{2}\bar{k}\boldsymbol{e} = \mathbf{0}. \quad (4.111b)$$

With the body-based approach we get a similar closed loop that is not displayed or discussed here.

As mentioned above, the transport map \mathbf{Q} contains terms with $1/\sin \theta_2$. Fortunately these terms cancel out in $\bar{\mathbf{M}}\mathbf{Q}$ and $\bar{\mathbf{D}}\mathbf{Q}$ in the closed loop equation (4.111a), so this singularity actually does not hurt in practice. This could also be expected since the particle based approach, which does not rely on the transport map, leads to the same closed loop.

A singularity that does hurt, is the inertia matrix with $\det \bar{\mathbf{M}} = (\frac{1}{2}\bar{m}l_1l_2 \sin \theta_2)^2$. This means that one can not compute the control law if $\sin \theta_2 = 0$. Recalling the mechanical model of the SCARA Figure 4.9, this singularity is evident from a geometric point of view: If $\sin \theta_2 = 0$ the tool can only move in a tangential direction to the boundary of the workspace but not radial. However, it should be stressed that this singularity is not a consequence of unsuitable configuration coordinates $\boldsymbol{x} = [\theta_1, \theta_2]^\top$. It is rather an intrinsic one resulting from forcing dynamics suitable for \mathbb{R}^2 on a system that has the configuration space \mathbb{S}^2 .

Simulation result. Figure 4.10 and Figure 4.11 show a simulation results for the SCARA robot with the two proposed parameterizations. The robot starts in a rather random initial configuration. The reference configuration is constant till $t = 1$ s, then follows a straight line for the tool position till $t = 4$ s and remains constant thereafter.

For both parameterizations the controlled total energy $\bar{\mathcal{W}}$ converges. The crucial difference between the two parameterizations is, though the tool position \boldsymbol{r}_T tracks its reference in both cases, the joint angles θ_1, θ_2 do not for the second parameterization. The reason for this is best understood when looking at the controlled potential energy $\bar{\mathcal{V}}$ illustrated in Figure 4.12: For parameterization 2 the potential has two minima $\bar{\mathcal{V}} = 0$ for which the tool is at its reference position, but with different joint angles. This is true for any tool position except the ones on the boundary of the workspace where $\theta_2 = 0$ or $\theta_2 = \pi$.

Which of the two parameterizations is “better” probably depends on the practical control task: If the actual joint configuration (θ_1, θ_2) matters then the control parameters

associated with them, i.e. ${}^0\bar{\Pi}_z, {}^0\bar{\Upsilon}_z, \dots$, are more suited for the control design. If one is only interested in the tool position \mathbf{r}_T , then the parameters of the parameterization 2 are useful.

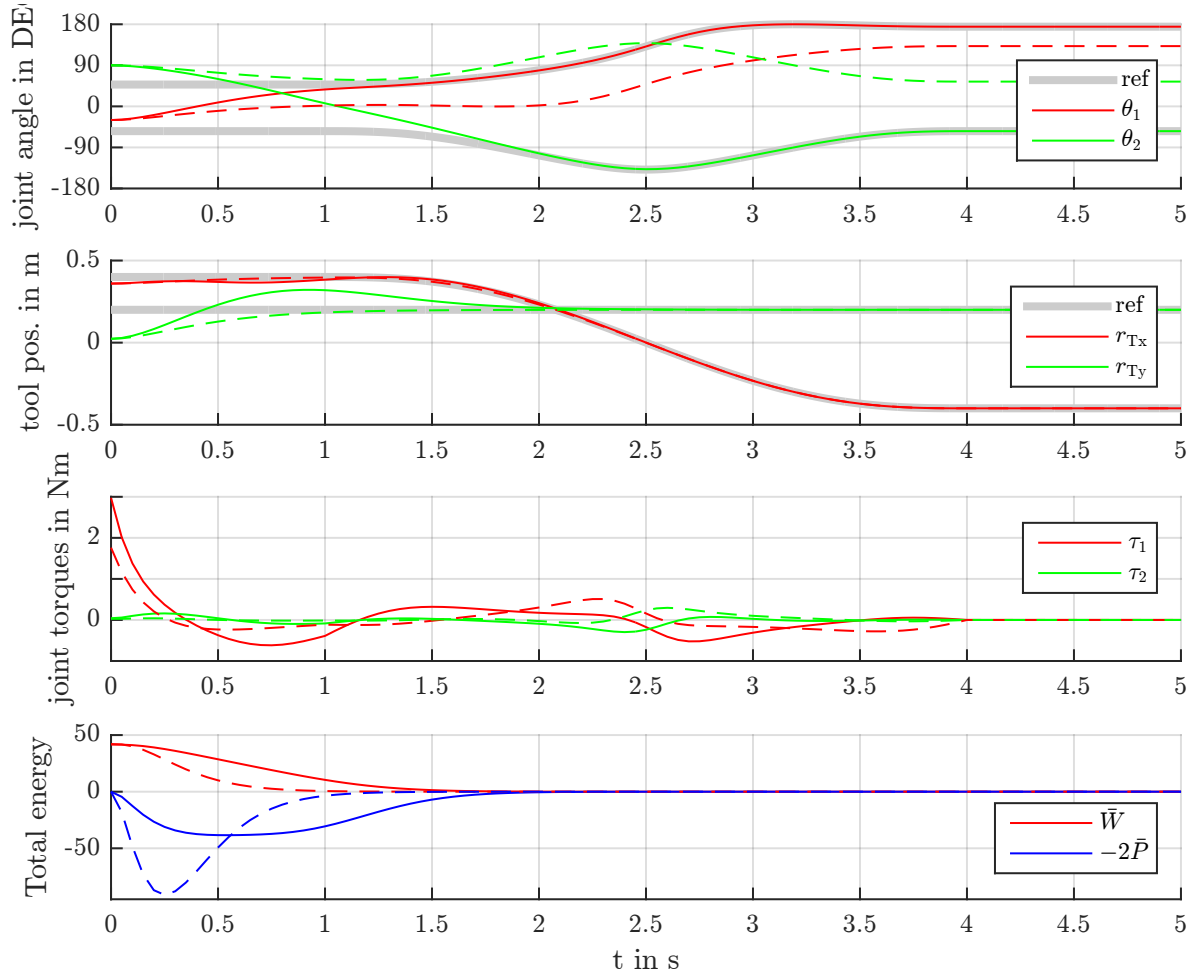


Figure 4.10: Simulation result for the SCARA with parameterization 1 (solid lines) and 2 (dashed lines)

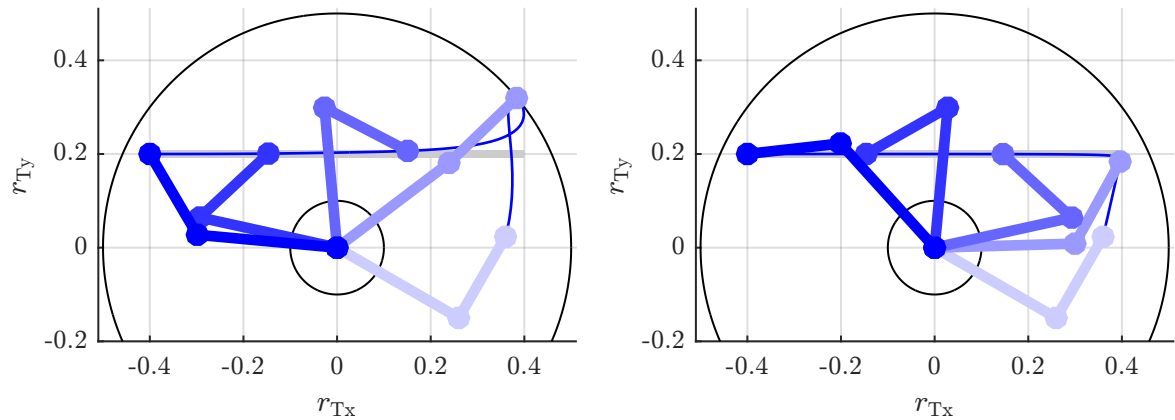


Figure 4.11: Snapshots for the simulation result for the SCARA with parameterization 1 (left) and 2 (right)

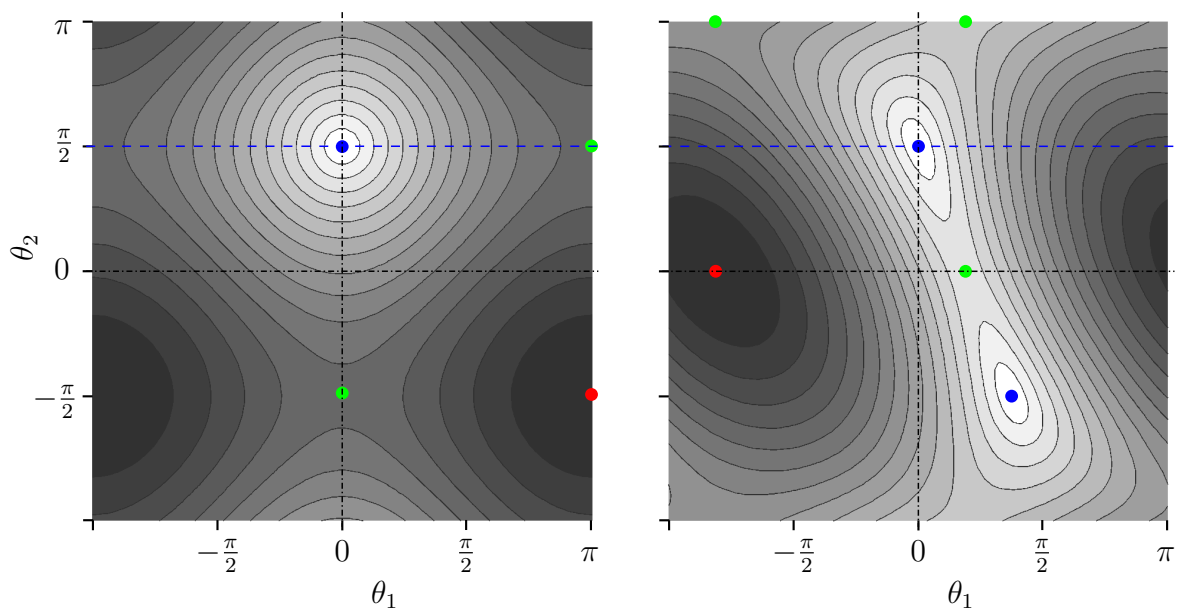


Figure 4.12: The controlled potential energy \mathcal{V} for parameterization 1 (left) and 2 (right) for $\theta_{1R} = 0$, $\theta_{2R} = \frac{\pi}{2}$. Blue dots are minima, red are maxima and green are saddle points.

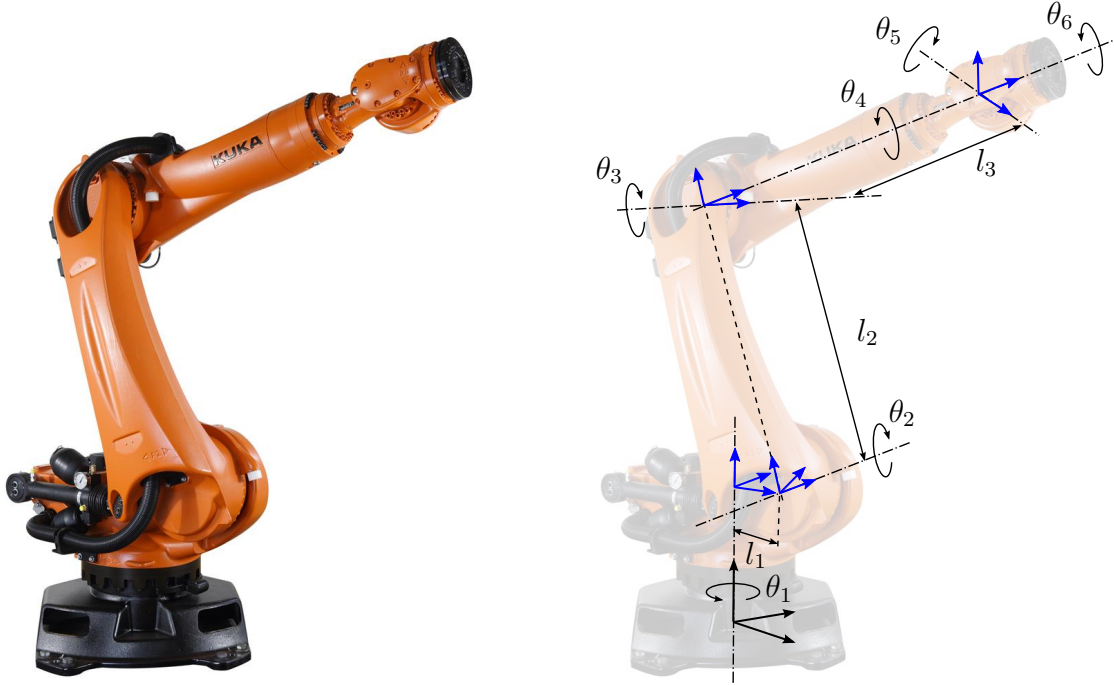


Figure 4.13: A model of a robot arm (background image from www.kuka.de)

4.7.7 Robot arm

As a more complex multibody system we consider a robot arm as illustrated in Figure 4.13. For this example the model equations and the resulting closed loop equations become quite cumbersome and are not displayed explicitly. However this displays some benefits of the proposed control approach: One does not have to look at e.g. the actual system inertia matrix but only at the much less cumbersome body inertia matrices to conclude e.g. stability of the closed loop.

Model. A reasonable choice of coordinates of the system are the joint angles $\boldsymbol{x} = [\theta_1, \dots, \theta_6]^\top$ and trivial kinematics $\boldsymbol{\xi} = \dot{\boldsymbol{x}}$. The body configurations can be computed from the following relative transformations

$$\begin{aligned}
 {}^0\mathbf{G} &= \begin{bmatrix} \cos \theta_1 & -\sin \theta_1 & 0 & 0 \\ \sin \theta_1 & \cos \theta_1 & 0 & 0 \\ 0 & 0 & 1 & 0 \\ 0 & 0 & 0 & 1 \end{bmatrix}, & {}^1\mathbf{G} &= \begin{bmatrix} \cos \theta_2 & 0 & \sin \theta_2 & l_1 \\ 0 & 1 & 0 & 0 \\ -\sin \theta_2 & 0 & \cos \theta_2 & 0 \\ 0 & 0 & 0 & 1 \end{bmatrix}, \\
 {}^2\mathbf{G} &= \begin{bmatrix} \cos \theta_3 & 0 & \sin \theta_3 & 0 \\ 0 & 1 & 0 & 0 \\ -\sin \theta_3 & 0 & \cos \theta_3 & l_2 \\ 0 & 0 & 0 & 1 \end{bmatrix}, & {}^3\mathbf{G} &= \begin{bmatrix} 1 & 0 & 0 & l_3 \\ 0 & \cos \theta_4 & -\sin \theta_4 & 0 \\ 0 & \sin \theta_4 & \cos \theta_4 & 0 \\ 0 & 0 & 0 & 1 \end{bmatrix}, \\
 {}^4\mathbf{G} &= \begin{bmatrix} \cos \theta_5 & 0 & \sin \theta_5 & 0 \\ 0 & 1 & 0 & 0 \\ -\sin \theta_5 & 0 & \cos \theta_5 & 0 \\ 0 & 0 & 0 & 1 \end{bmatrix}, & {}^5\mathbf{G} &= \begin{bmatrix} 1 & 0 & 0 & 0 \\ 0 & \cos \theta_6 & -\sin \theta_6 & 0 \\ 0 & \sin \theta_6 & \cos \theta_6 & 0 \\ 0 & 0 & 0 & 1 \end{bmatrix}. \tag{4.112}
 \end{aligned}$$

This together with the body inertia matrices and the gravity coefficients \mathbf{a}_G and the control forces, $\mathbf{u} = [\tau_1, \dots, \tau_6]^\top$ determines the equations of motion.

Controller parameterization 1: Joint space control. Like above we consider two different sets of controller parameterizations: For the first case, the nonzero control parameters are

$$\begin{aligned} {}^0\bar{\Pi}_{zz}, {}^1\bar{\Pi}_{yy}, {}^2\bar{\Pi}_{yy}, {}^3\bar{\Pi}_{xx}, {}^4\bar{\Pi}_{yy}, {}^5\bar{\Pi}_{xx} &\in \mathbb{R} > 0 \\ {}^0\bar{\Upsilon}_{zz}, {}^1\bar{\Upsilon}_{yy}, {}^2\bar{\Upsilon}_{yy}, {}^3\bar{\Upsilon}_{xx}, {}^4\bar{\Upsilon}_{yy}, {}^5\bar{\Upsilon}_{xx} &\in \mathbb{R} > 0 \\ {}^0\bar{\Theta}_{zz}, {}^1\bar{\Theta}_{yy}, {}^2\bar{\Theta}_{yy}, {}^3\bar{\Theta}_{xx}, {}^4\bar{\Theta}_{yy}, {}^5\bar{\Theta}_{xx} &\in \mathbb{R} > 0 \end{aligned} \quad (4.113)$$

A transport map for the resulting potential energy is $\mathbf{Q} = \mathbf{I}_6$. The resulting closed loop kinetics are 6 decoupled equations identical to the ones for the SCARA (4.106) resp. (4.107).

Controller parameterization 2: Work space control. As a second case consider: For many applications the task of the robot arm is to control the position and orientation of a tool mounted at the end of its kinematic chain. This tool might have a particularly meaningful center point (TCP) and principle axes. Let the configuration ${}^6\mathbf{G} = \text{const.}$ capture these tool specific parameters, for example the tip position and direction of a welding electrode as shown in Figure 4.14.

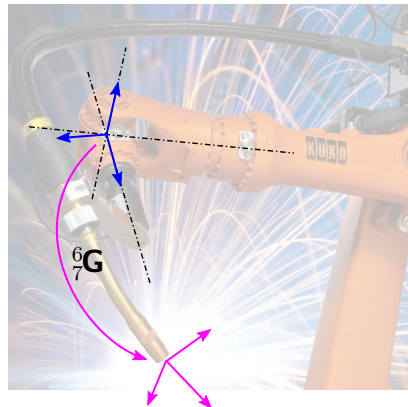


Figure 4.14: Welding tool attached to the robot arm (background image from www.kuka.de)

For this example it could be useful to control the tool as if it is a free rigid body (with its center of mass, damping and stiffness at the TCP) and not care about the particular mechanism that is used to give it this degree of freedom. This is achieved by the following nonzero control parameters

$${}^0\bar{k}, {}^0\bar{d}, {}^0\bar{m} \in \mathbb{R}^+, \quad {}^0\bar{\Pi}, {}^0\bar{\Upsilon}, {}^0\bar{\Theta} \in \text{SYM}^+(3). \quad (4.114)$$

The resulting potential and corresponding transport map are

$$\bar{\mathcal{V}}(\mathbf{x}, \mathbf{x}_R) = \frac{1}{2} \|({}^0\mathbf{G}(\mathbf{x}_R))^{-1} {}^0\mathbf{G}(\mathbf{x}) - \mathbf{I}_4\)^T\|_{\mathbf{K}'}^2, \quad \mathbf{Q}(\mathbf{x}, \mathbf{x}_R) = ({}^0\mathbf{J}(\mathbf{x}))^{-1} {}^0\mathbf{J}(\mathbf{x}_R). \quad (4.115)$$

The resulting closed loop dynamics of the robot arm may be written by plugging the absolute tool configuration ${}^0_7\mathbf{G}(\mathbf{x})$ and its reference ${}^0_7\mathbf{G}(\mathbf{x}_R)$ into the dynamics of a single rigid body for either of the three proposed approaches (4.14), (4.21) or (4.44).

The determinant of the transport map is

$$\det \mathbf{Q}(\mathbf{x}, \mathbf{x}_R) = \frac{\det {}^0_7\mathbf{J}(\mathbf{x}_R)}{\det {}^0_7\mathbf{J}(\mathbf{x})}, \quad \det {}^0_7\mathbf{J}(\mathbf{x}) = -l_2 l_3 (l_1 + l_2 \sin \theta_2 + l_3 \cos(\theta_2 + \theta_3)) \cos \theta_3 \sin \theta_5 \quad (4.116)$$

If the term in the brackets vanishes means that the wrist lies on the axis of θ_1 and $\cos \theta_3 = 0$ is the case if the arm is completely straight which is the singularity we already encountered with the SCARA robot. The last three axis with angles $\theta_4, \theta_5, \theta_6$ can be regarded as Euler angles in the sequence XYX and $\sin \theta_5 = 0$ is their singularity. Comparing this to the motivation example in section 1.2 we have the same problem but the other way around: The Euler angles are an absolutely appropriate choice of coordinates since the mechanism is realized like this. Consequently the configuration manifold of this part is $\mathbb{S}^1 \times \mathbb{S}^1 \times \mathbb{S}^1$ and we are assigning a control that was designed for $\mathbb{SO}(3)$.

Conclusion. The behavior of the two different parameterizations are quite analog to the two parameterizations of the SCARA robot. Which one is more suitable depends on the actual control task. Furthermore, the two presented parameterizations are just two special cases of which dynamics can be achieved with the more general approach of control of this work.

4.8 Examples of underactuated systems

4.8.1 Two masses connected by a spring

In order to illustrate the control approach for underactuated systems we consider the minimal example: Two bodies in prismatic joints connected by a linear spring but where only one is directly actuated by the force F as illustrated in Figure 4.15.

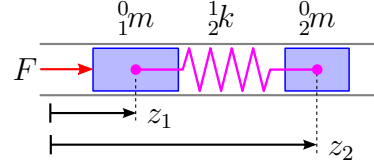


Figure 4.15: Model of two bodies connected by a spring

Model. We choose the absolute positions of the bodies as configuration coordinates $\mathbf{x} = [z_1, z_2]^\top$ and their derivative as velocity coordinates $\boldsymbol{\xi} = \dot{\mathbf{x}}$. With this the body configurations are

$${}^0_1\mathbf{G} = \begin{bmatrix} 1 & 0 & 0 & z_1 \\ 0 & 1 & 0 & 0 \\ 0 & 0 & 1 & 0 \\ 0 & 0 & 0 & 1 \end{bmatrix}, \quad {}^0_2\mathbf{G} = \begin{bmatrix} 1 & 0 & 0 & z_2 \\ 0 & 1 & 0 & 0 \\ 0 & 0 & 1 & 0 \\ 0 & 0 & 0 & 1 \end{bmatrix}. \quad (4.117)$$

With the total mass ${}_1^0m$, ${}_2^0m$ of the individual bodies and the spring stiffness ${}_2^1k$ the resulting equations of motion may be written as

$$\underbrace{\begin{bmatrix} {}_1^0m & 0 \\ 0 & {}_2^0m \end{bmatrix}}_M \begin{bmatrix} \ddot{z}_1 \\ \ddot{z}_2 \end{bmatrix} + \underbrace{\begin{bmatrix} {}_2^1k & -{}_2^1k \\ -{}_2^1k & {}_2^1k \end{bmatrix}}_K \begin{bmatrix} z_1 \\ z_2 \end{bmatrix} = \underbrace{\begin{bmatrix} 1 \\ 0 \end{bmatrix}}_B F. \quad (4.118)$$

Desired closed loop. We assume general body inertia ${}^0_1\mathbf{M}$, ..., damping and stiffness. The three proposed control approaches lead to identical desired closed loop dynamics:

$$\bar{\mathbf{M}}\ddot{\mathbf{e}} + \bar{\mathbf{D}}\dot{\mathbf{e}} + \bar{\mathbf{K}}\mathbf{e} = \mathbf{0}, \quad \mathbf{e} = \mathbf{x} - \mathbf{x}_R \quad (4.119)$$

where

$$\bar{\mathbf{M}} = \begin{bmatrix} {}_1^0\bar{m} + {}_2^1\bar{m} & -{}_2^1\bar{m} \\ -{}_2^1\bar{m} & {}_2^0\bar{m} + {}_1^1\bar{m} \end{bmatrix}, \quad \bar{\mathbf{D}} = \begin{bmatrix} {}_1^0\bar{d} + {}_2^1\bar{d} & -{}_2^1\bar{d} \\ -{}_2^1\bar{d} & {}_2^0\bar{d} + {}_1^1\bar{d} \end{bmatrix}, \quad \bar{\mathbf{K}} = \begin{bmatrix} {}_1^0\bar{k} + {}_2^1\bar{k} & -{}_2^1\bar{k} \\ -{}_2^1\bar{k} & {}_2^0\bar{k} + {}_1^1\bar{k} \end{bmatrix}. \quad (4.120)$$

The corresponding potential $\bar{\mathcal{V}} = \frac{1}{2}\mathbf{e}^\top \bar{\mathbf{K}} \mathbf{e}$ has the obvious transport map $\mathbf{Q} = \mathbf{I}_2$.

Matching. The matching condition (4.59) for this example may be written as

$$\boldsymbol{\lambda} = (\boldsymbol{B}^\perp)^\top (\bar{\boldsymbol{M}} \bar{\boldsymbol{M}}^{-1} (-\bar{\boldsymbol{M}} \ddot{\boldsymbol{x}}_R + \bar{\boldsymbol{D}}(\dot{\boldsymbol{x}} - \dot{\boldsymbol{x}}_R) + \bar{\boldsymbol{K}}(\boldsymbol{x} - \boldsymbol{x}_R)) - \boldsymbol{K}\boldsymbol{x}) = \mathbf{0}. \quad (4.121)$$

Since this equation is linear in the system coordinates we can separate the into

$$(\boldsymbol{B}^\perp)^\top (\bar{\boldsymbol{M}} \ddot{\boldsymbol{x}}_R + \boldsymbol{K}\boldsymbol{x}_R) = \mathbf{0}. \quad (4.122a)$$

$$(\boldsymbol{B}^\perp)^\top \bar{\boldsymbol{M}} \bar{\boldsymbol{M}}^{-1} \bar{\boldsymbol{D}} = \mathbf{0}, \quad (4.122b)$$

$$(\boldsymbol{B}^\perp)^\top \bar{\boldsymbol{M}} \bar{\boldsymbol{M}}^{-1} (\bar{\boldsymbol{K}} - \boldsymbol{K}) = \mathbf{0}, \quad (4.122c)$$

Choosing $\boldsymbol{B}^\perp = [0, 1]^\top$ this is explicitly

$$\ddot{z}_{2R} + \varpi(z_{2R} - z_{1R}) = 0 \quad (4.123a)$$

$$\begin{cases} {}^0\bar{m} {}^1\bar{d} - {}^1\bar{m} {}^0\bar{d} = 0 \\ {}^0\bar{m} {}^1\bar{d} + ({}^0\bar{m} + {}^1\bar{m}) {}^0\bar{d} = 0 \end{cases} \quad (4.123b)$$

$$\begin{cases} {}^0\bar{m} {}^1\bar{k} - {}^1\bar{m} {}^0\bar{k} = ({}^0\bar{m} {}^0\bar{m} + {}^0\bar{m} {}^1\bar{m} + {}^0\bar{m} {}^1\bar{m}) \varpi \\ {}^0\bar{m} {}^1\bar{k} + ({}^0\bar{m} + {}^1\bar{m}) {}^0\bar{k} = ({}^0\bar{m} {}^0\bar{m} + {}^0\bar{m} {}^1\bar{m} + {}^0\bar{m} {}^1\bar{m}) \varpi \end{cases} \quad (4.123c)$$

where $\varpi = {}^1k / {}^0m$ is the sole model parameter relevant for the matching condition. The first part (4.123a) is a constraint on the reference trajectory as it is independent of tunable parameters. It can be resolved by acknowledging that z_2 is a *flat output* of the system and planing the reference trajectory accordingly, i.e.

$$z_{1R} = z_{2R} - \ddot{z}_{2R}/\varpi. \quad (4.124)$$

The other conditions can be resolved by setting

$$\begin{aligned} {}^1\bar{k} &= \frac{{}^1\bar{m}}{{}^0m} {}^0\bar{k} + \frac{{}^0\bar{m} {}^0\bar{m} + {}^0\bar{m} {}^1\bar{m} + {}^0\bar{m} {}^1\bar{m}}{{}^0m} \varpi, & {}^0\bar{k} &= -\frac{{}^1\bar{m}}{{}^0m + {}^1\bar{m}} {}^0\bar{k}, & {}^1\bar{d} &= \frac{{}^1\bar{m}}{{}^0m} {}^0\bar{d}, & {}^0\bar{d} &= -\frac{{}^1\bar{m}}{{}^0m + {}^1\bar{m}} {}^0\bar{d}, \end{aligned} \quad (4.125)$$

which leaves the 5 tuning parameters ${}^0\bar{k}$, ${}^1\bar{d}$, ${}^0\bar{m}$, ${}^0\bar{m}$ and ${}^1\bar{m}$.

The resulting control law is

$$\begin{aligned} F = {}^0m \ddot{z}_{1R} + {}^1k(z_{1R} - z_{2R}) + & \left({}^1k + \frac{{}^0m({}^1\bar{m} {}^1\bar{k} + {}^0m({}^0\bar{k} - {}^1\bar{k}))}{{}^0m({}^0\bar{m} + {}^1\bar{m})} \right) e_1 \\ & - \left({}^1k - \frac{{}^0m({}^1\bar{m} {}^1\bar{k} - {}^0m {}^1\bar{k})}{{}^0m({}^0\bar{m} + {}^1\bar{m})} \right) e_2 - \frac{{}^0m({}^0\bar{d} + {}^1\bar{d})}{{}^0m + {}^1\bar{m}} \dot{e}_1 + \frac{{}^0m {}^1\bar{d}}{{}^0m + {}^1\bar{m}} \dot{e}_2. \end{aligned} \quad (4.126)$$

Pole placement. Tuning the design parameters under the given matching conditions might not be intuitive for this example. To resolve this we can fall back to the classical approach of placing the eigenvalues of the closed loop system (4.119). Taking into account the matching condition (4.125), the characteristic polynomial of (4.119) is

$$\frac{\det(\bar{\boldsymbol{M}} \lambda^2 + \bar{\boldsymbol{D}} \lambda + \bar{\boldsymbol{K}})}{\det \bar{\boldsymbol{M}}} = \lambda^4 + \underbrace{\frac{{}^0\bar{d}}{{}^0m}}_{p_3} \lambda^3 + \underbrace{\frac{{}^0\bar{k} + ({}^0\bar{m} + {}^1\bar{m}) \varpi}{{}^0m}}_{p_2} \lambda^2 + \underbrace{\frac{\varpi {}^0\bar{d}}{{}^0m + {}^1\bar{m}}}_{p_1} \lambda + \underbrace{\frac{\varpi {}^0\bar{k}}{{}^0m + {}^1\bar{m}}}_{p_0}. \quad (4.127)$$

This can be solved for

$${}^0\bar{k} = \frac{{}^1\bar{m} p_0 p_3}{\varpi p_3 - p_1}, \quad {}^0\bar{d} = \frac{{}^1\bar{m} p_1 p_3}{\varpi p_3 - p_1}, \quad {}^0\bar{m} = \frac{{}^1\bar{m} p_1}{\varpi p_3 - p_1}, \quad {}^0\bar{m} = \frac{{}^1\bar{m}(p_1 p_2 - p_0 p_3 - \varpi p_1)}{\varpi(\varpi p_3 - p_1)}. \quad (4.128a)$$

and ${}^1\bar{m} \in \mathbb{R} \neq 0$. Choosing any Hurwitz polynomial for the coefficients p_i guarantees the asymptotic stability of the closed loop. In order to conclude $\bar{\boldsymbol{M}} > 0$, $\bar{\boldsymbol{D}} \geq 0$ and $\bar{\boldsymbol{K}} > 0$ from the Hurwitz criterion ($p_0, p_1, p_2, p_3, p_1 p_2 - p_0 p_3, p_1 p_2 p_3 - p_1^2 - p_0 p_3^2 > 0$) we need $\text{sign } {}^1\bar{m} = \text{sign}(\varpi p_3 - p_1)$.

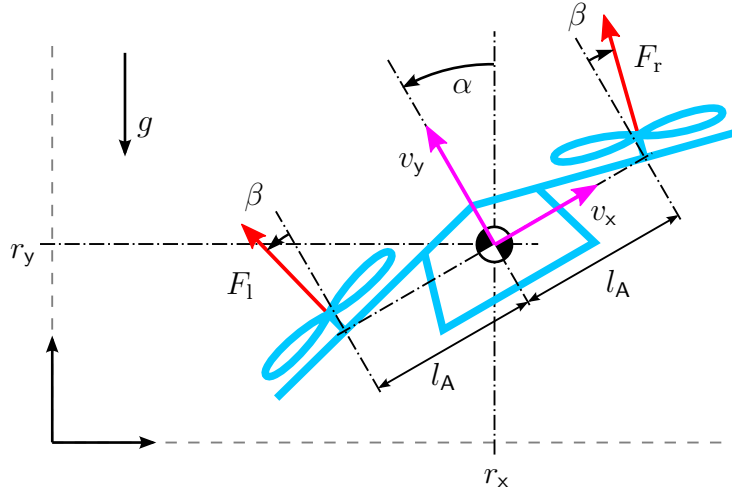


Figure 4.16: Model of the PVTOL

Conclusions. The resulting controller is equivalent to one that could be designed by standard linear state-feedback methods. However, this approach here might give some *physical* insight to the resulting closed loop system. For example that the closed loop system must have an inertial coupling ($\frac{1}{2}\bar{m} \neq 0$) of the two bodies, if one wants to tune all 4 poles.

4.8.2 PVTOL

The planar vertical take off landing aircraft (PVTOL) as depicted in Figure 4.16, is a common benchmark problem discussed in e.g. [Hauser et al., 1992] or [Fliess et al., 1999].

Model. The model of the PVTOL is a planar rigid body already discussed in subsection 4.7.4 supplemented with gravity and the specific actuation F_r , F_l depicted in Figure 4.16. Here, we chose the body fixed frame to be positioned at the center of mass, i.e. $s_x = s_y = 0$. The kinetic equation takes the form

$$\underbrace{\begin{bmatrix} m & 0 & 0 \\ 0 & m & 0 \\ 0 & 0 & \Theta_z \end{bmatrix}}_M \underbrace{\begin{bmatrix} \dot{v}_x \\ \dot{v}_y \\ \dot{\omega}_z \end{bmatrix}}_{\dot{\xi}} + \underbrace{\begin{bmatrix} m(g \sin \alpha - v_y \omega_z) \\ m(g \cos \alpha + v_x \omega_z) \\ 0 \end{bmatrix}}_b = \underbrace{\begin{bmatrix} \sin \beta & -\sin \beta \\ \cos \beta & \cos \beta \\ l_A \cos \beta & -l_A \cos \beta \end{bmatrix}}_B \underbrace{\begin{bmatrix} F_r \\ F_l \end{bmatrix}}_u. \quad (4.129)$$

Reference trajectory. For the following we chose $\mathbf{B}^\perp = [1, 0, -\frac{\sin \beta}{l_A \cos \beta}]$ as a left complement to \mathbf{B} . With this, the matching condition for the reference from (4.60) reads

$$\lambda^{\text{ZeroError}} = m \left(\dot{v}_{xR} - \underbrace{\frac{\Theta_z \sin \beta}{ml_A \cos \beta} \dot{\omega}_{zR}}_\varepsilon - \omega_{zR} v_{yR} + g \sin \alpha_R \right) = 0 \quad (4.130)$$

This can be fulfilled by parameterizing the configuration through the flat output $y_{1R} = r_{xR} - \varepsilon \sin \alpha_R$, $y_{2R} = r_{yR} + \varepsilon \cos \alpha_R$ (see e.g. [Fliess et al., 1999]), i.e.

$$r_{xR} = y_{1R} - \varepsilon \frac{\ddot{y}_{1R}}{\sqrt{\ddot{y}_{1R}^2 + (\ddot{y}_{2R} + g)^2}}, \quad (4.131)$$

$$r_{yR} = y_{2R} - \varepsilon \frac{\ddot{y}_{2R} - g}{\sqrt{\ddot{y}_{1R}^2 + (\ddot{y}_{2R} + g)^2}}, \quad (4.132)$$

$$\alpha_R = \text{atan2}(\ddot{y}_{1R}, \ddot{y}_{2R} + g). \quad (4.133)$$

Note that this parameterization fails if $\ddot{y}_{1R} = \ddot{y}_{2R} + g = 0$, i.e. the body is in free fall.

Closed loop. As for the model, the closed loop templates are the ones the planar rigid body from subsection 4.7.4. Due to symmetry reasons we set the parameters $\bar{h}_x = \bar{l}_x = \bar{s}_x = 0$.

Matching. The matching force λ from (4.57) with the orthogonal complement from above takes a rather cumbersome form and is not given explicitly here. Instead we will investigate its linear approximation about any reference trajectory with $\alpha_R = 0$: The matrices of the linearized model and desired closed loop are

$$\mathbf{M}_0 = \begin{bmatrix} m & 0 & 0 \\ 0 & m & 0 \\ 0 & 0 & J \end{bmatrix}, \quad \bar{\mathbf{M}}_0 = \begin{bmatrix} \bar{m} & 0 & -\bar{m}\bar{s}_y \\ 0 & \bar{m} & 0 \\ -\bar{m}\bar{s}_y & 0 & \bar{\Theta}_z + \bar{m}\bar{s}_y^2 \end{bmatrix}, \quad (4.134a)$$

$$\mathbf{D}_0 = \begin{bmatrix} 0 & 0 & 0 \\ 0 & 0 & 0 \\ 0 & 0 & 0 \end{bmatrix}, \quad \bar{\mathbf{D}}_0 = \begin{bmatrix} \bar{d} & 0 & -\bar{d}\bar{l}_y \\ 0 & \bar{d} & 0 \\ -\bar{d}\bar{l}_y & 0 & \bar{\Upsilon}_z + \bar{d}\bar{l}_y^2 \end{bmatrix}, \quad (4.134b)$$

$$\mathbf{K}_0 = \begin{bmatrix} 0 & 0 & mg \\ 0 & 0 & 0 \\ 0 & 0 & 0 \end{bmatrix}, \quad \bar{\mathbf{K}}_0 = \begin{bmatrix} \bar{k} & 0 & -\bar{k}\bar{h}_y \\ 0 & \bar{k} & 0 \\ -\bar{k}\bar{h}_y & 0 & \bar{\Pi}_z + \bar{k}\bar{h}_y^2 \end{bmatrix}. \quad (4.134c)$$

The conditions for $(\mathbf{B}^\perp)^\top (\mathbf{M}_0 \bar{\mathbf{M}}_0^{-1} \bar{\mathbf{D}}_0 - \mathbf{D}_0) = \mathbf{0}$ and $(\mathbf{B}^\perp)^\top (\mathbf{M}_0 \bar{\mathbf{M}}_0^{-1} \bar{\mathbf{K}}_0 - \mathbf{K}_0) = \mathbf{0}$ for the linearized matching force from (4.62) to vanish are equivalent to

$$\bar{k}(\bar{\Theta}_z - \bar{m}(\bar{h}_y - \bar{s}_y)(\bar{s}_y - \varepsilon)) = 0, \quad (4.135a)$$

$$\bar{m}\bar{\Pi}_z(\bar{s}_y - \varepsilon) - \bar{k}\bar{h}_y(\bar{\Theta}_z - \bar{m}(\bar{h}_y - \bar{s}_y)(\bar{s}_y - \varepsilon)) = \bar{\Theta}_z\bar{m}g, \quad (4.135b)$$

$$\bar{d}(\bar{\Theta}_z - \bar{m}(\bar{l}_y - \bar{s}_y)(\bar{s}_y - \varepsilon)) = 0, \quad (4.135c)$$

$$\bar{m}\bar{\Upsilon}_z(\bar{s}_y - \varepsilon) - \bar{d}\bar{l}_y(\bar{\Theta}_z - \bar{m}(\bar{l}_y - \bar{s}_y)(\bar{s}_y - \varepsilon)) = 0. \quad (4.135d)$$

One solution for this is

$$\bar{\Theta}_z = \bar{m}(\bar{h}_y - \bar{s}_y)(\bar{s}_y - \varepsilon), \quad \bar{l}_y = \bar{h}_y, \quad \bar{\Upsilon}_z = 0, \quad \bar{\Pi}_z = \bar{m}g(\bar{h}_y - \bar{s}_y) \quad (4.136)$$

which leaves the parameters $\bar{k}, \bar{d}, \bar{m}, \bar{h}_y, \bar{s}_y$ for tuning. For the energies to be positive (semi) definite, i.e. $\bar{\mathbf{M}} > 0$, $\bar{\mathbf{D}} \geq 0$ and $\bar{\mathcal{V}} > 0$ we need

$$\bar{k}, \bar{d}, \bar{m} > 0, \quad \bar{h}_y > \bar{s}_y > \varepsilon. \quad (4.137)$$

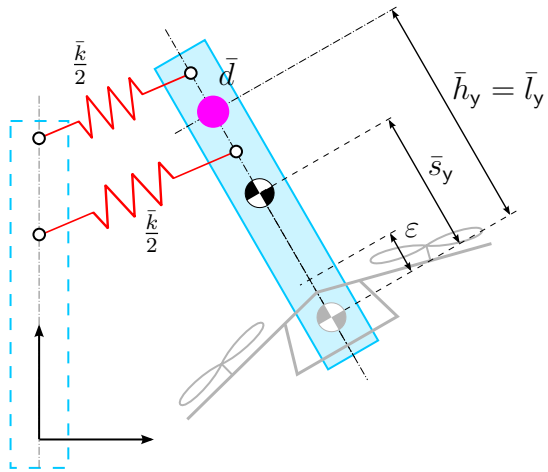


Figure 4.17: Interpretation of the controlled PVTOL as a mechanical system

The remaining matching force is

$$\tilde{\mathbf{b}} = \frac{\bar{m}(\bar{h}_y - \bar{s}_y)}{m(\bar{h}_y - \varepsilon)} \begin{bmatrix} 1 \\ 0 \\ -\varepsilon \end{bmatrix} \lambda \quad (4.138)$$

where λ for the corresponding approach is

$$\lambda^{\text{ParticleBased}} = m(a_{yR} - \varepsilon\omega_{zR}^2) \sin \alpha_E \quad (4.139a)$$

$$\lambda^{\text{BodyBased}} = m(a_{yR} \sin \alpha_E - r_{xE}\omega_{zR}^2 + 2v_{yE}\omega_{zR} + (\varepsilon(1 - \cos \alpha_E) - r_{yE})\dot{\omega}_{zR}) \quad (4.139b)$$

$$\lambda^{\text{EnergyBased}} = m(a_{yR} \sin \alpha_E - r_{xE}\omega_{zR}^2 + v_{yE}\omega_{zR} + (\varepsilon(1 - \cos \alpha_E) - r_{yE})\dot{\omega}_{zR}) \quad (4.139c)$$

where $a_{yR} = \dot{v}_{yR} + v_{xR}\omega_{zR} + g(\cos \alpha_R - 1)$. Note that for a constant reference motion $\dot{\mathbf{v}}_R = 0$ (which implies $\alpha_R = 0$) the matching force vanishes $\lambda = 0$ for all approaches.

Mechanical interpretation. The closed loop template is a planar rigid body with attached springs and dampers as motivated in section 3.3 but without gravity. Taking into account the parameter constraints (4.136), the controlled PVTOL corresponds to the mechanical system illustrated in Figure 4.17. The condition $\bar{h}_y > \bar{s}_y$ implies that the center of mass must be below the center of stiffness. As discussed in subsection 4.7.5, $\bar{h}_y \neq \bar{s}_y$ results in a coupling between translational and rotational motion. From a stability/attractiveness point of view this is necessary: As there is no inherent rotational dissipation $\bar{\Upsilon}_z = 0$, the corresponding energy is dissipated through its coupling to the translational motion. The coupling also reflects the characteristic behavior of the PVTOL that tilting is required for sideways motion.

Pole placement. Even if the tuning parameters might be mechanically intuitive, a classic pole placement approach can be instructive: The characteristic polynomial of the linearized system is

$$\begin{aligned} \det(\bar{\mathbf{M}}\lambda^2 + \bar{\mathbf{D}}\lambda + \bar{\mathbf{K}}) / \det \bar{\mathbf{M}} \\ = (\lambda^2 + \frac{\bar{d}}{\bar{m}}\lambda + \frac{\bar{k}}{\bar{m}})(\lambda^4 + \frac{\bar{d}(\bar{h}_y - \varepsilon)}{\bar{m}(\bar{s}_y - \varepsilon)}\lambda^3 + \frac{\bar{k}(\bar{h}_y - \varepsilon) + \bar{m}g}{\bar{m}(\bar{s}_y - \varepsilon)}\lambda^2 + \frac{\bar{d}g}{\bar{m}(\bar{s}_y - \varepsilon)}\lambda + \frac{\bar{k}g}{\bar{m}(\bar{s}_y - \varepsilon)}) \end{aligned} \quad (4.140)$$

From a desired polynomial of forth degree $\lambda^4 + p_3\lambda^3 + p_2\lambda^2 + p_1\lambda + p_0$ we get the parameters

$$\bar{k} = \frac{\bar{m}p_0p_1}{p_1p_2 - p_0p_3}, \quad \bar{h}_y = \varepsilon + \frac{gp_3}{p_1}, \quad \bar{\Theta}_z = \frac{\bar{m}g^2(p_1p_2p_3 - p_1^2 - p_0p_3^2)}{(p_1p_2 - p_0p_3)^2}, \quad (4.141)$$

$$\bar{d} = \frac{\bar{m}p_1^2}{p_1p_2 - p_0p_3}, \quad \bar{s}_y = \varepsilon + \frac{gp_1}{p_1p_2 - p_0p_3}, \quad \bar{H}_z = \frac{\bar{m}g^2(p_1p_2p_3 - p_1^2 - p_0p_3)}{p_1(p_1p_2 - p_0p_3)}, \quad (4.142)$$

and leaves an arbitrary choice for $\bar{m} > 0$. Note that the Hurwitz criterion ($p_0, p_1, p_2, p_3, p_1p_2 - p_0p_3, p_1p_2p_3 - p_1^2 - p_0p_3^2 > 0$) implies that $\bar{k}, \bar{d}, \bar{\Theta}_z, \bar{H}_z > 0$ which ultimately implies positive definiteness of the total energy and non-negativity of its derivative.

Simulation. A very similar control design approach for the PVTOL was presented in [Konz and Rudolph, 2016]. Therein on finds two exemplary simulation results for stabilization and tracking or a looping trajectory.

The PVTOL is a simpler version of the 3d bicopter which will be discussed in the following and the simulation results there also apply to the PVTOL.

4.8.3 Quadcopter

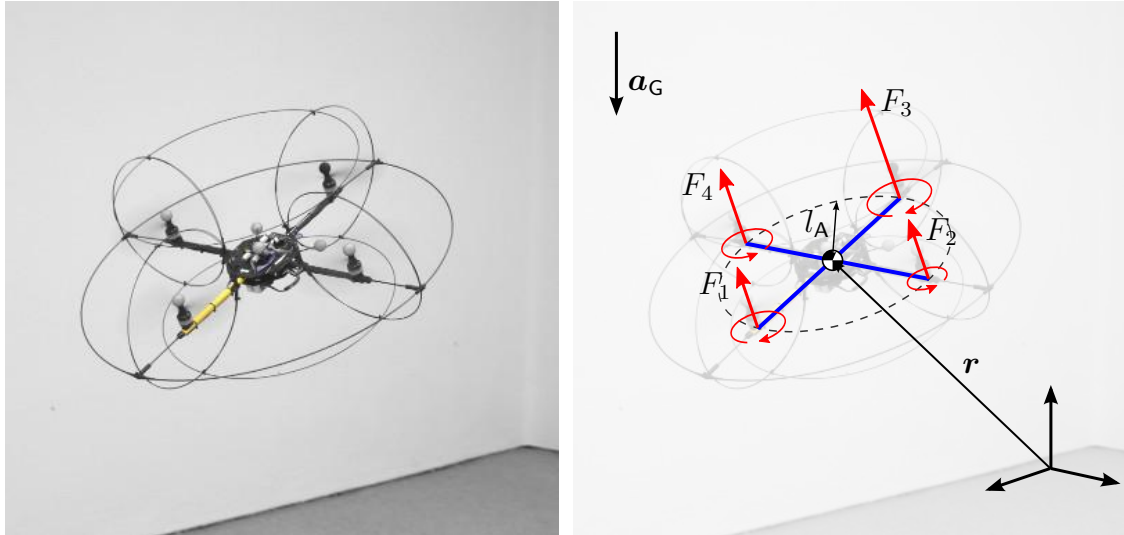


Figure 4.18: Model of the Quadcopter

Model. Mechanically, a quadcopter is a free 3d rigid body subject to gravity and the specific actuation as illustrated in Figure 4.18. It is reasonable to chose the center of mass as the reference point and assume that the body frame coincides with the principle axes

of inertia. Then the kinetic equation takes the form

$$\underbrace{\begin{bmatrix} m & 0 & 0 & 0 & 0 & 0 \\ 0 & m & 0 & 0 & 0 & 0 \\ 0 & 0 & m & 0 & 0 & 0 \\ 0 & 0 & 0 & \Theta_y & 0 & 0 \\ 0 & 0 & 0 & 0 & \Theta_x & 0 \\ 0 & 0 & 0 & 0 & 0 & \Theta_z \end{bmatrix}}_M \underbrace{\begin{bmatrix} \dot{v}_x \\ \dot{v}_y \\ \dot{v}_z \\ \dot{\omega}_x \\ \dot{\omega}_y \\ \dot{\omega}_z \end{bmatrix}}_{\dot{\xi}} + \underbrace{\begin{bmatrix} m(v_y\omega_z - v_z\omega_y + R_x^z g) \\ m(v_x\omega_z - v_z\omega_x + R_y^z g) \\ m(v_y\omega_x - v_x\omega_y + R_z^z g) \\ (\Theta_z - \Theta_y)\omega_y\omega_z \\ (\Theta_x - \Theta_z)\omega_x\omega_z \\ (\Theta_y - \Theta_x)\omega_x\omega_y \end{bmatrix}}_b = \underbrace{\begin{bmatrix} 0 & 0 & 0 & 0 \\ 0 & 0 & 0 & 0 \\ 1 & 1 & 1 & 1 \\ 0 & l_A & 0 & -l_A \\ -l_A & 0 & l_A & 0 \\ -b_F & b_F & -b_F & b_F \end{bmatrix}}_B \underbrace{\begin{bmatrix} F_1 \\ F_2 \\ F_3 \\ F_4 \\ u \end{bmatrix}}_u \quad (4.143)$$

Reference trajectory. An obvious left complement for B is

$$(B^\perp)^\top = \begin{bmatrix} 1 & 0 & 0 & 0 & 0 & 0 \\ 0 & 1 & 0 & 0 & 0 & 0 \end{bmatrix}. \quad (4.144)$$

With this, the matching condition for the reference from (4.60) are just the two first equations of (4.143):

$$\lambda^{\text{ZeroError}} = m \begin{bmatrix} \dot{v}_{xR} + v_{zR}\omega_{yR} - v_{yR}\omega_{zR} + R_{xR}^z g \\ \dot{v}_{yR} + v_{xR}\omega_{zR} - v_{zR}\omega_{xR} + R_{yR}^z g \end{bmatrix} = 0. \quad (4.145)$$

This may be easily resolved by formulating the reference trajectory in terms of the systems flat output r and some parameterization of the orientation about the body fixed z-axis as done in [Konz and Rudolph, 2013].

Closed loop template. As the quadcopter is just a free rigid body with a particular actuation, the closed loop templates coincide with the ones given in subsection 4.1.2, subsection 4.2.1 and subsection 4.3.3. Due to symmetry considerations we set $\bar{s}_x = \bar{s}_y = 0$, $\bar{\Theta}_{xx} = \bar{\Theta}_{yy}$, $\bar{\Theta}_{xy} = \bar{\Theta}_{xz} = \bar{\Theta}_{yz} = 0$ and analog for the stiffness and damping parameters.

Matching. The explicit matching conditions are too cumbersome to be displayed here. Instead we start again with the linearized version: The linearized system matrices for model and closed loop template are

$$\begin{aligned} M_0 &= \begin{bmatrix} m & 0 & 0 & 0 & 0 & 0 \\ 0 & m & 0 & 0 & 0 & 0 \\ 0 & 0 & m & 0 & 0 & 0 \\ 0 & 0 & 0 & \Theta_y & 0 & 0 \\ 0 & 0 & 0 & 0 & \Theta_x & 0 \\ 0 & 0 & 0 & 0 & 0 & \Theta_z \end{bmatrix}, \quad \bar{M}_0 = \begin{bmatrix} \bar{m} & 0 & 0 & 0 & \bar{m}\bar{s}_z & 0 \\ 0 & \bar{m} & 0 & -\bar{m}\bar{s}_z & 0 & 0 \\ 0 & 0 & \bar{m} & 0 & 0 & 0 \\ 0 & -\bar{m}\bar{s}_z & 0 & \bar{\Theta}_x + \bar{m}\bar{s}_z^2 & 0 & 0 \\ \bar{m}\bar{s}_z & 0 & 0 & 0 & \bar{\Theta}_x + \bar{m}\bar{s}_z^2 & 0 \\ 0 & 0 & 0 & 0 & 0 & \bar{\Theta}_z \end{bmatrix}, \\ D_0 &= \begin{bmatrix} 0 & 0 & 0 & 0 & 0 & 0 \\ 0 & 0 & 0 & 0 & 0 & 0 \\ 0 & 0 & 0 & 0 & 0 & 0 \\ 0 & 0 & 0 & 0 & 0 & 0 \\ 0 & 0 & 0 & 0 & 0 & 0 \\ 0 & 0 & 0 & 0 & 0 & 0 \end{bmatrix}, \quad \bar{D}_0 = \begin{bmatrix} \bar{d} & 0 & 0 & 0 & \bar{d}l_z & 0 \\ 0 & \bar{d} & 0 & -\bar{d}l_z & 0 & 0 \\ 0 & 0 & \bar{d} & 0 & 0 & 0 \\ 0 & -\bar{d}l_z & 0 & \bar{\Upsilon}_x + \bar{d}l_z^2 & 0 & 0 \\ \bar{d}l_z & 0 & 0 & 0 & \bar{\Upsilon}_x + \bar{d}l_z^2 & 0 \\ 0 & 0 & 0 & 0 & 0 & \bar{\Upsilon}_z \end{bmatrix}, \end{aligned}$$

$$\mathbf{K}_0 = \begin{bmatrix} 0 & 0 & 0 & 0 & -mg & 0 \\ 0 & 0 & 0 & mg & 0 & 0 \\ 0 & 0 & 0 & 0 & 0 & 0 \\ 0 & 0 & 0 & 0 & 0 & 0 \\ 0 & 0 & 0 & 0 & 0 & 0 \\ 0 & 0 & 0 & 0 & 0 & 0 \end{bmatrix}, \quad \bar{\mathbf{K}}_0 = \begin{bmatrix} \bar{k} & 0 & 0 & 0 & \bar{k}\bar{h}_z & 0 \\ 0 & \bar{k} & 0 & -\bar{k}\bar{h}_z & 0 & 0 \\ 0 & 0 & \bar{k} & 0 & 0 & 0 \\ 0 & -\bar{k}\bar{h}_z & 0 & \bar{\Pi}_x + \bar{k}\bar{h}_z^2 & 0 & 0 \\ \bar{k}\bar{h}_z & 0 & 0 & 0 & \bar{\Pi}_x + \bar{k}\bar{h}_z^2 & 0 \\ 0 & 0 & 0 & 0 & 0 & \bar{\Pi}_z \end{bmatrix}.$$

Taking into account the symmetries between x and y directions, the remaining linearized matching conditions are

$$\bar{k}(\bar{\Theta}_x - \bar{m}\bar{s}_z(\bar{h}_z - \bar{s}_z)) = 0 \quad (4.147a)$$

$$\bar{m}(\bar{\Theta}_x g - \bar{\Pi}_x \bar{s}_z) + \bar{k}\bar{h}_z(\bar{\Theta}_x - \bar{m}\bar{s}_z(\bar{h}_z - \bar{s}_z)) = 0 \quad (4.147b)$$

$$\bar{d}(\bar{\Theta}_x - \bar{m}\bar{s}_z(\bar{h}_z - \bar{s}_z)) = 0 \quad (4.147c)$$

$$-\bar{m}\bar{s}_z\bar{\Upsilon}_x + \bar{d}\bar{l}_z(\bar{\Theta}_x - \bar{m}\bar{s}_z(\bar{l}_z - \bar{s}_z)) = 0 \quad (4.147d)$$

It is not surprising that these are identical to the previously encountered conditions (4.135) for the PVTOL for $\varepsilon = 0$. Consequently we use the same solution

$$\bar{l}_z = \bar{h}_z, \quad \bar{\Theta}_x = \bar{\Theta}_y = \bar{m}\bar{s}_z(\bar{h}_z - \bar{s}_z), \quad \bar{\Upsilon}_x = \bar{\Upsilon}_y = 0, \quad \bar{\Pi}_x = \bar{\Pi}_y = \bar{m}g(\bar{h}_z - \bar{s}_z). \quad (4.148)$$

which leaves the tuning parameters \bar{m} , \bar{d} , \bar{k} , \bar{s}_z , \bar{h}_z and $\bar{\Theta}_z$, $\bar{\Upsilon}_z$, $\bar{\Pi}_z$.

Even with the linearized matching conditions fulfilled, the nonlinear matching condition is still to cumbersome to be displayed here. For the case of a constant reference velocity $\dot{\mathbf{v}}_R = \mathbf{0}$ and its implications on the reference attitude, $\omega_{xR} = \omega_{yR} = 0$, we have the residual matching force

$$\tilde{\mathbf{b}} = \frac{\bar{m}}{m\bar{h}_z} \begin{bmatrix} \bar{\Theta}_z \omega_x \omega_z - \frac{1}{2} \bar{\Pi}_z (R_{zE}^x + R_{xE}^z) \\ \bar{\Theta}_z \omega_y \omega_z - \frac{1}{2} \bar{\Pi}_z (R_{zE}^y + R_{yE}^z) \\ 0 \\ 0 \\ 0 \\ 0 \end{bmatrix}. \quad (4.149)$$

Tuning. The first set of parameters \bar{m} , \bar{d} , \bar{k} , \bar{s}_z , \bar{h}_z may be tuned just as presented for the PVTOL, see Figure 4.17. The parameters associated with the heading control may be set to $\bar{\Upsilon}_z = 2\bar{\Theta}_z \zeta \omega_0$ and $\bar{\Pi}_z = \bar{\Theta}_z \omega_0^2$ to obtain a desired bandwidth ω_0 and damping ratio ζ . The corresponding moment of inertia $\bar{\Theta}_z > 0$ may be adjusted in relation to $\bar{\Theta}_x$ as a priority factor between heading control and tilt control. This is most crucial if the quadcopter propellers are at their constraints and the control has to find a trade-off between maintaining its tilt (and consequently its position), or the heading. For most applications heading is less important than tilt so one may set $\bar{\Theta}_z = 0.1\bar{\Theta}_x$ as was done for the experiments with the LSR quadcopter presented in the next section.

Simulation results. The body based approach proposed here was also discussed in [Konz and Rudolph, 2021] which also showed simulation results for a looping trajectory. Furthermore, this approach was implemented for the experimental setup in the LSR quadcopter. The results are discussed in detail in the next chapter.

4.8.4 Bicopter

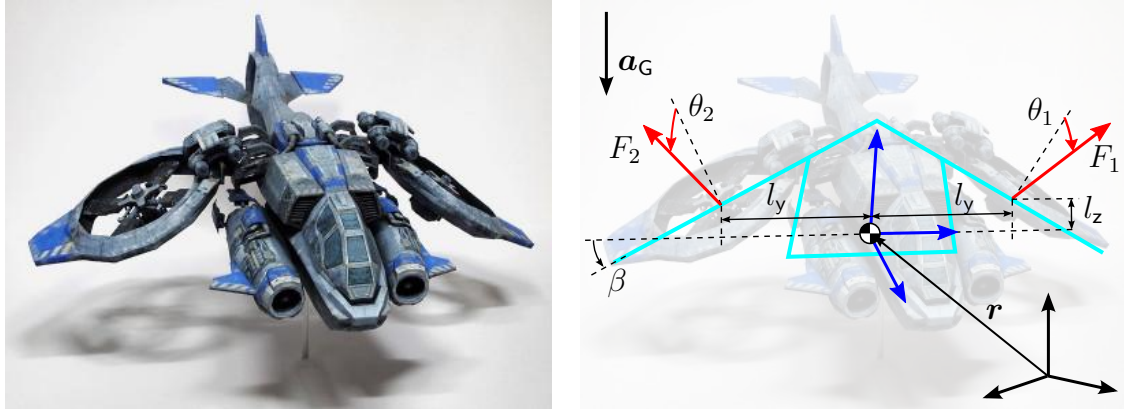


Figure 4.19: Model of a bicopter (background image: www.poppaper.net/80155164809)

Equations of motion. The bicopter considered here is a single rigid body with two tilttable propellers as illustrated in Figure 4.18. With the same coordinates as for the previous examples, the equations of motion are identical as well up to the generalized force from the propellers

$$\mathbf{f}^U = \underbrace{\begin{bmatrix} 1 & 0 & 1 & 0 \\ 0 & \sin \beta_F & 0 & -\sin \beta_F \\ 0 & \cos \beta_F & 0 & \cos \beta_F \\ 0 & l'_y & 0 & -l'_y \\ l_z & 0 & l_z & 0 \\ -l_y & 0 & l_y & 0 \end{bmatrix}}_B \underbrace{\begin{bmatrix} F_1 \sin \theta_1 \\ F_1 \cos \theta_1 \\ F_2 \sin \theta_2 \\ F_2 \cos \theta_2 \end{bmatrix}}_u. \quad (4.150)$$

with $l'_y = l_y \cos \beta_F - l_z \sin \beta_F$. The transformation of the actual control inputs F_1 , F_2 and θ_1 , θ_2 to a auxiliary input \mathbf{u} is used to achieve the linear form $\mathbf{f}^U = \mathbf{B}\mathbf{u}$. Within the input constraints $2\text{ N} \leq F_i \leq 14\text{ N}$, $-30^\circ \leq \theta_i \leq 30^\circ$, $i = 1, 2$ this transformation is bijective. To account for the original constraints in the transformed input $\mathbf{u} \in \mathbb{R}^4$, a convex approximation illustrated in Figure 4.20 is used. These constraints can be written in the required form $\mathbf{W}\mathbf{u} \leq \mathbf{l}$.

Reference trajectory. A possible left complement for \mathbf{B} is

$$(\mathbf{B}^\perp)^\top = \begin{bmatrix} l_z & 0 & 0 & 0 & -1 & 0 \\ 0 & l'_y & 0 & -\sin \beta_F & 0 & 0 \end{bmatrix} \quad (4.151)$$

With this, the matching condition for the reference from (4.60) is

$$\boldsymbol{\lambda}^{\text{ZeroError}} = \begin{bmatrix} ml_z(\dot{v}_x + v_y \omega_z - v_z \omega_y - \varepsilon_x(\dot{\omega}_y + \frac{\theta_x - \theta_z}{\theta_y} \omega_x \omega_z) + R_x^z g) \\ ml'_y(\dot{v}_y + v_x \omega_z - v_z \omega_x + \varepsilon_y(\dot{\omega}_x + \frac{\theta_z - \theta_y}{\theta_x} \omega_y \omega_z) + R_y^z g) \end{bmatrix} = \mathbf{0}. \quad (4.152)$$

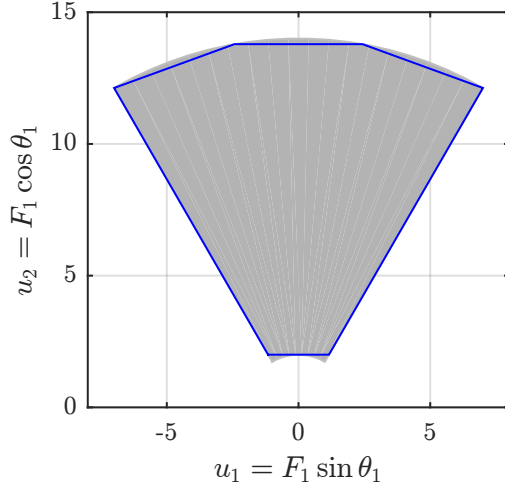


Figure 4.20: Approximation of the Bicopter input constraints

where

$$\varepsilon_x = -\frac{\Theta_y}{ml_z}, \quad \varepsilon_y = \frac{\Theta_x \sin \beta_F}{m(l_y \cos \beta_F - l_z \sin \beta_F)}. \quad (4.153)$$

For the general case⁴ $\varepsilon_x \neq \varepsilon_y$ this system is probably not flat, so parameterization of a feasible reference trajectory is not trivial.

Closed loop template. As for the quadcopter, the closed loop templates are that of a free rigid body i.e. subsection 4.1.2, subsection 4.2.1 and subsection 4.3.3. However, in contrast to the quadcopter there are no assumptions on symmetries in the constitutive parameters.

Matching. As before we first consider the linearized matching conditions: It turns out that asymmetries in the constitutive parameters are not useful for resolving matching constraints. So we set $\bar{\Theta}_{xy} = \bar{\Theta}_{xz} = \bar{\Theta}_{yz} = 0$, $\bar{s}_x = \bar{s}_y = 0$ and the same for damping and stiffness. The remaining linearized matching conditions may be fulfilled by constraining the parameters as

$$\bar{l}_z = \bar{h}_z, \quad \bar{\Upsilon}_x = \bar{\Upsilon}_y = 0, \quad \bar{\Pi}_x = \bar{\Pi}_y = \bar{m}g(\bar{h}_z - \bar{s}_z), \quad (4.154a)$$

$$\bar{\Theta}_x = \bar{m}(\bar{h}_z - \bar{s}_z)(\bar{s}_z - \varepsilon_y), \quad \bar{\Theta}_y = \bar{m}(\bar{h}_z - \bar{s}_z)(\bar{s}_z - \varepsilon_x), \quad (4.154b)$$

which leaves the tuning parameters \bar{m} , \bar{d} , \bar{k} , \bar{s}_z , \bar{h}_z and $\bar{\Theta}_z$, $\bar{\Upsilon}_z$, $\bar{\Pi}_z$. Note, in contrast to the quadcopter, that $\varepsilon_x \neq \varepsilon_y$ implies $\bar{\Theta}_x \neq \bar{\Theta}_y$ and since the remaining relevant parameters are identical, the closed loop dynamics for x and y are different from another.

⁴Even in the case $\varepsilon_x = \varepsilon_y \neq 0$ we would need $\Theta_x = \Theta_y = \Theta_z$ for $\mathbf{r} + \mathbf{R}\boldsymbol{\varepsilon}$ to be a flat output. The case $\varepsilon_x = 0$ implies $\Theta_y = 0$, which does not make physical sense.

The remaining matching force in the stabilization case $\xi_R = \mathbf{0}$ is

$$\tilde{\mathbf{b}} = \frac{\bar{m}}{m} \begin{bmatrix} \frac{1}{h_z - \varepsilon_x} & 0 \\ 0 & \frac{1}{h_z - \varepsilon_y} \\ 0 & 0 \\ 0 & -\frac{\varepsilon_y}{h_z - \varepsilon_y} \\ \frac{\varepsilon_x}{h_z - \varepsilon_x} & 0 \\ 0 & 0 \end{bmatrix} \begin{bmatrix} (\bar{\Theta}_z - \bar{m}(\bar{h}_z - \bar{s}_z)(\frac{\theta_x - \theta_z}{\theta_y} \varepsilon_x - \varepsilon_y)) \omega_y \omega_z - \frac{1}{2} \bar{\Pi}_z (R_{zE}^x + R_{xE}^z) \\ (\bar{\Theta}_z - \bar{m}(\bar{h}_z - \bar{s}_z)(\frac{\theta_y - \theta_z}{\theta_x} \varepsilon_y - \varepsilon_x)) \omega_x \omega_z - \frac{1}{2} \bar{\Pi}_z (R_{zE}^y + R_{yE}^z) \end{bmatrix} \quad (4.155)$$

Simulation result. Since the bicopter model is probably not flat, generation of a feasible reference trajectory is not trivial. For the simulation example here we exploited that, if we set $r_{xR} = 0$ and $R_{xR}^x = 1$, the motion is constrained to the yz plane and the remaining model is essentially a PVTOL. The reference trajectory chosen for this example is a vertical circle with constant arc speed in the yz plane, similar to the examples presented in [Konz and Rudolph, 2016] and [Konz and Rudolph, 2021]. As shown in subsection 4.8.2, the position trajectory determines the tilt trajectory through flatness. The circle arc speed was chosen such that the bicopter is upside down at the highest point of the circle.

As initial condition for the simulation we chose a position error of 0.5 m in all directions and heading error of 90°. This guarantees that all parts of the control are excited.

The simulation result for the position trajectory with snapshots of a bicopter mockup for the first 3 s is shown in Figure 4.21. The red lines indicate the propeller tilt and the thrust magnitude. The resulting time graphs are shown in Figure 4.22. Roughly, during the first loop, or the first 2 s, the state trajectory converges to its reference and tracks it for the remaining simulation time. This is also quantified by the error energy $\dot{\mathcal{W}}$ in the bottom of Figure 4.22. There, one may also see that $\dot{\mathcal{W}} \neq \bar{\mathcal{P}}$ which is most notably during the time around $t = 0.5$ s when input constraints are active, but also due to the non-vanishing matching force $\tilde{\mathbf{b}}$. Nevertheless, if we neglect the parts where the input constraints are active, the error energy is converging to zero. So, even for this arguably challenging example, the control objective is achieved.

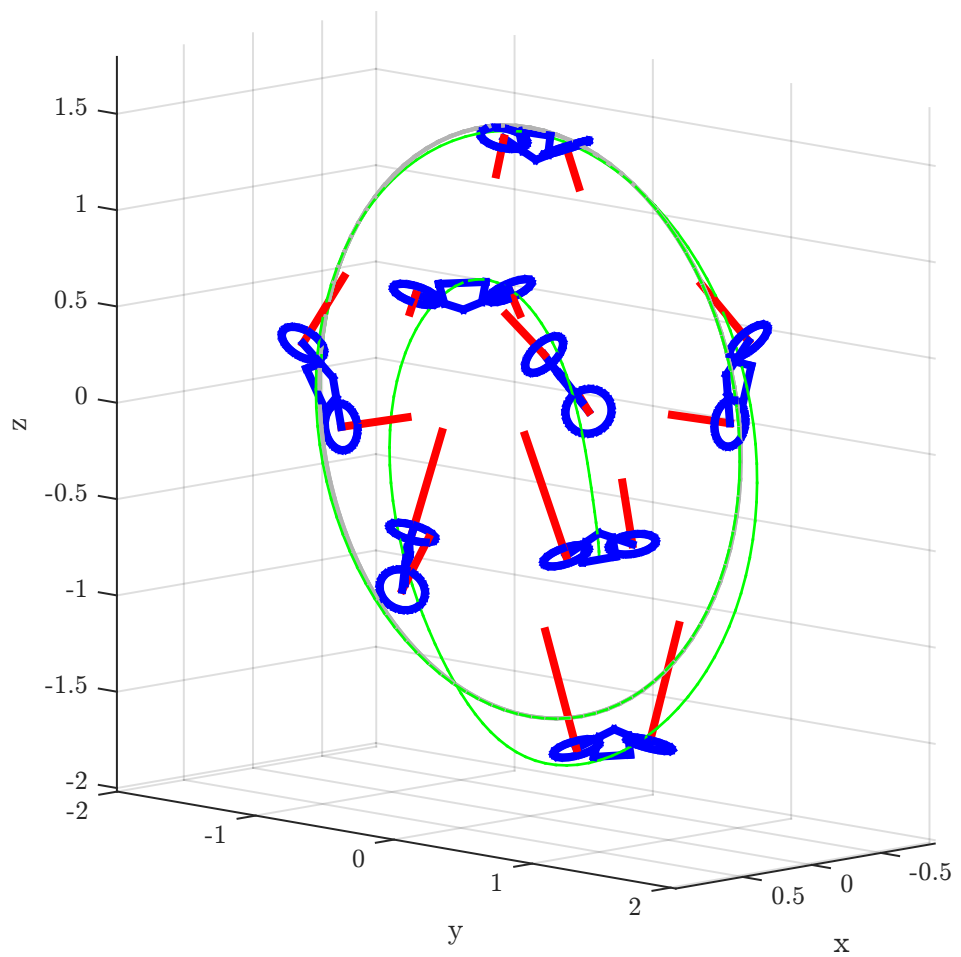


Figure 4.21: Snapshots for the simulation of the bicopter

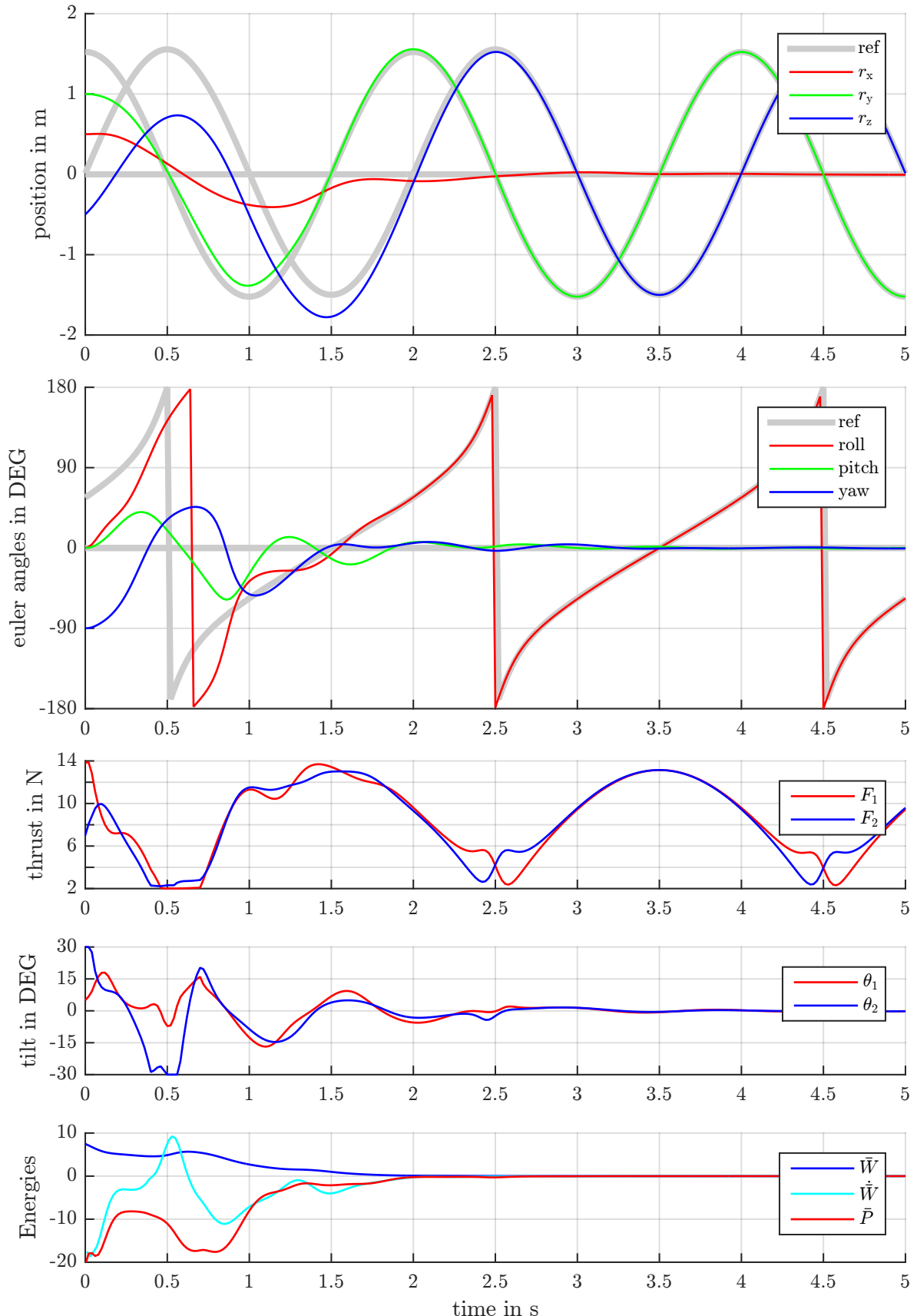


Figure 4.22: Simulation result for the bicopter

Chapter 5

Multicopter control realization

This chapter describes the realization and discusses the experimental results with the LSR-Multicopters, Figure 5.1. On the highest abstraction layer they can be regarded as a single rigid body with body fixed forces (the propeller forces and torques). As such they are used for practical validation of the modeling and control approaches of the previous chapters.

The LSR-quadcopter started as a student project in 2009, a time in which they were not as ubiquitous as these drones are nowadays, 15 years later. The original hardware, a kit from the online shop www.mikrokopter.de, was continuously improved and adapted for specific experiments until the only remaining original parts in 2018 were the motors and propellers. The final version has an outer diameter of 0.8 m and a weight of about 1 kg. With a maximal total propeller thrust of roughly 3.2 kg there is a lot of reserve for aggressive maneuvering.

Based on experiences with the quadcopter, the LSR-tricopter also started as a student project in 2012. It utilizes three tiltable propellers, which makes it from a control perspective a fully actuated free rigid body. Its propellers and outer dimensions are the same as the quadcopter. Due to the additional servo motors and the tilting joints the overall weight is higher at about 1.3 kg. Furthermore, due to the 120° arrangement of the arms, the propellers may counteract each other when tilted, reducing the efficiency.

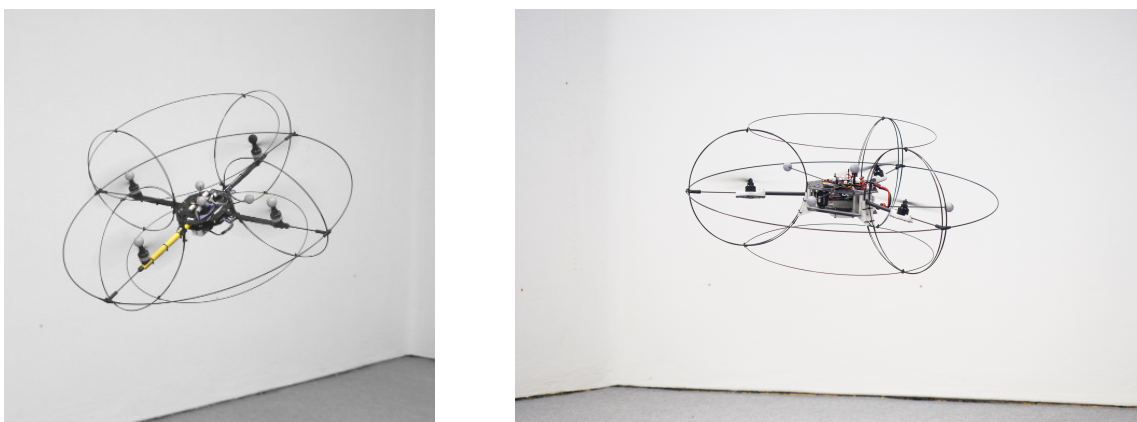


Figure 5.1: LSR-Quad- and Tricopter

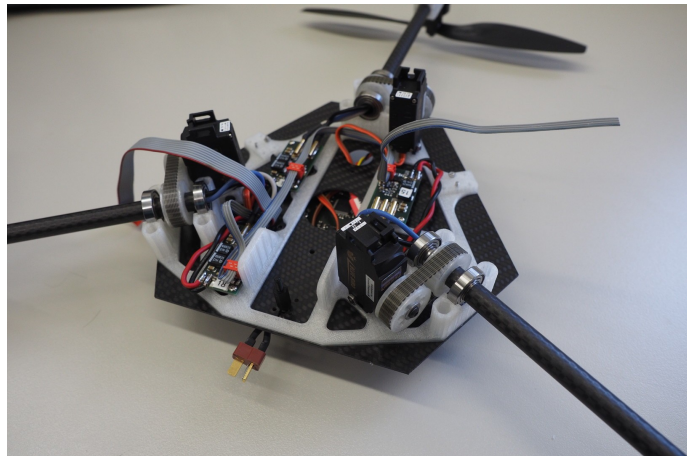


Figure 5.2: Disassembled central body of the LSR-tricopter

The ubiquity quadcopter is also reflected in the control literature. The tricopter design in contrast, is novel, with the LSR-tricopter probably being its first practical realization.

The LSR-multicopters were the platform for experiments in publications like [Kastelan et al., 2015], [Servais et al., 2015a], [Servais et al., 2015b], [Konz et al., 2018], [Irscheid et al., 2019], [Konz and Rudolph, 2021] and several student projects, bachelor and master theses.

5.1 Hardware & software realization

Mechanical frame. The mechanical design of the LSR-quat and tricopter (see Figure 5.1) is kept as simple as possible. A central body holds the electronic parts including the battery. It is a sandwich of two water jet cut carbon fiber plates that clamp together the internal 3d printed parts. These in turn clamp the carbon fiber tubes, the arms, or in the case of the tricopter its bearings, see Figure 5.2. From there, carbon fiber tubes (the arms) stretch out to hold the propeller motors. The propellers are directly bolted to their motors. The radius at which the propellers are attached is intentionally the same for quad and tricopter, $l_A = 240$ mm. The outer, flexible carbon-fiber rings serve as collision protection and landing skid.

Propeller drive. Quad and tricopter share the same $10'' = 254$ mm propellers, brushless DC motors and driver electronics. The driver electronics and firmware is also an LSR development but will not be discussed further in this work. Overall the drive allows for angular velocities up to 120 Hz, corresponding to a maximum thrust of about 8 N. More crucially, it allows for very fast response times including active braking by feeding current back into the battery.

For the tricopter, the tilting mechanism is driven by a hobbyist servo drive that is connected to a gear on the arm by a toothed-belt (see Figure 5.2) and allows for tilt angles of $\pm 75^\circ$.

Sensors. Quad and tricopter utilize the same sensors: An inertial measurement unit (IMU) VN100s from VECTORNAV is mounted on the central body to measure its angular velocity and inertial acceleration. It also contains an internal algorithm for bias and attitude estimation which is used for outdoor experiments which are not subject of this work.

Inside the LSR lab, a camera-based motion capture system from VICON measures position and attitude by way of reflective markers on the multicopters. The motion capturing software runs on the ground station Windows 7 PC and the measurements are transferred to the multicopter processor via wireless link. Overall, this results in a low sampling rate and significant latency in these measurements. The algorithm used to fuse the high bandwidth IMU measurements with the Vicon measurements will be presented in the following section.

User interface. A FUTABA two-joystick remote control with several additional analog and digital inputs is used as a reliable and near real-time user interface. It is used for manual piloting the multicopters as well as realizing security mechanisms like triggering emergency landing or even propeller shutdown.

The ground station computer runs a graphical user interface (GUI) implemented in MATLAB. It displays and may record realtime data and can issue discrete commands to the multicopter controller. Furthermore, this software also handles the forwarding of the Vicon data. The communication link is realized by two XBee S6B Wi-Fi modules.

Mainboard & processor. The center of the onboard electronics is a custom build mainboard. It transforms and distributes the battery power to the other components and connects the data lines of the sensors and actuators to the main processor: An Atmel AT32UC3C 32-bit, 66 MHz microcontroller with FPU.

Overall, the relevant hardware components of the LSR-Multicopters are illustrated in Figure 5.3.

Firmware. The firmware on the main processor does not utilize an operation system but is programmed directly using C & C++ code compiled by the `avr32-gcc`. It uses the Atmel software framework as low level interface to the microcontroller peripherals. On the top level, the template library EIGEN offers linear algebra objects and routines for the rigid body controller. A rough overview of the microcontroller firmware is given in Figure 5.4.

Multicopter agent. The critical control part of the multicopter firmware, here called *multicopter agent*, is also used in a SIMULINK simulation of the closed loop with a multicopter model. To be precise, the same cpp files are included in the either the firmware compilation as in the compilation of the SIMULINK block.

The multicopter model, the estimation of its parameters and experimental validation will be discussed in the next section. For this work, the feedback controller for quad and

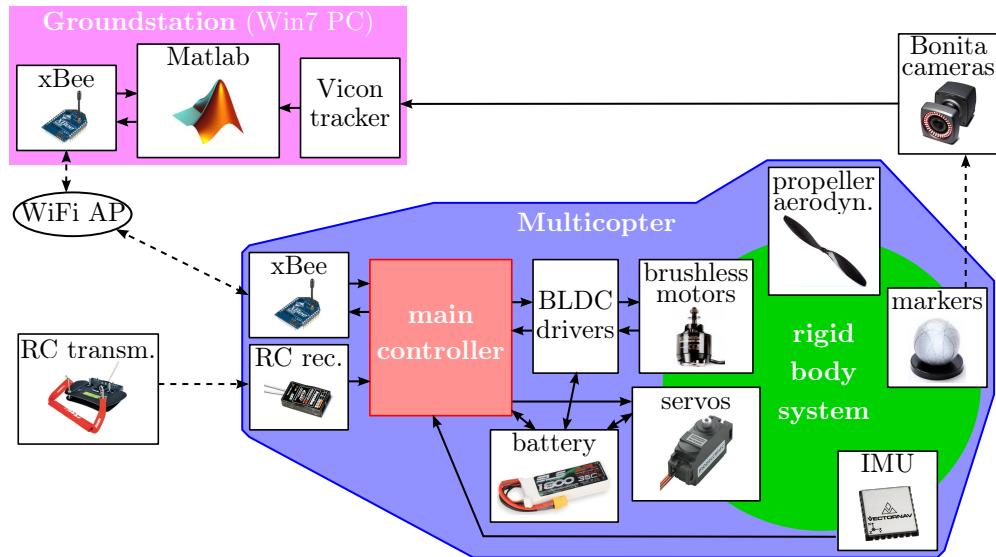


Figure 5.3: Multicopter Hardware realization

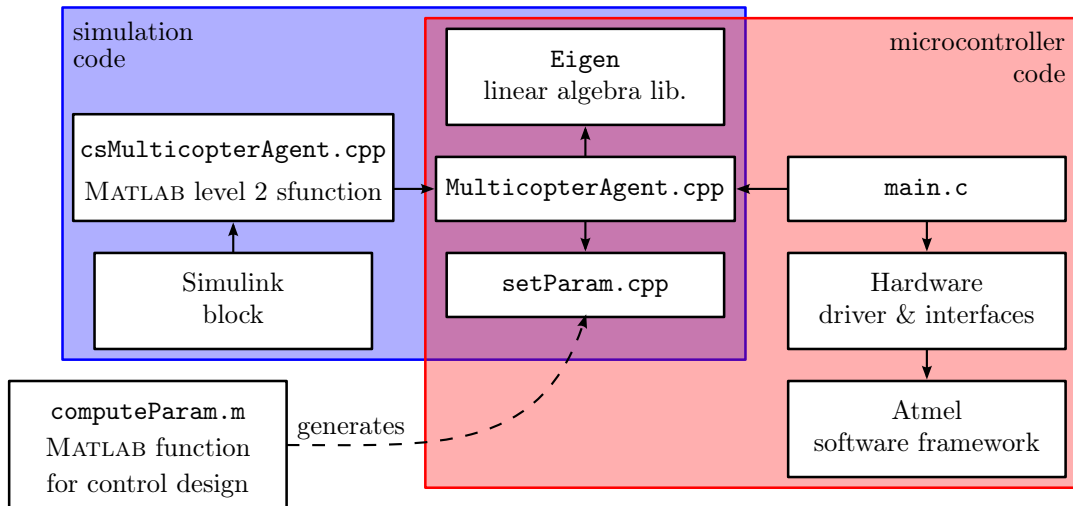


Figure 5.4: Controller code structure

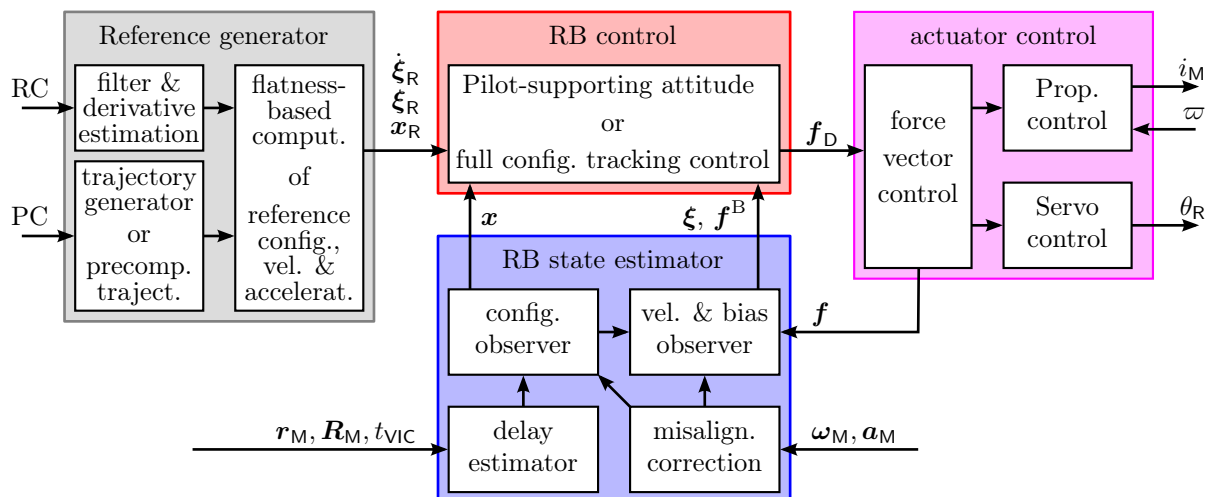


Figure 5.5: Structure of the Multicopter Agent

tricopter are of paramount interest. However, its realization depends on an accurate state estimation, the realization of the control forces and a reasonable reference generation. These are also parts of the multicopter agent, as illustrated in Figure 5.5 and will be subject of the next sections. A coarse overview for this is given in [Konz et al., 2018] and its book version [Konz et al., 2020].

5.2 Multicopter Models

This section derives a mathematical model for a multicopter based on the theory and the example from section 3.4. Furthermore, it covers parameter identification, model simplifications and validation with the LSR quad and tricopter. The resulting models are the basis for simulation and controller design.

5.2.1 Actuator models

Propeller motor. A multicopter propeller is mounted on a small brushless DC motor (BLDC) which is controlled by dedicated driver electronics. This driver implements the electronic commutation and a digital current control with sampling frequency of 64 kHz. It receives the desired, torque generating current i_M from the main controller with the sampling frequency of 200 Hz. Consequently we assume that all electrical dynamics of the propeller drive are negligible on the timescale of the main controller and the motor torque on the propeller is proportional to its current as

$$\tau_M = k_M i_M. \quad (5.1)$$

Servo motor. On the tricopter there are servo motors controlling the tilt θ of the propellers. These are standard hobbyist servos which combine a small motor, a gearbox, a potentiometer and some digital controller which takes the desired servo angle θ_R as input. The integrated controller is probably a fast PID controller since it handles constant loads as well as fast transitions quite well. However, at the main controller sampling frequency, 200 Hz, the fast internal dynamics are negligible and for modeling we only assume a PD controller

$$\tau_S = k_{PS}(\theta_R - \theta) - k_{DS}\dot{\theta}. \quad (5.2)$$

Comparison of the resulting model and actual measurements in Figure 5.13, show that this assumption is valid here.

Propeller aerodynamics. Propellers are designed to generate a force in its spinning direction. A general theory of propellers is quite sophisticated, see e.g. [Johnson, 1980]. However, for the small, rigid propellers used on the LSR quad and tricopter a simple model, which is also common in the corresponding literature e.g. [Hamel et al., 2002], [Mellinger et al., 2012] or [Fritsch, 2014], is sufficient:

$$F = \kappa_F \varpi^2, \quad \tau = -\kappa_T \varpi^2. \quad (5.3)$$

where ϖ is the angular velocity of the propeller. The propeller thrust F is directed along its spinning direction and the propeller drag τ acts opposing the spinning direction. The model parameters κ_F and κ_T arise from the propeller geometry but will be identified in dedicated experiments.

In [Bristeau et al., 2009] and [Martin and Salaun, 2010] a more sophisticated aerodynamic model for a quadcopter of about the same size as the one used here is proposed. It mainly adds dissipative forces that are bilinear in the propeller velocities ϖ and the rigid body velocities \mathbf{v} and $\boldsymbol{\omega}$. For this it introduces 8 additional constant model parameters. Even though their model has a nice physical motivation, it does not fit to the experimental observations done for this work. It does, however, motivate linear drag force and torques on the multicopter body.

Dissipative forces. We assume a general linear damping model for the overall multicopter as motivated in subsection 3.3.5

$$\begin{bmatrix} \mathbf{F}_D \\ \boldsymbol{\tau}_D \end{bmatrix} = \begin{bmatrix} \mathbf{D}_v & \mathbf{D}_v \text{ wed}(\mathbf{l})^\top \\ \text{wed}(\mathbf{l})\mathbf{D}_v & \boldsymbol{\Upsilon} \end{bmatrix} \begin{bmatrix} \mathbf{v} \\ \boldsymbol{\omega} \end{bmatrix} \quad (5.4)$$

where the parameters $\mathbf{D}_v = \text{diag}(d_x, d_y, d_z)$, $\mathbf{l} = [0, 0, l_z]^\top$, $\boldsymbol{\Upsilon} = \text{diag}(\Upsilon_x, \Upsilon_y, \Upsilon_z)$ reflect the geometric symmetries of the multicopters.

5.2.2 Rigid body model

A rigid body model for a tricopter with tilttable propellers has been discussed in section 3.4. Here we like to present a generic model for a multicopter with ρ tilttable propellers. The specific model for a quadcopter and a tricopter arises by application of special parameter values.

Coordinates and Kinematics. Recalling from section 3.4, we choose the configuration coordinates

$$\mathbf{x} = [\mathbf{r}^\top, \text{vec}(\mathbf{R})^\top, \boldsymbol{\theta}^\top, \boldsymbol{\psi}^\top]^\top \in \mathbb{R}^{12+2\rho} \quad (5.5)$$

where $\mathbf{r} \in \mathbb{R}^3$ is the position of the center body, $\mathbf{R} \in \mathbb{SO}(3)$ its orientation matrix, $\boldsymbol{\theta} = [\theta_1, \dots, \theta_\rho]^\top \in \mathbb{R}^\rho$ the arm tilt angles and $\boldsymbol{\psi} = [\psi_1, \dots, \psi_\rho]^\top \in \mathbb{R}^\rho$ the angles of the propellers, see Figure 5.6. Note that the propellers are designed only for either clockwise or counter-clockwise rotation, and will only rotate in this direction during operation. The propeller angles ψ_k are defined, such that $\dot{\psi}_k > 0$ during operation. To recover the spinning directions we use the parameter $\varepsilon_k = 1$ for a positive/counter-clockwise and $\varepsilon_k = -1$ for a negative/clockwise spinning propeller.

To capture the velocity state of the system we use the velocity coordinates

$$\boldsymbol{\xi} = [\mathbf{v}, \boldsymbol{\omega}, \dot{\boldsymbol{\theta}}, \boldsymbol{\varpi}]^\top \in \mathbb{R}^{6+2\rho}, \quad (5.6)$$

related to the configuration coordinates by

$$\dot{\mathbf{r}} = \mathbf{R}\mathbf{v}, \quad \dot{\mathbf{R}} = \mathbf{R} \text{ wed}(\boldsymbol{\omega}), \quad \dot{\boldsymbol{\psi}} = \boldsymbol{\varpi}. \quad (5.7)$$

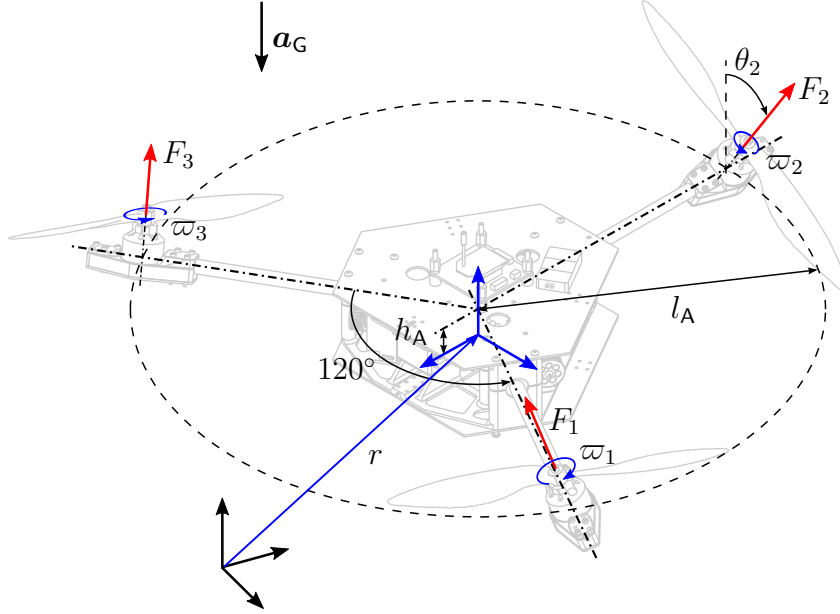


Figure 5.6: Mechanical model of the tricopter

Assumptions on the mass distribution. The algorithm proposed in section 3.4 does of course handle general mass distributions of the rigid bodies, but the resulting kinetic equations are far too cumbersome to display here explicitly. Instead we motivate some assumptions on the body inertia matrices that will lead to a greatly condensed system inertia matrix: Assume that the combined center of mass of one arms and its propeller lies on the tilt axis. This implies that the overall center of mass $\mathbf{s} \in \mathbb{R}^3$ of the complete system is constant w.r.t. the body fixed frame. This was one goal during the construction process of the Tricopter. Furthermore, we assume that the combined moment of inertia of one arm and propeller is symmetric about the tilt axis. This is not the case for the real inertia parameters. However, it is justified by the fact that the overall inertia Θ changes only slightly depending on the arm tilts θ or the propeller angles ψ .

A crucial part to get the overall dynamics right, is to explicitly consider the rotor of the servo motor. The relevant moment of inertia Θ_{Sxx} might be very small, but since it is located behind a gearbox with transmission ratio $c_S = 625$ its contribution to the system inertia matrix is significant. This is reflected in the different values within Θ_{AC} which contains $c_S\Theta_{Sxx}$ and Θ_A which contains $c_S^2\Theta_{Sxx}$. The validity of the model with these assumptions will be discussed later by comparison to experimental data.

Kinetic equation. With the above assumptions, and the propeller model (5.3), the kinetic equation for a multicopter takes the form

$$\mathbf{M}(\boldsymbol{\theta})\dot{\boldsymbol{\xi}} + \mathbf{c}(\boldsymbol{\theta}, \boldsymbol{\xi}) + \mathbf{D}\boldsymbol{\xi} + \mathbf{f}^G(\mathbf{R}) = \mathbf{f}^P(\boldsymbol{\theta}, \boldsymbol{\varpi}) + \mathbf{f}^U(\tau_M, \tau_S) + \mathbf{f}^B \quad (5.8)$$

where

$$\mathbf{M}(\boldsymbol{\theta}) = \begin{bmatrix} m\mathbf{I}_3 & m \text{wed}(\mathbf{s})^\top & 0 & 0 \\ m \text{wed}(\mathbf{s}) & \boldsymbol{\Theta} & \boldsymbol{\Theta}_{AC}\mathbf{H}_1 & \boldsymbol{\Theta}_P\mathbf{H}_3(\boldsymbol{\theta}) \text{diag}(\boldsymbol{\varepsilon}) \\ 0 & \boldsymbol{\Theta}_{AC}\mathbf{H}_1^\top & \boldsymbol{\Theta}_A\mathbf{I}_\rho & 0 \\ 0 & \boldsymbol{\Theta}_P \text{diag}(\boldsymbol{\varepsilon})\mathbf{H}_3^\top(\boldsymbol{\theta}) & 0 & \boldsymbol{\Theta}_P\mathbf{I}_\rho \end{bmatrix}, \quad (5.9a)$$

$$\mathbf{c}(\boldsymbol{\theta}, \boldsymbol{\xi}) = \begin{bmatrix} \text{wed}(\boldsymbol{\omega})\mathbf{p}_v \\ \text{wed}(\mathbf{v})\mathbf{p}_v + \text{wed}(\boldsymbol{\omega})\mathbf{p}_{\omega} + \Theta_{\mathbb{P}}\mathbf{H}_4(\boldsymbol{\theta}) \text{diag}(\dot{\boldsymbol{\theta}}) \text{diag}(\boldsymbol{\varepsilon})\boldsymbol{\varpi} \\ -\Theta_{\mathbb{P}} \text{diag}(\text{diag}(\boldsymbol{\varepsilon})\mathbf{H}_4^{\top}(\boldsymbol{\theta})\boldsymbol{\omega})\boldsymbol{\varpi} \\ \Theta_{\mathbb{P}} \text{diag}(\text{diag}(\boldsymbol{\varepsilon})\mathbf{H}_4^{\top}(\boldsymbol{\theta})\boldsymbol{\omega})\dot{\boldsymbol{\theta}} \end{bmatrix}, \quad (5.9b)$$

$$\mathbf{D} = \begin{bmatrix} \mathbf{D}_v & \mathbf{D}_v \text{wed}(\mathbf{l})^{\top} & 0 & 0 \\ \text{wed}(\mathbf{l})\mathbf{D}_v & \boldsymbol{\Upsilon} & 0 & 0 \\ 0 & 0 & 0 & 0 \\ 0 & 0 & 0 & 0 \end{bmatrix}, \quad \mathbf{f}^G(\mathbf{R}) = \begin{bmatrix} m\mathbf{I}_3 \\ m \text{wed}(\mathbf{s}) \\ 0 \\ 0 \end{bmatrix} \mathbf{R}^{\top}(-\mathbf{a}_{\mathbb{G}}), \quad (5.9c)$$

$$\mathbf{f}^P(\boldsymbol{\theta}, \boldsymbol{\varpi}) = \begin{bmatrix} \kappa_{\mathbb{F}}\mathbf{H}_3(\boldsymbol{\theta}) \\ \kappa_{\mathbb{F}}(l_{\mathbb{A}}\mathbf{H}_4(\boldsymbol{\theta}) + h_{\mathbb{A}}\mathbf{H}_2(\boldsymbol{\theta})) - \kappa_{\mathbb{T}}\mathbf{H}_3(\boldsymbol{\theta}) \text{diag}(\boldsymbol{\varepsilon}) \\ 0 \\ -\kappa_{\mathbb{T}}\mathbf{I}_{\rho} \end{bmatrix} \text{diag}(\boldsymbol{\varpi})\boldsymbol{\varpi}, \quad (5.9d)$$

$$\mathbf{f}^U(\tau_{\mathbb{M}}, \tau_{\mathbb{S}}) = \begin{bmatrix} 0 \\ 0 \\ \tau_{\mathbb{S}} \\ \tau_{\mathbb{M}} \end{bmatrix} \quad \mathbf{f}^B = \begin{bmatrix} \mathbf{F}_B \\ \boldsymbol{\tau}_B \\ 0 \\ \tau_{MB} \end{bmatrix} \quad (5.9e)$$

with the (just for readability) substituted momenta

$$\mathbf{p}_v = m(\mathbf{v} - \text{wed}(\mathbf{s})\boldsymbol{\omega}), \quad (5.9f)$$

$$\mathbf{p}_{\omega} = m \text{wed}(\mathbf{s})\mathbf{v} + \boldsymbol{\Theta}\boldsymbol{\omega} + \Theta_{AC}\mathbf{H}_1\dot{\boldsymbol{\theta}} + \Theta_{\mathbb{P}}\mathbf{H}_3(\boldsymbol{\theta}) \text{diag}(\boldsymbol{\varepsilon})\boldsymbol{\varpi}. \quad (5.9g)$$

and the sub-matrices

$$\mathbf{H}_1 = \begin{bmatrix} c_{\varphi_1} & \cdots & c_{\varphi_{\rho}} \\ s_{\varphi_1} & \cdots & s_{\varphi_{\rho}} \\ 0 & \cdots & 0 \end{bmatrix}, \quad \mathbf{H}_2(\boldsymbol{\theta}) = \begin{bmatrix} c_{\varphi_1}s_{\theta_1} & \cdots & c_{\varphi_{\rho}}s_{\theta_{\rho}} \\ s_{\varphi_1}s_{\theta_1} & \cdots & s_{\varphi_{\rho}}s_{\theta_{\rho}} \\ 0 & \cdots & 0 \end{bmatrix}, \quad (5.9h)$$

$$\mathbf{H}_3(\boldsymbol{\theta}) = \begin{bmatrix} s_{\varphi_1}s_{\theta_1} & \cdots & s_{\varphi_{\rho}}s_{\theta_{\rho}} \\ -c_{\varphi_1}s_{\theta_1} & \cdots & -c_{\varphi_{\rho}}s_{\theta_{\rho}} \\ c_{\theta_1} & \cdots & c_{\theta_{\rho}} \end{bmatrix}, \quad \mathbf{H}_4(\boldsymbol{\theta}) = \begin{bmatrix} s_{\varphi_1}c_{\theta_1} & \cdots & s_{\varphi_{\rho}}c_{\theta_{\rho}} \\ -c_{\varphi_1}c_{\theta_1} & \cdots & -c_{\varphi_{\rho}}c_{\theta_{\rho}} \\ -s_{\theta_1} & \cdots & -s_{\theta_{\rho}} \end{bmatrix}. \quad (5.9i)$$

Tricopter. To get the rigid body model equations for the tricopter (displayed in Figure 5.6) we plug the following parameters into (5.9)

$$\rho = 3, \quad \varphi = \frac{\pi}{3}[1, 3, 5]^{\top}, \quad \boldsymbol{\varepsilon} = [-1, +1, +1]^{\top}. \quad (5.10)$$

The model equations do not simplify too much and the special result is not displayed explicitly here.

Quadcopter. For the quadcopter model we have the parameters (see Figure 5.7)

$$\rho = 4, \quad \varphi = \frac{\pi}{2}[0, 1, 2, 3]^{\top}, \quad \boldsymbol{\varepsilon} = [+1, -1, +1, -1]^{\top}, \quad \boldsymbol{\theta} = [0, 0, 0, 0]^{\top}. \quad (5.11)$$

Here the model equations simplify significantly: Since the propellers do not tilt $\theta = 0$, the corresponding equations can be regarded as definition of reaction torques $\tau_{\mathbb{S}}$ and dropped

from the model equations. Overall the model for the quadcopter is

$$\mathbf{M} = \begin{bmatrix} m\mathbf{I}_3 & -m \text{wed}(\mathbf{s}) & 0 \\ m \text{wed}(\mathbf{s}) & \boldsymbol{\Theta} & \boldsymbol{\Theta}_{\mathbf{P}} \mathbf{H}_3 \text{diag}(\boldsymbol{\varepsilon}) \\ 0 & \boldsymbol{\Theta}_{\mathbf{P}} \text{diag}(\boldsymbol{\varepsilon}) \mathbf{H}_3^T & \boldsymbol{\Theta}_{\mathbf{P}} \mathbf{I}_4 \end{bmatrix}, \quad (5.12a)$$

$$\mathbf{c}(\boldsymbol{\xi}) = \begin{bmatrix} \text{wed}(\boldsymbol{\omega}) & 0 & 0 \\ \text{wed}(\mathbf{v}) & \text{wed}(\boldsymbol{\omega}) & 0 \\ 0 & 0 & 0 \end{bmatrix} \mathbf{M} \boldsymbol{\xi}, \quad \mathbf{f}^G(\mathbf{R}) = \begin{bmatrix} m\mathbf{I}_3 \\ m \text{wed}(\mathbf{s}) \\ 0 \end{bmatrix} \mathbf{R}^T(-\mathbf{a}_G), \quad (5.12b)$$

$$\mathbf{f}^P(\boldsymbol{\varpi}) = \begin{bmatrix} \kappa_F \mathbf{H}_3 \\ \kappa_F l_A \mathbf{H}_4 - \kappa_T \mathbf{H}_3 \text{diag}(\boldsymbol{\varepsilon}) \\ -\kappa_T \mathbf{I}_4 \end{bmatrix} \text{diag}(\boldsymbol{\varpi}) \boldsymbol{\varpi}, \quad \mathbf{f}^U(\tau_M) = \begin{bmatrix} 0 \\ 0 \\ \tau_M \end{bmatrix} \quad (5.12c)$$

with the sub-matrices

$$\mathbf{H}_3 = \begin{bmatrix} 0 & 0 & 0 & 0 \\ 0 & 0 & 0 & 0 \\ 1 & 1 & 1 & 1 \end{bmatrix}, \quad \mathbf{H}_4 = \begin{bmatrix} 0 & 1 & 0 & -1 \\ -1 & 0 & 1 & 0 \\ 0 & 0 & 0 & 0 \end{bmatrix}. \quad (5.12d)$$

Note that the system inertia matrix \mathbf{M} is constant, but there is still an inertial coupling between the propeller velocities $\boldsymbol{\varpi}$ and ω_z . The same model up to different dissipative forces, requiring $\mathbf{s} = \mathbf{0}$ and using Euler angles, has been derived in [Martin and Salaun, 2010].

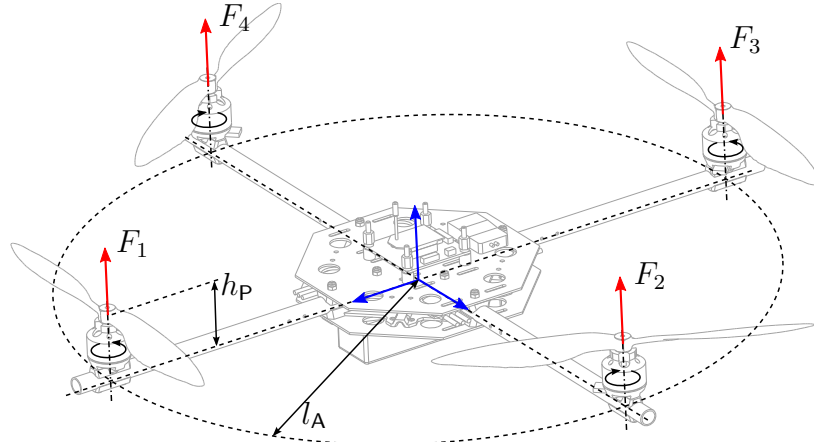


Figure 5.7: Propeller forces on the Quadcopter

5.2.3 Parameter identification

The preceding mathematical model for the multicopters contains various constant parameters of which only the total mass m and the arm radius l_A can be measured directly. Some crucial parameters are identified in dedicated experimental setups which will be discussed in the following. The remaining parameters are estimated by the method of least squares based on the system model and actual in-flight measurements.

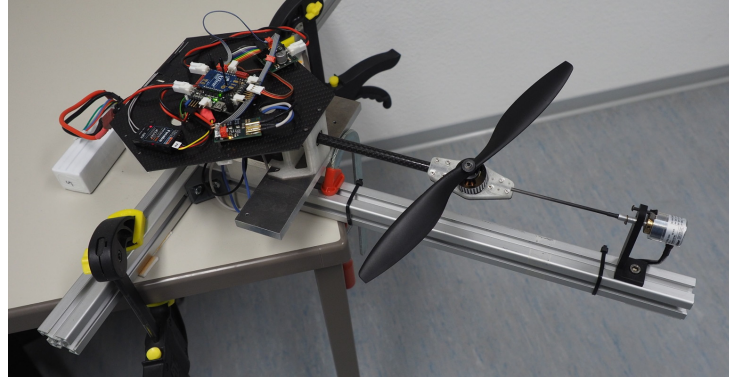


Figure 5.8: Test bench for the propeller and tilting mechanism

Propeller and servo drive. For the identification of the propeller drive and its tilting mechanism we use a dedicated test bench, see Figure 5.8. It is essentially one tricopter arm with additional absolute encoder for the tilt angle θ and an incremental encoder for the propeller velocity ϖ .

The equations of motion for the test bench are

$$\dot{\varpi} + \underbrace{\frac{\kappa_T}{\Theta_P}}_{p_{P1}} \varpi^2 = \underbrace{\frac{k_M}{\Theta_P} i_M}_{p_{P2}} + \underbrace{\frac{\tau_{MB}}{\Theta_P}}_{p_{P3}} \quad (5.13)$$

$$\ddot{\theta} + \underbrace{\frac{k_{DS}}{\Theta_A}}_{p_{S1}} \dot{\theta} + \underbrace{\frac{k_{PS}}{\Theta_A}}_{p_{S0}} \theta = \underbrace{\frac{k_{PS}}{\Theta_A}}_{p_{S0}} \theta_U \quad (5.14)$$

The equations are normalized, yielding the parameters p_{P1} , p_{P2} , p_{P3} and p_{S0} , p_{S1} , which will become more convenient later. These parameters can be directly estimated from measured timeseries using Savitzky-Golay derivative estimation and the method of least squares. The inertia parameters Θ_P and Θ_A are computed from a detailed CAD model of the multicopters. With them one could recover the original parameters κ_T , k_{PS} , etc.. The identified parameter values are summarized in Table 5.1.

The accuracy of the proposed model and its identified parameters can be seen from the results in Figure 5.13 and Figure 5.14 in section 5.3. An online estimation of the bias parameter p_{P3} by means of an observer will be discussed there as well.

Propeller thrust. For identification of the thrust constant κ_F , a propeller drive was mounted horizontally on a 1 m tall pole. The pole in turn stands on a digital scale and the “weight” was recorded at different propeller speeds ϖ . From this “weight” we can compute the corresponding propeller thrust F . The measurements are displayed in Figure 5.9 together with the model $F = \kappa_F \varpi^2$ with the identified parameter value $\kappa_F = 1.44 \cdot 10^{-5} \text{ N s}^2$.

Rigid body inertia. A dedicated experiment was conducted for identification of the inertia parameters Θ_{xx} , Θ_{yy} and Θ_{zz} for quad and tricopter. The body is suspended by two strings as shown on the left side of Figure 5.10. The basic idea is that a rotation of the body about the vertical axis results in an upward movement of the body which is

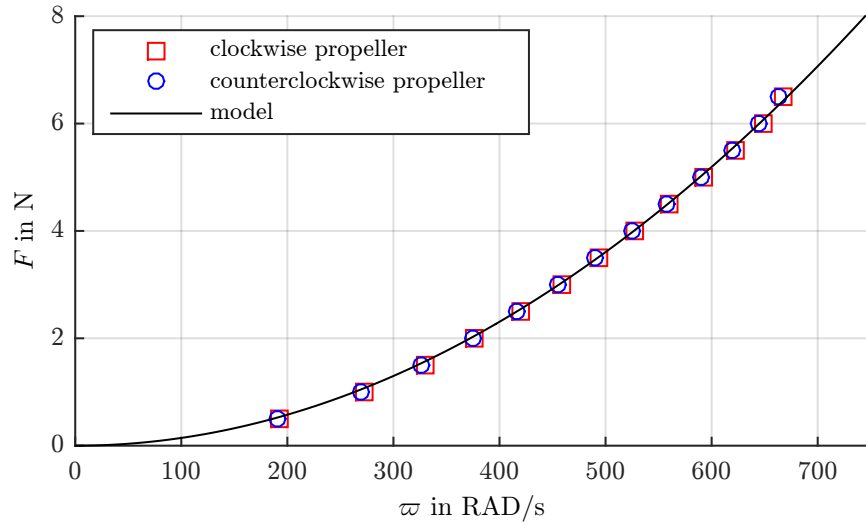
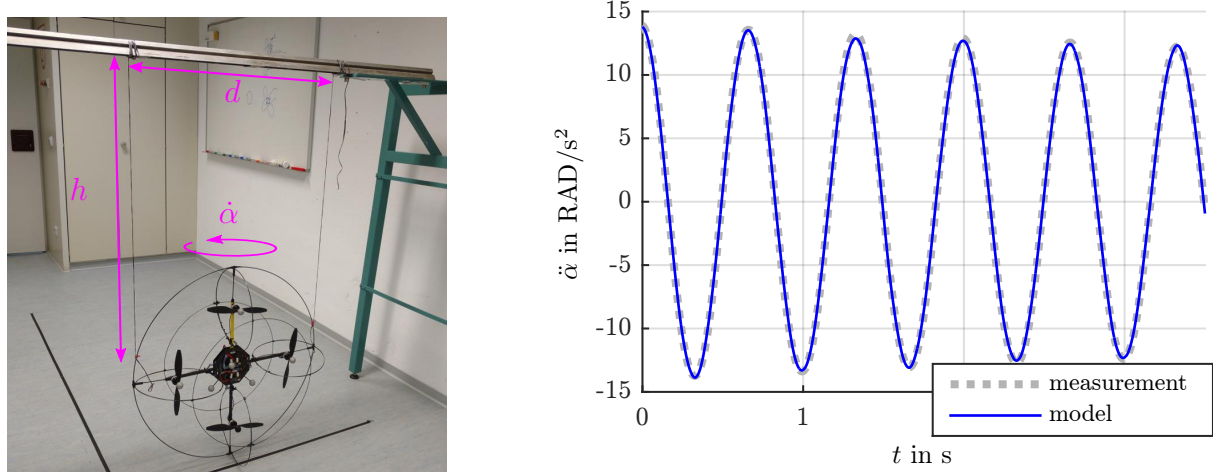


Figure 5.9: Measured propeller thrust compared to proposed model

Figure 5.10: Experimental setup and identification result for Θ_{xx} of the Quadcopter

countered by gravity. So we basically have a torsional spring, which, together with the inertia forms an oscillator whose frequency is proportional to the moment of inertia.

The equation of motion for the vertical rotation with angle α in this setup is

$$\Theta \ddot{\alpha} + \Upsilon \dot{\alpha} + mg \frac{d^2 \sin \alpha}{4\sqrt{h^2 - \frac{d^2}{2}(1 - \cos \alpha)}} = 0. \quad (5.15)$$

Here m indicated the total mass of the copter, $g = 9.81 \text{ m/s}^2$ is the gravitational acceleration, d and h are the distance and length of the strings. From the measured trajectory $t \mapsto \alpha$ of the twist angle we can estimate the inertia Θ and damping Υ about the corresponding axis.

On the right side of Figure 5.10, the acceleration $\ddot{\alpha}$ computed from the model (5.15) with the estimated parameters is plotted against the measured acceleration, computed from the onboard gyroscope readings.

This test was conducted for all three axis, i.e. for Θ_{xx} , Θ_{yy} and Θ_{zz} for Tri- and Quadcopter and the resulting parameters are given in Table 5.1. The identified parameters match the values computed from a detailed CAD model by $\pm 10\%$.

Parameter identification from flight test. The model (5.8) still contains several so far unknown parameters: The coordinates of the center of mass $\mathbf{s} = [s_x, s_y, s_z]^\top$, the off-diagonal entries Θ_{xy} , Θ_{xz} and Θ_{yz} , the translational damping d_x , d_z , the rotational damping Υ_x , Υ_z and the coordinate l_z of the center of damping.

With some auxiliary transformation ($\tilde{l}_z = d_x l_z$, $\tilde{\Upsilon}_x = \Upsilon_x + d_z l_z^2$) the first 6 model equations (5.8) are linear in the remaining unknown parameters. So we can identify these by the method of least squares from flight test measurements. Table 5.1 summarizes the identified parameter values from this flight test as well as the ones from the previously discussed dedicated experiments. These are the values that are used for the simulator.

From this experiment we have the first estimate for the overall center of mass \mathbf{s} of tri- and quadcopter. The identified value s_z is then used to adjust the body fixed frame in the vertical direction such that $s_z = 0$ m. For the Tricopter this determines also the parameter h_A . The values for s_x and s_y are small so we stick to the geometric center in the horizontal directions.

The damping parameter values for the tricopter are greater than the ones for the quadcopter. This could be explained by the model from [Martin and Salaun, 2010] and the fact that the propellers of the Tricopter nominally spin 40% faster than on the Quadcopter. Also the identified value for l_z is roughly the distance from the body fixed frame to the propeller plane which fits well to their model. On the other hand, the identified translational damping d_z in the vertical direction is greater than the horizontal damping d_x . This contradicts the model proposed in [Martin and Salaun, 2010] which would imply $d_z = 0$.

Table 5.1 also shows identified constant bias forces \mathbf{F}_B and torques $\boldsymbol{\tau}_B$ for this particular experiment. These mean values probably result from small misalignments of the propellers and servos rather than constant side wind or anything similar. In the practical application the bias forces will be estimated online by means of an observer, so can vary slowly. However, the magnitudes of the displayed identified values are less than 3% compared to the maximal available propeller forces \mathbf{f}^P in the corresponding directions, so their influence on the overall identification result should be small.

symbol	tricopter value	quadcopter value	source
m	1.251 kg	1.001 kg	directly measured
s_x	$1.7 \cdot 10^{-3}$ m	$-1.8 \cdot 10^{-3}$ m	flight test
s_y	$0.6 \cdot 10^{-3}$ m	$0.6 \cdot 10^{-3}$ m	flight test
s_z	$0.0 \cdot 10^{-3}$ m	$0.0 \cdot 10^{-3}$ m	manually adjusted
Θ_{xx}	$19.2 \cdot 10^{-3}$ kg m ²	$17.9 \cdot 10^{-3}$ kg m ²	pendulum test
Θ_{yy}	$19.2 \cdot 10^{-3}$ kg m ²	$18.0 \cdot 10^{-3}$ kg m ²	pendulum test
Θ_{zz}	$30.8 \cdot 10^{-3}$ kg m ²	$30.7 \cdot 10^{-3}$ kg m ²	pendulum test
Θ_{xy}	$-0.8 \cdot 10^{-3}$ kg m ²	$-0.7 \cdot 10^{-3}$ kg m ²	flight test
Θ_{xz}	$-1.2 \cdot 10^{-3}$ kg m ²	$0.2 \cdot 10^{-3}$ kg m ²	flight test
Θ_{yz}	$-2.1 \cdot 10^{-3}$ kg m ²	$0.0 \cdot 10^{-3}$ kg m ²	flight test
d_x	0.29 kg/s	0.30 kg/s	flight test
d_z	0.45 kg/s	0.36 kg/s	flight test
l_z	$4.0 \cdot 10^{-3}$ m	$12 \cdot 10^{-3}$ m	flight test
Υ_x	$8.5 \cdot 10^{-3}$ kg m ² /s	$-1.5 \cdot 10^{-3}$ kg m ² /s	flight test
Υ_z	$14 \cdot 10^{-3}$ kg m ² /s	$10 \cdot 10^{-3}$ kg m ² /s	flight test
α_G	$[0, 0, -9.81]^\top$ m/s ²		
l_A	$240 \cdot 10^{-3}$ m	$240 \cdot 10^{-3}$ m	directly measured
h_A	$-6 \cdot 10^{-3}$ m	-	manually adjusted
Θ_A	0.9 kg m ²	-	CAD model
Θ_{AC}	0.002 kg m ²	-	prop. test bench
k_{PS}	1400 Nm s ²	-	prop. test bench
k_{DS}	66 Nm s	-	prop. test bench
Θ_P	$3.6 \cdot 10^{-5}$ kg m ²		CAD model
κ_F	$1.44 \cdot 10^{-5}$ N s ²		prop. test bench
κ_T	$2.45 \cdot 10^{-7}$ Nm s ²		prop. test bench
k_M	0.0105 Nm/A		prop. test bench
τ_{MB}	0.005 Nm		prop. test bench
F_{Bx}	-0.21 N	0.09 N	flight test
F_{By}	-0.02 N	0.02 N	flight test
F_{Bz}	0.03 N	-0.09 N	flight test
τ_{Bx}	0.037 Nm	0.049 Nm	flight test
τ_{By}	-0.024 Nm	-0.015 Nm	flight test
τ_{Bz}	-0.003 Nm	-0.012 Nm	flight test

Table 5.1: Parameter values for tri- and quadcopter model

5.2.4 Model validation and simplification

In the previous subsections we proposed a quite detailed model for tri- and quadcopter. Now we like to validate this model by comparing it to experimental data. From this quantitative analysis we can also motivate which parts of the model can be neglected to obtain a simplified model that is still accurate enough for our working domain.

Tricopter. Figure 5.11 shows the accelerations $\dot{\xi}$ during a benchmark fight test for the tricopter. The data corresponds to a 20 s sample at the beginning of the video available here¹. The gray lines are obtained by applying a Savitzky-Golay derivative filter to the measured generalized velocities ξ . The blue lines are the accelerations $\dot{\xi}$ computed from the model (5.8) with the parameters from Table 5.1 and the measured configuration, velocity and inputs. The dashed red lines are the accelerations computed in the same way but from a simplified model that will be proposed now:

For the simplified model of the tricopter we drop all off diagonal entries in the system inertia matrix \mathbf{M} . This means in particular $s = 0$ and $\Theta = \text{diag}(\Theta_x, \Theta_y, \Theta_z)$. Furthermore we drop the damping parameters $l_z = 0$, $\gamma_x = \gamma_z = 0$ and assume isotropic translational damping $D_v = d\mathbf{I}_3$ with $d = \frac{1}{3}(2d_x + d_z)$. The resulting model equations are summarized as follows:

Simplified tricopter model. Rigid body dynamics

$$\dot{r} = \mathbf{R}\mathbf{v}, \quad m(\dot{\mathbf{v}} + \text{wed}(\boldsymbol{\omega})\mathbf{v} - \mathbf{R}^\top \mathbf{a}_G) + d\mathbf{v} = \mathbf{F} + \mathbf{F}_B, \quad (5.16a)$$

$$\dot{\mathbf{R}} = \mathbf{R} \text{wed}(\boldsymbol{\omega}), \quad \Theta \dot{\boldsymbol{\omega}} + \text{wed}(\boldsymbol{\omega})\Theta \boldsymbol{\omega} = \tau + \boldsymbol{\tau}_B, \quad (5.16b)$$

Generalized force from propellers

$$\underbrace{\begin{bmatrix} F_x \\ F_y \\ F_z \\ \tau_x \\ \tau_y \\ \tau_z \end{bmatrix}}_f = \underbrace{\begin{bmatrix} 0 & 0 & 0 & \frac{\sqrt{3}}{2} & 0 & -\frac{\sqrt{3}}{2} \\ 0 & 0 & 0 & -\frac{1}{2} & 1 & -\frac{1}{2} \\ 1 & 1 & 1 & 0 & 0 & 0 \\ \frac{\sqrt{3}l_A}{2} & 0 & -\frac{\sqrt{3}l_A}{2} & \frac{h_A}{2} + \frac{\sqrt{3}\kappa_T}{2\kappa_F} & h_A & \frac{h_A}{2} + \frac{\sqrt{3}\kappa_T}{2\kappa_F} \\ -\frac{l_A}{2} & l_A & -\frac{l_A}{2} & \frac{\sqrt{3}h_A}{2} - \frac{\kappa_T}{2\kappa_F} & \frac{\kappa_T}{\kappa_F} & \frac{\kappa_T}{2\kappa_F} - \frac{\sqrt{3}h_A}{2} \\ \frac{\kappa_T}{\kappa_F} & -\frac{\kappa_T}{\kappa_F} & -\frac{\kappa_T}{\kappa_F} & -l_A & -l_A & -l_A \end{bmatrix}}_B \underbrace{\begin{bmatrix} \mathbf{F}_1^V \\ \mathbf{F}_2^V \\ \mathbf{F}_3^V \\ \mathbf{F}_1^H \\ \mathbf{F}_2^H \\ \mathbf{F}_3^H \end{bmatrix}}_{\mathbf{F}^{VH}} \quad (5.16c)$$

$$\mathbf{F}_j^V = F_j \cos \theta_j, \quad \mathbf{F}_j^H = F_j \sin \theta_j, \quad F_j = \kappa_F \varpi_j^2, \quad j = 1, 2, 3 \quad (5.16d)$$

Propeller drive dynamics

$$\Theta_P \dot{\varpi}_j + \kappa_T \varpi_j^2 = k_M i_{Mj} - \tau_{MBj}, \quad j = 1, 2, 3 \quad (5.16e)$$

Servo dynamics

$$\ddot{\theta}_j + p_{S1} \dot{\theta}_j + p_{S0} \theta_j = p_{S0} \theta_{Uj}, \quad j = 1, 2, 3 \quad (5.16f)$$

¹<https://youtu.be/oS5PHr6H0K4>

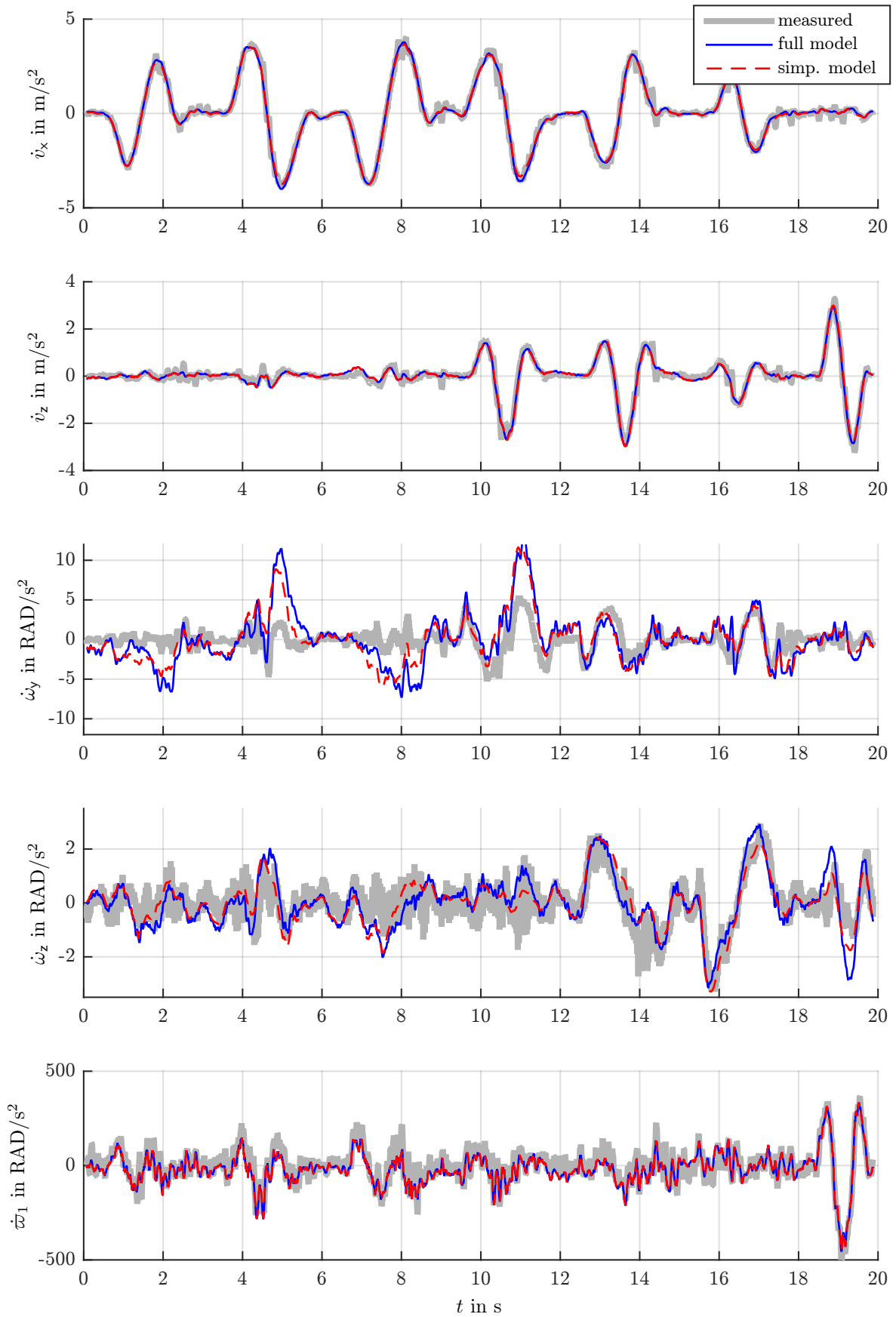


Figure 5.11: Model vs. measured accelerations for the tricopter

Comparing the computed accelerations flight test in Figure 5.11 one finds the following observations: For the translational \dot{v}_x , \dot{v}_z and the propeller acceleration $\dot{\varpi}_1$ the two models can not be distinguished and they match the measured accelerations quite well. For the angular accelerations $\dot{\omega}_x$ and $\dot{\omega}_z$ the models differ slightly. Unfortunately, one cannot say that the full model matches the measured accelerations better than the simplified. This means that there are unmodeled effects that have a greater influence than the ones we dropped for the simplified model. Overall the simplified model (5.16) captures the Tricopter dynamics reasonably well and is due to its simplicity a good starting point for the model based control design.

Quadcopter. As simplifications for the quadcopter model we neglect the inertial couplings between the center body and propeller except $\Theta_P \mathbf{H}_1 \dot{\varpi}$. Furthermore, we assume $s = 0$ and $\boldsymbol{\Theta} = \text{diag}(\Theta_x, \Theta_x, \Theta_z)$. The resulting model reads:

Simplified quadcopter model. Rigid body dynamics

$$\dot{\mathbf{r}} = \mathbf{R} \mathbf{v}, \quad m(\dot{\mathbf{v}} + \text{wed}(\boldsymbol{\omega})\mathbf{v} - \mathbf{R}^\top \mathbf{a}_G) + d\mathbf{v} = F_z e_3 + \mathbf{F}_B, \quad (5.17a)$$

$$\dot{\mathbf{R}} = \mathbf{R} \text{wed}(\boldsymbol{\omega}), \quad \boldsymbol{\Theta} \dot{\boldsymbol{\omega}} + \text{wed}(\boldsymbol{\omega}) \boldsymbol{\Theta} \boldsymbol{\omega} = \boldsymbol{\tau} + \boldsymbol{\tau}_B, \quad (5.17b)$$

Generalized force from propeller rotation

$$\begin{bmatrix} F_z \\ \tau_x \\ \tau_y \\ \tau_z \end{bmatrix} = \underbrace{\begin{bmatrix} 1 & 1 & 1 & 1 \\ 0 & l_A & 0 & -l_A \\ -l_A & 0 & l_A & 0 \\ -\frac{\kappa_T}{\kappa_F} & \frac{\kappa_T}{\kappa_F} & -\frac{\kappa_T}{\kappa_F} & \frac{\kappa_T}{\kappa_F} \end{bmatrix}}_B \underbrace{\begin{bmatrix} \kappa_F \varpi_1^2 \\ \kappa_F \varpi_2^2 \\ \kappa_F \varpi_3^2 \\ \kappa_F \varpi_4^2 \end{bmatrix}}_F - \begin{bmatrix} 0 \\ 0 \\ 0 \\ \Theta_P (\dot{\varpi}_1 - \dot{\varpi}_2 + \dot{\varpi}_3 - \dot{\varpi}_4) \end{bmatrix} \quad (5.17c)$$

Propeller drive dynamics

$$\Theta_P \dot{\varpi}_j + \kappa_T \varpi_j^2 = k_{Mj} i_{Mj} - \tau_{MBj}, \quad j = 1, \dots, 4. \quad (5.17d)$$

Up to a change in velocity coordinates this model is identical to the one proposed in [Hamel et al., 2002, eq. 7–12].

As discussed above for the tricopter, the validation result for the quadcopter is shown in Figure 5.12 which is the first 20 s from <https://youtu.be/x66sua3M6RQ>. The full model and simplified model can hardly be distinguished, so one may say that the simplifications are justified. The measured translational accelerations and the propeller acceleration fit the model quite well. For the angular accelerations there are slightly varying offsets between model and measurements. These are probably aerodynamic disturbances rather than mechanical modeling errors. Nevertheless, this motivates the use of a disturbance observer which will be discussed in a following section.

In contrast to the tricopter simplifications, the simplified quadcopter model did not drop the inertial coupling between the propellers and the yaw dynamics. The reason for this is twofold: The tricopter may generate yaw torque by tilting the propellers, whereas the

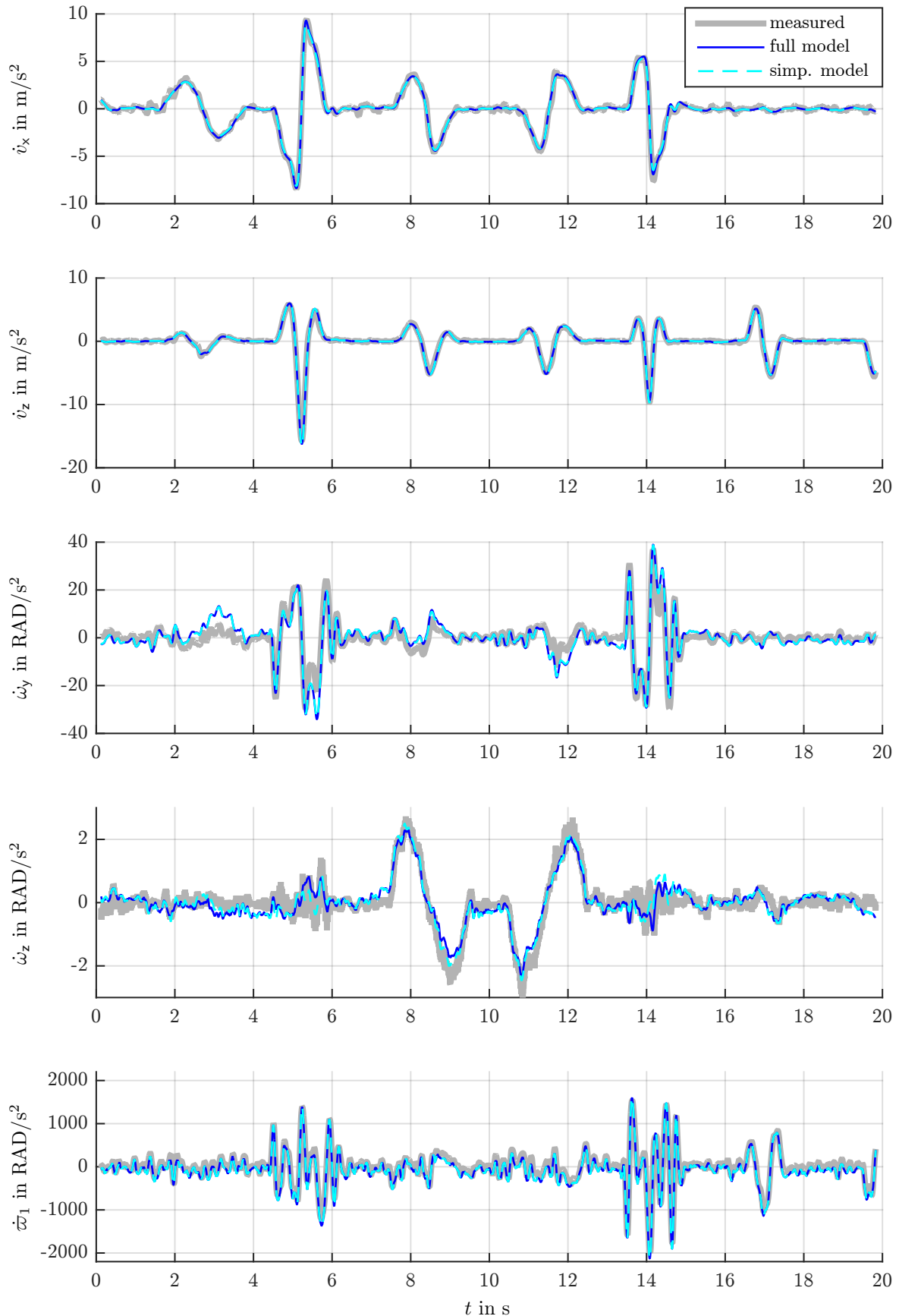


Figure 5.12: Model vs. measured accelerations on the quadcopter

quadcopter relies on the propeller drag and the inertial coupling, which are nominally much smaller. Secondly, the experiments with the quadcopter perform much more dynamic maneuvers which result in higher propeller accelerations as can be seen exemplary by comparing Figure 5.12 to Figure 5.11.

5.3 Control of the generalized force

The rigid body controller computes a *desired* generalized force \mathbf{f}_D for the corresponding multicopter. This force cannot be realized instantaneously as its subject to its own actuator dynamics, see section 5.2. This section describes a control approach for the generalized force \mathbf{f}

Since the force \mathbf{f} itself is subject , it is not possible to realize it instantaneously. However, we can pursue to realize it reasonably fast, which is the subject of this section. At the same time we need an accurate estimate for the current generalized force for the rigid body observer. The coarse structure was already given in Figure 5.5.

5.3.1 Servo simulation

The integrated servo controller uses an internal angle measurement but this is not available for the main controller. A dedicated test bench (see Figure 5.8) with an absolute encoder for the tilt angle θ was used for validation of the servo dynamics (5.16f) and identification of its parameters p_{S0} and p_{S1} . Since the model is asymptotically stable, a simple online simulation of the model with the known servo setpoint $\theta_U[k]$ is sufficient to get an estimate of the current servo angle. For this a simple forward Euler discretization of (5.16f) is implemented on the main controller

$$\hat{\theta}[k+1] = \hat{\theta}[k] + T_S \dot{\hat{\theta}}[k] \quad (5.18a)$$

$$\dot{\hat{\theta}}[k+1] = \dot{\hat{\theta}}[k] + T_S (p_{S0}(\theta_U[k] - \hat{\theta}[k]) - p_{S1}\dot{\hat{\theta}}[k]). \quad (5.18b)$$

In Figure 5.13 its result is compared to the measurement of the encoder. To be close to the real application on the Tricopter, the propeller on the test bench is spinning with about 70 Hz during the experiment. This explains the vibration seen in the encoder measurements. If the propeller is switched off, the estimation error is always less than ± 0.5 DEG.

5.3.2 Propeller tracking control

The forward Euler discretization of the propeller model (5.17d) is

$$\varpi[k+1] = \varpi[k] + T_S (p_{P2}i_M[k] - p_{P3} - p_{P1}(\varpi[k])^2), \quad (5.19)$$

Measurement model. From the commutation algorithm of the BLDC driver we get an estimate ϖ_M of the propeller velocity which relies on its *angle* ψ estimation used for

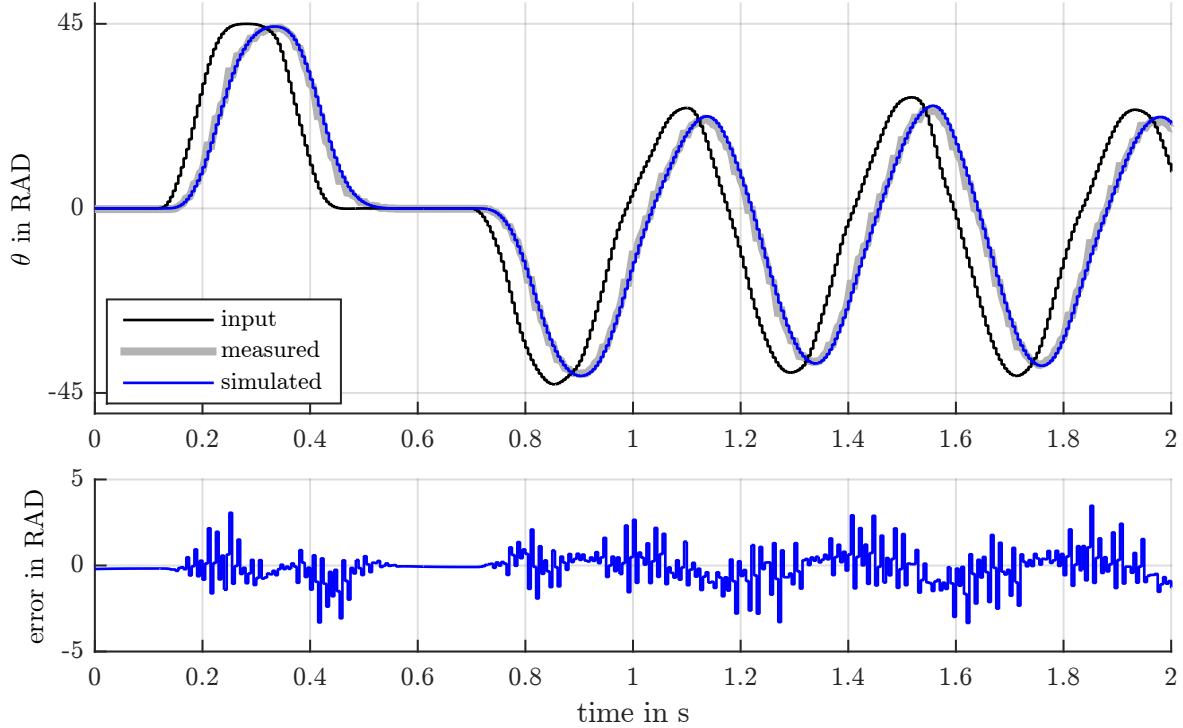


Figure 5.13: Servo simulation validation

the commutation, which is

$$\varpi_M[k] = \frac{1}{T_S} (\psi[k] - \psi[k-1]). \quad (5.20)$$

Assuming that the angular acceleration $\dot{\varpi}$ is roughly constant within one sampling step, we have the relations

$$\psi[k] = \psi[k-1] + \varpi[k-1]T_S + \frac{1}{2}\dot{\varpi}[k-1]T_S^2, \quad \dot{\varpi}[k-1] = \frac{1}{T_S}(\varpi[k] - \varpi[k-1]). \quad (5.21)$$

So the estimate corresponds to the mean velocity between the current and the last sampling step, i.e.

$$\varpi_M[k] = \frac{1}{2}(\varpi[k] + \varpi[k-1]). \quad (5.22)$$

Observer. The velocity estimate ϖ_M from the BLDC driver is quite noisy, so it should not be used directly in a feedback. The scaled model (5.19) also contains the a friction parameter $p_{P3} = \frac{\tau_{MB}}{\theta_P}$ which we like to estimate online for each propeller drive individually. To address these two aspects, an observer for each propeller drive is implemented on the main controller. It is essentially a copy of the discrete model (5.19) supplemented with a linear error feedback

$$e[k] = \varpi_M[k] - \frac{1}{2}(\hat{\varpi}[k] + \hat{\varpi}[k-1]) \quad (5.23a)$$

$$\hat{\varpi}[k+1] = \hat{\varpi}[k] + T_S(p_{P2}i_M[k] - \hat{p}_{P3}[k] - p_{P1}(\hat{\varpi}[k])^2 + l_{P1}e[k]), \quad (5.23b)$$

$$\hat{p}_{P3}[k+1] = \hat{p}_{P3}[k] + T_S l_{P2} e[k]. \quad (5.23c)$$

where $l_{P1}, l_{P2} \in \mathbb{R}$ are the feedback gains. For quantitative analysis of the observer we consider the linearization of the observer error dynamics about a general expansion point $\varpi = \bar{\varpi} > 0$. Its characteristic polynomial is

$$\lambda^3 + \left(\frac{T_S}{2}(4p_{P1}\bar{\varpi} + l_{P1}) - 2\right)\lambda^2 + \left(1 - \frac{T_S}{2}(4p_{P1}\bar{\varpi} + T_S l_{P2})\right)\lambda - \frac{T_S}{2}(l_{P1} + T_S l_{P2}) = 0 \quad (5.24)$$

The roots λ for the given parameters are shown in (fixme).

Tracking controller. Assume that we have a given trajectory $k \mapsto \hat{\varpi}_D[k]$ and we want the trajectory of the propeller velocity $k \mapsto \varpi[k]$ (actually its estimate $\hat{\varpi}$) to converge to it. Being at the sampling step k the available control input is the motor current $i_M[k+1]$ for the *next* step. From the observer (5.23) we have estimates for the velocity $\hat{\varpi}[k+1]$ and the friction $\hat{p}_{P3}[k+1]$ at the next sampling step. Taking this into account we propose the control law:

$$e[k+1] = \hat{\varpi}_D[k+1] - \hat{\varpi}[k+1], \quad (5.25a)$$

$$i_M[k+1] = \frac{1}{p_{P2}} \left(\frac{\hat{\varpi}_D[k+2] - \hat{\varpi}_D[k+1]}{T_S} + p_{P1} (\hat{\varpi}_D[k+1])^2 + \hat{p}_{P3}[k+1] + k_P e[k+1] \right), \quad (5.25b)$$

It is essentially a (shifted) copy of the discrete model (5.19) supplemented with a linear error feedback with the gain $k_P \in \mathbb{R}$. Plugging the control law (5.25) into the model (5.19) and assuming the observer has converged, i.e. $\hat{\varpi}[k] = \varpi[k]$ and $\hat{p}_{P3}[k] = p_{P3}$, yields the tracking error dynamics

$$e[k+1] + (T_S(2p_{P1}\varpi[k] + k_P) - 1)e[k] + T_S p_{P1} (e[k])^2 = 0. \quad (5.26)$$

For a the linearization about the expansion point $e = 0$, $\varpi = \bar{\varpi}$ the corresponding characteristic polynomial has the root

$$\lambda = 1 - T_S(2p_{P1}\bar{\varpi} + k_P). \quad (5.27)$$

5.3.3 Tricopter force control

The generalized force \mathbf{f} on the tricopter is a static transformation of the propeller velocities $\varpi_1, \dots, \varpi_3$ and the servo angles $\theta_1, \dots, \theta_3$ as given in (5.16c). For a given desired generalized force \mathbf{f}_D we can (partially) invert this relation to obtain the corresponding propeller thrusts F_{D1}, \dots, F_{D3} and servo angles $\theta_{D1}, \dots, \theta_{D3}$ as

$$\mathbf{F}_D^{VH} = B^{-1} \mathbf{f}_D, \quad F_{Dj} = \sqrt{(\mathbf{F}_{Dj}^V)^2 + (\mathbf{F}_{Dj}^H)^2}, \quad \theta_{Dj} = \text{atan2}(\mathbf{F}_{Dj}^H, \mathbf{F}_{Dj}^V), \quad j = 1, 2, 3. \quad (5.28)$$

In addition the computed values are saturated to $0.3 \text{ N} \leq F_{Di} \leq 7.0 \text{ N}$ and $-45^\circ \leq \theta_{Di} \leq 45^\circ$, $i = 1, 2, 3$ to incorporate the practical limitations of the actuators. The desired servo angles θ_{Di} are directly forwarded to the servo controllers. In contrast, for the desired thrusts F_i a first order filter is applied:

$$\hat{F}_D[k+2] = c_F \hat{F}_D[k+1] + (1 - c_F) F_D[k+1], \quad \hat{\varpi}_D[k+2] = \sqrt{\hat{F}_D[k+2]/\kappa_F}. \quad (5.29)$$

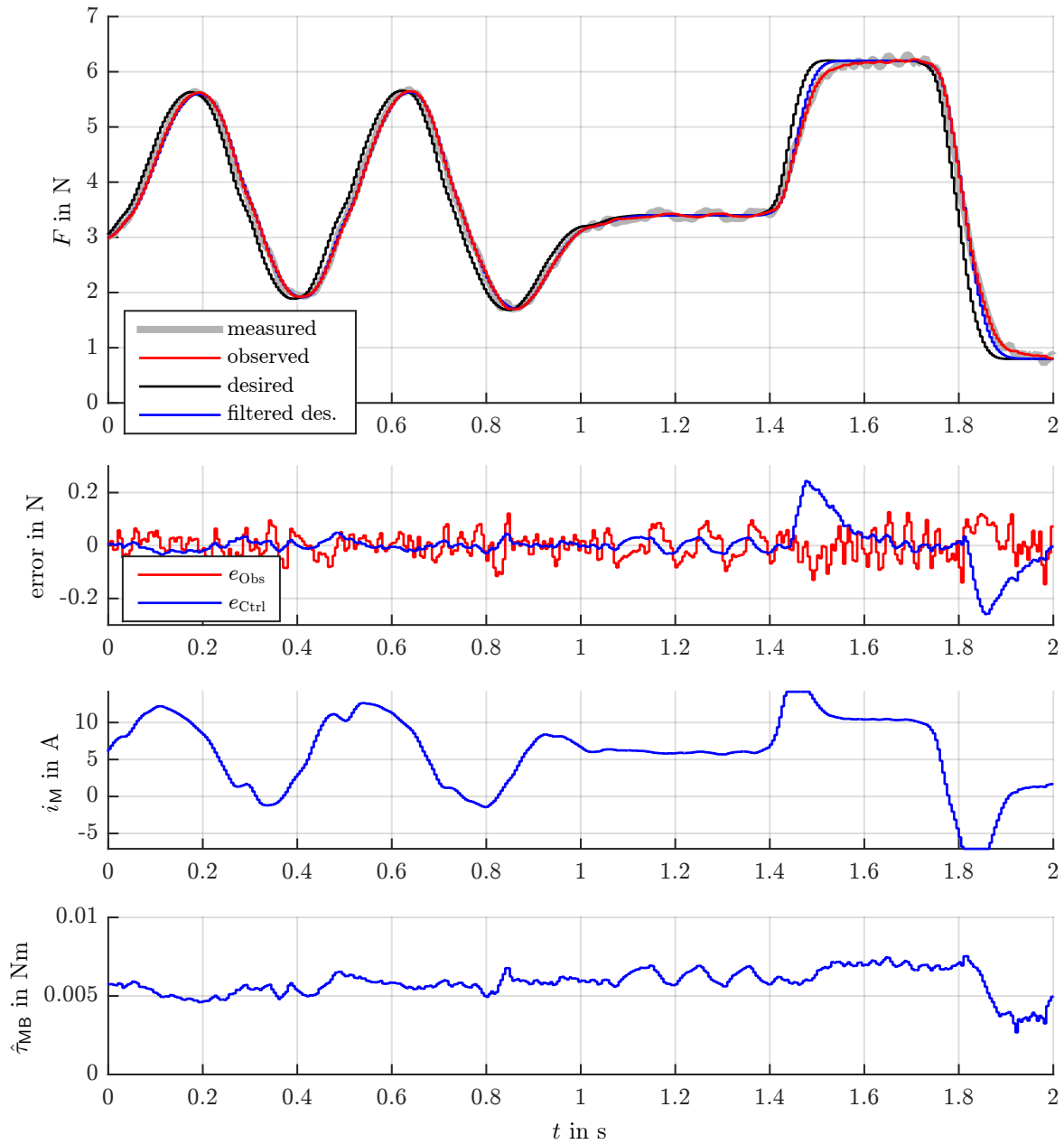


Figure 5.14: Propeller control validation

This yields the desired propeller velocities $\hat{\omega}_{\text{D}i}[k+1]$ and $\hat{\omega}_{\text{D}i}[k+2]$ for the next two sampling steps which are required for the propeller *tracking* controller. After the propeller controller has converged, i.e. $F_i = \hat{F}_{\text{D}i}$, the thrust dynamic is completely determined by this filter.

Overall we can combine the discrete servo dynamics (5.18), the thrust filter (5.29) and the static transformations (5.16c) and (5.28) to obtain a nonlinear dynamic system with the input \mathbf{f}_D and the output \mathbf{f} , the *tricopter actuator dynamics*. For a quantitative analysis its first order approximation about a general expansion point $(\bar{F}_1, \bar{F}_2, \bar{F}_3, \bar{\theta}_1, \bar{\theta}_2, \bar{\theta}_3)$ is considered. Using the z -transformation $\mathcal{Z}\{\cdot\}$ the linearized dynamics between \mathbf{f} and \mathbf{f}_D can be written as

$$\mathcal{Z}\{\Delta \mathbf{f}\} = G_f(z) \mathcal{Z}\{\Delta \mathbf{f}_D\}. \quad (5.30)$$

The discrete transfer function

$$G_f(z) = J \text{diag}(G_F(z), G_F(z), G_F(z), G_\theta(z), G_\theta(z), G_\theta(z)) J^{-1} \quad (5.31)$$

consists of $G_F(z)$, the transfer function of the thrust filter (5.29), $G_\theta(z)$, the transfer function of the controlled servo (5.18):

$$G_F(z) = \frac{1 - c_F}{z - c_F}, \quad G_\theta(z) = \frac{p_{S0} T_S^2}{(z - 1)^2 + p_{S1} T_S(z - 1) + p_{S0} T_S^2}. \quad (5.32)$$

and J is the Jacobian matrix of the force transformation (5.16c) at the expansion point.

$$J = B \begin{bmatrix} \cos \bar{\theta}_1 & 0 & 0 & -\bar{F}_1 \sin \bar{\theta}_1 & 0 & 0 \\ 0 & \cos \bar{\theta}_2 & 0 & 0 & -\bar{F}_2 \sin \bar{\theta}_2 & 0 \\ 0 & 0 & \cos \bar{\theta}_3 & 0 & 0 & -\bar{F}_3 \sin \bar{\theta}_3 \\ \sin \bar{\theta}_1 & 0 & 0 & \bar{F}_1 \cos \bar{\theta}_1 & 0 & 0 \\ 0 & \sin \bar{\theta}_2 & 0 & 0 & \bar{F}_2 \cos \bar{\theta}_2 & 0 \\ 0 & 0 & \sin \bar{\theta}_3 & 0 & 0 & \bar{F}_3 \cos \bar{\theta}_3 \end{bmatrix}. \quad (5.33)$$

Note that \bar{F} cancels out in (5.31), i.e. G_f is independent of it.

From the structure of G_f in (5.31) it is clear that its entries are linear combinations of the transfer functions the the thrust and the servos, G_F and G_θ . Also it is evident that if $G_F = G_\theta$, then G_f would be diagonal. Since this is not the case we do have off-diagonal entries in the transfer matrix G_f . This so-called crosstalk between the components of the generalized force \mathbf{f} depends mainly on the expansion point of the servo angles $\bar{\theta}$.

For a better quantitative analysis of the off-diagonal entries of G_f , the transfer function is normalized as $\tilde{G}_f = S^{-1} G_f S$ where $S = \text{diag}(F_{x,\text{Max}}, \dots, \tau_{z,\text{Max}})$ contains the maximal magnitudes of the corresponding forces and torques. Figure 5.15 shows exemplary the bode magnitude plot of \tilde{G}_f for the hover case $\bar{\theta} = [0, 0, 0]^\top$ (left) and for a forward force with $\bar{\theta} = [\pi/4, 0, -\pi/4]^\top$ (right). In the hover case the diagonal entries for F_z , τ_x and τ_y coincide with the thrust dynamics G_F , whereas the diagonal entries for F_x and F_y coincide with the servo dynamics G_θ . The diagonal entry for τ_z is dominated by the servo dynamics G_θ but also has a small influence from G_F due to the propeller drag (terms involving κ_T in (5.16c)). The propeller drag is also responsible for the small off-diagonal entries in the hover case. For the forward force case it is evident that the diagonal entries are linear combinations of G_F and G_θ . Furthermore, the off-diagonal entries have a significantly larger magnitude.

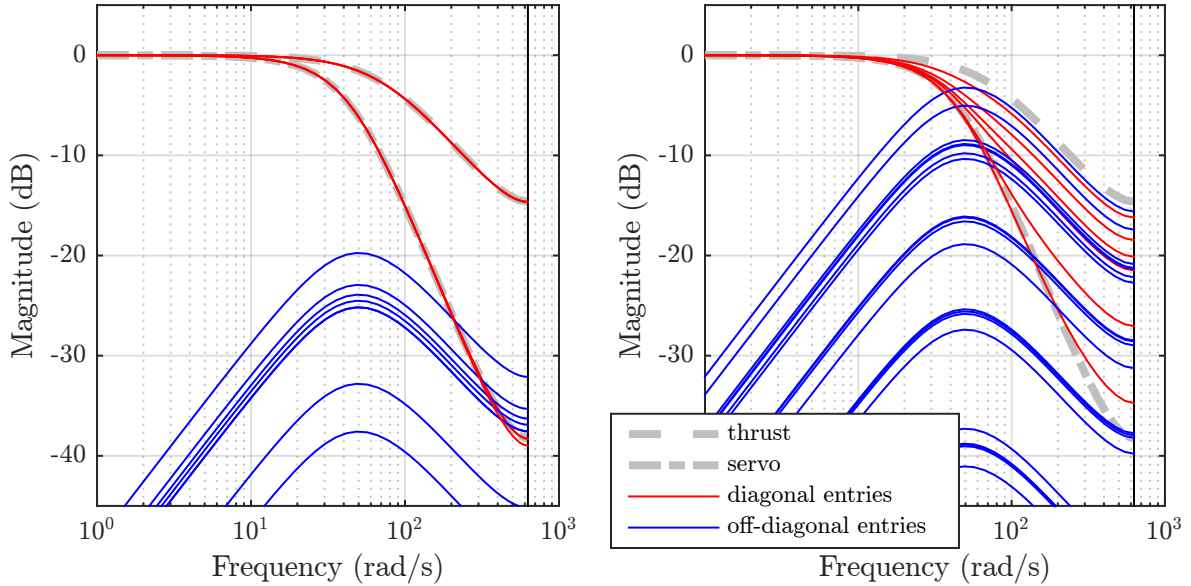


Figure 5.15: Bode magnitude plot of the normalized tricopter actuator dynamics transfer function \tilde{G}_f at different expansion points

5.3.4 Quadcopter force vector control

Model. The model of the generalized force on the quadcopter from (5.17c) can be split into a static part f^{stat} , proportional to the squares of the propeller velocities ϖ , and a dynamic part f^{dyn} proportional to the propeller accelerations $\dot{\varpi}$, as

$$f(\varpi, \dot{\varpi}) = \underbrace{\begin{bmatrix} \kappa_F & \kappa_F & \kappa_F & \kappa_F \\ 0 & \kappa_F l_A & 0 & -\kappa_F l_A \\ -\kappa_F l_A & 0 & \kappa_F l_A & 0 \\ -\kappa_T & \kappa_T & -\kappa_T & \kappa_T \end{bmatrix}}_{f^{\text{stat}}(\varpi)} \underbrace{\begin{bmatrix} \varpi_1^2 \\ \varpi_2^2 \\ \varpi_3^2 \\ \varpi_4^2 \end{bmatrix}}_{B} - \underbrace{\begin{bmatrix} 0 \\ 0 \\ 0 \\ \Theta_P(\dot{\varpi}_1 - \dot{\varpi}_2 + \dot{\varpi}_3 - \dot{\varpi}_4) \end{bmatrix}}_{f^{\text{dyn}}(\dot{\varpi})}. \quad (5.34)$$

Filter dynamics. The task here is to design a filter which outputs the desired propeller velocities $\varpi[k]$ and $\varpi[k+1]$ for the next two sampling steps based on the given desired generalized force $f_D[k]$. Note that f is *not* a flat output of (5.34), so a simple low-pass filter for f_D does not do the trick. However, the propeller velocities ϖ form a flat output and so we propose the following continuous time filter

$$\frac{d^2}{dt^2}(f^{\text{stat}}(\hat{\varpi}_D)) + K_1 \frac{d}{dt}(f^{\text{stat}}(\hat{\varpi}_D)) + K_0(f(\hat{\varpi}_D, \dot{\hat{\varpi}}_D) - f_D) = 0. \quad (5.35)$$

With introduction of the auxiliary state $\hat{h} = \frac{d}{dt}(f^{\text{stat}}(\hat{\varpi}_D)) + K_1 f^{\text{stat}}(\hat{\varpi}_D)$ this can be rewritten in an explicit first order form

$$\dot{\hat{\varpi}}_D = \text{diag}(2\kappa_F \hat{\varpi}_D)^{-1} B^{-1} (\hat{h} - K_1 f^{\text{stat}}(\hat{\varpi}_D)), \quad (5.36a)$$

$$\dot{\hat{h}} = K_0(f_D - f(\hat{\varpi}_D, \dot{\hat{\varpi}}_D)). \quad (5.36b)$$

For the time discrete implementation we add the forward Euler approximation of the derivatives

$$\hat{\varpi}_D[k+1] = \hat{\varpi}_D[k] + T_S \dot{\hat{\varpi}}_D[k], \quad \hat{h}[k+1] = \hat{h}[k] + T_S \dot{\hat{h}}[k]. \quad (5.37)$$

With this representation of the filter dynamics it is very simple to add a saturation $\varpi_{\min} \leq \hat{\varpi}_D \leq \varpi_{\max}$ to take into account the practical limitations of the propellers. The combination of (5.36) and (5.37) constitute a time discrete nonlinear system with the input $f_D[k]$ and the output $\hat{\varpi}_D[k]$, $\hat{\varpi}_D[k+1]$, the *quadcopter actuator dynamics*.

Tuning. The filter gains K_1 and K_2 are chosen as diagonal matrices and for symmetry considerations the gains corresponding to τ_x and τ_y are identical, i.e.

$$K_0 = \text{diag}(k_{\text{mag}0}, k_{\text{tilt}0}, k_{\text{tilt}0}, k_{\text{head}0}), \quad K_1 = \text{diag}(k_{\text{mag}1}, k_{\text{tilt}1}, k_{\text{tilt}1}, k_{\text{head}1}). \quad (5.38)$$

For a quantitative analysis of the actuator dynamics we consider its linearization for a general expansion point $(\bar{\varpi}_1, \dots, \bar{\varpi}_4) \in [\varpi_{\min}, \varpi_{\max}]^4$. Using the z -transformation we get the following transfer matrix

$$\mathcal{Z}\{\Delta f\} = G_f(z) \mathcal{Z}\{\Delta f_D\}, \quad G_f(z) = \begin{bmatrix} G_{11}(z) & 0 & 0 & 0 \\ 0 & G_{22}(z) & 0 & 0 \\ 0 & 0 & G_{33}(z) & 0 \\ G_{41}(z) & G_{42}(z) & G_{43}(z) & G_{44}(z) \end{bmatrix} \quad (5.39)$$

with the components

$$G_{11}(z) = \frac{k_{\text{mag}0}}{\left(\frac{z-1}{T_S}\right)^2 + k_{\text{mag}1} \frac{z-1}{T_S} + k_{\text{mag}0}} \quad (5.40a)$$

$$G_{22}(z) = G_{33}(z) = \frac{k_{\text{tilt}0}}{\left(\frac{z-1}{T_S}\right)^2 + k_{\text{tilt}1} \frac{z-1}{T_S} + k_{\text{tilt}0}} \quad (5.40b)$$

$$G_{44}(z) = \frac{k_{\text{head}0} (p_4 \frac{z-1}{T_S} + 1)}{\left(\frac{z-1}{T_S}\right)^2 + (k_{\text{head}0} p_4 + k_{\text{tilt}1}) \frac{z-1}{T_S} + k_{\text{head}0}} \quad (5.40c)$$

$$G_{4j}(z) = \frac{p_j G_{jj}(z) \left(\frac{z-1}{T_S}\right)^2 \left(\frac{z-1}{T_S} + k_{\text{head}1}\right)}{\left(\frac{z-1}{T_S}\right)^2 + (k_{\text{head}0} p_4 + k_{\text{tilt}1}) \frac{z-1}{T_S} + k_{\text{head}0}}, \quad j = 1, 2, 3 \quad (5.40d)$$

and the (expansion point dependent) model parameters

$$p_1 = \frac{\Theta_P}{8\kappa_F} \left(\frac{1}{\bar{\varpi}_4} - \frac{1}{\bar{\varpi}_3} + \frac{1}{\bar{\varpi}_2} - \frac{1}{\bar{\varpi}_1} \right), \quad p_2 = \frac{\Theta_P}{4\kappa_F l_A} \left(\frac{1}{\bar{\varpi}_2} - \frac{1}{\bar{\varpi}_4} \right), \quad (5.41a)$$

$$p_4 = \frac{\Theta_P}{8\kappa_T} \left(\frac{1}{\bar{\varpi}_1} + \frac{1}{\bar{\varpi}_2} + \frac{1}{\bar{\varpi}_3} + \frac{1}{\bar{\varpi}_4} \right), \quad p_3 = \frac{\Theta_P}{4\kappa_F l_A} \left(\frac{1}{\bar{\varpi}_1} - \frac{1}{\bar{\varpi}_3} \right). \quad (5.41b)$$

The transfer behaviors for F_z , τ_x and τ_y are uncorrelated and independent of the expansion point. Their parameters are chosen to form a second order Butterworth filter.

Unfortunately, the transfer behavior for τ_z is not that nice: It is in general affected by all components of f_D and the corresponding transfer functions $G_{4j}, j = 1, \dots, 4$ depend on the expansion point. However, for the hover case $\bar{\varpi}_1 = \bar{\varpi}_2 = \bar{\varpi}_3 = \bar{\varpi}_4 = \sqrt{mg/4\kappa_F}$ we

have $p_1 = p_2 = p_3 = 0$ and $p_4 = \frac{\Theta_p}{\kappa_T} \sqrt{\kappa_F/mg}$. We choose $k_{\text{head1}} = 1/p_4 = \frac{\kappa_T}{\Theta_p} \sqrt{mg/\kappa_F}$ such that at this particular expansion point we have a pole-zero cancellation. The remaining parameter k_{head0} is then used to adjust the cut-off frequency of the filter.

Figure 5.16 shows the Bode magnitude plot of the normalized transfer matrix \tilde{G}_f coefficients from (5.40) with the used filter parameters. The left side corresponds to the most common hover case $\bar{\omega}_1 = \bar{\omega}_2 = \bar{\omega}_3 = \bar{\omega}_4 = \sqrt{mg/4\kappa_F}$ whereas the right side captures the “worst case” expansion points where $(\bar{\omega}_1, \dots, \bar{\omega}_4) \in \{\bar{\omega}_{\min}, \bar{\omega}_{\max}\}^4$. Obviously the pole-zero cancellation only holds for the hover case but even for the worst case points G_{44} only differs slightly from its design. Furthermore one can see that the influence of the off-diagonal entries is restricted to high frequencies.

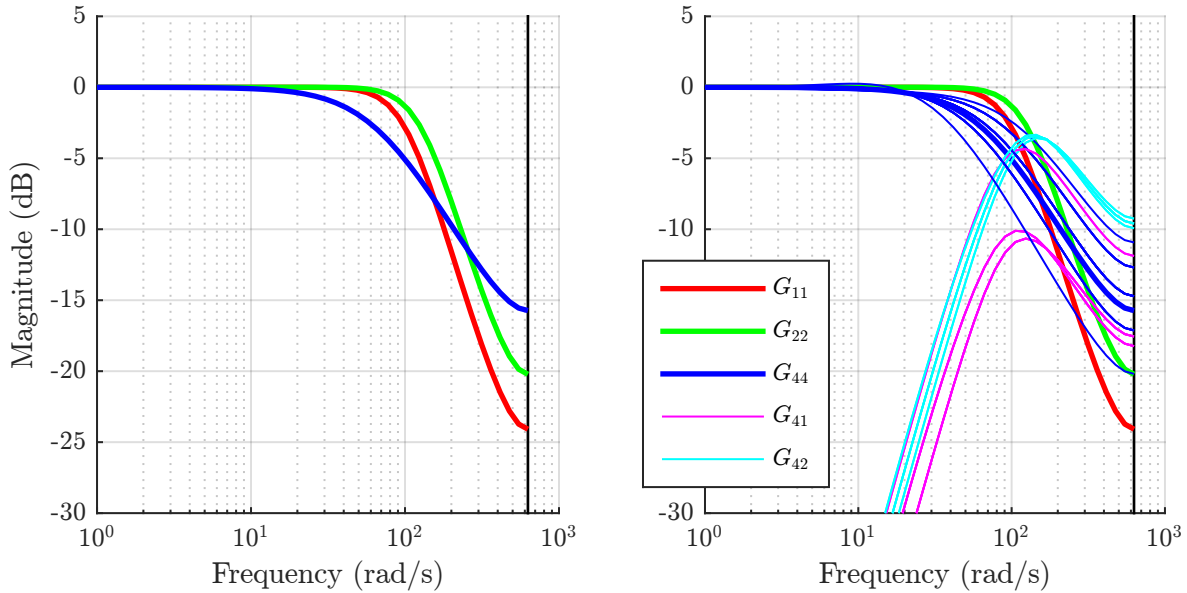


Figure 5.16: Bode magnitude plot of the normalized transfer matrix \tilde{G}_f at different expansion points

Comparison to static approach. The proposed filter (5.35) might seem complicated. In particular one might argue that the dynamic part f^{dyn} in the model (5.34) is negligible, as is done in most publications on this subject.

To answer this question we can replace (5.35) by

$$\frac{d^2}{dt^2}(f^{\text{stat}}(\hat{\omega}_D)) + K_1 \frac{d}{dt}(f^{\text{stat}}(\hat{\omega}_D)) + K_0(f^{\text{stat}}(\hat{\omega}_D) - f_D) = 0 \quad (5.42)$$

what essentially neglects the dynamics part f^{dyn} in the generalized force $f = f^{\text{stat}} + f^{\text{dyn}}$. As before we now consider the transfer matrix G_f for the linearized filter at a general expansion point. The components differing from (5.40) are

$$G_{44}(z) = \frac{k_{\text{head0}}(p_4 \frac{z-1}{T_S} + 1)}{\left(\frac{z-1}{T_S}\right)^2 + k_{\text{tilt1}} \frac{z-1}{T_S} + k_{\text{head0}}} \quad G_{4j}(z) = p_j \frac{z-1}{T_S} G_{jj}(z), \quad j = 1, 2, 3. \quad (5.43)$$

Now one can chose the gains K_0 and K_1 such that (5.42) forms 4 decoupled second order Butterworth filters with inputs f_D and outputs f^{stat} . However, since the real force on the

quadcopter does contain the dynamic part as well the behavior from f_D to $f = f^{\text{stat}} + f^{\text{dyn}}$ is quite different, as can be seen in (5.43). The Bode magnitude plot of the transfer functions is displayed in Figure 5.17 on the left side. Even for the hover case (thick lines) the transfer function G_{44} for τ_z has an unacceptable overshoot.

In order to improve the behavior we can do the same as before: adjust the parameters in G_{44} , i.e. $k_{\text{head}0}$ and $k_{\text{head}1}$, such that there is a pole-zero cancellation at the hover expansion point. The resulting Bode magnitude plot is shown on the right side of Figure 5.17. It is already a significant improvement compared to the left side but is much worse as the previous result shown in Figure 5.16. Moreover, the magnitude of the off-diagonal transfer functions at low frequencies is much higher for both cases in Figure 5.17 than in Figure 5.16.

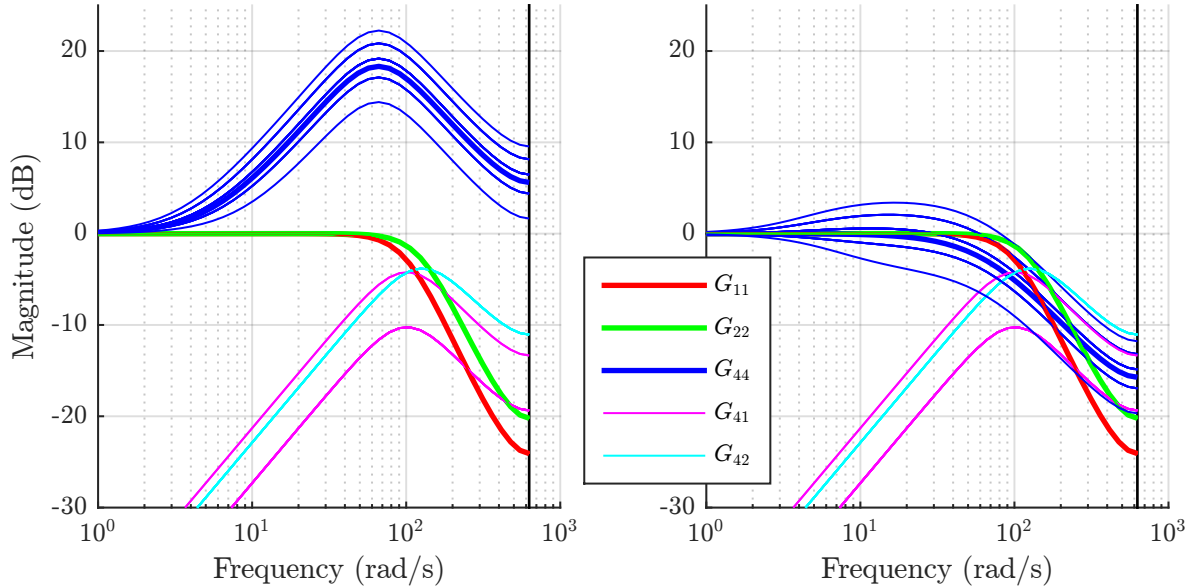


Figure 5.17: Bode magnitude plot of the normalized transfer matrix \tilde{G}_f at different expansion points (static approach)

Overall this discussion should justify the filter design in (5.35) and justify the consideration of the dynamic model (5.34) for the present case. For other quadcopters with smaller ratios Θ_P/κ_T or less aggressively tuned multicopters like the previously discussed tricopter, however, the situation can be different.

5.4 State estimation

The rigid body controller requires the current rigid body state (position, velocity, attitude and angular velocity) and the assumed offset force and torque. The subject of this section is the estimation of these values based on the available measurements from IMU and motion capturing system.

Rigid body dynamics. The rigid body attitude may be parameterized by a unit quaternion $\mathbf{q} = [q_w, q_x, q_y, q_z] \in \mathbb{S}^3$ which allows for a more efficient implementation of the microcontroller and is pretty common in this field. The corresponding kinematics may be derived as proposed in section 2.1. Furthermore, using the velocity coefficients $\dot{\mathbf{r}}$ w.r.t. the reference frame, the rigid body dynamics are

$$m(\ddot{\mathbf{r}} - \mathbf{a}_G) + d\dot{\mathbf{r}} = \mathbf{R}_{\text{quat}}(\mathbf{q})(\mathbf{F} + \mathbf{F}_B) \quad (5.44a)$$

$$\dot{\mathbf{q}} = \mathbf{A}_{\text{quat}}(\mathbf{q})\boldsymbol{\omega}, \quad \boldsymbol{\Theta}\dot{\boldsymbol{\omega}} + \text{wed}(\boldsymbol{\omega})\boldsymbol{\Theta}\boldsymbol{\omega} = \boldsymbol{\tau} + \boldsymbol{\tau}_B \quad (5.44b)$$

with

$$\mathbf{R}_{\text{quat}}(\mathbf{q}) = \begin{bmatrix} 1 - 2(q_y^2 + q_z^2) & 2(q_y q_x - q_w q_z) & 2(q_z q_x + q_w q_y) \\ 2(q_y q_x + q_w q_z) & 1 - 2(q_x^2 + q_z^2) & 2(q_y q_z - q_w q_x) \\ 2(q_z q_x - q_w q_y) & 2(q_y q_z + q_w q_x) & 1 - 2(q_x^2 + q_y^2) \end{bmatrix} \quad (5.44c)$$

$$\mathbf{A}_{\text{quat}}(\mathbf{q}) = \frac{1}{2} \begin{bmatrix} -q_x & -q_y & -q_z \\ q_w & -q_z & q_y \\ q_z & q_w & -q_x \\ -q_y & q_x & q_w \end{bmatrix} \quad (5.44d)$$

IMU measurements. The VECTORNAV VN100S contains a 3-axis accelerometer, gyroscope and magnetometer connected to microcontroller which implements an extended Kalman filter to estimate the attitude quaternion and gyroscope biases. While the attitude estimate is used for outdoor applications with the multicopter, it is not used here, as in the lab the more precise estimate from the motion capturing system available.

Gyroscope and accelerometer measure the *inertial* angular velocity and acceleration. While for tactical and navigation grade IMUs the angular velocity of the Earth is an integral part of the navigation algorithms, see e.g. [Savage, 1998], for the consumer grade IMU here, it cannot be distinguished from the reminiscent bias in gyroscope. Similarly, the coriolis acceleration on the accelerometer may be ignored and the only external parameter is Earth's gravity \mathbf{a}_G at the current position.

The IMU is mounted to the corresponding multicopter to roughly align with its body fixed frame, more precisely the body fixed frame determined by the reflective markers for the motion capture. We will call the remaining, constant misalignment $\mathbf{R}_B \in \mathbb{SO}(3)$. While the gyroscope bias is compensated, the accelerometer contains a noticeable slowly varying bias $\mathbf{a}_B \in \mathbb{R}^3$. Furthermore, both sensors contain a noticeable noise $\boldsymbol{\omega}_N[k], \mathbf{a}_N[k] \in \mathbb{R}^3$ which is not further investigated here. Overall, with a constant sampling time $T_S = 0.005\text{s}$, we assume the IMU measurements $\boldsymbol{\omega}_M$ and \mathbf{a}_M to be related to the rigid body state by:

$$\boldsymbol{\omega}_M[k] = \mathbf{R}_B \boldsymbol{\omega}(kT_S) + \boldsymbol{\omega}_N[k], \quad (5.45)$$

$$\mathbf{a}_M[k] = \mathbf{R}_B \mathbf{R}^\top(kT_S)(\ddot{\mathbf{r}}(kT_S) - \mathbf{a}_G) + \mathbf{a}_B + \mathbf{a}_N[k]. \quad (5.46)$$

VICON measurements. The VICON motion capturing system measures the position \mathbf{r} and the attitude, reported as quaternion \mathbf{q} , by means of tracking the reflective markers on the multicopters. The reference frame of the system was carefully adjusted to align with gravity using a pendulum with reflective markers.

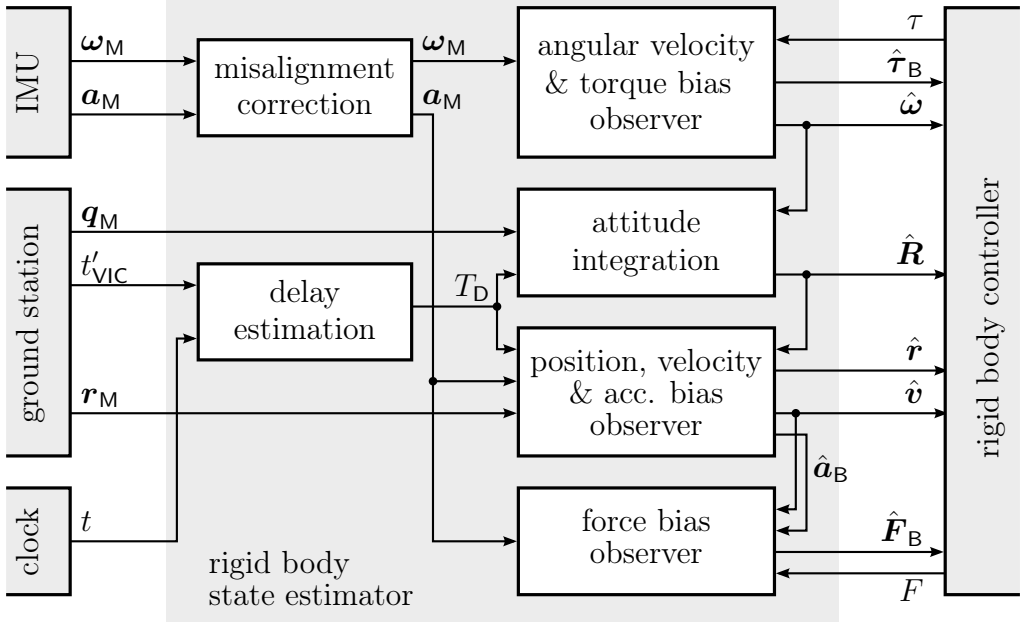


Figure 5.18: Overall structure of the state estimation

In contrast to the IMU measurements, there is no evidence for systematic errors in the measurements for the VICON system. However, their processing and transmission to the multicopter processor results in a substantial latency, i.e. measurements corresponding to time t are available to the controller only after time $t+T_D$. Furthermore, as non-realtime systems are involved, the latency varies slightly. Mostly due to bandwidth limitations on the wireless transmission, the sampling time is only $T_S' = 0.1$ s while the main controller runs at $T_S = 0.005$ s. The measurements \mathbf{r}_M and \mathbf{q}_M are related to the rigid body state by

$$\mathbf{r}_M[k'] = \mathbf{r}(k'T_S' - T_D), \quad \mathbf{q}_M[k'] = \mathbf{q}(k'T_S' - T_D). \quad (5.47)$$

Overall observer design. Instead of designing one large observer, the estimation problem is split into smaller subproblems as illustrated in Figure 5.18. The following subsections will discuss these.

5.4.1 IMU misalignment correction

For a static $\mathbf{x} = \text{const.}$ multicopter the accelerometer model reads

$$\mathbf{a}_M[k] = -\mathbf{R}_B \mathbf{R}^\top \mathbf{a}_G + \mathbf{a}_B + \mathbf{a}_N[k]. \quad (5.48)$$

Here we are interested in the value \mathbf{R}_B , but for the estimation proposed here we also need to estimate the accelerometer bias \mathbf{a}_N . For a short time measurement ($\Delta t < 10$ min) it can be assumed to be constant. Taking into account that the reference frame was carefully aligned, and the official gravitation value for Saarland, we have $\mathbf{a}_G = [0, 0, -9.8107]^\top \frac{\text{m}}{\text{s}^2}$.

The multicopter is placed in different random orientations while the accelerometer measurements \mathbf{a}_M and the attitude \mathbf{R} is recorded. To compensate the noise $\mathbf{a}_N[k]$ we take the mean value $\bar{\mathbf{a}}_M$ over 10 s. For each measurement with index i and different attitudes $\mathbf{R}[i]$ we have the mean accelerometer measurement $\bar{\mathbf{a}}_M[i]$. With this, we estimate the values for misalignment \mathbf{R}_B and bias \mathbf{a}_B as the ones that minimize the sum over the squared errors of the experiments:

$$\mathcal{J}(\mathbf{R}_B, \mathbf{a}_B) = \frac{1}{2} \sum_i \|\bar{\mathbf{a}}_M[i] + \mathbf{R}_B \bar{\mathbf{R}}^\top[i] \mathbf{a}_G + \mathbf{a}_B\|^2 \quad (5.49)$$

Note that this minimization problem is mathematically identical to the one considered in subsection 3.3.4.

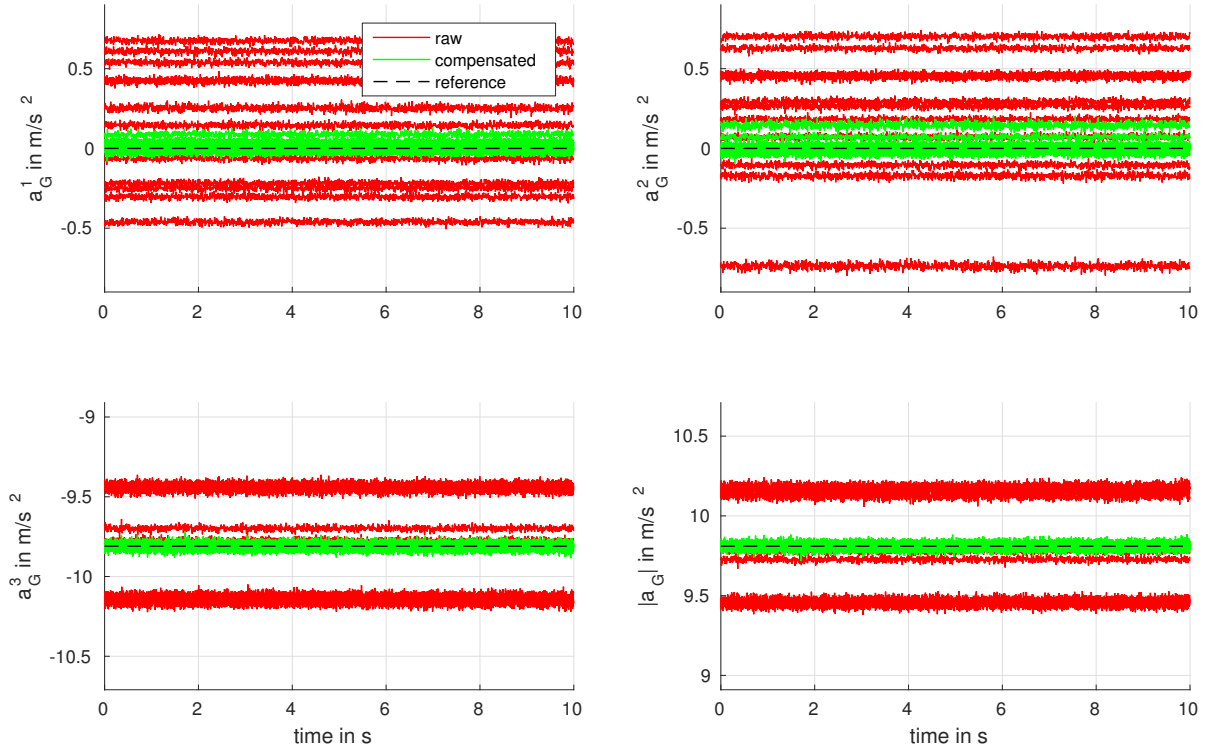


Figure 5.19: Accelerometer measurements and identification result

For validation Figure 5.19 displays the measured gravity coefficients \mathbf{a}_G within the 20 experiments with different orientations. The red lines are the raw measurements $\mathbf{a}_G = \mathbf{R}_M \mathbf{a}_M$, the green lines incorporate the identified values $\mathbf{a}_G = \mathbf{R}_M \mathbf{R}_B (\mathbf{a}_M + \mathbf{a}_B)$ and the black line is the reference value $\mathbf{a}_G = [0, 0, -9.81]^\top$. Most notably one can see that even the magnitude $\|\mathbf{a}_G\|$ of the raw acceleration is off by about 5% for some experiments whereas the compensated values are all within a window of about 0.2%.

5.4.2 Angular velocity and torque bias

Recall the mechanical model of the angular velocity $\boldsymbol{\omega}$, disturbance torque $\boldsymbol{\tau}_B$ and gyroscope $\boldsymbol{\omega}_M$ motivated above:

$$\boldsymbol{\Theta} \dot{\boldsymbol{\omega}} + \text{wed}(\boldsymbol{\omega}) \boldsymbol{\Theta} \boldsymbol{\omega} = \boldsymbol{\tau} + \boldsymbol{\tau}_B, \quad \dot{\boldsymbol{\tau}}_B = \mathbf{0}, \quad \boldsymbol{\omega}_M = \boldsymbol{\omega} + \boldsymbol{\omega}_N. \quad (5.50)$$

The input torque τ is known as discussed in section 5.3.

The multicopters implement a simple Luenberger observer based on the forward Euler discretization and scalar gains L_ω, L_τ :

$$\hat{\omega}[k+1] = \hat{\omega}[k] + T_S \Theta^{-1} (\tau[k] + \hat{\tau}_B[k] - \text{wed}(\hat{\omega}[k]) \Theta \hat{\omega}[k]) + L_\omega (\omega_M[k] - \hat{\omega}[k]) \quad (5.51a)$$

$$\hat{\tau}_B[k+1] = \hat{\tau}_B[k] + L_\tau (\omega_M[k] - \hat{\omega}[k]). \quad (5.51b)$$

In practice, the gains $L_\omega = 0.2$ and $L_\tau = 0.01$ did yield good results. The disturbance observer here takes the place of the integral controller, as the rigid body controller is "just" a PD controller.

5.4.3 Configuration measurement latency

The configuration measurement $(\mathbf{r}_M, \mathbf{q}_M)$ is done by a VICON motion capturing system. This measurement relies on the optical tracking of reflective markers fixed on the multicopters by infrared cameras mounted at the walls of the lab and connected to the ground station, a Windows 7 PC. The groundstation software is written in MATLAB. It runs a timer at $T'_S = 0.1$ ms which reads the measurement, validates and forwards it to the xBee radio module. Finally, the multicopter microcontroller receives the measurements through its radio module. The radio module also handles other transmissions like receiving commands and sending measurements to the groundstation.

As a result of this chain of non realtime elements, the latency at which the configuration measurements are available to the multicopter is *not* constant, but varies by several main sampling steps T_S in addition to its average value. Actual timings of these measurements are presented in Figure 5.22 for actual measurements. The estimation of the resulting *variable time delay* $T_D[k']$ is the subject of this subsection.

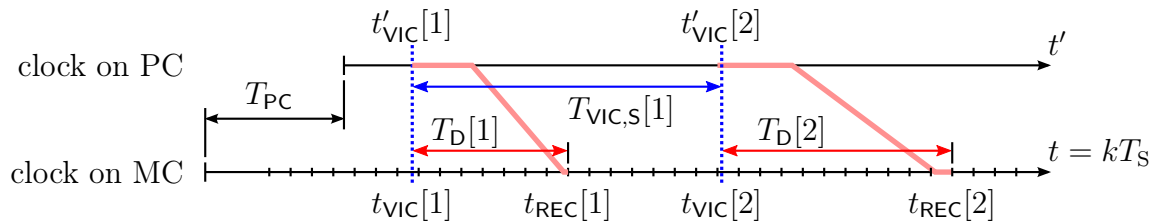


Figure 5.20: Illustration of the measurement time at the PC and when it is available on the microcontroller (MC)

To get an estimate $\hat{T}_D[k']$ for this delay we utilize the clocks on the ground station PC, t' , and the microcontroller, t . The clocks are assumed to be synchronous but have an unknown offset $T_{PC} = t - t' = \text{const.}$ depending on when each device was powered. Figure 5.20 illustrates the time $t'_VIC[k']$ at which a measurement was taken and the time $t_{REC}[k']$ at which it is received/available on the microcontroller. Taking a large enough sample of these times we have the relation

$$\text{mean}(t_{REC}[1, \dots, K'] - t'_VIC[1, \dots, K']) = T_{PC} + \text{mean}(T_D[1, \dots, K']), \quad K' \gg 1. \quad (5.52)$$

Whereas T_{PC} changes whenever the ground station or the microcontroller restarts, the average delay $\bar{T}_D = \text{mean}(T_D[1, \dots, K'])$ remains constant.

Experimental average delay identification. The identification of the average delay \bar{T}_D is done in a dedicated experiment: A multicopter is mounted on an incremental encoder directly connected to the multicopter main processor. It serves as a reference for the yaw-angle and is assumed to have negligible latency. The encoder signal and the yaw-angle from the motion capture system are recorded by the multicopter microcontroller. The experimental data here is about 1 min long and captures about $K' = 600$ VICON frames. Now we can plot the reference encoder angle $\varphi[k]$ at the sampling points $t = kT_S$ and the yaw angle $\varphi_M[k']$ received from the Vicon system at the shifted time $t'_{VICON}[k'] + \text{mean}(t_{REC}[1, \dots, K'] - t'_{VICON}[1, \dots, K'])$. If the previous assumption (5.52) hold these signals should be similar up to a shift of the mean delay \bar{T}_D .

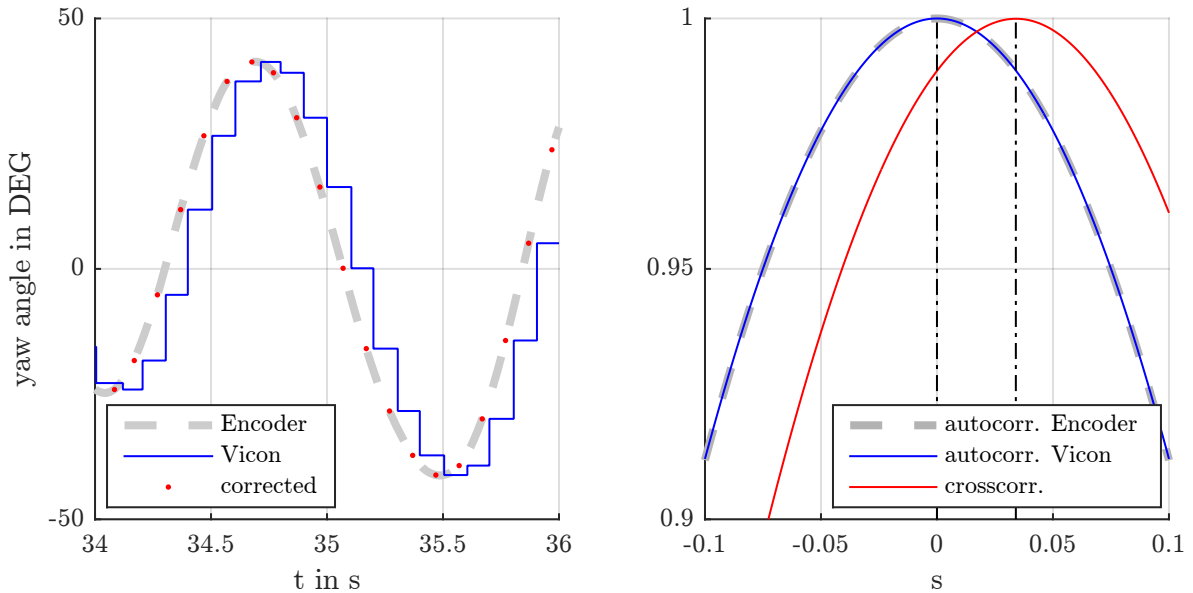


Figure 5.21: A small sample of the yaw-angle measurements (left) and the correlations (right) of the complete 60 s measurements for the identification of the average time delay

Figure 5.21 shows a small sample of the measured yaw angle and the correlations of the two measurements. The identified average delay is where the cross-correlation has its maximum at $\bar{T}_D = 0.034$ s. In order to achieve this resolution the measurements were up-sampled to 1 ms by cubic interpolation.

Clock offset estimation. For the realtime implementation, (5.52) is approximated by a slow ($c_{PC} = 0.99$) low-pass filter

$$\hat{T}_{PC}[k'] = c_{PC}\hat{T}_{PC}[k'-1] + (1 - c_{PC})(t_{REC}[k'] - t'_{VICON}[k'] - \bar{T}_D) \quad (5.53)$$

yielding the estimate \hat{T}_{PC} for the constant clock offset T_{PC} . Finally, the estimated delay of the k' -th Vicon measurement is

$$\hat{T}_D[k'] = t_{REC}[k'] - (t'_{VICON}[k'] + \hat{T}_{PC}[k']). \quad (5.54)$$

Figure 5.22 shows the estimated clock offset \hat{T}_{PC} and the resulting estimated delay \hat{T}_D for the previous example measurement.

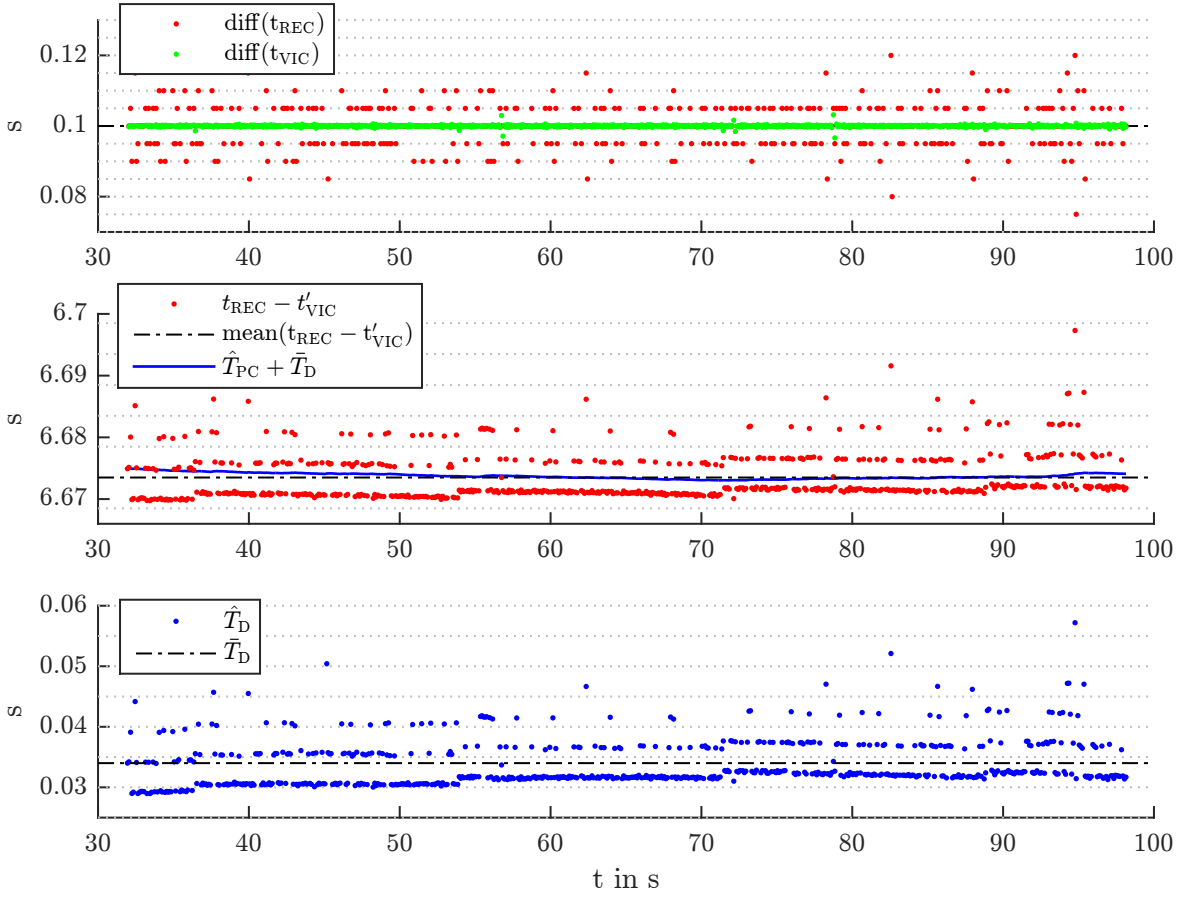


Figure 5.22: Measured timings

5.4.4 Attitude integration

Once the latency $\hat{T}_{\text{D}}[k']$ of the attitude measurement \mathbf{q}_M is known, the current attitude is simply integrated based on buffered angular velocity measurements. The quaternion kinematics (5.44) supplemented with a stabilization term for the constraint $\mathbf{q} \in \mathbb{S}^3$, as motivated in section A.2, reads

$$\underbrace{\frac{d}{dt} \begin{bmatrix} q_w \\ q_x \\ q_y \\ q_z \end{bmatrix}}_{\mathbf{q}} = \underbrace{\frac{1}{2} \begin{bmatrix} -q_x & -q_y & -q_z \\ q_w & -q_z & q_y \\ q_z & q_w & -q_x \\ -q_y & q_x & q_w \end{bmatrix}}_{\mathbf{A}_{\text{quat}}(\mathbf{q})} \underbrace{\begin{bmatrix} \omega_x \\ \omega_y \\ \omega_z \end{bmatrix}}_{\boldsymbol{\omega}} - \underbrace{\frac{1}{2} \begin{bmatrix} q_w \\ q_x \\ q_y \\ q_z \end{bmatrix}}_{\left(\frac{\partial \phi}{\partial \mathbf{q}} \right)^+} \lambda \underbrace{(\|\mathbf{q}\|^2 - 1)}_{\phi(\mathbf{q})}. \quad (5.55)$$

The actual implementation uses the forward Euler discretization with the stabilization gain $\lambda = 2/T_S$, i.e.

$$\mathbf{q}[k+1] = \mathbf{q}[k] + T_S \mathbf{A}_{\text{quat}}(\mathbf{q}[k]) \boldsymbol{\omega}[k] - (\|\mathbf{q}[k]\|^2 - 1) \mathbf{q}[k]. \quad (5.56)$$

Note that with this particular gain the stabilization coincides with the 1st order Taylor expansion of the normalization $\mathbf{q}/\|\mathbf{q}\| \approx \mathbf{q} - (\|\mathbf{q}\|^2 - 1)\mathbf{q}$ for $\|\mathbf{q}\| \approx 1$. In contrast to the exact normalization, the approximation avoids the expensive computation of a square root and division.

5.4.5 Position, velocity and accelerometer bias

For the translational dynamics we have a similar situation as for the attitude kinematics: We have an accurate but low sampled and delayed position measurement \mathbf{r}_M and a biased and noisy measurement of the acceleration \mathbf{a}_M . From this we want to estimate the current position \mathbf{r} and velocity $\dot{\mathbf{r}}$ required for the controller implementation.

The differential relation between position and accelerometer measurement is given in (5.45). For the following we assume a constant bias $\dot{\mathbf{a}}_B = \mathbf{0}$ and drop the noise term $\mathbf{a}_N = \mathbf{0}$. Furthermore, the IMU misalignment has already been corrected, i.e. $\mathbf{R}_B = \mathbf{I}_3$. Introducing the state $\mathbf{z} = [\mathbf{r}^\top, \dot{\mathbf{r}}^\top, \mathbf{a}_B^\top]^\top \in \mathbb{R}^9$ we may write

$$\underbrace{\frac{d}{dt} \begin{bmatrix} \mathbf{r} \\ \dot{\mathbf{r}} \\ \mathbf{a}_B \end{bmatrix}}_{\mathbf{z}} = \underbrace{\begin{bmatrix} 0 & \mathbf{I}_3 & 0 \\ 0 & 0 & -\mathbf{R} \\ 0 & 0 & 0 \end{bmatrix}}_A \begin{bmatrix} \mathbf{r} \\ \dot{\mathbf{r}} \\ \mathbf{a}_B \end{bmatrix} + \underbrace{\begin{bmatrix} 0 \\ \mathbf{I}_3 \\ 0 \end{bmatrix}}_B (\mathbf{a}_G + \mathbf{R}\mathbf{a}_M), \quad \mathbf{r}_M = \underbrace{[\mathbf{I}_3, \mathbf{0}, \mathbf{0}]}_C \begin{bmatrix} \mathbf{r} \\ \dot{\mathbf{r}} \\ \mathbf{a}_B \end{bmatrix} \quad (5.57)$$

Estimator implementation. The implemented estimation algorithm on the microcontroller works as follows: After having received 2 subsequent position measurements $\mathbf{r}_M[1]$, $\mathbf{r}_M[2]$ and their reconstructed time $t_{VIC}[1]$, $t_{VIC}[2]$ with $T'_S[1] = t_{VIC}[2] - t_{VIC}[1]$ we set the initial value for the estimator state $\hat{\mathbf{z}} = [\hat{\mathbf{r}}^\top, \hat{\dot{\mathbf{r}}}^\top, \hat{\mathbf{a}}_B^\top]^\top$ as

$$\hat{\mathbf{r}}(t_{VIC}[2]) = \mathbf{r}_M[2], \quad \hat{\dot{\mathbf{r}}}(t_{VIC}[2]) = \frac{\mathbf{r}_M[2] - \mathbf{r}_M[1]}{T'_S[1]} \quad \mathbf{a}_B(t_{VIC}[2]) = \mathbf{0}. \quad (5.58)$$

Then we use the zero order hold discretization of (5.57) to integrate the current state based on (ring) buffered accelerometer measurements \mathbf{a}_M and estimated attitudes $\hat{\mathbf{R}}$:

$$\underbrace{\begin{bmatrix} \hat{\mathbf{r}}[k+1] \\ \hat{\dot{\mathbf{r}}}[k+1] \\ \hat{\mathbf{a}}_B[k+1] \end{bmatrix}}_{\hat{\mathbf{z}}[k+1]} = \underbrace{\begin{bmatrix} \mathbf{I}_3 & T_S \mathbf{I}_3 & -\frac{T_S^2}{2} \hat{\mathbf{R}}[k] \\ 0 & \mathbf{I}_3 & -T_S \hat{\mathbf{R}}[k] \\ 0 & 0 & \mathbf{I}_3 \end{bmatrix}}_{\hat{\mathbf{A}}_S[k]} \underbrace{\begin{bmatrix} \hat{\mathbf{r}}[k] \\ \hat{\dot{\mathbf{r}}}[k] \\ \hat{\mathbf{a}}_B[k] \end{bmatrix}}_{\hat{\mathbf{z}}[k]} + \underbrace{\begin{bmatrix} \frac{T_S^2}{2} \mathbf{I}_3 \\ T_S \mathbf{I}_3 \\ 0 \end{bmatrix}}_{\hat{\mathbf{B}}_S} (\mathbf{a}_G + \hat{\mathbf{R}}[k] \mathbf{a}_M[k]) \quad (5.59)$$

Note that the measurement time $t_{VIC}[2]$ usually does not coincide with a sampling step, see Figure 5.20. Consequently the value T_S in (5.59) has to be adjusted to match the time from the initial value to the subsequent sampling step.

After this initial procedure, (5.59) is computed once every sampling step with the most recent accelerometer measurement $\mathbf{a}_M[k]$ yielding the most recent predictions for the position and velocity. The position estimates $\hat{\mathbf{r}}[k]$ for the last 64 sampling steps are stored in a ring buffer.

When a new configuration measurement $(\mathbf{r}_M[k'], \mathbf{R}_M[k'])$ and its timestamp $t_{VIC}[k']$ are available, the corresponding estimate $\hat{\mathbf{r}}(t_{VIC}[k'])$ is interpolated. This is used to correct the estimate at the measurement time $t_{VIC}[k']$ with yet to define gains $\mathbf{L}_r, \mathbf{L}_v, \mathbf{L}_a \in \mathbb{R}^{3 \times 3}$:

$$\underbrace{\begin{bmatrix} \hat{\mathbf{r}}(t_{VIC}[k']) \\ \hat{\dot{\mathbf{r}}}(t_{VIC}[k']) \\ \hat{\mathbf{a}}_B(t_{VIC}[k']) \end{bmatrix}}_{\hat{\mathbf{z}}(t_{VIC}[k'])} \leftarrow \underbrace{\begin{bmatrix} \hat{\mathbf{r}}(t_{VIC}[k']) \\ \hat{\dot{\mathbf{r}}}(t_{VIC}[k']) \\ \hat{\mathbf{a}}_B(t_{VIC}[k']) \end{bmatrix}}_{\hat{\mathbf{z}}(t_{VIC}[k'])} + \underbrace{\begin{bmatrix} \mathbf{L}_r[k'] \\ \mathbf{L}_v[k'] \\ \mathbf{L}_a[k'](\mathbf{R}_M[k'])^\top \end{bmatrix}}_{\mathbf{L}[k']} (\mathbf{r}_M[k'] - \hat{\mathbf{r}}(t_{VIC}[k'])). \quad (5.60)$$

Finally, the state estimate for current time is again integrated from (5.59).

Error dynamics and tuning. To chose reasonable correction gains \mathbf{L}_r , \mathbf{L}_v and \mathbf{L}_a we investigate the resulting error dynamics of the estimation algorithm above. Assuming the attitude is constant and perfectly known $\hat{\mathbf{R}} = \mathbf{R}$ the matrix A in the continuous model (5.57) is constant and is denoted by $\bar{\mathbf{A}}$.

From measurement time $t_{\text{VIC}}[k']$ till the next one at $t_{\text{VIC}}[k'+1]$ there are several prediction steps (5.59): The first from the measurement time till the subsequent sampling step with integration time T_l . Then several steps with integration time T_S till the sampling step before $t_{\text{VIC}}[k'+1]$, and finally a step integration time T_F till $t_{\text{VIC}}[k'+1]$. Overall this results in the dynamic matrix

$$\bar{\mathbf{A}}'_S = \exp(\bar{\mathbf{A}} T_l) \exp(\bar{\mathbf{A}} T_S) \cdots \exp(\bar{\mathbf{A}} T_S) \exp(\bar{\mathbf{A}} T_F) = \exp(\bar{\mathbf{A}} T'_S), \quad (5.61)$$

where $T'_S[k'] = T_l[k'] + T_S + \dots + T_S + T_F[k'] = t_{\text{VIC}}[k'] - t_{\text{VIC}}[k'-1]$.

Finally, adding one correction step (5.60) and subtracting the estimator from the discretization of the model (5.57), we obtain the relation for the error $\mathbf{e} = \mathbf{z} - \hat{\mathbf{z}}$ for one correction/measurement cycle from $t_{\text{VIC}}[k']$ to the next one at $t_{\text{VIC}}[k'+1]$ as

$$\mathbf{e}(t_{\text{VIC}}[k'+1]) = \underbrace{(\mathbf{I}_9 - \bar{\mathbf{L}}[k']\mathbf{C})\bar{\mathbf{A}}'_S[k']\mathbf{e}(t_{\text{VIC}}[k'])}_{\bar{\mathbf{A}}'_e[k']} \quad (5.62)$$

where

$$\bar{\mathbf{A}}_e[k'] = \begin{bmatrix} \mathbf{I}_3 - \mathbf{L}_r[k'] & T'_S(\mathbf{I}_3 - \mathbf{L}_r[k']) & \frac{(T'_S[k'])^2}{2}(\mathbf{L}_r[k'] - \mathbf{I}_3)\bar{\mathbf{R}} \\ -\mathbf{L}_v[k'] & \mathbf{I}_3 - T'_S[k']\mathbf{L}_v[k'] & T_S(\frac{T'_S[k']}{2}\mathbf{L}_v[k'] - \mathbf{I}_3)\bar{\mathbf{R}} \\ -\mathbf{L}_a[k']\bar{\mathbf{R}}^\top & -T'_S[k']\mathbf{L}_a[k']\bar{\mathbf{R}}^\top & \mathbf{I}_3 + \frac{T'_S[k']^2}{2}\mathbf{L}_a[k'] \end{bmatrix} \quad (5.63)$$

Scaling the gains with the variable integration time $T'_S[k']$ between two correction steps as

$$\mathbf{L}_r[k'] = l_r \mathbf{I}_3, \quad \mathbf{L}_v[k'] = \frac{l_v}{T'_S[k']} \mathbf{I}_3, \quad \mathbf{L}_a[k'] = \frac{2l_a}{(T'_S[k'])^2} \quad (5.64)$$

yields the characteristic polynomial with constant coefficients

$$\det(\lambda \mathbf{I}_9 - \bar{\mathbf{A}}'_e[k']) = \left(\lambda^3 + (l_r + l'_v - l'_a - 3)\lambda^2 + (3 - 2l_r - l'_v - l'_a)\lambda + l_r - 1 \right)^3. \quad (5.65)$$

However, it should be noted here that constant eigenvalues of the time varying matrix $\bar{\mathbf{A}}'_e[k']$ can not conclude stability of the time-varying system.

In practice the eigenvalues $\text{eig}(\bar{\mathbf{A}}'_e) = \{0, 0.5, 0.9\}$ and the resulting gains $l_r = 1$, $l_v = 0.575$, $l_a = -0.025$ did result in quite good estimation performance. These rather fast eigenvalues also reflect a high confidence in the position measurement.

5.4.6 Force bias

Combining the translational multicopter model (5.44) and the accelerometer model (5.45), we may write

$$\mathbf{F}_B = m(\mathbf{a}_M - \mathbf{a}_N - \mathbf{a}_B) + d\mathbf{R}^\top \dot{\mathbf{r}} - \mathbf{F}. \quad (5.66)$$

From the previous sections we have estimates for the all quantities on the right hand side except the measurement noise \mathbf{a}_N . This motivates a simple low-pass to obtain the estimate $\hat{\mathbf{F}}_B$ for the force bias

$$\hat{\mathbf{F}}_B[k+1] = l_F \hat{\mathbf{F}}_B[k] + (1 - l_F) (m(\mathbf{a}_M[k] - \hat{\mathbf{a}}_B[k]) + d(\hat{\mathbf{R}}[k])^\top \hat{\mathbf{r}}[k] - \hat{\mathbf{F}}[k]). \quad (5.67)$$

In practice the low-pass gain $l_F = 0.98$ did yield reasonable results.

5.5 Reference generation

There are two ways for the user to interact with the multicopters: With a two joystick remote control (RC) or by sending various commands from the ground station PC. For each approach we need to generate reasonable reference values $(\mathbf{r}_R, \mathbf{R}_R, \mathbf{v}_R, \boldsymbol{\omega}_R, \dot{\mathbf{v}}_R, \dot{\boldsymbol{\omega}}_R)[k]$ for the multicopter controller.

Euler angles and flat output. For the vast majority of multicopter maneuvers it is tilted less than 45° , so a minimal parameterization with singularities outside this working domain is tolerable. A very popular parameterization for the rigid body attitude are the Euler angles in the roll-pitch-yaw convention $\boldsymbol{\varepsilon} = [\alpha, \beta, \varphi]^\top$:

$$\mathbf{R}(\boldsymbol{\varepsilon}) = \begin{bmatrix} c_\varphi c_\beta & -s_\varphi c_\alpha + c_\varphi s_\beta s_\alpha & s_\varphi s_\alpha + c_\varphi s_\beta c_\alpha \\ s_\varphi c_\beta & c_\varphi c_\alpha + s_\varphi s_\beta s_\alpha & -c_\varphi s_\alpha + s_\varphi s_\beta c_\alpha \\ -s_\beta & c_\beta s_\alpha & c_\beta c_\alpha \end{bmatrix}, \quad \boldsymbol{\omega}(\boldsymbol{\varepsilon}, \dot{\boldsymbol{\varepsilon}}) = \begin{bmatrix} \dot{\alpha} - s_\beta \dot{\varphi} \\ c_\beta s_\alpha \dot{\varphi} + c_\alpha \dot{\beta} \\ c_\beta c_\alpha \dot{\varphi} - s_\alpha \dot{\beta} \end{bmatrix} \quad (5.68)$$

previously discussed in section 1.2.

As the tricopter is fully actuated, any minimal parameterization of its configuration space is a flat output. One such parametrization is $\mathbf{y} = (r_x, r_y, r_z, \alpha, \beta, \varphi)$.

For the quadcopter, flatness was already discussed in subsection 4.8.3. A reasonable flat output is $\mathbf{y} = (r_x, r_y, r_z, \varphi)$. The remainder of the attitude is then computed from the translational dynamics as

$$\mathbf{R}_z = \frac{\ddot{\mathbf{r}} - \mathbf{a}_G}{\|\ddot{\mathbf{r}} - \mathbf{a}_G\|}, \quad \alpha = \arcsin(c_\varphi R_z^y - s_\varphi R_z^x), \quad \beta = \text{atan2}(c_\varphi R_z^x + s_\varphi R_z^y, R_z^z). \quad (5.69)$$

From these relations its clear that a feasible reference trajectory $t \mapsto \mathbf{r}_R(t)$ for the position must be 4 times differentiable in order to compute the reference trajectory $t \mapsto \dot{\boldsymbol{\omega}}_R(t)$ for the angular acceleration. The singularity for $\ddot{\mathbf{r}} = \mathbf{a}_G$, is practically not realizable, since the propellers have a minimum thrust, i.e. free fall is not feasible.

Real-time trajectory generator. The multicopter firmware includes a real-time trajectory generator for the corresponding flat output discussed above. It knows the current reference $\mathbf{y}_R(t), \dots, \mathbf{y}_R^{(4)}(t)$ and when receiving a new static setpoint $\mathbf{y}_R(t+T) = \text{const.}$, with a given transition time T , it computes and evaluates the interpolating polynomials of sufficient degree. The actual reference values $(\mathbf{r}_R, \mathbf{R}_R, \mathbf{v}_R, \boldsymbol{\omega}_R, \dot{\mathbf{v}}_R, \dot{\boldsymbol{\omega}}_R)[k]$ for the main rigid body controller are computed from (5.69), (5.68) and their derivatives.

The set points are the standard command interface for the multicopter GUI on the ground-station PC. The results in Figure 5.24 and Figure 5.25 which are discussed in the next section utilized these trajectories.

Precomputed position trajectories. For specific maneuvers it's also possible to execute a precomputed, sampled position trajectory $k \mapsto \mathbf{r}_R[k]$ stored on the multicopter controller. For the tricopter, the attitude is held constant during the maneuver. This mode was used for the experimental results in [Irscheid et al., 2019].

Analog to this, for the quadcopter, we could hold the yaw angle constant. However, this mode is used for aerobatic maneuvers where the singularities of the Euler angles are unacceptable. Also, as discussed in [Konz and Rudolph, 2013], the hairy ball theorem [Brouwer, 1912] implies that any flat output of the quadcopter model must have a singularity somewhere. On the other hand, we usually do not care too much about the actual heading of the copter, but only want it to be somewhat steady about this degree of freedom.

So instead of parameterizing the heading we use the angular velocity ω_{zR} and *integrate* the remaining attitude from:

$$\mathbf{R}_{zR} = \frac{\ddot{\mathbf{r}}_R - \mathbf{a}_G}{\|\ddot{\mathbf{r}}_R - \mathbf{a}_G\|}, \quad \dot{\mathbf{R}}_{zR} = \frac{\mathbf{r}_R^{(3)} - \langle \mathbf{r}_R^{(3)}, \mathbf{R}_{zR} \rangle \mathbf{R}_{zR}}{\|\ddot{\mathbf{r}}_R - \mathbf{a}_G\|}, \quad (5.70a)$$

$$\dot{\mathbf{R}}_{xR} = \omega_{zR} \mathbf{R}_{yR} - \omega_{yR} \mathbf{R}_{zR}, \quad \omega_{yR} = \mathbf{R}_{xR}^\top \dot{\mathbf{R}}_{zR} \quad (5.70b)$$

$$\dot{\mathbf{R}}_{yR} = \omega_{xR} \mathbf{R}_{zR} - \omega_{zR} \mathbf{R}_{xR}, \quad \omega_{xR} = -\mathbf{R}_{yR}^\top \dot{\mathbf{R}}_{zR}. \quad (5.70c)$$

This trajectory generation mode with $\omega_{zR} = 0$ was used for the quadcopter looping (Figure 5.26) and the quadcopter flip experiment (Figure 5.27).

Remote control mode. In this mode the position measurements are not available or not used, e.g. in outdoor experiments. Instead a human pilot is tasked with controlling the multicopter with a two joystick remote control (RC).

The parameters of the rigid body controller, see chapter 4, are set as follows: The desired inertia coincides with the model inertia, i.e. $\bar{m} = m$, $\bar{\Theta} = \Theta$, $\bar{s} = \mathbf{0}$. The center of damping and stiffness coincides with the center of mass $\bar{l} = \bar{h} = \mathbf{0}$. As previously discussed in subsection 4.7.5, this decouples the rotational part of the closed loop dynamics. As the pilot is charged with controlling the position, we set vanishing translational stiffness $\bar{k} = 0$ and damping $\bar{d} = 0$. For the particle based approach (see subsection 4.1.2) this results in the trivial closed loop dynamics $\ddot{\mathbf{r}} = \ddot{\mathbf{r}}_R$ and the translational part of the explicit control law reads

$$\mathbf{F} = m \mathbf{R}^\top (\ddot{\mathbf{r}}_R - \mathbf{a}_G) \quad (5.71)$$

Unfortunately, for the body-based and energy based approaches, terms with $\mathbf{r} - \mathbf{r}_R$ and $\dot{\mathbf{r}} - \dot{\mathbf{r}}_R$ still appear in gyroscopic terms. For the actual microcontroller implementation these terms were simply set to zero which ultimately implies the same translational control as for the particle based approach (5.71).

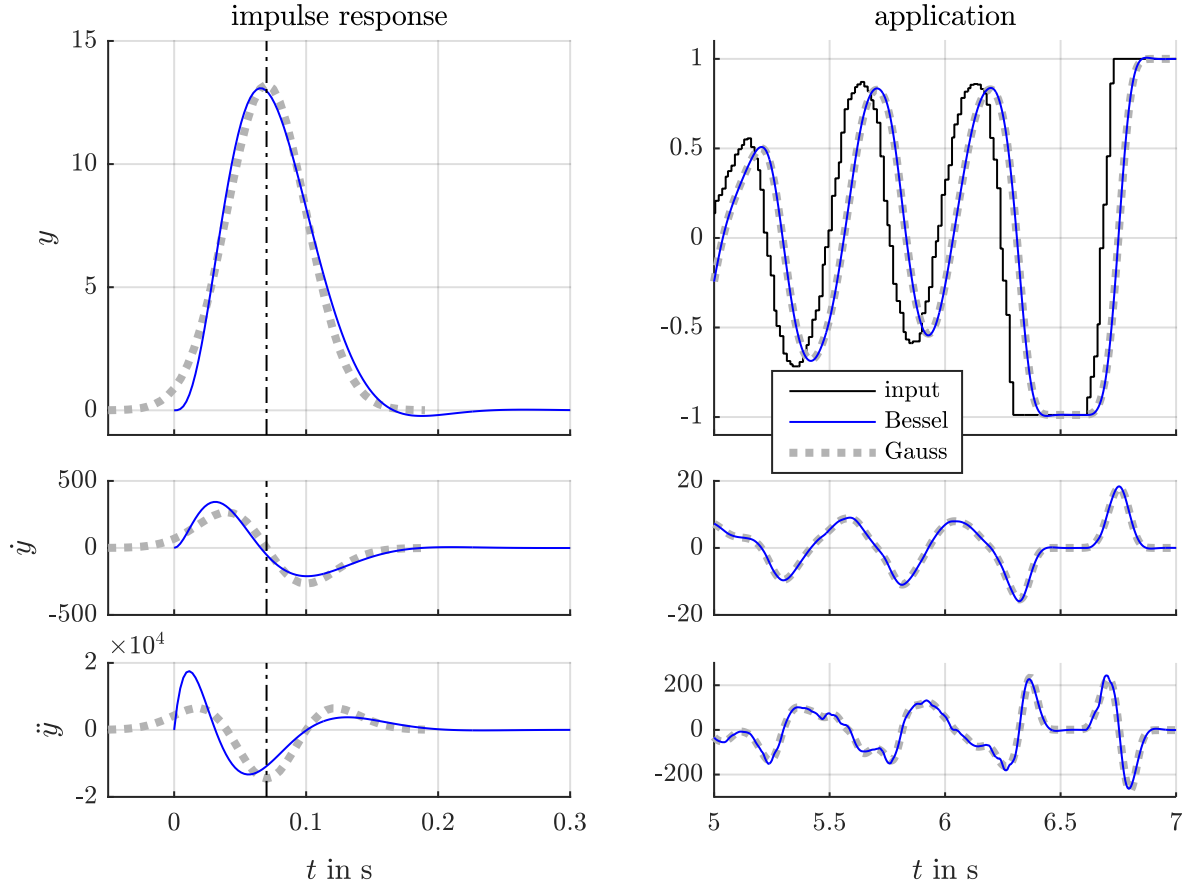


Figure 5.23: Application of the filter to the RC input

In practice, the forward direction of the multicopter is more intuitive to a pilot than the e.g. the north directions. With similar arguments [Kastelan et al., 2015] proposes the use of a heading referenced acceleration $\mathbf{a}_R = \mathbf{R}_Z^\top(\varphi_R)\ddot{\mathbf{r}}_R$ which is used in the following as well. Furthermore, its practical to set the yaw rate $\dot{\varphi}_R$ and integrate the angle within the controller. Overall, the analog channels of the RC are associated with the the reference quantities $(a_{xR}, a_{yR}, a_{zR}, \alpha_R, \beta_R, \dot{\varphi}_R)$ for the tricopter and $(a_{xR}, a_{yR}, a_{zR}, \dot{\varphi}_R)$ for the quadcopter.

In order to smoothen the RC signals u_{RC} and obtain the required derivatives at the same time we utilize a simple low pass filter

$$\frac{d}{dt} \begin{bmatrix} y_{RC} \\ \dot{y}_{RC} \\ \ddot{y}_{RC} \\ y_{RC}^{(3)} \end{bmatrix} = \begin{bmatrix} 0 & 1 & 0 & 0 \\ 0 & 0 & 1 & 0 \\ 0 & 0 & 0 & 1 \\ -a_0 & -a_1 & -a_2 & -a_3 \end{bmatrix} \begin{bmatrix} y_{RC} \\ \dot{y}_{RC} \\ \ddot{y}_{RC} \\ y_{RC}^{(3)} \end{bmatrix} + \begin{bmatrix} 0 \\ 0 \\ 0 \\ a_0 \end{bmatrix} u_{RC} \quad (5.72)$$

The filter coefficients a_i are chosen to resemble a (continuous) Bessel filter with cutoff frequency 7 Hz, see e.g. [Tietze and Schenk, 1999, sec. 13.1.3]. A Bessel filter is characterized by having a maximally flat group delay, i.e. it preserves the (time-domain) shape of the signal in the passband (opposed to a Butterworth filter which preserves the amplitude in the frequency domain). With rising order the (IIR) Bessel filter converges to a (FIR) Gaussian filter [Rabiner and Gold, 1975, sec. 4.9.2].

The actual implementation is the exact discretization of (5.72). Figure 5.23 shows the impulse response and application to a measured example RC-channel of the used Bessel filter and a corresponding Gaussian filter (window length 43). Even though the difference is visible on the impulse response, the result of the implemented filter and the Gauss filter are indistinguishable in the practical application.

5.6 Experimental results

In this section finally discusses results of actual flight tests. The task for the experiments is to track different reference trajectories while using the same controller and parameter values. As the tracking errors for the following experiments were small, there was no distinguishable difference between the particle, body and energy based approaches. The data for the presented figures were recorded while using the body based control approach.

The controller parameters for the following experiments are summarized in Table 5.2. Note that the values for inertia etc. are w.r.t. the body fixed frame and not w.r.t. the (closed loop) center of mass as done in subsection 4.8.3. Consequently the some values differ from what the matching conditions in (4.148) would suggest.

Error quantization. In order to quantify the tracking performance we use the scalar quantities

$$e_r = \|\hat{\mathbf{r}} - \mathbf{r}_R\|, \quad (5.73a)$$

$$e_R = \cos^{-1} \left(\frac{1}{2} (\text{tr } \mathbf{R}_E - 1) \right), \quad \mathbf{R}_E = \mathbf{R}_R^\top \hat{\mathbf{R}}, \quad (5.73b)$$

$$e_\varphi = |\text{atan2}(R_{xE}^y - R_{yE}^x, R_{xE}^x + R_{yE}^y)|. \quad (5.73c)$$

The position error e_r is the Euclidean distance between estimated position $\hat{\mathbf{r}}$ and its reference \mathbf{r}_R . The attitude error e_R is the angle of the rotation matrix \mathbf{R}_E which rotates the reference attitude \mathbf{R}_R to the estimated attitude $\hat{\mathbf{R}}$. The heading error e_φ is roughly the yaw angle of the error attitude \mathbf{R}_E .

There are two reasons for considering the heading error e_φ in addition to the attitude error e_R : Firstly the copters behave differently for the tilting degree of freedom and the heading. This is also reflected by the different controller parameters for the respective directions. Secondly, for the quadcopter, the tilting is used to compensate a horizontal position error. A horizontal bias force implies a tilt error and consequently an attitude error. Note that there is the relation $e_R \geq e_\varphi$.

To quantify the errors for an experiment containing N sampling steps we use the root-mean-square

$$\text{rms}(e_r) = \sqrt{\frac{1}{N} \sum_{k=1}^N (e_r[k])^2}. \quad (5.74)$$

As an indicator for the dynamic of the reference trajectory for one experiment we consider the maximal velocity

$$\max(\|\mathbf{v}_R\|) = \max (\|\mathbf{v}_R[1]\|, \dots, \|\mathbf{v}_R[N]\|) \quad (5.75)$$

symbol	tricopter value	quadcopter value	comment
T_S		0.005 s	main sampling time
\bar{m}	1.251 kg	1.001 kg	same as model
\bar{s}_z	0 m	0.043 m	center of mass
$\bar{\Theta}_{xx} = \bar{\Theta}_{yy}$	0.0192 kg m ²	0.0095 kg m ²	tilt inertia
$\bar{\Theta}_{zz}$	0.0308 kg m ²	0.0307 kg m ²	same as model
\bar{d}	6 $\frac{\text{kg}}{\text{s}}$	4.4 $\frac{\text{kg}}{\text{s}}$	translation damping
\bar{l}_z	0 m	0.255 m	center of damping
$\bar{T}_{xx} = \bar{T}_{yy}$	0.3 $\frac{\text{kg m}^2}{\text{s}}$	0.4 $\frac{\text{kg m}^2}{\text{s}}$	tilt damping
\bar{T}_{zz}	0.25 $\frac{\text{kg m}^2}{\text{s}}$	0.1 $\frac{\text{kg m}^2}{\text{s}}$	yaw damping
\bar{k}	8 $\frac{\text{kg}}{\text{s}^2}$	8 $\frac{\text{kg}}{\text{s}^2}$	translation stiffness
\bar{h}_z	0 m	0.255 m	center of stiffness
$\bar{I}_{xx} = \bar{I}_{yy}$	1.7 $\frac{\text{kg m}^2}{\text{s}}$	2.6 $\frac{\text{kg m}^2}{\text{s}}$	tilt stiffness
\bar{I}_{zz}	0.7 $\frac{\text{kg m}^2}{\text{s}}$	0.2 $\frac{\text{kg m}^2}{\text{s}}$	yaw stiffness
l_{P1}		0.1	propeller obs. gain 1
l_{P2}		0.01 Hz	propeller obs. gain 2
k_P		0.25	propeller control gain
c_F	0.1		thrust filter param
ω_{mag}		100 $\frac{\text{RAD}}{\text{s}}$	thrust mag. bandwidth
ζ_{mag}		0.707	thrust mag. damp. ratio
ω_{tilt}		125 $\frac{\text{RAD}}{\text{s}}$	tilt torque bandwidth
ζ_{tilt}		0.707	tilt torque damp. ratio
ω_{head}		66 $\frac{\text{RAD}}{\text{s}}$	head. torque bandwidth
L_ω	0.2		ang. vel. obs. gain
L_τ	0.01		torque bias obs. gain
c_{PC}	0.99		clock offset estimator root
l_r	1		pos. obs. fb. gain 1
l_v	0.575		pos. obs. fb. gain 2
l_a	-0.025		pos. obs. fb. gain 3
l_F	0.01		force bias obs. fb. gain

Table 5.2: Parameter values for tri- and quadcopter controller

and in the same way the maximal acceleration $\max(\|\dot{\mathbf{v}}_R\|)$, the maximal angular velocity $\max(\|\omega_R\|)$ and the maximal angular acceleration $\max(\|\dot{\omega}_R\|)$.

The resulting values for the following four experiments are collected in Table 5.3. Evidently, the quadcopter experiments are much more dynamic. This is due to the fact that the quadcopter has a much better thrust to mass and torque to inertia ratio.

	tricopter transitions	quadcopter transitions	quadcopter looping	quadcopter flip
$\max(\ \mathbf{v}_R\)$ in $\frac{\text{m}}{\text{s}}$	2.2	3.4	4.2	2.3
$\max(\ \dot{\mathbf{v}}_R\)$ in $\frac{\text{m}}{\text{s}^2}$	3.9	8.2	17.1	17.5
$\max(\ \omega_R\)$ in $\frac{\text{deg}}{\text{s}}$	318	271	537	736
$\max(\ \dot{\omega}_R\)$ in $\frac{\text{deg}}{\text{s}^2}$	497	1380	1610	2480
$\text{rms}(e_r)$ in m	0.013	0.017	0.027	0.026
$\text{rms}(e_R)$ in deg	1.1	1.3	2.5	2.1
$\text{rms}(e_\varphi)$ in deg	0.95	0.3	1.2	0.8

Table 5.3: Statistical values for the multicopter experiments

Tricopter transitions. Figure 5.24 shows measurements of the tricopter tracking polynomial transitions between constant configurations. A video of this experiment is available here².

In the first 10 s the tricopter does some horizontal movement while maintaining the attitude and height. For the next 10 s it tracks similar trajectories, but this time using the body tilt to generate the necessary horizontal force. The difference between the approaches is obvious in the trajectories for the servo angles for the first case and the roll and pitch angle for the second case. Furthermore a 90° heading transition is added to the last two position transitions. In the last third of the maneuver the tricopter tilts while maintaining its position. One can see that for a body tilt of 15° the servos have to tilt more than 30°. The last transition is a 360° heading rotation and 1 m height transition in 2 s. This is the part where we have the maximal attitude error of about 5°. Here in particular one can see that the heading error e_φ is the major part of the attitude error e_R .

Comparing the performance of this tricopter experiment with the following quadcopter experiments, see Table 5.3, one can see that the tricopter has the lowest position and attitude error. However, the comparison is not really fair since the quadcopter trajectories are much more dynamic.

Quadcopter transitions. Figure 5.25 shows measurements of the quadcopter tracking polynomial transitions between constant configurations. A video of this and the following experiments is available here³.

²<https://youtu.be/oS5PHr6H0K4>

³<https://youtu.be/x66sua3M6RQ>

The reference trajectories are very similar to the previous transitions for the tricopter, but with reduced transitions times. The maximal velocity and acceleration, see Table 5.3, are achieved at about 12 s, for a 2 m horizontal transition in 1.5 s. Since the tilt here is almost 45° it is evident that the acceleration must be almost $\|\mathbf{a}_G\|$. The last transition is a 360° heading rotation in 4 s, which is much slower as the corresponding maneuver for the tricopter due to the limited control torque of the quadcopter. On the other hand the heading error e_φ during this maneuver is much better as with the tricopter. This might be a positive result of the sophisticated thrust controller from section 5.3.

Quadcopter looping. Figure 5.26 shows measurements of the quadcopter tracking four looping trajectories. The reference trajectory for r_x and r_z is essentially a vertical circle with 2 m diameter, see Figure 1.4. The individual looping takes about 3 s from rest to rest.

This is the first maneuver which involves that the quadcopter is upside down, i.e. $\mathbf{R}_{RE_z} = -\mathbf{e}_z$, so an appropriate method for the heading reference generation is required here. Though the accelerations are quite high as well, this experiment has in comparison to the others the highest translational velocity. The fact that it has largest position and attitude errors could suggest that there are large model errors and/or unknown disturbances related to higher translational velocity.

Quadcopter flip. Figure 5.27 shows measurements of the quadcopter tracking six flip trajectories about different axis. A flip is a trajectory where the quadcopter does a 360° tilt transition while trying to minimize translational movement. The maneuver here requires a vertical clearance of less than 1 m and just a few centimeters horizontally. The individual flip takes less than 2 s from rest to rest.

This maneuver contains the largest translational and angular accelerations of the four experiments. The maximal linear acceleration of $17.5 \frac{\text{m}}{\text{s}^2}$ obviously appears when the quadcopter is upside down. Here gravity pulls it with $9.81 \frac{\text{m}}{\text{s}^2}$ and the propellers generate significant thrust in the same direction.

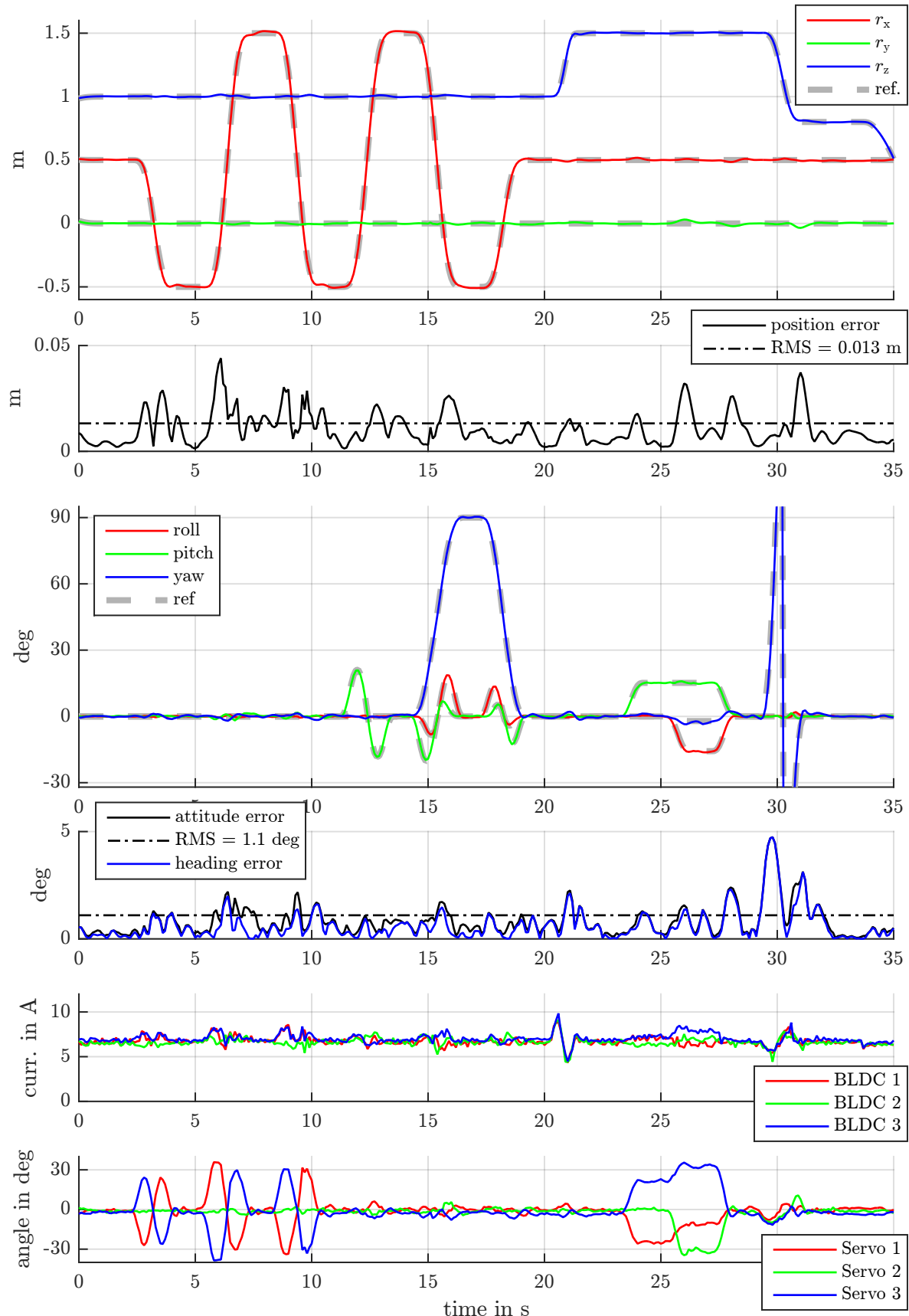


Figure 5.24: Tricopter flight test result for polynomial transition trajectories

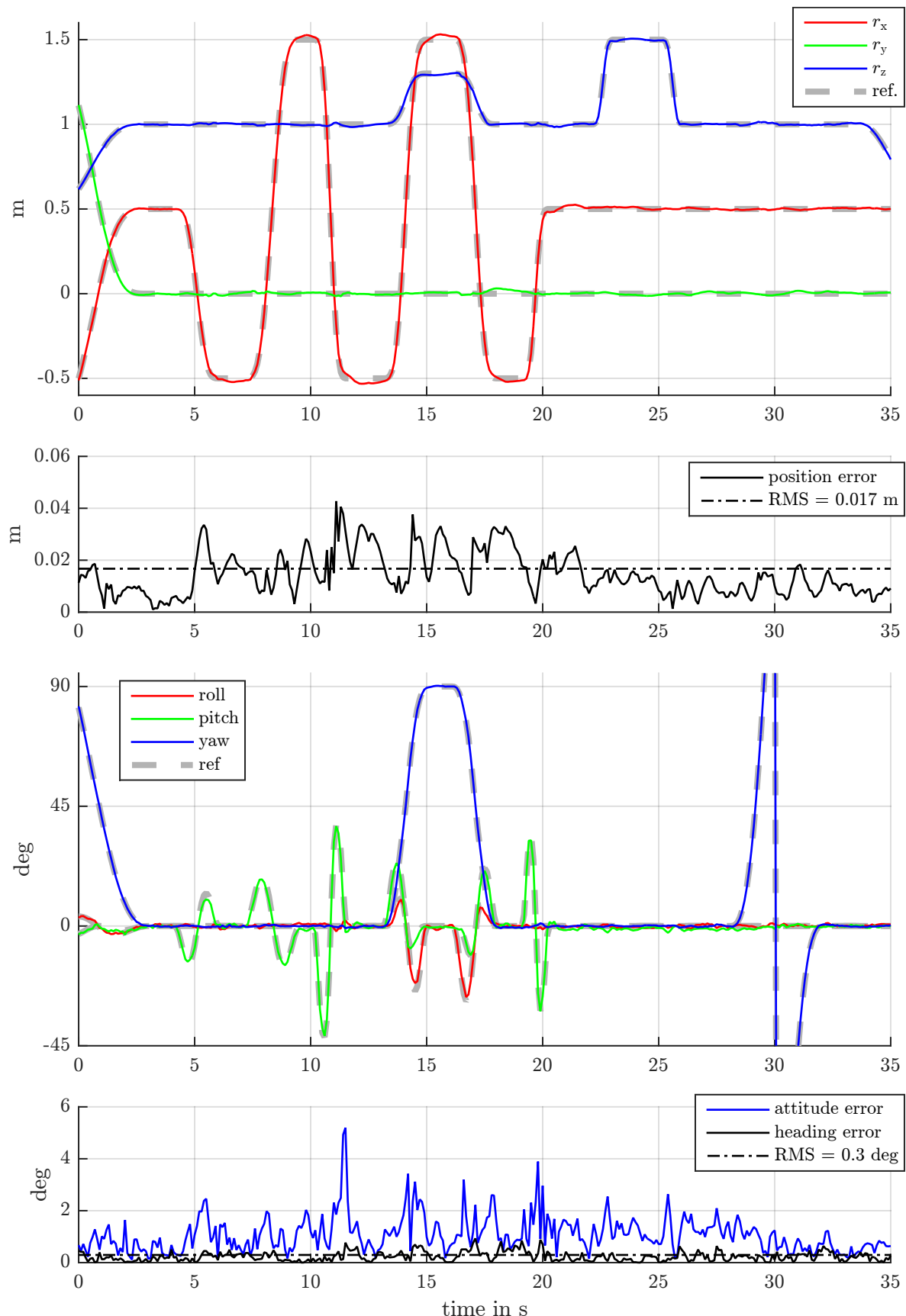


Figure 5.25: Quadcopter flight test result for polynomial transition trajectories

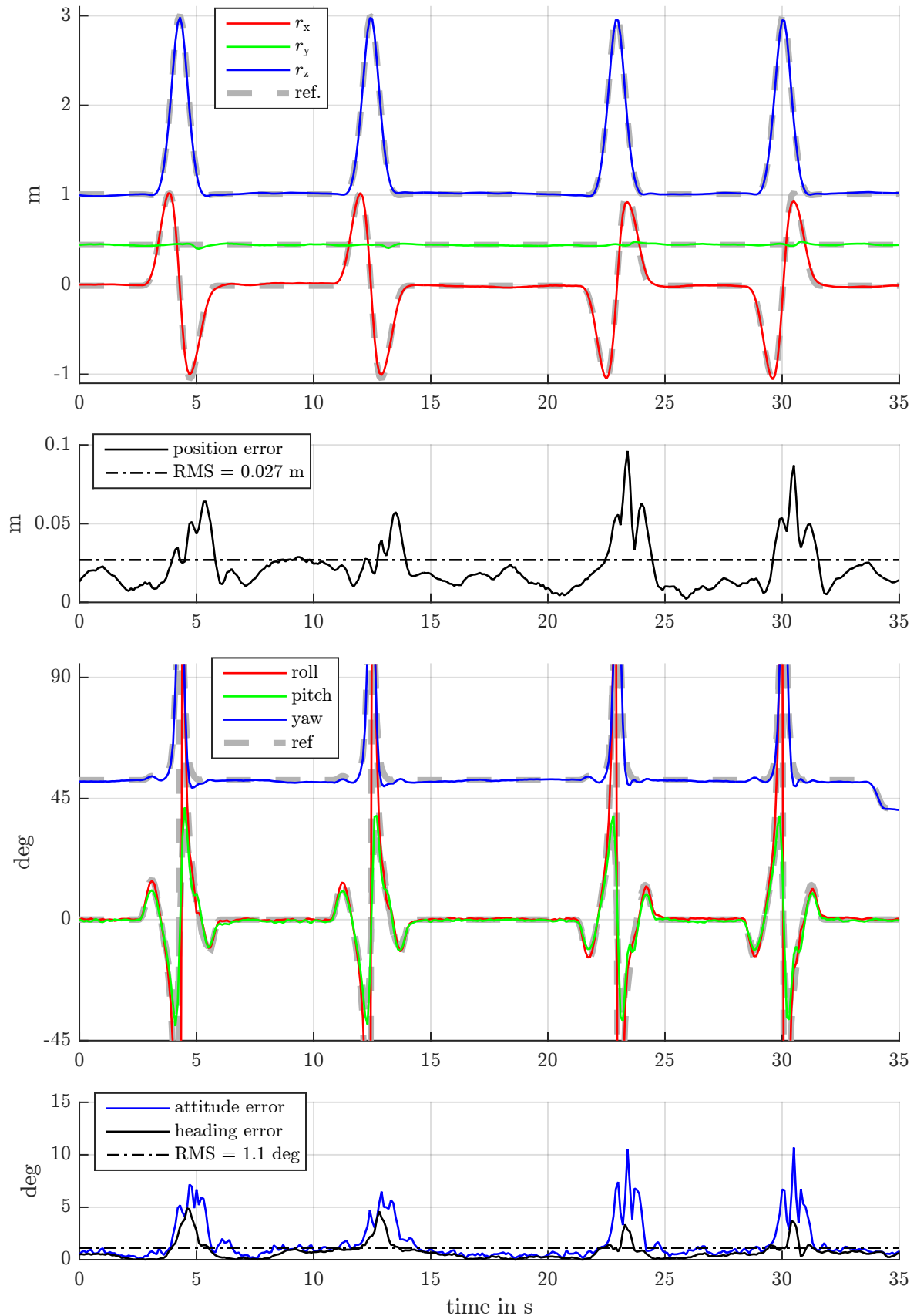


Figure 5.26: Quadcopter flight test result for looping trajectories

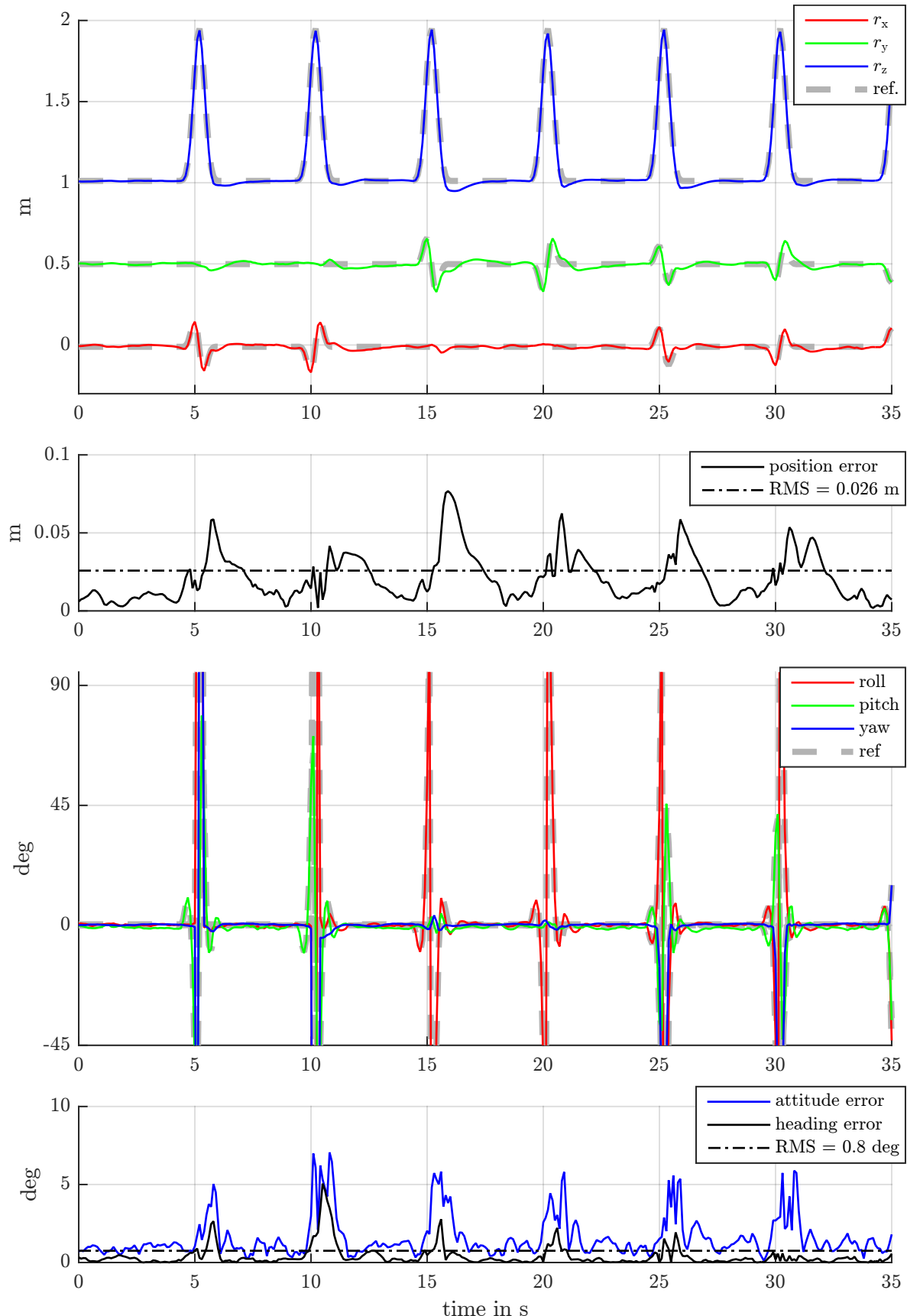


Figure 5.27: Quadcopter flight test result for the flip trajectories

Chapter 6

Summary and Conclusions

This work discussed the modeling and tracking control of rigid body systems. Both subjects are well covered in the dedicated literature. However, the literature is somewhat split into two viewpoints: Small academic examples are treated independently with a lot of emphasis on the particular geometry like e.g. [Marsden and Ratiu, 1998]. Larger multibody systems are handled by general formalisms, but treated by minimal generalized coordinates as if their configuration manifold is \mathbb{R}^n as in e.g. [Roberson and Schwertassek, 1988]. This work attempts to combine both these points of view: The proposed recipe for the equations of motion holds for general multibody systems *and* allows a parameterization through redundant configuration coordinates that respect the underlying geometry of the system.

While inertia is arguably the core aspect of a rigid body system, this work also investigated into analog, natural stiffness and damping formulations. The resulting damping and stiffness parameters, are not presented, maybe even unknown, in the dedicated literature. The way e.g. the moment of stiffness matrix $\boldsymbol{\Pi}$ was derived here, it is just as natural as the (absolutely established) moment of inertia matrix $\boldsymbol{\Theta}$.

For control design, it is a common approach to design the desired closed loop dynamics and derive the actually required control law from it. Flatness based control formalizes this approach but the vast majority combines it with linear error dynamics, thus treating the system as if its configuration manifold is \mathbb{R}^p . This work proposes desired closed loop dynamics based on a general mechanical model of a rigid body system. As a result, the closed loop dynamics are invariant to the choice of coordinates in the same way as the motion of a mechanical system is unchanged by the choice of coordinates with which it is parameterized. Furthermore, all control parameters have intrinsic mechanical interpretation, so should be intuitive for tuning.

Motivated by this basic idea, this work proposed three candidates for closed loop tracking dynamics: One motivated by the dynamics of a particle system, one motivated by the rigid body energies and one motivated by the total energy of the system. When dealing with the stabilization of a constant reference, the three approaches coincide and resemble an actual rigid body system subject to inertia, viscous damping and linear springs but not gravity. For this case, the total energy is a Lyapunov function. For tracking a general reference trajectory, only the third approach guarantees stability. In contrast, this approach has

the drawback of requiring an additional ingredient, the transport map, whose existence is not guaranteed. Though not necessarily being a Lyapunov function, each approach comes with a formulation for a total energy that is positive definite, i.e. positive and zero if, and only if, the tracking objective is fulfilled, usually $\mathbf{x} = \mathbf{x}_R$ and $\boldsymbol{\xi} = \boldsymbol{\xi}_R$.

The three control approaches were applied to various examples of rigid body systems and tested in simulation with reasonable reference trajectories and initial conditions. While the total energy was not always monotonically decreasing, it always eventually converged to zero. So the general control objective was always achieved.

Finally, the proposed rigid body controller was successfully tested on the LSR-quad and tricopter. The realization also required trajectory generation, state estimation and underlying actuator control which were each challenging control tasks in their own right. From a coding perspective, the actual rigid body controller is less than 1 % of the microcontroller C code. The presented experiments show the viability of the proposed control design in a practical environment with imperfect measurements and disturbances. The quadcopter showed good tracking performance even while following aerobatic trajectories like loops and flips.

Appendix A

TBD

A.1 On error coordinates

Error coordinates. Introduce (possibly redundant) error coordinates $\mathbf{e} \in \mathbb{R}^{\nu_e}$ as

$$\mathbf{e} = \chi_E(\mathbf{x}, \mathbf{x}_R), \quad \phi_E(\mathbf{e}) = 0. \quad (\text{A.1})$$

and require that this relation is invertible with $\mathbf{x} = \chi(\mathbf{e}, \mathbf{x}_R)$, i.e. $\chi(\chi_E(\mathbf{x}, \mathbf{x}_R), \mathbf{x}_R) = \mathbf{x} \forall \mathbf{x} \in \mathbb{X}$. The inverse function theorem now implies that the differential $\nabla \chi_E = \frac{\partial \chi_E}{\partial \mathbf{x}} \mathbf{A}$ has full rank: $\text{rank}(\nabla \chi_E) = \dim \mathbb{X} = n$.

Let Φ_E be the linear independent rows of $\partial \phi_E / \partial \mathbf{e}$. Then the derivative of the geometric constraint $\dot{\phi}_E = 0$ implies

$$\Phi_E \nabla \chi_E = 0, \quad \Phi_E \nabla_R \chi_E = 0, \quad (\text{A.2})$$

Since the matrices $\nabla \chi_E$ and Φ_E have full rank, their pseudo-inverses are

$$(\nabla \chi_E)^+ = ((\nabla \chi_E)^\top (\nabla \chi_E))^{-1} (\nabla \chi_E)^\top, \quad (\nabla \chi_E)^+ (\nabla \chi_E) = \mathbf{I}_n \quad (\text{A.3})$$

$$\Phi_E^+ = \Phi_E^\top (\Phi_E \Phi_E^\top)^{-1}, \quad \Phi_E \Phi_E^+ = \mathbf{I}_{\nu_e - n}. \quad (\text{A.4})$$

Furthermore, due to the orthogonality $\Phi_E \nabla \chi_E = 0$ we have

$$(\nabla \chi_E) (\nabla \chi_E)^+ + \Phi_E^+ \Phi_E = \mathbf{I}_{\nu_e}. \quad (\text{A.5})$$

Error potential. We require that the potential $\bar{\mathcal{V}}$ can be expressed as a function $\bar{\mathcal{V}}_E$ of the error coordinates \mathbf{e} alone, i.e.

$$\bar{\mathcal{V}}(\mathbf{x}, \mathbf{x}_R) = \bar{\mathcal{V}}_E(\chi_E(\mathbf{x}, \mathbf{x}_R)). \quad (\text{A.6})$$

Now the requirement (4.30) for the transport map \mathbf{Q} can be written as

$$\begin{aligned} \nabla_{\mathbf{R}} \bar{\mathcal{V}} + \mathbf{Q}^T \nabla \bar{\mathcal{V}} &= (\nabla_{\mathbf{R}} \chi_E + \nabla \chi_E \mathbf{Q})^T \frac{\partial \bar{\mathcal{V}}_E}{\partial \mathbf{e}} \\ &= \left(\underbrace{((\nabla \chi_E)(\nabla \chi_E)^+ + \Phi_E^+ \Phi_E)}_{\mathbf{I}_{\nu_e}} \nabla_{\mathbf{R}} \chi_E + \nabla \chi_E \mathbf{Q} \right)^T \frac{\partial \bar{\mathcal{V}}_E}{\partial \mathbf{e}} \\ &= ((\nabla \chi_E)^+ (\nabla_{\mathbf{R}} \chi_E) + \mathbf{Q})^T (\nabla \chi_E)^T \frac{\partial \bar{\mathcal{V}}_E}{\partial \mathbf{e}} + \Phi_E^+ \underbrace{\Phi_E \nabla_{\mathbf{R}} \chi_E}_{0} \frac{\partial \bar{\mathcal{V}}_E}{\partial \mathbf{e}} = 0 \quad (\text{A.7}) \end{aligned}$$

which has the simple solution

$$\mathbf{Q} = -(\nabla \chi_E)^+ (\nabla_{\mathbf{R}} \chi_E). \quad (\text{A.8})$$

Error kinematics. With the same approach as above we can derive a kinematic relation between the error coordinates \mathbf{e} and the error velocity $\boldsymbol{\xi}_E = \boldsymbol{\xi} - \mathbf{Q} \boldsymbol{\xi}_R$ as

$$\begin{aligned} \dot{\mathbf{e}} &= (\nabla \chi_E) \boldsymbol{\xi} + (\nabla_{\mathbf{R}} \chi_E) \boldsymbol{\xi}_R \\ &= (\nabla \chi_E) \boldsymbol{\xi} + \underbrace{((\nabla \chi_E)(\nabla \chi_E)^+ + \Phi_E^+ \Phi_E)}_{\mathbf{I}_{\nu_e}} \nabla_{\mathbf{R}} \chi_E \boldsymbol{\xi}_R \\ &= (\nabla \chi_E) \underbrace{(\boldsymbol{\xi} + (\nabla \chi_E)^+ (\nabla_{\mathbf{R}} \chi_E) \boldsymbol{\xi}_R)}_{\boldsymbol{\xi}_E} + \Phi_E^+ \underbrace{\Phi_E (\nabla_{\mathbf{R}} \chi_E)}_0 \boldsymbol{\xi}_R \quad (\text{A.9}) \end{aligned}$$

A.2 Constraint stabilization

In practice we might run into trouble with flawed initial conditions $\phi(x_0) \neq 0$ or with the flaws of numerical integration. To counter this we can add a *stabilization term* $-\Lambda \phi$ to the kinematic equation:

$$\dot{\mathbf{x}} = \underbrace{[\mathbf{A} \ \boldsymbol{\Psi}]}_{\mathbf{A}_{\square}} \begin{bmatrix} \boldsymbol{\xi} \\ -\Lambda \phi \end{bmatrix}. \quad (\text{A.10})$$

This results in

$$\frac{d}{dt} \phi = \frac{\partial \phi}{\partial \mathbf{x}} \dot{\mathbf{x}} = \underbrace{\frac{\partial \phi}{\partial \mathbf{x}} \mathbf{A}}_0 \boldsymbol{\xi} - \underbrace{\frac{\partial \phi}{\partial \mathbf{x}} \boldsymbol{\Psi}}_{\mathbf{I}_{n-\nu}} \Lambda \phi = -\Lambda \phi \quad (\text{A.11})$$

i.e. for an appropriate $\Lambda \in \mathbb{R}^{(\nu-n) \times (\nu-n)}$ the error to the geometric constraint converges exponentially. For the example of the rigid body orientation (A.10) can also be written in the probably more intuitive matrix form

$$\dot{\mathbf{R}} = \mathbf{R} (\widehat{\boldsymbol{\omega}} - \Lambda (\mathbf{R}^T \mathbf{R} - \mathbf{I}_3)) \quad (\text{A.12})$$

with a symmetric positive definite matrix $\Lambda = \Lambda^T \in \mathbb{R}^{3 \times 3} > 0$.

The resulting EoM with Lagrangian multipliers (3.130) only consider the derivatives of the constraints, e.g. $\ddot{\psi} = 0$ or $\dot{\eta} = 0$. As before, for the case of bad initial conditions or

the errors of numerical integration, we should add a stabilization term: In the case of kinematic constraints this is

$$\underbrace{\frac{\partial \eta}{\partial \xi}}_z \dot{\xi} = \underbrace{-\nabla \eta \xi - \frac{\partial \eta}{\partial t}}_z \underbrace{-\Lambda \eta(\mathbf{x}, \xi, t)}_{\text{stabilization}} \Leftrightarrow \dot{\eta} + \Lambda \eta = 0 \quad (\text{A.13a})$$

and for a geometric constraints

$$\underbrace{\nabla \psi}_z \dot{\xi} = \underbrace{-\frac{d}{dt}(\nabla \psi) \xi - \Lambda_1 \nabla \psi(\mathbf{x}) \xi - \Lambda_0 \psi(\mathbf{x})}_{\text{stabilization}} \Leftrightarrow \ddot{\psi} + \Lambda_1 \dot{\psi} + \Lambda_0 \psi = 0. \quad (\text{A.13b})$$

consult [Bremer, 2008, sec. 3.5.2.4]

A.3 A possible generalization of the rigid body energies

Note that any symmetric, positive matrix $\mathbf{K} \in \mathbb{SYM}^+(6)$ can be decomposed into

$$\mathbf{K} = \begin{bmatrix} \mathbf{I}_3 & \mathbf{0} \\ \mathbf{H} & \mathbf{I}_3 \end{bmatrix} \begin{bmatrix} \mathbf{K}_r & \mathbf{0} \\ \mathbf{0} & \mathbf{K}_R \end{bmatrix} \begin{bmatrix} \mathbf{I}_3 & \mathbf{H}^\top \\ \mathbf{0} & \mathbf{I}_3 \end{bmatrix} = \begin{bmatrix} \mathbf{K}_r & \mathbf{K}_r \mathbf{H}^\top \\ \mathbf{H} \mathbf{K}_r & \mathbf{K}_R + \mathbf{H} \mathbf{K}_r \mathbf{H}^\top \end{bmatrix} \quad (\text{A.14})$$

where $\mathbf{K}_r, \mathbf{K}_R \in \mathbb{SYM}^+(3)$ and $\mathbf{H} \in \mathbb{R}^{3 \times 3}$. For variables $\mathbf{x}_i \in \mathbb{R}^3$ and $\mathbf{Y}_i \in \mathbb{R}^{3 \times 3}$ collected in the square matrix $\Xi_i = [\mathbf{Y}_i \ \mathbf{x}_i \ \mathbf{0}]$ define the inner product as

$$\langle \Xi_1, \Xi_2 \rangle_{\mathbf{K}} = \tilde{\mathbf{x}}_1^\top \mathbf{K}_r \tilde{\mathbf{x}}_2 + \text{tr}(\mathbf{Y}_1 \text{Vee}(\mathbf{K}_R) \mathbf{Y}_2^\top), \quad (\text{A.15})$$

where $\tilde{\mathbf{x}}_i = \mathbf{x}_i + \frac{1}{2}\mathbf{Y}_i \text{vee2}(\mathbf{H}) + \frac{1}{4}(\mathbf{H} + \mathbf{H}^\top) \text{vee2}(\mathbf{Y}_i)$. To prove that this is indeed an inner product one can use the same argument as in [sec:RBSMathInnerProduct](#) and note that positive definiteness of \mathbf{K}_R implies positive definiteness of $\text{Vee}(\mathbf{K}_R)$. For the special parameters $\mathbf{K}_r = k\mathbf{I}_3$ and $\mathbf{H} = \text{wed}(\mathbf{h}), \mathbf{h} \in \mathbb{R}^3$ this inner product coincides with the definition of (2.47). For the special arguments $\mathbf{Y}_i = \text{wed}(\mathbf{y}_i), \mathbf{y}_i \in \mathbb{R}^3$ we have the following simplifications $\tilde{\mathbf{x}}_i = \mathbf{x}_i + \mathbf{H}^\top \mathbf{y}_i$ and $\text{tr}(\text{wed}(\mathbf{y}_1) \text{Vee}(\mathbf{K}_R) \text{wed}(\mathbf{y}_2)^\top) = \mathbf{y}_1^\top \mathbf{K}_R \mathbf{y}_2$. So, for the case $\Xi_i = \text{wed}(\xi_i), \xi_i = [\mathbf{x}_i^\top, \mathbf{y}_i^\top]^\top$ the inner product (A.15) simplifies to

$$\langle \text{wed}(\xi_1), \text{wed}(\xi_2) \rangle_{\mathbf{K}} = \xi_1^\top \mathbf{K} \xi_2. \quad (\text{A.16})$$

For any inner product we may define an induced norm and metric as

$$\|\Xi\|_{\mathbf{K}} = \sqrt{\langle \Xi, \Xi \rangle_{\mathbf{K}}}, \quad d_{\mathbf{K}}(\Xi_1, \Xi_2) = \|\Xi_1 - \Xi_2\|_{\mathbf{K}}. \quad (\text{A.17})$$

Note that the same inner product, norm and metric can also be defined for elements of the form $\Xi_i = [\mathbf{Y}_i \ \mathbf{x}_i \ \mathbf{0}]$.

With this we may define the following energies as the square of the metrics

$$\mathcal{V} = \frac{1}{2} d_{\mathbf{K}}^2(\mathbf{G}, \mathbf{G}_R), \quad \mathbf{K} \in \mathbb{SYM}^+(6), \quad (\text{A.18a})$$

$$\mathcal{R} = \frac{1}{2} d_{\mathbf{D}}^2(\dot{\mathbf{G}}, \dot{\mathbf{G}}_R), \quad \mathbf{D} \in \mathbb{SYM}^+(6), \quad (\text{A.18b})$$

$$\mathcal{T} = \frac{1}{2} d_{\mathbf{M}}^2(\ddot{\mathbf{G}}, \ddot{\mathbf{G}}_R), \quad \mathbf{M} \in \mathbb{SYM}^+(6). \quad (\text{A.18c})$$

For the special parameters $\mathbf{K}_r = k\mathbf{I}_3$ and $\mathbf{H} = \text{wed}(\mathbf{h}), \mathbf{h} \in \mathbb{R}^3$ this coincides with the energies defined in (4.11). Alternatively, using $\mathbf{G}_E = \mathbf{G}_R^{-1}\mathbf{G}$, we may define

$$\mathcal{V} = \frac{1}{2}d_{\mathbf{K}}^2(\mathbf{G}_E, \mathbf{I}_4), \quad \mathbf{K} \in \text{SYM}^+(6), \quad (\text{A.19a})$$

$$\mathcal{R} = \frac{1}{2}d_{\mathbf{D}}^2(\dot{\mathbf{G}}_E, \mathbf{0}), \quad \mathbf{D} \in \text{SYM}^+(6), \quad (\text{A.19b})$$

$$\mathcal{T} = \frac{1}{2}d_{\mathbf{M}}^2(\ddot{\mathbf{G}}_E, \mathbf{0}), \quad \mathbf{M} \in \text{SYM}^+(6), \quad (\text{A.19c})$$

For the special parameters mentioned above, this coincides with the energies defined in (4.20).

The inner product and its induced norm and metric can be regarded as a generalization of the inner product (with 10 parameters) proposed in [sec:RBSMathInnerProduct](#) in the sense that it incorporates all 21 independent coefficients of the symmetric matrix $\mathbf{K} \in \text{SYM}^+(6)$. This results in more tuning parameters for the control design. On the downside, the translation invariance [eq:InnerProductSE3Translation](#) and the physical interpretation of the parameters are lost for the general case.

Bibliography

- [Abraham and Marsden, 1978] Abraham, R. and Marsden, J. E. (1978). *Foundations of Mechanics*. Westview Press.
- [Appell, 1900] Appell, P. E. (1900). Sur une forme générale des équations de la dynamique. *J. Reine Angew. Math.*, 121:310–319.
- [Arnold, 1989] Arnold, V. I. (1989). *Mathematical Methods of Classical Mechanics*, volume 60 of *Graduate Texts in Mathematics*. Springer, New York.
- [Bloch et al., 2000] Bloch, A. M., Leonard, N. E., and Marsden, J. E. (2000). Controlled Lagrangians and the stabilization of mechanical systems. I. The first matching theorem. *IEEE Trans. on Automatic Control*, 45(12):2253–2270.
- [Boltzmann, 1897] Boltzmann, L. (1897). *Vorlesungen ueber die Pincipe der Mechanik*. Johann Ambrosius Barth.
- [Boltzmann, 1902] Boltzmann, L. (1902). Über die Form der Lagrangeschen Gleichungen für nichtholome, generalisierte Koordinaten. In *Wissenschaftliche Abhandlungen*, volume 3, pages 682–692. Johann Ambrosius Barth.
- [Bremer, 2008] Bremer, H. (2008). *Elastic Multibody Dynamics: A Direct Ritz Approach*. Springer.
- [Bristeau et al., 2009] Bristeau, P.-J., Martin, P., Salaün, E., and Petit, N. (2009). The role of propeller aerodynamics in the model of a quadrotor uav. In *Proc. ECC 2009*, pages 683–688.
- [Brouwer, 1912] Brouwer, L. (1912). Über Abbildung von Mannigfaltigkeiten. *Mathematische Annalen*, 71:97–115.
- [Bryson, 1975] Bryson, A. E. (1975). *Applied optimal control: optimization, estimation and control*. CRC Press.
- [Bullo and Murray, 1999] Bullo, F. and Murray, R. M. (1999). Tracking for fully actuated mechanical systems: A geometric framework. *Automatica*, 35(1):17–34.
- [Courant and Hilbert, 1924] Courant, R. and Hilbert, D. (1924). *Methoden der Mathematischen Physik*. Julius Springer.
- [Davenport, 1968] Davenport, P. B. (1968). A vector approach to the algebra of rotations with applications. *NASA Technical Note D-4696*.

- [Denavit and Hartenberg, 1955] Denavit, J. and Hartenberg, R. (1955). A kinematic notation for lower-pair mechanisms based on matrices. *Journal of Applied Mechanics*, 22(2):215–221.
- [Desloge, 1987] Desloge, E. A. (1987). Relationship between Kane's equations and the Gibbs-Appell equations. *Journal of Guidance, Control, and Dynamics*, 10(1):120–122.
- [Einstein, 1916] Einstein, A. (1916). Hamiltonsches Prinzip und allgemeine Relativitätstheorie. *Sitzungsberichte der Preussischen Akademie der Wissenschaften zu Berlin*.
- [Fliess et al., 1995] Fliess, M., Lévine, J., Martin, P., and Rouchon, P. (1995). Flatness and defect of non-linear systems: introductory theory and examples. *International Journal of Control*, 61(6):1327–1361.
- [Fliess et al., 1999] Fliess, M., Lévine, J., Martin, P., and Rouchon, P. (1999). A Lie-Bäcklund approach to equivalence and flatness of nonlinear systems. *IEEE Trans. Automat. Contr.*, 44(5):922–937.
- [Frankel, 1997] Frankel, T. (1997). *The Geometry of Physics*. Cambridge University Press.
- [Fritsch, 2014] Fritsch, O. (2014). *Energiebasierte Lage- und Positionsfolgeregelung für einen Quadrocopter*. PhD thesis, Technische Universität München.
- [Galilei, 1638] Galilei, G. (1638). *Discorsi e dimostrazioni matematiche intorno a due nuove scienze*. Appresso gli Elsevirii.
- [Gauß, 1829] Gauß, C. F. (1829). Über ein neues allgemeines Grundgesetz der Mechanik. *Journal für die reine und angewandte Mathematik*.
- [Gibbs, 1879] Gibbs, J. W. (1879). On the fundamental formulae of dynamics. *Am. J. Math.*, 2(1):49–64.
- [Goldstein, 1951] Goldstein, H. (1951). *Classical Mechanics*. Addison-Wesley.
- [Golub and Loan, 1996] Golub, G. H. and Loan, C. F. V. (1996). *Matrix Computations*. Johns Hopkins.
- [Gould et al., 2001] Gould, N., Hribar, M., and Nocedal, J. (2001). On the solution of equality constrained quadratic programming problems arising in optimization. *SIAM Journal on Scientific Computing*, 23(4):1376–1395.
- [Grafarend and Kühnel, 2011] Grafarend, E. W. and Kühnel, W. (2011). A minimal atlas for the rotation group $\text{SO}(3)$. *GEM-International Journal on Geomathematics*, 2(1):113–122.
- [Hall, 2015] Hall, B. (2015). *Lie Groups, Lie Algebras, and Representations*, volume 222 of *Graduate Texts in Mathematics*. Springer, 2nd edition.
- [Hamel, 1904a] Hamel, G. (1904a). Die Lagrange-Eulerschen Gleichungen der Mechanik. *Z. für Mathematik u. Physik*, 50:1–57.

- [Hamel, 1904b] Hamel, G. (1904b). Über die virtuellen Verschiebungen in der Mechanik. *Mathematische Annalen*, 59:416–434.
- [Hamel, 1949] Hamel, G. (1949). *Theoretische Mechanik*. Springer.
- [Hamel et al., 2002] Hamel, T., Mahony, R., Lozano, R., and Ostrowski, J. (2002). Dynamic Modelling and configuration stabilization for an X4-Flyer. In *Proc. 15th Triennial IFAC World Congress*, pages 217–222.
- [Hauser et al., 1992] Hauser, J., Sastry, S., and Meyer, G. (1992). Nonlinear control design for slightly non-minimum phase systems: Application to V/STOL aircraft. *Automatica*, 28(4):664–679.
- [Hooke, 1678] Hooke, R. (1678). *Lectures De Potentia Restitutiva, or of Spring. Explaining the Power of Springing Bodies*. Printed for John Martyn Printer to the Royal Society.
- [Horn and Johnson, 1985] Horn, R. A. and Johnson, C. R. (1985). *Matrix Analysis*. Cambridge University Press.
- [Irscheid et al., 2019] Irscheid, A., Konz, M., and Rudolph, J. (2019). A flatness-based approach to the control of distributed parameter systems applied to load transportation with heavy ropes. In Kondratenko, Y. P., Chikrii, A. A., Gubarev, V. F., and Kacprzyk, J., editors, *Advanced Control Techniques in Complex Engineering Systems: Theory and Applications*, pages 279–294. Springer.
- [Johnson, 1980] Johnson, W. (1980). *Helicopter Theory*. Princeton University Press.
- [Kabsch, 1976] Kabsch, W. (1976). A solution for the best rotation to relate two sets of vectors. *Acta Crystallographica*, A32(5):922.
- [Kane and Levinson, 1985] Kane, T. R. and Levinson, D. A. (1985). *Dynamics*. McGraw Hill.
- [Kastelan et al., 2015] Kastelan, D., Konz, M., and Rudolph, J. (2015). Fully actuated tricopter with pilot-supporting control. In *Proc. 1st IFAC Workshop on Advanced Control and Navigation for Autonomous Aerospace Vehicles ACNAAV 15*, pages 79–84.
- [Klein, 1926] Klein, F. (1926). *Vorlesungen über die Entwicklung der Mathematik im 19. Jahrhundert*. Julius Springer.
- [Koditschek, 1989] Koditschek, D. E. (1989). The Application of Total Energy as a Lyapunov Function for Mechanical Control Systems. In Marsden, J. E., Krishnaprasad, P. S., and Simo, J. C., editors, *Dynamics and Control of Multibody Systems*, volume 97 of *Contemporary Mathematics*, pages 131–157. American Mathematical Society.
- [Konz et al., 2018] Konz, M., Kastelan, D., Gerbet, D., and Rudolph, J. (2018). Practical challenges of fully-actuated tricopter control. In *Proc. of MECHATRONICS 2018*, pages 128–135.

- [Konz et al., 2020] Konz, M., Kastelan, D., and Rudolph, J. (2020). Tracking Control for a Fully-Actuated UAV. In Yan, X., Bradley, D., Russell, D., and Moore, P., editors, *Reinventing Mechatronics*, pages 127–144. Springer.
- [Konz and Rudolph, 2013] Konz, M. and Rudolph, J. (2013). Quadrotor tracking control based on a moving frame. In *Proc. 9th IFAC Symposium on Nonlinear Control Systems*, pages 80–85.
- [Konz and Rudolph, 2015] Konz, M. and Rudolph, J. (2015). Equations of motion with redundant coordinates for mechanical systems on manifolds. In *Proc. 8th Vienna Int. Conf. on Mathematical Modelling*, pages 681–682.
- [Konz and Rudolph, 2016] Konz, M. and Rudolph, J. (2016). Beispiele für einen direkten Zugang zu einer globalen, energiebasierten Modellbildung und Regelung von Starrkörperpersystemen. *at - Automatisierungstechnik*, 64(2):96–109.
- [Konz and Rudolph, 2018] Konz, M. and Rudolph, J. (2018). Redundant configuration coordinates and nonholonomic velocity coordinates in analytical mechanics. In *Proc. 9th Vienna Int. Conf. on Mathematical Modelling*, page 409–414.
- [Konz and Rudolph, 2021] Konz, M. and Rudolph, J. (2021). Gauss’s principle and tracking control of underactuated mechanical systems. In *Proc. 7th IFAC Workshop on Lagrangian and Hamiltonian Methods for Nonlinear Control LHMNC*, pages 365–370.
- [Lanczos, 1986] Lanczos, C. (1986). *The Variational Principles of Mechanics*. Dover Publications, 4 edition.
- [Landau and Lifshitz, 1960] Landau, L. D. and Lifshitz, E. M. (1960). *Mechanics*, volume 1 of *Course of Theoretical Physics*. Pergamon Press.
- [Landau and Lifshitz, 1971] Landau, L. D. and Lifshitz, E. M. (1971). *The Classical Theory of Fields*, volume 2 of *Course of Theoretical Physics*. Pergamon Press.
- [Lee, 2003] Lee, J. M. (2003). *Introduction to Smooth Manifolds*. Springer.
- [Lesser, 1992] Lesser, M. (1992). A Geometric Interpretation of Kane’s Equations. *Proceedings of the Royal Society of London*, 436(1896):69–87.
- [Lewis, 1996] Lewis, A. D. (1996). The geometry of the Gibbs-Appell equations and Gauss’s Principle of Least Constraint. *Reports on Mathematical Physics*, 38(1):11–28.
- [Luenberger and Ye, 2015] Luenberger, D. G. and Ye, Y. (2015). *Linear and Nonlinear Programming*. Springer, 4th edition.
- [Lurie, 2002] Lurie, A. I. (2002). *Analytical Mechanics*. Springer.
- [Marsden and Ratiu, 1998] Marsden, J. E. and Ratiu, T. S. (1998). *Introduction to Mechanics and Symmetry*. Springer, Berlin Heidelberg, 2nd edition.
- [Martin et al., 1997] Martin, P., Murray, R. M., and Rouchon, P. (1997). Flat systems, equivalence and trajectory generation. In *Mini-course ECC’97*.

- [Martin and Salaun, 2010] Martin, P. and Salaun, E. (2010). The true role of accelerometer feedback in quadrotor control. In *IEEE Int. Conf. on Robotics and Automation*, pages 1623–1629.
- [Mellinger et al., 2012] Mellinger, D., Michael, N., and Kumar, V. (2012). Trajectory Generation and Control for Precise Aggressive Maneuvers with Quadrotors. *Int. J. Rob. Res.*, 31(5):664–674.
- [Misner et al., 1973] Misner, C. W., Thorne, K. S., and Wheeler, J. A. (1973). *Gravitation*. W. H. Freeman and Company.
- [Murray et al., 1994] Murray, R. M., Li, Z., and Sastry, S. S. (1994). *A Mathematical Introduction to Robotic Manipulation*. CRC Press.
- [Murray et al., 1995] Murray, R. M., Rathinam, M., and Sluis, W. (1995). Differential flatness of mechanical control systems: A catalog of prototype systems. In *Proceedings of the ASME International Congress and Exposition*.
- [Neimark and Fufaev, 1972] Neimark, J. I. and Fufaev, N. A. (1972). *Dynamics of Nonholonomic Systems*. Amer. Mathem. Society.
- [Newton, 1687] Newton, I. (1687). *Philosophiae naturalis principia mathematica*. Jussu Societatis Regiae ac Typis Josephi Streator.
- [Newton, 1846] Newton, I. (1846). *The Mathematical Principles of Natural Philosophy, Translated into English by A. Motte and N. W. Chittenden*. Daniel Adee.
- [Nocedal and Wright, 2006] Nocedal, J. and Wright, S. J. (2006). *Numerical Optimization*. Springer, 2nd edition.
- [Olfati-Saber, 2001] Olfati-Saber, R. (2001). *Nonlinear Control of Underactuated Mechanical Systems with Applications to Robotics and Aerospace Vehicles*. PhD thesis, Massachusetts Institute of Technology, Cambridge, MA.
- [Papastavridis, 2002] Papastavridis, J. G. (2002). *Analytical Mechanics*. World Scientific.
- [Penrose, 1955] Penrose, R. (1955). A generalized inverse for matrices. *Mathematical proceedings of the Cambridge philosophical society*, 51(3):406–413.
- [Pfeiffer and Glocker, 1996] Pfeiffer, F. and Glocker, C. (1996). *Multibody Dynamics with unilateral contacts*. Wiley-VCH.
- [Päsler, 1968] Päsler, M. (1968). *Prinzip der Mechanik*. Walter de Gruyter & Co.
- [Rabiner and Gold, 1975] Rabiner, L. R. and Gold, B. (1975). *Theory and Application of Digital Signal Processing*. Prentice-Hall.
- [Rathinam and Murray, 1998] Rathinam, M. and Murray, R. M. (1998). Configuration flatness of lagrangian systems underactuated by one control. *SIAM Journal of Control and Optimization*, 36(1):164–179.
- [Rayleigh, 1877] Rayleigh, J. W. S. B. (1877). *The Theory of Sound*. Macmillan and Co.

- [Roberson and Schwertassek, 1988] Roberson, R. E. and Schwertassek, R. (1988). *Dynamics of Multibody Systems*. Springer.
- [Savage, 1998] Savage, P. G. (1998). Strapdown inertial navigation integration algorithm design part 1: Attitude algorithms. *Journal of Guidance, Control, and Dynamics*, 1(21):19–28.
- [Schlacher and Schöberl, 2007] Schlacher, K. and Schöberl, M. (2007). Construction of flat outputs by reduction and elimination. *CD Proceedings IFAC Symposium on Non-linear Control Systems*, pages 666–671.
- [Servais et al., 2015a] Servais, E., d’Andréa Novel, B., and Mounier, H. (2015a). Ground control of a hybrid tricopter. In *2015 International Conference on Unmanned Aircraft Systems (ICUAS)*, pages 945–950.
- [Servais et al., 2015b] Servais, E., Mounier, H., and d’Andréa Novel, B. (2015b). Trajectory tracking of trirotor uav with pendulum load. In *2015 20th International Conference on Methods and Models in Automation and Robotics (MMAR)*, pages 517–522.
- [Shabana, 2005] Shabana, A. A. (2005). *Dynamics of Multibody Systems*. Cambridge University Press, 3 edition.
- [Slotine and Li, 1991] Slotine, J.-J. and Li, W. (1991). *Applied Nonlinear Control*. Springer.
- [Spivak, 1999] Spivak, M. (1999). *A Comprehensive Introduction to Differential Geometry*. Publish or Perish.
- [Spong et al., 2006] Spong, M. W., Hutchinson, S., and Vidyasagar, M. (2006). *Robot Modeling and Control*. Wiley.
- [Szabó, 1956] Szabó, I. (1956). *Höhere Technische Mechanik*. Springer.
- [Tietze and Schenk, 1999] Tietze, U. and Schenk, C. (1999). *Halbleiter-Schaltungstechnik*. Springer, 11 edition.
- [Wahba, 1965] Wahba, G. (1965). A least squares estimate of satellite attitude. *SIAM Review*, 7(3):409.
- [Wittenburg, 2008] Wittenburg, J. (2008). *Dynamics of Multibody Systems*. Springer, 2 edition.